Continuous Earth-Moon Payload Exchange Using Motorised Tethers With Associated Dynamics

by

Christopher Murray

B.Sc., B.Sc.(Honours), M.Sc.

Submitted in fulfillment of the requirements for the

Degree of Doctor of Philosophy

School of Engineering

University of Glasgow

June, 2011

Abstract

A means of conducting continuous payload exchanges between the Earth and Moon would allow materials to be transported between them on a regular basis and could be used to supply vital resources to a permanent lunar colony. In addition to this, it could provide a means of returning materials, extracted from the mineral rich lunar surface, back to Earth. The use of symmetrically laden motorised momentum exchange tethers would allow these transfers to be conducted free of any conventional propulsion, purely by the exchange of momentum between the payloads, and without the subsequent loss of orbital altitude experienced by asymmetrical tether configurations. Although this is an exciting prospect it is not without its challenges, for example, if the Moon orbited a spherical Earth adhering to Kepler's laws, the transport of materials would be conducted with clockwork precision and the colonisation of the Moon would already have taken place. However, Kepler's laws are idealised to the two body motion of perfectly spherical bodies and are applicable only in the most simplified of circumstances. The Moon's motion is in reality complex and the establishment of such a system is made even more so by the oblateness effects of a non-spherical Earth acting on the tether system in Earth orbit. Adding to this complexity is the less significant but noticeable effect of the Moon's oblateness acting on a tether in lunar orbit. Other challenges include the design of a device to capture the payloads at the tether's tips at orbital velocity in addition to effecting their release at the correct instant; and the tether system's reaction to mechanical shocks which are a real possibility if velocity mismatches between the tether tips and payloads are significant. Restricting the scope of this investigation, the aim of the following is: to determine whether such a system can be realistically established when taking into account the complex nature of the Moon and resulting opportunities for payload exchanges; to establish the logistical design of the system required to conduct these regular two-way exchanges; to determine suitable config-

urations of the Earth and Moon orbiting tethers for conducting these exchanges when planetary oblateness effects are taken into account in addition to the complex motion of the Moon about Earth; to configure the trajectory design of the payloads between these tethers such that the logistical requirements are satisfied; and finally to investigate an anomaly observed whilst conducting simulations of the motion of a symmetrically laden tether in orbit about Earth which relates to the theory behind the concept of gravity gradient stabilisation.

Contents

Bibliography 227

List of Tables

List of Figures

Nomenclature

A	Tether cross sectional area
a	Semi-major axis
a_{EM}	Semi-major axis of EMMET's orbit
a_h	Semi-major axis of payload's hyperbola about the Moon
$\vec{a}_{l-eq}$	Equatorial acceleration vector of EMMET's lower tip
$\vec{a}_{Lp}$	Lunavator central facility's perifocal acceleration vector
$\vec{a}_{Lpu}$	Lunavator upper tip's perifocal acceleration vector
$\vec{a}_{Lsu}$	Lunavator upper tip's selenocentric frame acceleration vector
$\vec{a}_{Lu}$	Lunavator upper tip's body frame acceleration vector
a_{min}	Minimum payload semi-major axis for lunar transfer
a_o	Magnitude of acceleration vector acting on EMMET's central facility
$a_{payload}$	Payload semi-major axis upon release from upper tip
$Apoapse$	Point of orbit furthest from the central body
$Apogee$	Point of orbit furthest from Earth
$Apolune$	Point of orbit furthest from the Moon
$a(s)$	Magnitude of acceleration acting at point s along sub-span

$\vec{a}_{u-eq}$	Equatorial acceleration vector of EMMET's upper tip
$\vec{a}_{u-per}$	Perifocal acceleration vector of EMMET's upper tip
c_1	Transfer time harmonic between EMMET's orbital period and trans-luna flight time
c_2	Transfer time harmonic between EMMET's orbital period and trans-Earth flight time
d_w	Delay harmonic between Lunavator's orbital period and wait time
e	EMMET central facility's magnitude of eccentricity
E	Eccentric anomaly
E_{EM}	Specific energy of EMMET's orbit
e_f	Magnitude of eccentricity of final orbit
e_h	Magnitude of eccentricity of the payload's hyperbola
e_i	Magnitude of eccentricity of initial orbit
E_l	Lower payload's energy upon release
E_{min}	Minimum payload energy for lunar transfer
$EMMET$	Earth orbiting MMET
E_u	Upper payload's energy upon release
$\vec{F}_g$	Force of gravity vector
G	Universal gravitation constant
H	Hyperbolic anomaly

h	EMMET central facility's magnitude of specific angular momentum
h_f	Magnitude of angular momentum in final orbit
h_i	Magnitude of angular momentum in initial orbit
h_z	Magnitude of the specific angular momentum vector projected along the equatorial z-axis
I	3x3 identity matrix
i	Orbital inclination
$\vec{i}_{AN}$	Unit vector directed towards Lunavator's selenocentric ascending node
i_c	Critical inclination of 63.4°
i_h	Inclination of payload's hyperbola about the Moon
$\vec{i}_L$	Unit vector from Moon to point on LSI
$\vec{i}_s$	Unit vector directed along tether sub-span
$\vec{i}_W$	Direction of satellite's angular momentum vector relative to equatorial frame
J_2	Earth's second zonal harmonic
J_{2m}	Moon's second zonal harmonic
KE	System kinetic energy
$KE_{specific}$	Specific kinetic energy of MMET
L	EMMET sub-span's length
L_L	Lunavator tether sub-span length

LSI	Lunar Sphere of Influence
$Lunavator$	Moon orbiting MMET
m	Orbital harmonic between EMMET and Moon orbital periods
M_E	Mass of Earth
M_e	Mean anomaly
M_M	Moon's mass
$MMET$	Motorised Momentum Exchange Tether
m_p	Payload mass
m_T	Tether sub-span mass
$\vec{N}$	Orbit's node line vector
n	Orbital harmonic between Lunavator and EMMET orbital periods
p	EMMET central facility's orbital parameter
$Perigee$	Point of orbit closest to Earth
$Periapse$	Point of orbit closest to the central body
$Perilune$	Point of orbit closest to the Moon
p_L	Orbital parameter of Lunavator central facility's orbit
p_r	Rotational harmonic between EMMET and sub-spans periods
q	Generalised coordinate

$\dot{q}$	System generalised velocity
q_r	Rotational harmonic between Lunavator and sub-spans periods
r_a	Payload's distance from Earth at LSI arrival
$\vec{r}_{ap}$	Payload's perifocal position vector at LSI arrival relative to Earth
R_{cf}	Central facility position vector for Lagrangian formulation
$\vec{R}_{cg}$	System's centre of gravity position vector
$\vec{R}_{cp}$	System's centre of energy position vector
r_d	Payload's distance from Earth at LSI departure
$\vec{r}_{dp}$	Payload's perifocal position vector at LSI departure relative to Earth
R_E	Radius of Earth
$\vec{r}_{eq}$	Position vector in Earth's equatorial frame
$\vec{r}_f$	Position vector in final orbit
R_G	Perifocal to equatorial transformation matrix
$\dot{R}_G$	First derivative with respect to time of perifocal to equatorial transformation matrix
$\ddot{R}_G$	Second derivative with respect to time of perifocal to equatorial transformation matrix
$\vec{r}_i$	Position vector in initial orbit

R_K — Rotation matrix about equatorial frame pole

R_{K_m} — Rotation matrix about selenocentric frame pole

$\vec{r}_L$ — Position vector of LSI contact point

r_L — Lunavator central facility's perilune radius

r_L — Payload distance from Moon at LSI contact

r_{L-a} — Payload's distance from Moon at LSI arrival

r_{L-d} — Payload's distance from Moon at LSI departure

R_{lower} — Lower tip vector for Lagrangian formulation

$\vec{r}_{Lp}$ — Lunavator central facility's perifocal position vector

$\vec{r}_{Lpu}$ — Lunavator upper tip's perifocal position vector

$\vec{r}_{Lsu}$ — Lunavator upper tip's selenocentric frame position vector

$\vec{r}_{Lu}$ — Lunavator upper tip's body frame position vector

R_{LV} — Lunavator's perifocal to selenocentric frame transformation matrix

$\dot{R}_{LV}$ — First derivative with respect to time of Lunavator's perifocal to selenocentric frame transformation matrix

$\ddot{R}_{LV}$ — Second derivative with respect to time of Lunavator's perifocal to selenocentric frame transformation matrix

R_M — Moon's radius

r_m — Lunavator minimum lower tip distance

$\vec{r}_{moon}$	Position of Moon in Earth's equatorial frame
$\vec{r}_o$	Origin of body frame coinciding with EMMET's central facility
r_o	EMMET central facility's distance from Earth
$\vec{r}_{o-eq}$	Position vector of central facility in equatorial frame
$\vec{r}_{per}$	Position vector in satellite's perifocal frame
$\vec{r}_{perifocal}$	Position of Moon in perifocal frame of its orbit
$r_{perigee}$	EMMET perigee radius
$\vec{r}_{perilune}$	Perilune position vector
$r_{perilune}$	Perilune distance
$\vec{r}_{ps}$	Payload's perilune position relative to selenocentric frame
R_S	Payload's perifocal to selenocentric transformation matrix
R_{sp}	Selenocentric to perifocal transformation matrix
$\vec{r}_u$	Body frame position vector of EMMET's upper tip
$\vec{r}_{u-eq}$	Equatorial position vector of EMMET's upper tip
$\vec{r}_{u-per}$	Perifocal position vector of EMMET's upper tip
R_{upper}	Upper tip position vector for Lagrangian formulation
R_W	Body frame to perifocal frame transformation matrix
$\dot{R}_W$	First derivative with respect to time of body to perifocal frame transformation matrix

$\ddot{R}_W$	Second derivative with respect to time of body to perifocal frame transformation matrix
R_{W_L}	Lunavator's body to perifocal frame transformation matrix
$\dot{R}_{W_L}$	First derivative with respect to time of the Lunavator's body to perifocal frame transformation matrix
$\ddot{R}_{W_L}$	Second derivative with respect to time of the Lunavator's body to perifocal frame transformation matrix
R_{W_m}	Rotation matrix between Lunavator's initial and final argument's of perilune
$R(\Delta i)$	Rotation matrix for change in inclination between Lunavator's initial and final orbits
s	Arbitrary length along tether sub-span
S	3x3 skew symmetric matrix of unit vector directed along rotation axis
S_{an}	Skew symmetric matrix for Lunavator's angle of ascending node adjustment
S_{ap}	Skew symmetric matrix of Lunavator's perifocal pole relative to selenocentric frame
SF	Factor of safety
S_i	Skew symmetric matrix for unit vector directed towards Lunavator's selenocentric ascending node
T	Orbital period

T_{EM}	Orbital period of EMMET's orbit
T_{EM-LV}	Transfer time between EMMET and Lunavator upper tips
T_{EM-ROT}	Rotational period of EMMET's sub-spans
$\vec{T}_L$	Tension vector acting at connection point due to tether sub-span mass
$\vec{T}_l$	Tension vector acting at connection point due to payload mass
$\vec{T}_{l-p}$	Tension vector acting on lower payload
T_{LV}	Orbital period of Lunavator's orbit
T_{LV-EM}	Transfer time between Lunavator and EMMET upper tips
T_{LV-ROT}	Rotational period of Lunavator's sub-spans
T_{moon}	Orbital period of the Moon about Earth
$\vec{T}_{net}$	Vector of net tension acting on payload and tether sub-span
$T_{net-lower}$	Magnitude of net tension acting at lower connection point
$T_{net-upper}$	Vector of net tension acting on upper tether connection point
t_p	Time since perigee
$t_{perilune}$	Time to perilune from LSI entry

$\vec{T}_U$	Vector of tension acting along upper tether sub-span
$\vec{T}_u$	Tension acting on central facility due to payload mass
$\vec{T}_{u-p}$	Vector of tension acting on upper payload
$\vec{T}_{u-s}$	Tension acting on upper tether sub-span element at distance s
T_w	Wait time at Lunavator between capture and launch operations
U	System potential energy
$\vec{v}_{EQ}$	Velocity vector in Earth's equatorial frame
$\vec{v}_f$	Velocity vector in final orbit
$\vec{v}_i$	Velocity vector in initial orbit
v_l	Magnitude of lower payload's velocity upon release
v_L	Lunavator central facility's perilune speed
$\vec{v}_{Lp}$	Lunavator central facility's perifocal velocity vector
$\vec{v}_{Lu}$	Lunavator upper tip's body frame velocity vector
$\vec{v}_{Lpu}$	Lunavator upper tip's perifocal velocity vector
$\vec{v}_{Lsu}$	Lunavator upper tip's selenocentric frame velocity vector
$\vec{v}_{moon}$	Velocity of Moon in Earth's equatorial frame
$\vec{v}_{mpa}$	Perifocal velocity of the Moon at LSI entry
$\vec{v}_{mpd}$	Perifocal velocity of the Moon at LSI exit

$\vec{v}_O$	Velocity vector of perifocal frame origin
$\vec{v}_{PER}$	Velocity vector in satellite's perifocal frame
$\vec{v}_{perilune}$	Payload's velocity vector at perilune
$v_{perilune}$	Perilune speed
$\vec{v}_{ps}$	Payload's perilune velocity relative to selenocentric frame
v_u	Magnitude of upper payload's velocity upon release
$\vec{v}_{u-per}$	Perifocal velocity vector of EMMET's upper tip
x_i	x-axis coordinate of initial orbit
x_f	x-axis coordinate of final orbit
y_i	y-axis coordinate of initial orbit
y_f	y-axis coordinate of final orbit
α	Angle between the Earth-Moon line and the point on the boundary of the LSI
δ_a	LSI arrival latitude
δ_d	LSI departure latitude
ΔE_l	Change in lower payload's energy upon release
ΔE_u	Change in upper payload's energy upon release
δ_L	LSI contact latitude
δm	Infinitesimal mass element
δs	Infinitesimal length element

Δt_l	Payload perigee to LSI entry flight time
Δt_r	LSI exit to payload perigee flight time
$\Delta \vec{v}$	Change in velocity
$\Delta \vec{v}_{entry}$	Change in payload's velocity vector at LSI entry
$\Delta \vec{v}_{exit}$	Change in payload's velocity vector at LSI exit
$\Delta \vec{v}_{LV-AN}$	Velocity change required for Lunavator's angle of ascending node adjustment
$\Delta \vec{v}_{LV-AP}$	Velocity change required for Lunavator's argument of perilune adjustment
$\Delta \vec{v}_{LV-i}$	Velocity change required to adjust Lunavator's inclination
$\Delta \vec{v}_{perigee-l}$	Change in payload's velocity vector at EMMET launch
$\Delta \vec{v}_{perigee-r}$	Change in payload's velocity vector for capture at EMMET's upper tip
$\Delta \vec{v}_{ps}$	Change in payload's velocity vector at Lunavator's upper tip
$\Delta \theta$	Change in true anomaly of Lambert's transfer
$\Delta \omega$	Change in argument of perigee/perilune
$\Delta \Omega_f$	Change in angle of ascending node
η_L	Payload arrival time at LSI after system input time
θ	True anomaly of point in orbit
$\dot{\theta}$	EMMET central facility's orbital angular velocity

θ_a	True anomaly of Moon at payload arrival
θ_{AN}	True anomaly at Lunavator's ascending node
θ_d	True anomaly of Moon at payload departure
θ_f	True anomaly in final orbit
θ_i	True anomaly in initial orbit
θ_{in}	True anomaly of payload's hyperbolic orbit at LSI entry
θ_L	Lunavator's true anomaly
ΘT_{LV}	Time between payload entry and exit from the LSI
μ	Earth's gravitational parameter
μ_m	Moon's gravitational parameter
σ	Tether sub-span material's tensile strength
σ_{max}	Tether sub-span material's maximum tensile strength
ϕ_a	LSI arrival longitude
ϕ_d	LSI departure longitude
ϕ_L	LSI contact longitude
ψ	EMMET sub-span's rotation angle
$\dot{\psi}$	Angular velocity of tether sub-span's rotation
$\ddot{\psi}$	Angular acceleration of tether sub-span's rotation
$\dot{\psi}_L$	Maximum rotational velocity of Lunavator's sub-spans
$\dot{\psi}_{max}$	Maximum tether rotation rate

Ω Angle of ascending node

$\dot{\Omega}$ Precession rate of the orbit's angle of ascending node

$\ddot{\Omega}$ Change in precession rate of the orbit's angle of ascending node

Ω_{EM} Angle of ascending node of the EMMET's orbit

Ω_f Final angle of ascending node

Ω_h Angle of ascending node of payload's hyperbola about the Moon

$\dot{\Omega}_h$ Rate of precession of Lunavator's ascending node

Ω_i Initial angle of ascending node

Ω_m Angle of ascending node of the Moon's orbit

$\vec{\Omega}_{PER}$ Angular velocity vector of satellite's perifocal frame

ω Argument of perigee when referenced to Earth, argument of perilune when referenced to the Moon

$\dot{\omega}$ Precession rate of argument of perigee/perilune

$\ddot{\omega}$ Change in precession rate of argument of perigee/perilune

ω_f Argument of perigee/perilune of final orbit

ω_h Argument of perilune of payload's hyperbola about the Moon

$\dot{\omega}_h$ Rate of precession of Lunavator's argument of perilune

ω_i Argument of perigee/perilune of initial orbit

1. Introduction

The concept of tethering satellites together in space using long wires with the aim of utilising the exchange of momentum between one satellite or another or to take advantage of a planet's magnetic field for power generation or thrust has been around for a considerable amount of time, innumerable practical applications for these systems have been proposed in addition to alternative proposals for their use too extensive to list. The application which is the main focus of this thesis is the use of symmetrically laden motorised momentum exchange tethers to conduct continuous payload exchanges between the Earth and Moon for each rotation of the Moon about Earth.

The concept of momentum exchange utilises the propensity of two bodies to orbit a planet at the distance and angular velocity of their common centre of mass, naturally aligned along the local gravity gradient. This results in the satellite at the tether end furthest from Earth having a greater linear velocity and subsequently linear momentum than the satellite at the tether body closest to Earth with the lower satellite having effectively transferred part of its momentum to the upper satellite. If the two satellites are disconnected from the tether, the upper satellite has a velocity too large to stay on its current orbit and it traverses a trajectory to a distance further from Earth; the lower satellite has too little velocity to stay on its current orbit and traverses a trajectory closer to Earth. The upper satellite's orbit has been effectively raised and the lower satellite has in fact been de-orbited.

To enhance this raising and lowering of the satellites, librating and spinning tether configurations have been conceived and with a motor driven torque applied to spinning tether systems; analysis has shown that the gain in upper satellite's distance renders it capable of reaching the Moon or leaving Earth orbit altogether. Many concepts use an asymmetrical tether system consisting of a satellite tethered to a large central motor driven hub, for example Puig-Suari *et al* [1] and Cartmell

and Zeigler [2], with the aim of raising the orbit of these satellites but it was found that the de-orbit experienced, even if the hub's mass was considerably larger than that of the satellite, was still of an unacceptable magnitude. The solution to this, in terms of a re-usable system which maintained its orbital altitude after payload release, was found by Cartmell and Zeigler [2] to be a symmetrically laden motorised momentum exchange tether. By simultaneously releasing the upper and lower satellites, or alternatively payloads, from the free ends of tethers attached symmetrically to a centrally located motorised hub; any gain in momentum by the upper payload was offset by the loss of momentum by the lower payload. Furthermore, it was found that this motorised system could impart sufficient velocity for payload transfers to the Moon and in conjunction with it retaining its orbital altitude throughout; a system for continuous transportation to the Moon was conceived [2].

It was proposed that a continuous Earth-Moon payload exchange method could be established by utilising two of these symmetrically laden momentum exchange tethers, one orbiting Earth and the other the Moon, by passing payloads between one another at opportune moments in the Moon's motion about Earth. The great advantage of this would be that once the system was established, the exchange of payloads would become effectively free with no or very little chemical propulsion required and conducted simply through the exchange of momentum between the payloads. There are a great many reasons why such a system would be advantageous: the Moon has a wealth of untapped mineral resources which could be mined and transported back to Earth using this system but this would require that people actually resided on the Moon to conduct these activities however, all necessary food; water and oxygen (initially); shelter; and fuel could all be transported to the Moon on a regular basis using this system. In addition to this, the idea of setting up an interplanetary launch facility in orbit about the Moon is becoming an ever more popular and this would be aided by the establishment of such a system.

The engineering challenges associated with establishing this system are numerous, firstly the Moon's motion about Earth is extremely com-

plex and a system that exchanges these payloads must account for variations in the Moon's orbit which are a direct result of the perturbing accelerations of the Sun and other planets within the Solar System. This results in the required system having a flexible logistical design in addition to the trajectories between the Earth and Moon tether systems also being flexible enough to accommodate these variations. Secondly, the capture of payloads is conducted at extremely high velocities and a reliable system must be established which can achieve this and in the event of any failed captures a payload recovery procedure must be in place. Thirdly, however well the transfer trajectories have been designed the possibility of mechanical shock occurring as a result of velocity mismatches between the payload being captured and the tether tip are a very real possibility and the tether system must be designed robustly enough to handle this. Finally, the tether systems themselves will be subjected to perturbing accelerations mostly as a result of the oblateness effects of their respective central bodies therefore, a method to account for variations in the tether orbits must also be established. The following does not attempt to solve all of these issues but focuses on the logistical and trajectory designs necessary to account for the complex motion of the Moon in addition to the motion of the tether systems as a result of Earth's oblateness.

1.1   Space Tethers Concept

In 1895 Tsiolkovskii [3], conceived the first ever tethered space system with his concept of creating artificial gravity on a spacecraft attached to a counterweight using a 0.5 km chain and rotating about the centre of mass of the system. According to Beletsky and Levin [4], F.Tsander conceived a tapered tether extending from the surface of the Moon to the near vicinity of Earth in 1910 but the concept was subsequently overlooked in his ciphered diaries until it was deciphered and published in 1978. In the mean time, Tsander's concept was re-invented by Artsutanov in 1960; Isaaks *et al* in 1966; and Pearson in 1979. Modern day tethers consist of high strength wires or cables connecting satellites in orbit and fall

into two major categories; momentum exchange tethers which utilise the orbital dynamics of the common centre of mass of the tether system to impart or detract energy and altitude from the satellites; and electrodynamic tethers which utilise the Lorentz Force induced by a high velocity conductive tether moving through Earth's magnetic field in low Earth orbit to produce a thrust on the system or to generate electrical power. A large amount of activity has occurred in tether research in the last 40 years and new concepts and applications are continually being conceived.

1.1.1 Gravity Gradient Stabilisation

The concept of pseudo-gravity arising between tethered spacecraft was first investigated by Chobotov in 1963 [5] and consisted of rotating two tethered satellites about the centre of mass of the system at a rate greater than orbital velocity, this effect was practically demonstrated by tethering the GEMINI-11 spacecraft to the AGENA rocket stage in 1966 [6] with a tether rotation rate 13.5 times greater than orbital velocity. Gravity gradient stabilisation is one of the most fundamental applications of tether systems in orbit and allows two tethered satellites aligned along the local gravity gradient, with a rotational rate about the systems centre of mass equal to the orbital rate, to remain in this vertical position for extended time periods. The concept of gravity gradient stabilisation utilises the increments in gravitational and centrifugal forces arising due to the proximity of the tether system to Earth in addition to the rotational velocity and physical extension of the body. For two masses attached at either end of a vertically aligned tether, the gravitational force at the mass closest to Earth is greater than the centrifugal force arising due to its separation from the systems centre of mass, furthermore, the centrifugal force at the tip furthest from Earth is greater than the gravitational force acting on the system. The result of these net forces acting at either tip is a stable vertical configuration for the system with a restoring force arising when any displacement from this vertical position occurs. According to Cosmo and Lorenzini [7], these gravitational and centrifugal forces are balanced only at a single location corresponding to the centre of mass of the tethered system and this constrains the system to orbit

Earth at the same angular velocity as the centre of mass. Furthermore, the resulting forces acting as a result of these increments in gravitational and centrifugal forces result in the tension along the tether and the artificial gravity force being equal to the gravity gradient force along the tether. This gravity gradient stabilisation was practically demonstrated in 1966 when the GEMINI-12 spacecraft was tethered to the AGENA rocket stage [6].

There are many applications for artificial gravity in orbit such as creating more natural conditions for humans in space and biological processes in orbit in addition to facilitating refueling between orbiting spacecraft as there are technical problems associated with performing this in zero gravity conditions [8]. The tether lengths required to provide sufficient micro-gravity conditions to overcome the surface tension of varying fuel types was investigated by Kroll [9] and found to vary between 30 and 1200 m depending upon the fuel used. In addition to this, concepts such as an interferometer in orbit [10], consisting of two receivers separated by a 5 km tether, and a solar power station consisting of a gravity gradient stabilised tether bearing solar power collectors have been conceived. Furthermore, gravity gradient forces can be utilised in the stabilisation of tethered constellations which could be used for low gravity of micro-gravity labs [7].

1.1.2 Electrodynamic Tethers

According to Cosmo and Lorenzini [7], an electrodynamic tether is a long conductive wire extended from a spacecraft which utilises the magnetic field of Earth to induce an electromotive force along the wire's length. As a result of this, a difference in electric potential occurs along the wire with the upper end becoming positive relative to the lower end. By utilising the highly ionised particles, or plasma, resulting from motion within Earth's ionosphere, the wire becomes part of a current loop which incorporates the wire and the ionosphere itself. Plasma contactors are attached to each end to allow the collection of electrons at the positively charged upper tip and the emission of electrons at the lower tip which results in regions of net positive and negative charges at the

upper and lower tips, respectively. The current path from the upper tip within the ionosphere is therefore along the magnetic field lines to the lower ionosphere and the migration of electrons between these field lines occurs when the free charges collide with neutral particles in the lower ionosphere allowing the circuit to be completed. In addition to this, the tether current density at each tip should not exceed the external ionospheric current density and the plasma contactors are used to spread the tether current over large areas to reduce the current densities. Three configurations using different types of plasma contactor have been suggested (1) a passive large area conductor at each end of the tether (2) a passive large area conductor at one end and an electron gun at the other (3) a plasma generating hollow cathode at both ends. The first configuration utilises the upper conductor to collect electrons whilst the lower collector is utilised to collect ions; the second configuration achieves higher currents by ejecting the electrons at high energy using an electron gun at the lower end however, the electron gun requires a power supply; the third configuration is, according to Cosmo and Lorenzini [7], the most promising configuration as the system does not rely on passive means and utilises the hollow cathodes to generate clouds of highly conductive plasma. The hollow cathodes also require power supplies in addition to a gas supply to operate but require less power than electron guns with the gas supply not adding significant weight to the system. However, Beletsky and Levin [4] advise against relying upon current optimistic estimates when considering the use of hollow cathode contactors.

There are many applications of electrodynamic tethers and according to Bekey [11], by configuring a vertically aligned gravity gradient stabilised insulated conductive tether with a passive collector at the upper tip and an electron gun at the lower tip orbiting at a low inclination about Earth, the tether can be utilised as an electric generator as a result of the Lorentz force converting kinetic energy to electrical energy. The tether will generate 200 V/km with estimates that 10-100 kW of power could easily be produced with a tether length between 20-100 km and an energy conversion efficiency between kinetic and electrical energy of around 70%: as this electrical energy is being gained at the expense

of the system's kinetic energy it corresponds to a loss in altitude which can only be rectified by means of corrective maneouvres. However, in the event that some altitude loss could be tolerated it could function as an emergency power supply for a space station. This particular application is the focus of research by the US company *Tethers Unlimited Inc*™, they aim to use their *Terminator Tether*™ which utilises passive electrodynamic tether drag, arising in conjunction with the generation of electric power, to rapidly de-orbit spacecraft from low Earth orbit [12]. Numerical analysis of this system suggests that a 5-10km long tether weighing 2-3% of the satellite's mass can de-orbit a satellite within months, and a further system has been developed called *Terminator Tape*™ specially aimed at microsatellite systems weighing less than 500kg.

According to Drell, Foley and Rudderman [13], under the circumstances that a tether could drive a solar array generated current along the wire in conjunction with reversing the passive collector/electron gun configuration; this operation could be reversed and the Lorentz force acting on the tether would produce orbit altitude gain without the use of propellants. Furthermore, a study conducted by Vas *et al* [14] on the possibility of re-boosting the decaying orbit of the international space station estimated savings of over \$1 billion as a direct result of the reduction in flights to deliver fuel and there were also suggestions that the tether would improve the micro-gravity environment of the station.

Another application of electrodynamic tethers are as high powered ultra/extremely/very low frequency (ULF/ELF/VLF) antennas, according to Grossi [15], and utilise a side effect of the induced current along the tether; that as the electrons are emitted from the contactor into the plasma, electromagnetic waves are produced in the ionosphere. The current flow generating the waves can be provided by a transmitter such that the tether becomes part of the antenna and these waves are modulated by turning the electron gun or hollow cathode on or off at the desired frequency. It is believed that the ionosphere acts as a wave guide extending the area for effective signal reception and may allow instant worldwide communication. There are many other applications of electrodynamic tethers but as these are not the focus of this thesis our attention will

move away from them.

1.1.3 Momentum Exchange Tethers

The fundamental concept which led to the research presented in this thesis is the concept of momentum exchange between two tethered bodies in orbit. The concept is as follows; two tethered bodies will orbit a central gravitational force at their common centre of mass at the angular velocity of this centre of mass and due to gravity gradient stabilisation forces the bodies will align themselves along the local vertical with the payload at the upper end of the tether having the same angular velocity as the centre of mass but a greater linear velocity and the lower body also having the same angular velocity but a lower linear velocity. As a result of the non-uniform gravitational field, the velocity along the tangent to the orbit required for the lower payload to remain on the same orbit if released at this point is greater than the current linear velocity furthermore, the velocity along the tangent velocity required for the upper payload to remain on the same orbit after release is smaller than its current velocity. The upper body has gained linear momentum, mv, as a result of it having the same angular velocity as the centre of mass and it being a greater distance from Earth, meanwhile the lower body has lost a corresponding amount of linear momentum as a result of this angular velocity and closer proximity to Earth; the lower body has effectively transferred part of its momentum to the upper body. If both payloads were released at this point, the upper payload would have sufficient velocity to traverse an elliptic path from its point of release at the perigee of its acquired orbit to a point further from Earth at the apogee of this orbit. The upper payload has effectively used the momentum gained from the lower payload to raise the altitude of its orbit relative to Earth. At the same instant, the lower payload also traverses an elliptical path but in this case the loss of momentum results in the point of release occurring at the apogee of the payload's acquired orbit and this results in the payload traveling to the perigee of its orbit closer to Earth, so the lower payload has been effectively de-orbited due to this momentum exchange. The addition of a spin or swing in the direction of orbital motion will increase

the velocity of the upper payload and decrease the velocity of the lower payload and result in a greater exchange in momentum with the result that the upper payload's apogee distance will be even greater after release in addition to the lower payload's perigee being diminished even further. A spin or swing in the direction opposite to the direction of orbital motion will result in a less efficient exchange of momentum between the upper and lower payloads.

Bekey and Penzo [16] considered payload release from a hanging tether in a circular orbit about Earth and found that the apogee distance of the payload released from the upper tether position was greater than its perigee position by approximately 7 times the tether length. They considered utilising this method for raising a large observatory from low Earth orbit to geostationary Earth orbit using a shuttle in an elliptical orbit but practical problems such as the unacceptable altitude loss of the shuttle at the lower tip upon release and the required tether length of 5000km being unable to support its own mass without even considering the mass of the observatory rendered this particular practical application obsolete, however the idea remained with a reusable spinning two stage tether system being considered for transferring masses up to 4000 kg from low Earth orbit to geostationary Earth orbit by Lorenzini *et al* [17] with results that indicated that the system was lighter than a single stage tether system and more competitive on a mass basis than a chemical upper stage after two transfers. It was estimated by Bekey and Penzo [16] and additionally Carrol [18] that a payload released from a swinging tether could have an apogee distance 14 times the tether length greater than the perigee distance and according to Cosmo and Lorenzini [7] a spinning tether will provide a gain even greater than 14 times the tether sub-span length. The velocity gain that a spinning momentum exchange tether could impart when the system's centre of mass was in an elliptical orbit about Earth was investigated by Crellin and Janssens [19] in 1996 and they found a maximum change in velocity of 102.8 m/s for a 100 km tether which highlighted the need for a torque driven tether system if significant changes in orbital parameters were to be achieved.

The rotovator concept was conceived by Artsutanov in 1967 and rein-

vented by Moravec [20] in 1977 and is a method of obtaining low tether tip velocities as a result of a rapidly spinning tether. By arranging this system in orbit about a planet with little or no atmosphere, to negate drag effects, such that it touches the surface at the periapse of its orbit with zero relative velocity; payloads can be easily picked up or placed onto the surface without loss of momentum. A prime example for its application would be about Earth's Moon and in this instance the system is termed a Lunavator.

The concept of the addition of a torque to spin the tether was first published by Puig-Suari *et al* [1] in 1995 when it was suggested that orbital velocity for interplanetary exploration could be achieved by the continuous application of a solar power generated continuous torque to a tether sling and cites the lack of propulsive manoeuvre and virtually inexhaustible capacity as advantageous in the launch of deep space probes. To ensure that the tether is capable of supporting its own mass and that of the probes, a tapered tether configuration was endorsed. In this case however, chemical propulsion was found to provide a better mass ratio for high energy transfers. Two further issues arose concerning this configuration, the connection between the hub and tether is not located at the centre of mass resulting in a precession of the spin axis and additionally extremely high spin rates for the hub resulting from the torque required to spin up the tether would become unacceptably large. To rectify the precession of the hub, it was suggested that a second identical tether was attached symmetrically to the hub and furthermore, to reduce the spin rate a massive hub could be employed. Independently of this, Cartmell and Zeigler [2] proposed a symmetrically laden motorised momentum exchange tether for application to an interplanetary two-way exchange concept. This system consisted of a hub (or central facility) containing the motor and power supply, two symmetrically configured propulsion tethers with the payloads at their free ends and two outrigger tethers with masses at their free ends to provide the reaction force for the motor torque. By using a motor to drive the tether in conjunction with employing a staged tether system, as conceived by Hoyt and Forward [21] in 1997, for payload transport from sub-Earth orbit to the point of

orbital injection, the velocity for injection into interplanetary trajectories could be achieved at the upper tip and in addition to this, by ensuring that the upper and lower payloads were released simultaneously the orbital altitude of the hub could be retained. Attention focused on the Earth-Moon two-way exchange and it was proposed that a modified Lunavator tether would capture the payload from Earth and simultaneously pick up a payload from the Moon's surface to preserve the mass balance across the system. At a later time the Lunavator would send the payload from the Moon back to Earth whilst simultaneously placing the payload, previously from Earth, on to the Moon's surface.

The performance and efficiency of this symmetrically laden motorised momentum exchange tether was explored in 1998 and publsihed by Zeigler and Cartmell [22] in 2001 and was found to improve on the performance and efficiency of a librating tether by two orders of magnitude, which itself improved on the hanging tether by a factor of two. A series of terrestrial scale model tests of the motorised momentum exchange propulsion tether was conducted by Cartmell and Zeigler [23] in 2001 with the aims of investigating: the start up of the system and impulses along the tethers due to payload release; the use of outrigger tethers to limit the reaction motions of the drive motor stator; the potential for interference between the drive and outrigger tethers; the de-spin of the motor and payloads; and payload release in double ended systems. Some important observations and conclusions drawn from this were: that a small impulse was experienced by the tethers at the instant of payload release but they quickly returned to their required configuration; and payload release asymmetry was extremely significant and induced large overall system displacements. The development of this concept has continued with the work of McKenzie and Cartmell [24] in 2004 with *Performance of a Motorised Tether using a Ballistic Launch Method* which gives an example of a mission designed to transfer a payload from low Earth orbit to capture at the Moon; the work of Chen and Cartmell [25] in 2007 with *Multi-Objective Optimisation on Motorised Momentum Exchange Tether for Payload Orbital Transfer* which focuses on the multi-objective optimisation methods of genetic algorithms to improve tether performance;

and finally, the work of Murray and Cartmell [26] in 2008 with *A Continuous Earth-Moon Payload Exchange Using Symmetrically Laden Motorised Momentum Exchange Tethers* which focused on the logistical and trajectory designs required for a continuous two-way exchange between the Earth and Moon.

1.1.4 Interplanetary Tether Transfer

A Cislunar Tether Transport System consisting of a 89km long rotating momentum exchange tether in an elliptical, equatorial orbit about Earth exchanging payloads with a second 200km long momentum exchange tether in a low lunar orbit was shown to be theoretically possible by Forward [27] using little or no propellant. However, this used many simplifying assumptions and this system was re-investigated in 1999 by Hoyt and Uphoff [28], removing these assumptions and developing an architecture for the system. The basic operational procedure for this is as follows: the tether at Earth captures a payload from low Earth orbit (LEO), imparts its momentum and releases the payload on a trajectory to the Moon. At arrival at the Moon, the payload is captured by the Lunavator [20] which detracts energy from the payload and places it onto the Moon's surface with zero relative velocity. Furthermore, by also picking up payloads from the Moon's surface the Lunavator can return payloads back to Earth, by imparting some of its momentum, where they will be captured by the tether at Earth and released down into LEO. The orbital configuration used was a combination of a tether in an elliptical, equatorial Earth orbit and the Lunavator in a circular polar Lunar orbit with payloads transferred when the Moon crosses its ascending node. Several tether boost configurations were considered for raising the payload at Earth from LEO in order to make the orbital dynamics as manageable as possible. The most effective configuration to impart the desired velocity to the payload occurs when capture and launch operations are conducted by the tether at the perigee of an elliptical orbit about Earth however, as a result of the Earth tether's equatorial inclination, there is a precession of the line of apsides of this orbit due to Earth's oblateness which it is suggested can be overcome by arranging its orbital param-

eters such that its precessional period is in resonance with the Moon's orbit, alternatively, tether reeling manoeuvres are suggested to exchange momentum between the orbit and rotation of the system. It was found that upon capture at the Moon that to place a payload on to the surface with zero relative velocity that the tip would need a velocity relative to the tether's centre of mass equal to the orbital velocity of this centre of mass relative to the Moon. To achieve this an extremely high energy hyperbolic trajectory for the payload would be required which would add additional requirements and strains to the tether at Earth. This however could be remedied by configuring the Lunavator such that its central facility could alter its position relative to the payload and a counter mass at the other end to increase the angular rate of the system without modifying its momentum. Using this system the velocity changes required were estimated at 25m/s for small corrections with electrodynamic reboost of the tether systems envisaged to account for altitude drops as a result of them imparting momentum to the payloads.

Further work on a continuous Earth-Moon payload exchange concept was undertaken by Cartmell, McInnes and McKenzie [29] in 2004 and proposed a preliminary design architecture for the system. Utilising a staged tether system in orbit, first proposed by Hoyt and Forward [21] in 1997, to impart the payloads with the necessary velocity for lunar transfers; payloads are boosted to sub-Earth orbit (SEO) and captured by the lower tip of a MMET in low-Earth orbit (LEO) which simultaneously receives a payload from the lower tip of a MMET in an extremely elliptical orbit (EEO) to conserve mass balance across the system. This coincides with the release of a payload from the EEO tether's upper tip onto a Moon bound trajectory. Upon arrival at the Moon, the payload is captured by a double ended Moravec Lunavator and placed onto the Moon's surface; at a later time the payload previously picked up from the Moon's surface is released onto a trajectory back to Earth where it will rendezvous with the upper tip of the EEO tether. The staging of the tethers about Earth is of interest and introduces the concept of the two tethers with orbital periods which are harmonic to allow the passage of payloads between them when they arrive at the perigee of their respective

orbits about Earth. The transfer method used between the EEO tether and the Moravec Lunavator was the weak stability boundary transfer which gives a payload just enough energy to pass through the Lagrange point L_1 and enter the Moon's gravitational influence leading to a minimum energy transfer. It was found that the velocity required to perform this minimum energy transfer was 2.5% lower than that theoretically obtainable for this staged configuration. Other concepts for interplanetary exploration or transport included a tether sling as proposed by Puig-Suari *et al* [1] in 1995 in addition to rotating tether configurations similar to those employed for the Cislunar Transport System which were considered by Forward and Nordley [30] in 1999 for transporting payloads to Mars in as little as 90 days.

1.2   Past Tether Missions

It has been almost 45 years since the first tether mission was conducted by NASA during the GEMINI-11 mission of 1966 in which a 30m long tether connected the GEMINI-11 to the AGENA rocket stage which resulted in the first demonstration of artificial gravity occurring as a result of the spacecraft rotation about their common centre of mass [6]. A second experiment was conducted on the GEMINI 12 spacecraft, again tethered to the AGENA rocket stage using a 30m long tether and in this case the first demonstration of gravity gradient stabilisation was made [6].

The OEDIPUS-A mission was launched from a site in Norway in 1989 and was a collaboration between the Canadian National Research Council, NASA, and various other organisations. OEDIPUS is an acronym for Observations of Electric-field Distribution in the Ionospheric Plasma - a Unique Strategy, with the aim of making passive observations of the auroral ionosphere; to measure the response of a large probe in the ionospheric plasma; and to seek new insights into plane- and sheath-wave radio frequency propagation in plasma [7]. The tether system consisted of two spinning payloads with a mass of 84 and 131 kg, each being self-contained experiment and telemetry systems and these were connected by a 958 m long conductive tether. The mission objectives were success-

fully completed however, the payloads experienced rapid and unexpected increase in their coning angle due to the dynamic interaction of the tether with the payloads. OEDIPUS-C was launched in 1995 with similar mission objectives to its predecessor but to a higher altitude with a tether length of 1174m and as a result of this it had a greater range in plasma density and provided a better perspective on plane and sheath waves and their interaction with the plasma [7].

According to Cosmo and Lorenzini [7], the purpose of the Tethered Satellite System (TSS) missions was to demonstrate the capability of deploying a satellite on a long, gravity-gradient stabilised tether from the Space Shuttle where it would provide a research facility for investigations in space physics and plasma-electrodynamics. TSS-1 was launched in July 1992 and deployed a 268 m long tether directly above the Orbiter in low Earth orbit, which provided over 20 hours of stable deployment. This mission was a technology demonstrator for the gravity gradient stabilisation technique allowing the TSS-1R mission to be focused on science objectives. The TSS-1R mission was launched in February 1996 and deployed a conducting tether to a length of 19.7km. According to Cosmo and Lorenzini [7], high voltages were generated across the tether and large currents were extracted from the ionosphere, which, as a result of this, created several plasma phenomena. The deployment of the tether lasted more than five hours and significant results were that currents were observed three times greater than numerical predictions at the time; energetic electrons were detected which possibly resulted from wave-particle interactions; and observations implied that an enhancement in plasma density occurred as a result of ionisation of neutral gases emitted by the satellite thrusters.

The SEDS missions, Small Expendable Deployer Systems, flew as secondary payloads on Delta II launches of GPS satellites, and after the third stage separation the end-mass was deployed from the second stage. SEDS-1 was launched in March 1993 and its objectives were to demonstrate that the SEDS hardware could be used to deploy a payload using a 20km tether, when fully deployed the tether was cut proving that the the system was capable of de-orbiting a 25kg payload and allowing

its re-entry to be studied [7]. SEDS-2 was launched in March 1994 and its objectives were to demonstrate the use of a closed loop control law to deploy a tethered payload along the local vertical, the system was placed in a 350km circular orbit but, according to Cosmo and Lorenzini [7], the tether was allegedly cut by a micro-meteoroid or debris after five days.

The Plasma Motor-Generator(PMG) experiment was launched in 1993 by NASA as a secondary payload on a Delta II rocket and placed into an orbit with a 25.7 ° inclination with the objective of testing the ability of a hollow cathode assembly to make the electrical connection between the spacecraft and the ionosphere. The 500m long tether was deployed using a modified SEDS system used with the aim of demonstrating that such a configuration could function either as a orbit-boosting motor or as a generator converting orbital energy into electricity, according to Cosmo and Lorezini [7]. During the mission the current was shown to be fully reversible allowing operation either as a generator system with electron current flow down the tether or as a motor with electron current driven up the tether.

The Tether Physics and Survivability (TiPS) mission was launched in 1996 as a joint veture between the Naval Center for Space Technology (NCST) and the National Reconnaissance Office (NRO), and the aim of the experiment was to study the long term dynamics and survivability of tethered space systems. It consists of two end bodies connected by a 4 km non-conducting tether [7]. The motion of the end-bodies was observed by a ground based Satellite Laser Ranging (SLR) network and by ground based visual observations and the system survived for 15 months.

The Advanced Tether Experiment (ATEx) was a follow up to the TiPS mission launched on-board the Space Technology Experiment (STEX) spacecraft on October 1998 into a 751km circular orbit. The tether system consisted of upper and lower end bodies attached to a 6.05km tether housed within the STEX spacecraft, and its objectives were to demonstrate tether system stability and end-body attitude determination and control, however no mission objectives were achieved as the system was jettisoned by the STEX spacecraft as a safety precaution due to a deviation in its departure angle.

The Multi-Application Survivable Tether (MAST) experiment was launched into low Earth orbit with the objective of investigating the dynamics of tethered formations of spacecraft and the survivability of tethers in the space environment. The system consisted of three pico-satellites stacked together which were to separate deploying a 1 km tether, however the system failed to deploy [31]

The most recent tether mission was launched in August 2010 by JAXA, the Japanese Space Agency, called the Tether Technologies Rocket Experiment (TREX) which deployed a 300m long electrodynamic tether with the aim of conducting experiments of the interaction of the tether with the ionosphere and to control the attitude of a robot using a tether under the micro-gravity environment during a 10 minute sub-orbital flight of a sounding rocket to its maximum altitude of 300km. The tether was successfully deployed and the high-speed ignition function of the hollow cathode was verified [32].

1.3   Alternative Concepts

The Hypersonic Airplane Space Tether Orbital Launch (HASTOL) concept is an Earth to orbital launch system which consists of a re-usable air breathing sub-sonic to hyper-sonic dual-fuel aeroplane which is used to transport a payload from the ground to a point in the upper atmosphere, at this point a spinning tether system in orbit captures the payload and takes it into orbit. The advantages of this system are that it minimises the use of rockets for injection of payloads into orbit. It is envisaged that a Boeing designed DF-9 hypersonic plane will be utilised which can carry a payload up to 14 tonnes and deliver the payload to an altitude of 100km, and this will be used in conjunction with rotavator tethers composed of presently available fibres and lengths between 400 and 1600km. The system has several issues such as: tether survivability due to collisions with space debris and micrometeorites, overcoming the engineering challenges of operating at hypersonic speeds in the upper atmosphere in addition to safety and reliability issues [33]

The LEO-GTO Tether Boost Facility is a combination of momentum

exchange tether techniques with electrodynamic tether propulsion and its aim is to provide a reusable system to repeatedly boost payloads up to 2500kg from low Earth orbit to geostationary transfer orbit without the use of propellant by imparting a velocity change up to 2.4km/s and is envisaged to be capable of injecting 1000kg payloads into lunar transfer orbits. Electrodynamic propulsion will be used to re-boost the tether system on each occasion after it has imparted part of its momentum in raising the payload's orbit [34]. A follow on to this idea is the MXER Tether Boost Station which has refined the combination of momentum exchange techniques and electrodynamic tethers to raise payloads from LEO-GTO.

A possible future application of electrodynamic tethers is as power generators for future missions to the Jovian system where solar arrays rapidly degraded as a result of high radiation levels and the radioactive thermal generators previously used having safety issues relating to a risk of releasing plutonium into Earth's environment [35]. Preliminary analysis estimates that a 10km tether could generate approximately 1Mw of power and experience over 50N of thrust.

Applications of tethers currently in development include the work of the company *Tethers Unlimited Inc*™ with the *Terminator*™ *Tether* and *Tape*, which was referred to earlier, and utilised for satellite de-orbit applications in addition to a deployable net system *GRASP*™ which can be used to capture space debris [36]. This company is also working on a *Micro-satellite Propellantless Electrodynamic Tether Propulsion System* named μPET™ which used electrodynamic tethers to provide propellantless propulsion for micro-satellites [37]. A further application in development by *Tether's Unlimited Inc*™ for the *HiVOLT*™ system [38] which will use conductive tethers deployed in the Van Allen Belts to scatter the energetic particles causing them to leave the Van Allen Belts. A further research project currently under way is *BETS* which is the Bare Electrodynamic Tethers Project funded by the European Commission FP7 with the aim of developing a de-orbiting system for satellites in LEO using electrodynamic tethers [39].

1.4   Aims and Objectives

The main focus of this thesis is the application of symmetrically laden motorised momentum exchange tethers to a continuous Earth-Moon payload exchange. Solving all of the engineering challenges presented by this system would demand greater time than permissible for this work, therefore the following will focus on:

i. The basic logistical requirements necessary to establish a continuous payload exchange, and the analysis of their application.

ii. Assessment of possible configurations for the Earth tether's orbit suitable for conducting payload exchanges with the Moon whilst taking into account the complexity of the Moon's motion in addition to the oblateness effects acting on the Earth tether's orbit.

iii. The basic kinematic equations for the Earth tether and payloads attached at its tip will be derived with the aim of incorporating the velocity and accelerations resulting from the variation in its orbital elements as a result of Earth's oblateness.

iv. The tension acting along the Earth tether will be derived as a result of the tether's orbital and rotational motion incorporating these oblateness effects with the aim of determining the limitations of the system using current materials.

v. An investigation into the limiting factors for suitable Earth tether configurations in addition to estimates of the performance and efficiency will be obtained by numerical analysis of the system.

vi. Trajectory design for the payload exchange will be undertaken taking into account the logistical requirements outlined previously.

vii. The basic kinematic equations and limitations of the Moon orbiting tether will be undertaken with particular attention being paid to the effects of the Moon's less significant oblateness on its orbit. In addition to this, expressions for the tension acting along the Moon tether will be derived accounting for inertial forces arising from the oblateness effects of the Moon on the tether.

viii. Numerical analysis and simulations of the circumlunar trajectory design which conform to the required logistics will be undertaken.

ix. Alterations to the currently accepted theory of gravity gradient stabilisation as a result of observations of data anomalies of symmetrical tethers in orbit about Earth will be undertaken.

2. Logistical Requirements

To set up a continuous Earth-Moon payload exchange with *motorised momentum exchange tethers* (MMETs) being utilised to impart the velocity impulse required to transfer payloads between Earth and the Moon, the most fundamental criteria that must be satisfied are the logistical requirements of the system which allow the MMET's to perform these exchanges, in addition to the return of the entire system to its original configuration in a time period that is synchronous with the Moon's orbital period about Earth in preparation for a repeat of this operational procedure. To gain a clear understanding of the logistical requirements, we begin by defining this operational procedure and it is from this that we establish the logistical requirements. The standard logistical operation of the system will then be described in detail and the chapter will conclude with a discussion of the conditions under which modifications to the logistical operations of the system may be necessary and how these can be implemented.

2.1 System Operations Definition

The aim of the system is to exchange payloads at regular intervals between two MMETs, one orbiting Earth and the second orbiting the Moon, using the principle of momentum exchange. At the beginning of each operational phase, the *MMET in a prograde orbit about Earth* (EMMET) is fully laden with payloads attached symmetrically to its upper and lower tips which are spinning in the same direction as the orbital motion. At the same instant the MMET in a retrograde orbit about the Moon, termed the *Lunavator*, is completely unladen with its tether sub-spans spinning in the same direction as its orbital motion. Payloads are released from the upper and lower tips of the EMMET at the same instant. This occurs at the *perigee*, closest point of approach to Earth, of the EMMET's orbit with its tether sub-spans aligned along the local gravity gradient. As a

result of the direct addition of the rotational to the orbital velocity this is the best performing configuration for payload raising. Furthermore, this symmetrical launch is important for maintaining the orbital altitude of the tether system's central facility after payload release, with significant effects of an asymmetrical release noted by Cartmell and Zeigler [23] in their terrestrial tests of 2001. The payload released from the upper tip of the EMMET has the same orbital angular velocity as the central facility at perigee, which is coincident with the systems centre of mass, and this is greater than the orbital angular velocity required to stay on the same trajectory after release. In addition to this, as the direction of rotation of the tether sub-spans are in the same prograde direction as the orbital motion it gains an additional velocity increment when it is at the upper tip position relative to the central facility. These orbital and rotational velocities add to give a larger velocity than required at this position and after release the payload embarks upon a large prograde trajectory bound for the Moon with its position at the upper tip coinciding with the perigee of its outbound orbit. The payload released from the lower tip of the EMMET also has the same orbital angular velocity as the central facility, which is lower than the orbital angular velocity required to stay on the same trajectory, and again as the direction of rotation of the tether sub-spans is in the same prograde direction as the orbital motion it loses the same magnitude of velocity, and subsequently linear momentum, that the upper tip has gained. After release, this payload embarks upon a prograde trajectory to a position closer to Earth with its position at the lower tip coinciding with the *apogee*, furthest point from Earth, of its trajectory. At the perigee of its orbit, the payload released from the lower tip is captured by a space-plane and returned to Earth possibly using a system similar the reverse operation of the HASTOL system [33]. When the system is initially set up and begins its first phase of operation, a dummy payload would be attached to the EMMET's lower tip to preserve the mass symmetry of the system and this would be allowed to burn up upon entry into Earth's atmosphere. An elliptical trajectory is the lowest energy orbit for the payload released from the upper tip to reach the Moon and this is undertaken until the payload reaches
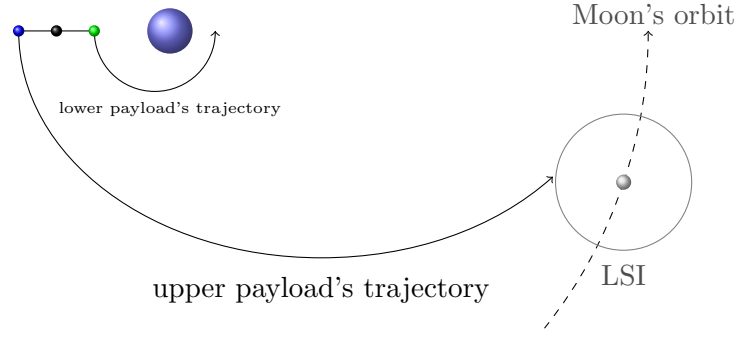
Figure 2.1: Earth-Moon elliptic transfer phase

the boundary between the dominating influence of Earth's gravity and the Moon's gravity. This boundary is denoted the *lunar sphere of influence* which is abbreviated to LSI. Upon entry into the LSI, the payload's velocity relative to the Moon results in it undertaking a retrograde hyperbolic trajectory to its closest point of approach to the Moon, denoted the *perilune* of the orbit and located on the far side of the Moon from Earth, at which point it is captured by the upper tip of the Lunavator, also at the perilune of its orbit. The Lunavator is designed such that its orbit about the Moon is elliptical, and when it is at the perilune of its orbit and the tether sub-spans are aligned along the gravity gradient the lower tip touches the Moon's surface and this is the systems similarity to Moravec's concept [20] and hence the label Lunavator. At the instant of capture, the incoming payload from Earth is captured at the upper
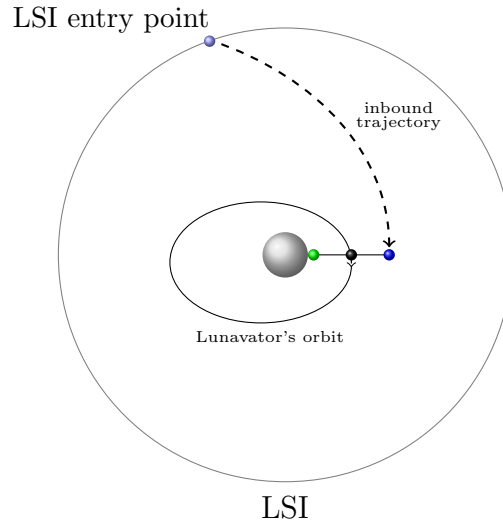
Figure 2.2: Earth-Moon hyperbolic transfer phase
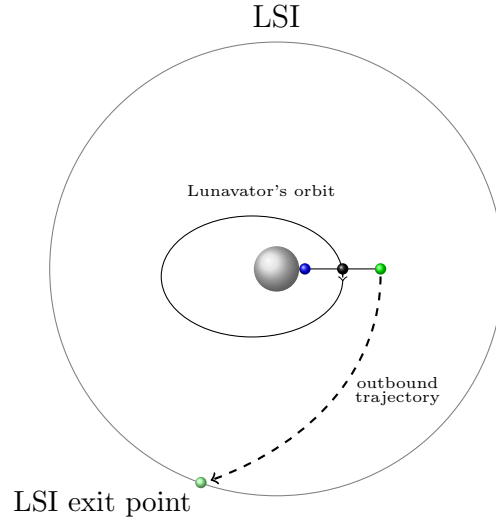
Figure 2.3: Moon-Earth hyperbolic transfer phase

tip whilst the lower tip picks up a payload from the Moon's surface to preserve mass balance across the system and maintain the central facility's orbital altitude. A waiting period between the Lunavator's capture and launch operations ensues which is designed to allow the Lunavator's upper and lower tips to exchange positions and allow payload launch to take place. After the waiting period, the payload previously picked up from the surface is released from the upper tip position on a retrograde hyperbolic LSI escape trajectory whilst the lower payload previously from Earth is placed onto the Moon's surface. When the outbound payload reaches the boundary of the LSI, it has a lower velocity relative to Earth and follows a prograde elliptical trajectory back to perigee. At perigee, the payload is captured by the upper tip of the EMMET which is at the perigee of its orbit with the tether sub-spans aligned along the local
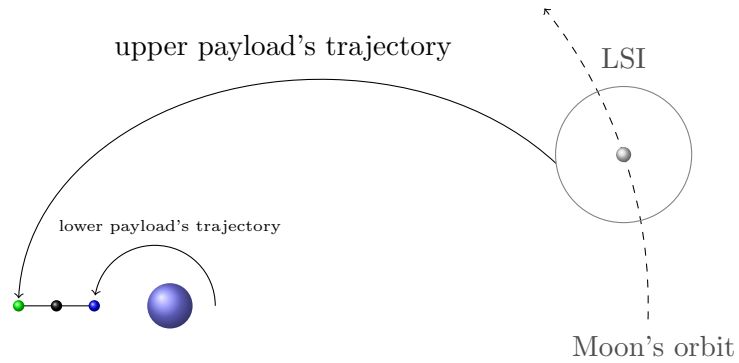
Figure 2.4: Moon-Earth elliptic transfer phase

gravity gradient. At the instant of capture at the upper tip, the lower tip also captures a payload to preserve the mass balance and central facility altitude. At this point the lower payload is at the apogee of its orbit, having previously been brought up from Earth's surface and released at the perigee of its orbit a half orbital period prior to capture, in this case an identical system to HASTOL may be useful. When the Moon again returns to the same initial position relative to the Earth the procedure is repeated.

2.2   System Logistics

Having defined the operational procedure to be undertaken by the system each time the Moon reaches a specified starting point in its orbit about Earth, the theoretical design of the system can begin in earnest. The logistical design will specify the most fundamental criteria that the system must adhere to for any functionality to be achieved and which satisfy the top level objective: to design an efficient system which is capable of transferring payloads between the Earth and Moon at regular intervals using symmetrically laden motorised momentum exchange tethers. Ignoring, for the moment, any of the more complex problems of actually satisfying the logistical requirements by trajectory design, utilisation of gravitational perturbations or orbital manoeuvers we shall focus solely on the requirements themselves. The most basic logistical requirements which must be satisfied can be stated as follows:

i. The EMMET must attain the same configuration relative to Earth and the Moon periodically with the Moon's orbit about Earth to allow payload capture and launch operations to take place.

ii. The Lunavator must attain the same configuration relative to Earth, the Moon and the EMMET periodically with the Moon's orbit about Earth again, to allow payload capture and launch operations to take place.

iii. The EMMET and Lunavator should be at the perigee and perilune of their respective orbits when these configurations occur to ensure

the system has maximum orbital velocity at these points.

iv. The EMMET and Lunavator tether sub-spans should be aligned along their local gravity gradients when these configurations occur to ensure maximum rotational increment to orbital velocity is achieved.

v. The EMMET and Lunavator systems should be capable of transporting payloads along the length of their system from upper to lower tips and vice-versa to allow propulsion-less transport of payloads between the lower and upper tip positions.

vi. The passage of payloads between the EMMET and Lunavator should take place within a time period compatible with these configurations.

vii. The entire time period between payload launch from the EMMET's upper tip and the arrival of a return payload from the Lunavator should also take place within a time period compatible with these configurations.

viii. The Lunavator must be capable of placing and collecting a payload from the Moon's surface.

Having stated these basic requirements we will now proceed with a description of how they can be satisfied:

To ensure that the EMMET periodically attains the same configuration relative to Earth and the Moon, the Moon's orbital period about Earth must be an integer multiple of the EMMET's orbital period about Earth. This ensures that each time the Moon reaches a pre-determined true anomaly of its orbit the EMMET arrives at a pre-determined true anomaly of its orbit. We describe the orbital periods of the EMMET and the Moon as being integer harmonic to one another and relate the orbital period of the Moon's orbit to the orbital period of the EMMET's orbit by defining the integer variable, m, and the following relation:

$$T_{EM} = \left(\frac{T_{moon}}{m} \right) \qquad m \epsilon \mathbb{N} \qquad (2.1)$$

where T_{EM} is the *EMMET's orbital period about Earth* and m is a positive integer which will be denoted as the *orbital variable m* as it is defined as the ratio of two orbital periods. This requirement is similar to, though not based upon, Hoyt and Uphoff's concept of orbital resonance between the apsidal rate of the Earth orbiting tether in the Cislunar Tether Transport System [28] and the arrival of the Moon at the ascending node of its orbit. For the Lunavator to periodically attain the same configuration relative to Earth, the Moon and the EMMET; the EMMET's orbital period about Earth, must be an integer multiple of the Lunavator's orbital period about the Moon and this corresponds to the Lunavator's orbital period about the Moon being integer harmonic with the EMMET's orbital period about Earth and subsequently the Moon's orbital period about Earth. This ensures that each time the Moon reaches a pre-determined true anomaly of its orbit the Lunavator arrives at a pre-determined true anomaly of its orbit and this is achieved by defining integer variable, n, and the Lunavator's orbital period by the following relation:

$$T_{LV} = \left(\frac{T_{EM}}{n}\right) = \left(\frac{T_{moon}}{m.n}\right) \qquad m, n \epsilon \mathbb{N} \qquad (2.2)$$

where n is a positive integer and will be denoted as the *orbital variable n* as this is also defined as the ratio of two orbital periods. By arranging the orbits of the EMMET and Lunavator such that they arrive at their respective periapses, the points of closest approach to the central body, when the Moon arrives at a pre-determined true anomaly of its orbit and by maintaining the relations defined in equations (2.1) and (2.2), the EMMET and Lunavator will arrive at the periapses of their orbits with the arrival of the Moon at its pre-determined true anomaly. To ensure that the tether sub-spans are aligned along the local gravity gradients when the EMMET and Lunavator arrive at the periapses of their orbits, the rotational periods of the sub-spans must be integer harmonic with the orbital periods of their respective tether systems. In addition to this, to allow the propulsion-less passage of payloads between the upper and lower payload positions, the integer harmonic in this case must take only odd integer values, with an additional half rotation of the tether sub-spans to allow alternate tips to occupy the upper and lower tip positions

at successive periapse arrivals. The rotational rates for the EMMET and Lunavator can be defined as follows:

$$T_{EM-ROT} = \left(\frac{T_{EM}}{p_r + 0.5} \right) \qquad p_r \epsilon \mathbb{N} \qquad (2.3)$$

and

$$T_{LV-ROT} = \left(\frac{T_{LV}}{q_r + 0.5} \right) \qquad q_r \epsilon \mathbb{N} \qquad (2.4)$$

where p_r and q_r are odd positive integers and are denoted by the rotational variables p_r and q_r as they are defined as *the ratio of the rotational to orbital periods for the tether systems.* To allow more flexibility in the payload's transfer trajectory design, equations (2.3) and (2.4) can be adjusted to add additional quarter or three-quarter rotations instead of the additional half rotation, with the addition of constraints to satisfy the systems operational procedure and this will be discussed later in this chapter. To ensure that the passage of payloads between the EMMET and Lunavator takes place within a time period compatible with these configurations and to ensure that this is also the case for the entire transfer time between EMMET capture and launch operations; transfer times between the EMMET and Lunavator must be integer multiples of the EMMET's orbital period, as must any waiting time between Lunavator capture and launch operations. This is satisfied by the transfer times between the EMMET and Lunavator satisfying the following relations for transfer variables c_1 and c_2:

$$T_{EM-LV} = c_1 T_{EM} \qquad c_1 \epsilon \mathbb{N} \qquad (2.5)$$

and

$$T_{LV-EM} = c_2 T_{EM} \qquad c_2 \epsilon \mathbb{N} \qquad (2.6)$$

The wait time constraints between payload capture and launch operations by the Lunavator can be satisfied by:

$$T_w = d_w T_{LV} \qquad d_w \epsilon \mathbb{N} \qquad (2.7)$$

The application of these requirements result in the logistical design of the system and this will be the focus of the following section.

2.3   Logistical Requirements

Having defined the logistical requirements that must be satisfied for the system operations to take place, the logistical operations of the system will be given in detail for the standard operation of a system where both tethers have integer harmonic rotational rates plus additional half rotations. Once this has been described, the operations of the system will be given when the rotations differ from this additional half rotation. The chapter will conclude with a description of the logistical adjustments required when combinations of rotations are used; or when no waiting time between Lunavator capture and launch operations is possible; or when additional adjustments may be required when orbital perturbations are taken into account.

2.3.1   Standard Operational Requirements

The logistical requirements for a continuous payload exchange when the rotational variables of both MMETs are some positive integers plus additional half rotations and satisfying equations (2.3) and (2.4), respectively, can be stated as follows:

i. The orbital variable, m, between the orbital periods of the EMMET and the Moon must take only even values such that the EMMET and Lunavator return to their initial configuration at the same true anomaly of the Moon's orbit.

ii. The rotational variable, p_r, between the EMMET and the tether sub-spans must only take odd values to ensure that alternating tips occupy alternating positions at each succeeding occurrence of the EMMET at the perigee of its orbit.

iii. The rotational variable, q_r, between the Lunavator and the tether sub-spans must only take odd values to ensure that alternating tips occupy alternating positions at each succceding occurrence of the Lunavator at the perilune of its orbit.

iv. The orbital variable, n, between the Lunavator and the EMMET

29

must only take odd values to ensure that when both the Lunavator and EMMET arrive simultaneously at their respective periapses, that alternating Lunavator tips occupy alternating positions at each succeeding occurrence. This is important in allowing the entire logistics of the system to be achieved easily as a function of the EMMET's orbital variable

v. The wait time variable, d_w, between Lunavator capture and launch operations must only take odd values to ensure that the upper and lower Lunavator's tips have exchanged positions to allow the release of a payload back to Earth from the upper tip.

vi. Transfer time variables, c_1 and c_2, between EMMET launch and Lunavator capture operations, and vice versa, should only take even values to ensure that the same tips perform the same operation in each operational phase.

To illustrate these requirements, a numerical example with diagrams showing each phase of the logistical operation will now be given:

Let orbital variable m be equal to 130, orbital variable n be equal to 9, rotational variables p_r and q_r equal to 7 and 15, respectively, transfer time variables c_1 and c_2 both equal 8 and wait time variable d_w be equal to 27. These numerical values are arbitrary and can be altered as long as the requirements described in this section are adhered to. At the instant prior to payload launch from the EMMET, both the EMMET and Lunavator are at the periapses of their orbits with their tether subspans aligned along the local gravity gradient. The EMMET is fully laden with the payload bound for the Moon (blue) at the upper tip
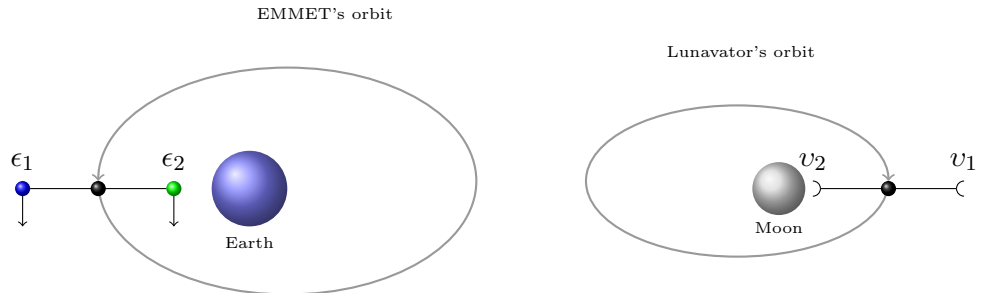
Figure 2.5: EMMET launch configuration

position ϵ_1 and the payload to be returned to Earth (green) at the lower tip position ϵ_2. At this point, the Lunavator is fully unladen with the lower tip position denoted υ_2 and the upper tip position denoted by υ_1, the system configuration at this instant is shown in Figure (2.5). At the instant of payload capture by the Lunavator, the payload from Earth has traversed a path between the EMMET's upper tip and the Lunavator's upper tip in a time period equal to 8 times the EMMET's orbital period. In addition to this, the Lunavator has arrived at perilune after completing 72 revolutions of the Moon and its tether sub-spans have completed 1116 rotations with the tip denoted by υ_2 remaining at the lower tip position and tip υ_1 remaining at the upper tip position. The upper tip, υ_1, has captured the incoming payload (blue) from Earth and the lower tip, υ_2, has picked up the payload (red) from the Moon's surface. The EMMET is now fully unladen and at the perigee of its orbit having traversed about Earth 8 times, the EMMET's sub-spans have rotated 60 times and ϵ_1 remains at the upper tip position whilst ϵ_2 remains at the lower tip position, the system configuration at this instant is shown in Figure (2.6). After a waiting time between capture and launch operations, the Lunavator has returned to perilune after orbiting the Moon 27 times, its tether sub-spans have rotated a further 418.5 times since payload capture from Earth and pick up from the Moon. Its upper and lower tips have exchanged positions with υ_1 now at the lower tip position which allows it to place the payload (blue) initially from Earth on to the Moon's surface, the payload (red) previously picked up from the surface is now launched from tip υ_2 on to an Earth bound trajectory. At the same instant, the still unladen EMMET is again at the perigee of its orbit having orbited
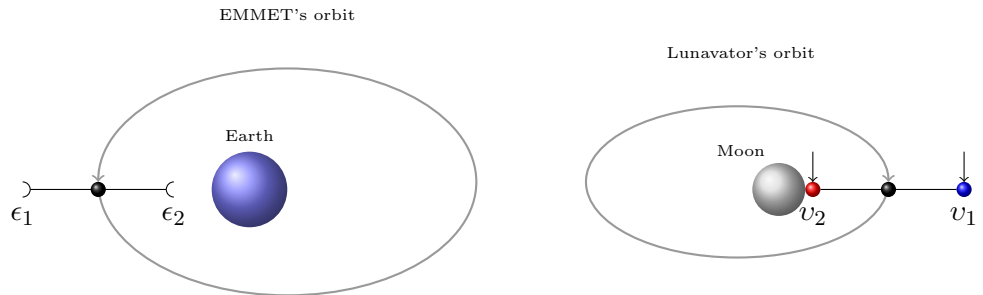
Figure 2.6: Lunavator capture configuration
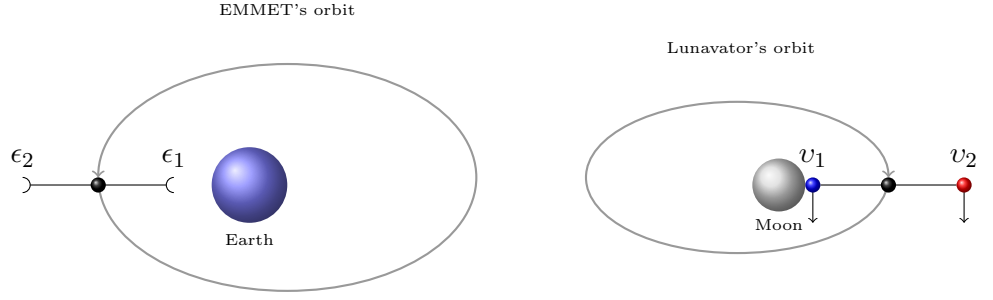
Figure 2.7: Lunavator launch configuration

Earth a further 3 times. Its tips have rotated a further 22.5 times and have alternated positions, with ϵ_2 now at the upper position and ϵ_1 at the lower position, the system configuration at this instant is shown in Figure (2.7). After a payload transfer time between the Lunavator's upper tip and the EMMET's upper tip of 8 times the orbital period of the EMMET, the EMMET has orbited Earth a further 8 times and its tether sub-spans have rotated a further 60 times. The inbound payload (red) from the Moon is therefore captured by the tip denoted by ϵ_2 at the upper tip position and the payload (cyan) from Earth is captured by ϵ_1 at the lower tip position. The Lunavator is again fully unladen and has traversed a further 72 orbits with its sub-spans having rotated a further 1116 times with the tip denoted by υ_2 remaining at the upper tip position and the tip denoted υ_1 remaining at the lower tip position, the system configuration at this instant is shown in Figure (2.8). After a further 111 EMMET orbital periods the Moon and system have returned to their original configuration, the EMMET has traversed Earth a further 111 times and is again at the perigee of its orbit. The EMMET's sub-spans have rotated a further 832.5 times with the tip denoted by ϵ_1 at the
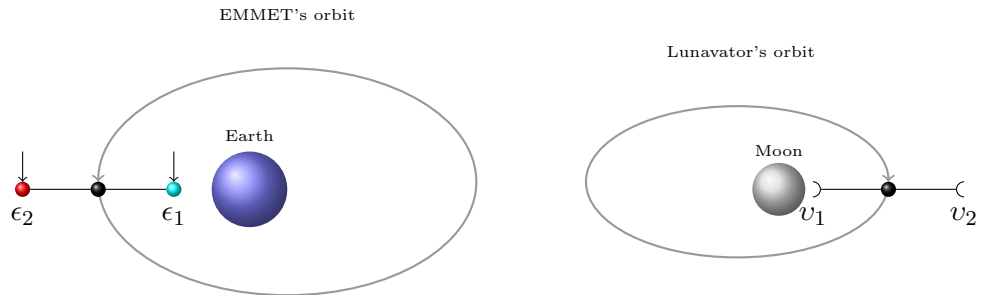
Figure 2.8: EMMET capture configuration
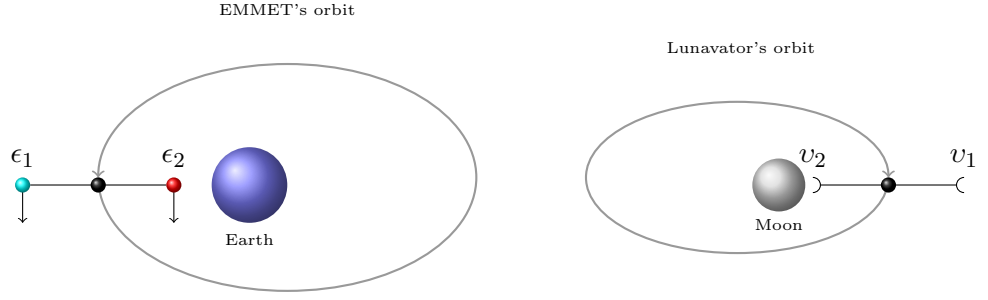
Figure 2.9: EMMET re-launch configuration

upper tip position and the tip denoted by ϵ_2 at the lower tip position. The payload (cyan) brought up from Earth at the previous capture operation is at the upper tip position and can be launched to the Moon whilst the payload from the Moon is at the lower position and can be released down to Earth. At the same instant, the Lunavator remaining fully unladen has traversed a further 999 orbits and at perigee with its sub-spans having rotated a further 15484.5 times with v_2 at the lower tip position and v_1 at the upper tip position. The entire system has returned to its original configuration in synchronisation with the Moon's orbital period about Earth and is prepared to launch a new payload towards the Moon in a second phase of operations, as shown in Figure (2.9).

2.4   Logistical Adjustments

When taking into account variations in the orbital elements of the Moon's orbit about Earth, resulting from the perturbations arising from the gravitational forces of the other planets in the Solar system and the Sun, in addition to the perturbations acting on the EMMET as a result of a non-spherical Earth and to a lesser extent those acting on the Lunavator as a result of the Moon's own oblateness; some flexibility must be introduced into the logistical design of the payload exchange mechanism to allow operational procedures to be undertaken under a variety of configurations and conditions. Another factor which requires a flexible logistical design is the launch velocity of the payloads from the tether tips when designing the trajectories between the Earth and Moon. Only under a very limited set of circumstances will the velocity at which the payload is

released from the EMMET's upper tip be the ideal velocity to allow the payload to traverse the optimum trajectory to the Lunavator's upper tip and vice-versa. Under all other conditions the EMMET and Lunavator supply the payloads with the majority of the velocity that they require to undertake the optimum trajectory with the remainder being supplied by an on-board chemical propulsion system. The amount of energy supplied by this chemical system can be minimised by matching as closely as possible the upper tip velocity of the EMMET and Lunavator to the required velocity for the transfer trajectory.

When the orbital perturbations acting on the Moon are introduced into the system, some modifications to the logistical design must be introduced, for example, when arranging an Earth orbiting system to arrive at the perigee of its orbit each time a secularly regressing Moon arrives at the ascending node of its orbit. To accomplish this, the orbital variable m of the EMMET's orbit should be modified to be integer harmonic with the orbital period of the Moon minus the time period between the true anomalies of successive ascending node positions. Obviously this would affect the other logistical requirements but as these are fundamentally based upon the EMMET's orbital period no further modifications would be necessary. This could also be applied to ensure that the EMMET arrives at its perigee each time the Moon arrives at the perigee of its orbit, with the Moon's argument of perigee regressing as a result of orbital perturbations, and this would be achieved by the modification of orbital variable m of the EMMET orbit to be integer harmonic with the Moon's orbital period about Earth minus the time period between successive perigee passages. However, the Moon's motion is not as simple as this and the modification utilised and applicable, importantly in this case, is when a particular feature of the Moon's orbit oscillates about a mean value relative to Earth, for example the Moon's ascending node. When attempting to arrange the payload exchange system to carry out its operational procedure each time the Moon arrives at the ascending node of its orbit, and in the case where the Moon's ascending node is at a larger true anomaly than that for which the logistical system was originally setup; the whole operational procedure is delayed by a time

period which is an even integer harmonic of the Moon's orbital period about Earth whilst conserving the other logistical requirements. This, however, will result in a timing discrepancy between the optimum transfer trajectory for the system's current configuration and the one that will be undertaken as a result of the variation in the Moon's ascending node. This discrepancy cannot be resolved and the logistical requirements must be maintained, therefore the payload is launched at the EMMET's arrival at perigee closest to the time of the optimum configurations launch from perigee whilst maintaining the flight time of the payload to LSI. As a result of the timing discrepancy, the payload will arrive at a different point of the LSI to that of the optimum configuration and will therefore undertake a different trajectory about the Moon: this results in a variation in the payload's perilune parameters, and therefore adjustments to the Lunavator's orbital elements to accommodate this are a necessity. Later in this thesis it will become obvious that adjustments to the Lunavator's parameters are necessary to accommodate the varying distance of the Moon at its ascending node due to variations in its true anomaly and reduce the magnitude of the velocity adjustments necessary for the payload exchanges which are more easily accommodated by the Lunavator due to the lesser gravitational attraction of the Moon than making adjustments to the EMMET. The same is possible for operations to be undertaken earlier than the original setup of the system and when the ascending node is at a lesser true anomaly of the Moon's orbit, the whole operation is brought forward by a time period an even integer multiple of the EMMET's orbital period, and again an unresolvable timing discrepancy is expected which is accommodated in a similar way.

To match the upper tip velocity of the EMMET and Lunavator more closely to the required payload velocity for an optimum trajectory, some alterations can be made to the rotational rates of the EMMET and Lunavator in order to reduce any velocity discrepancy. To allow alternate tips to occupy alternate tether tip positions at different points in the operational procedure, the rotational rates must take integer values plus additional of either half, quarter or three-quarter rotations. The logistical operation for the additional half rotation case has already been

outlined and the remainder of this chapter will consist of a description of the logistical requirements for the other two cases, and combinations of rotational rates in addition to the logistical requirements for a payload exchange procedure consisting of no waiting time at perilune which may be a necessity for certain transfer configurations.

2.4.1 Non-Standard Operational Requirements

Under the circumstances that a more favourable transfer configuration and velocity match between the payload's required transfer velocity and the tether sub-span's tip velocity can be had by adjustments to the rotational rates of the tether sub-spans, there are certain additional rotation rates that are applicable with some minor modifications to the logistical design. The operational procedure outlined previously can still be obtained by retaining tether sub-span rotation rates which are integer harmonic with their respective tether systems but with additional quarter or three-quarter rotations, however, certain adjustments must be made to the overall logistical design to accommodate this. The requirement still remains of alternate tips occupying alternate positions at certain points in the logistical arrangement to allow capture and launch operations to be conducted at different points in the operational procedure and this requires that these additional half rotations still occur. When using additional quarter or three-quarter rotations, additional half rotations occur when time periods between one configuration and another are odd integer multiples of twice the rotational period. Additionally, full rotations occur when the time periods between two configurations are even integer multiples of twice the rotational period. The modified logistical requirements for the quarter or three quarter rates are the same in both cases and can be stated as follows:

i. The orbital variable, m, is an even integer whilst remaining integer harmonic with the Moon's orbital period about Earth.

ii. The rotational variable, p_r, between the EMMET and its tether sub-spans must only take odd values to ensure that alternating tips can occupy alternating positions at successive occurrences of

the EMMET at the perigee of its orbit.

iii. The rotational variable, q_r, between the Lunavator and its tether sub-spans must only take odd values to ensure that alternating tips can occupy alternating positions at successive occurrences of the Lunavator at the perilune of its orbit.

iv. The orbital variable, n, remains odd integer harmonic with the EMMET's orbital period.

v. The wait time variable, d_w, between Lunavator capture and launch operations must only take odd integer multiples of twice the rotational period of the Lunavator's sub-spans to ensure that alternate Lunavator tips occupy alternate tip positions between capture and launch configurations thus satisfying the logistical design.

vi. Transfer time variables, c_1 and c_2, between EMMET launch and Lunavator capture operations and vice versa should only take even integer multiples of twice the EMMET's orbital period to ensure that the payloads arrive at the correct upper tips and allow the same tips perform the same operation in each operational time period.

The operation of the system using additional quarter rotations can again be most easily demonstrated with an illustrative example as follows: Setting the orbital variable m equal to 100, n equal to 9, rotational variables p_r and q_r equal to 7 and 15, respectively, transfer time variables c_1 and c_2 both equal to 16 and wait time variable d_w equal to 54 we achieve the configurations shown in Figure (2.10). At the initial launch of the payloads from the upper and lower tips of the EMMET, denoted by $t = 0$, the Lunavator and EMMET are both at periapse and aligned along the local gravity gradients. At launch, the payload (blue) released from the upper tip is launched on to a lunar trajectory and the payload (green) released from the lower tip is on a return trajectory to Earth. After a transfer time equal to 16 times the EMMET's orbital period, the EMMET and Lunavator are again at periapse. The EMMET has traversed Earth 16 times and its tether sub-spans have completed 116
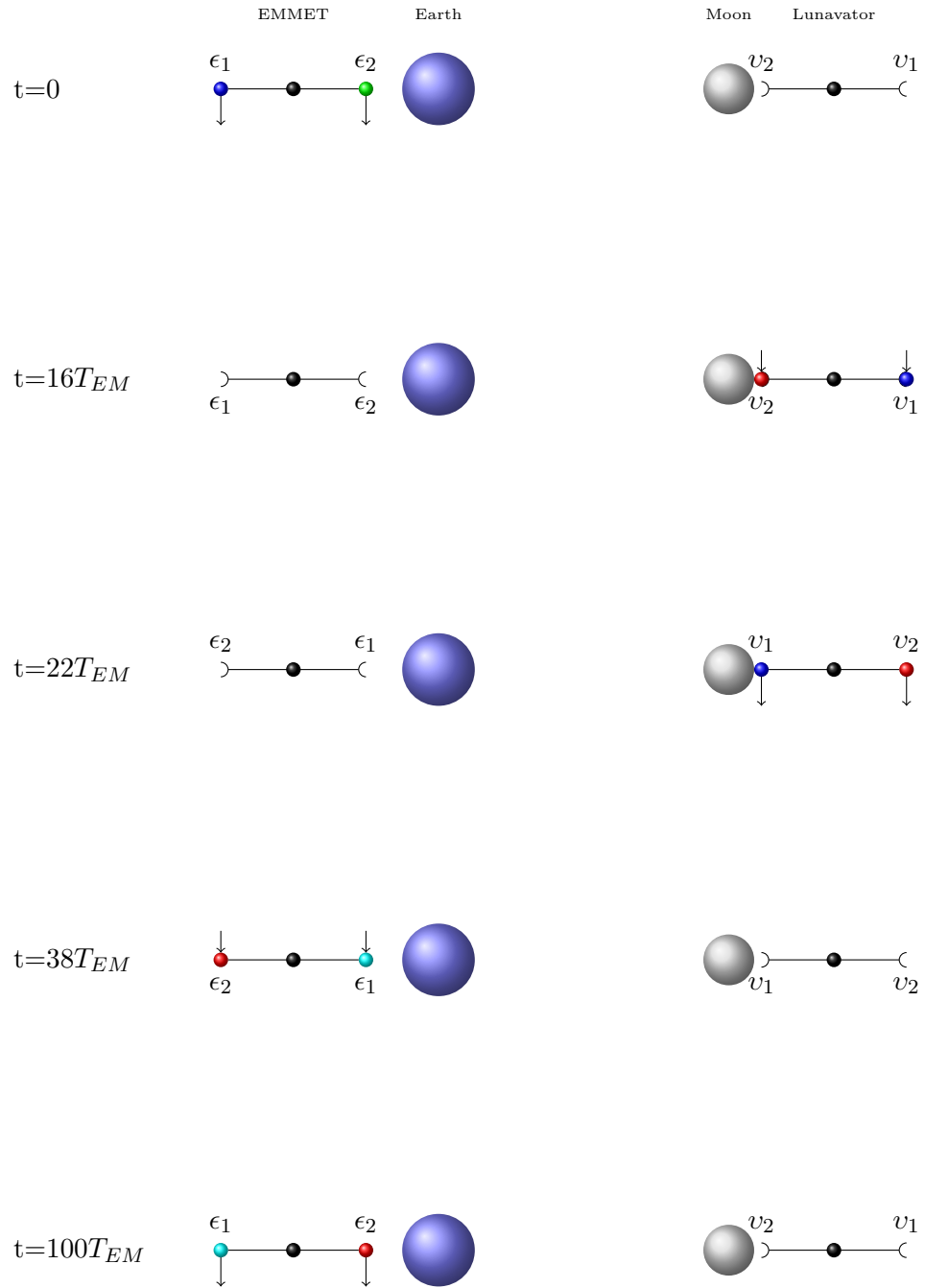
Figure 2.10: Additional one-quarter rotation logistical arrangement

rotations about the central facility, the Lunavator has orbited about the Moon 144 times and its sub-spans have rotated about the central facility 2196 times. The payload (blue) from Earth is then captured by tip υ_1 at the upper tip position and a payload (red) is picked up from the Moon's surface by tip υ_2 at the lower tip position. After 54 Lunavator orbits of the Moon, equal to 6 times the EMMET's orbit, the EMMET and Lunavator are again at the periapse of their respective orbits. The EMMET sub-spans have rotated 43.5 times in this period and the upper and lower tips have exchanged positions with tip ϵ_1 at the lower tip position and ϵ_2 at the upper tip position. The Lunavator tips have also exchanged position with the payload (red) previously from the Moon launched on an Earth bound trajectory from tip υ_2 now at the upper tip position and the payload (blue) previously from Earth placed on to the Moon's surface by tip υ_1 now at the lower tip position. After a time period equal to a further 16 times the EMMET's orbital period, the EMMET and Lunavator are again at the periapse of their respective orbits. The payload (red) from the Moon arrives at the upper tip position of the EMMET and is captured by tip ϵ_2 with the sub-spans having rotated a further 116 times, at the same instant, the lower tip captures the payload (cyan) brought up from Earth. The fully unladen Lunavator has orbited the Moon 144 times and the sub-spans have completed a further 2196 rotations. After 100 EMMET rotations, the system has returned to its original configuration with the payload (cyan) at the upper tip of the EMMET ready for transfer to the Moon, and the payload (red) at the lower tip will be returned to Earth at the same instant.

2.4.2 Combined Rates and Further Modifications

Having defined the logistics for the operational procedure where both the EMMET and Lunavator have the same fractional addition to their respective rotational variables; there may be cases where combinations of these fractional additions become necessary to ensure that the most efficient transfer trajectory between the tether tips can be had. The logistics for a system where the EMMET has an additional half rotation and the Lunavator an additional quarter or three-quarter rotation are

almost identical to the case for both tethers having additional quarter or three-quarter rotations with a single modification: the payload's Moon-Earth transfer trajectory must occur in a time period an odd integer multiple of the EMMET's orbital period, which allows the EMMET's tips to alternate their position and maintain the logistical requirements. This can be very simply accommodated into the system by extending the transfer time between the Lunavator's and EMMET's upper tips by a time period equal to a single EMMET orbital period. In the case that the Lunavator has an additional half rotation and the EMMET has an additional quarter or three-quarter rotation, two modifications must be made to the logistical design used when both tethers have additional quarter or three-quarter rotations: the first modification is that the wait time between Lunavator capture and launch operations must be extended by a single EMMET orbital period to ensure that there is an odd integer multiple of the EMMET's orbital period between capture and launch operations to allow alternate tips to exchange positions and the second is that the transfer time between the Lunavator and EMMET's upper tips are reduced or extended by a single EMMET orbital period to maintain the logistical design.

No-Wait Time Operations

A further modification and one which alters the operational procedure itself was suggested by Cartmell [40] and concerned the necessity for either of the MMETs ever becoming fully unladen. Under the circumstances that the trajectory design requires that no waiting time is possible to allow the Lunavator's tips to exchange positions, the operational procedure and logistical requirements can be modified to accommodate this. By configuring the Lunavator's upper tip such that when the payload is released onto an Earth-bound trajectory it is instantly replaced by the incoming payload from Earth and configuring its lower tip such that at the instant of release a payload is picked from the Moon's surface the mass balance and momentum across the system can be maintained. However, certain modifications to the logistical design of the system must be made to accommodate this. The modification necessary is to adjust succes-

sively the Lunavator to EMMET transfer time such that it is an odd integer harmonic whilst the EMMET to Lunavator remains even integer harmonic and on the next transfer procedure to adjust the EMMET to Lunavator transfer time such that it is odd integer harmonic whilst the Lunavator to EMMET transfer time returns to being even integer harmonic. A final illustrative example will be used to convey this process over three successive payload transfer procedures. Using an EMMET orbital variable m of 130, a Lunavator orbital variable n of 3, rotational variables p_r and q_r both equal to 7 and both with additional half rotations; we set the transfer variable between the EMMET and Lunavator upper tips, c_1, to 16 and the transfer variable between the Lunavator and EMMET upper tips, c_2, to 17:

At the instant of launch in Figure (2.11), the payload (blue) bound for the Moon is launched from the EMMET's tip denoted by ϵ_1 at the upper tip position and at the same instant a payload (green) is released to Earth from the tip denoted by ϵ_2 at the lower tip position. The Lunavator is fully laden at this point with a payload (green) attached to tip υ_2 at the lower tip position and a payload (yellow) attached to the tip υ_1 at the upper tip position. After a flight time equal to 16 times the EMMET's orbital period, the payload (blue) from Earth arrives at the Lunavator's tip υ_1 at the upper tip position and is captured at the instant of release of the return payload (yellow) to Earth. At this same instant, a payload (green) is placed onto the Moon's surface by υ_2 at the lower

Figure 2.11: No wait time (phase 1)

tip position and instantly afterwards another payload (red) is picked up from the surface to preserve the mass balance across the system, and so the EMMET is fully unladen at this point. After a flight time equal to 17 times the EMMET's orbital period, the EMMET and Lunavator tips have exchanged positions and the payload (yellow) released from the Lunavator's upper tip arrives back at the EMMET's upper tip and is captured by the tip denoted by ϵ_2 and at the same instant the tip denoted ϵ_1 at the lower position captures a payload (cyan) brought up from Earth, resulting in the Lunavator remaining fully laden at this point.

After a revolution of the Moon about the Earth, as shown in in Figure (2.12), the EMMET and Lunavator have returned to their original configurations with the payload (yellow) from the Moon attached to the EMMET's ϵ_2 tip at the lower position and the payload (cyan) previously brought up from Earth attached to the ϵ_1 tip at the upper position, therefore the Lunavator remains fully laden at this point. Again, the payload at the EMMET's upper tip is launched to the Moon and the payload at the lower tip is released to Earth. After a flight time equal to 17 times the EMMET's orbital period, the EMMET and Lunavator tips have exchanged positions and the payload (cyan) from Earth arrives at the Lunavator's tip υ_2 at the upper tip position and is captured at the instant of release of the return payload (red) to Earth which was picked up from the Moon's surface on the Moon's previous orbit about Earth. At this same instant, the payload (blue), previously from Earth,

Figure 2.12: No wait time (phase 2)
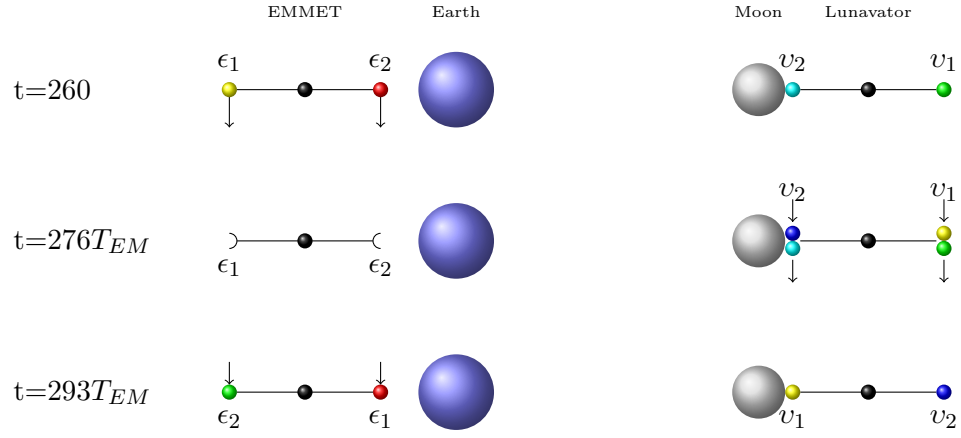
Figure 2.13: No wait time (phase 3)

is placed onto the Moon's surface by υ_1 at the lower tip position and instantly afterwards another payload (green) is picked up from the surface to preserve the mass balance across the system, and the EMMET is fully unladen at this point. After a flight time equal to 16 times the EMMET's orbital period, the Lunavator and EMMET tips remain in the same positions and the payload (red) released from the Lunavator's upper tip arrives back at the EMMET's upper tip and is captured by the tip denoted ϵ_2 and at the same instant the tip denoted by ϵ_1 at the lower position captures a payload (yellow) brought up from Earth, the Lunavator remaining fully laden at this point.

After a second revolution of the Moon about the Earth, shown in in Figure (2.13), the EMMET and Lunavator have again returned to their original configurations with the payload (red) from the Moon attached to the EMMET's ϵ_2 tip at the lower position and the payload (yellow) previously brought up from Earth attached to the ϵ_1 tip at the upper position, the Lunavator remains fully laden at this point. Again, the payload at the EMMET's upper tip is launched to the Moon and the payload at the lower tip is released to Earth. After a flight time equal to 16 times the EMMET's orbital period, the EMMET and Lunavator tips remain in the same positions and the payload (yellow) from Earth arrives at the Lunavator's tip υ_1 at the upper tip position and is captured at the instant of release of the return payload (green) to Earth which was picked up from the Moon's surface on the Moon's previous orbit about Earth. At this same instant, the payload (cyan), previously from Earth,

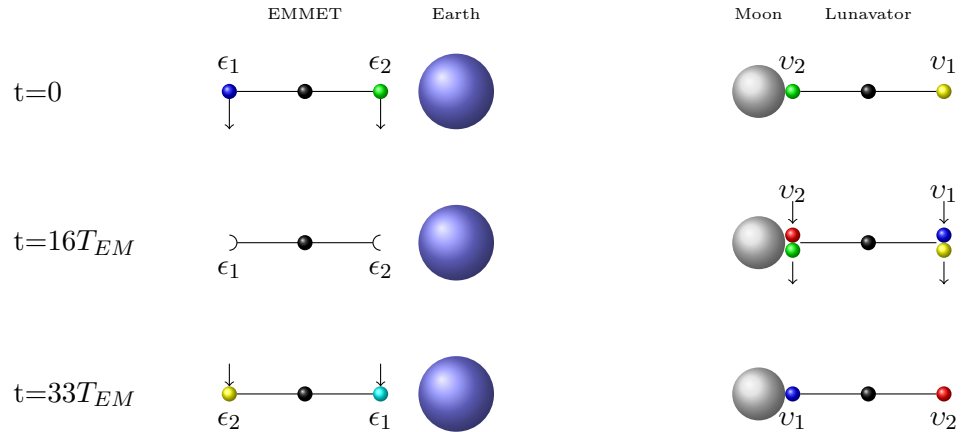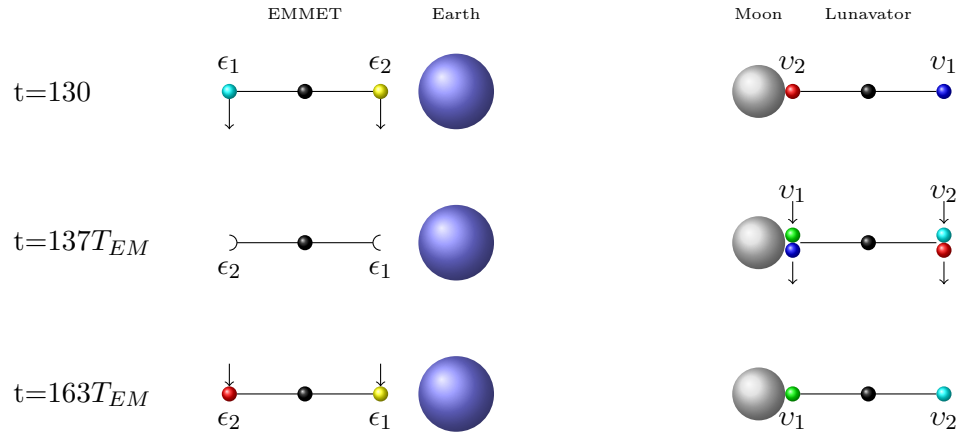is placed onto the Moon's surface by υ_2 at the lower tip position and instantly afterwards another payload (blue) is picked up from the surface to preserve the mass balance across the system, so that the EMMET is fully unladen at this point. After a flight time equal to 17 times the EMMET's orbital period, both the EMMET and Lunavator tips have exchanged positions and the payload (green) released from the Lunavator's upper tip arrives back at the EMMET's upper tip and is captured by the tip denoted by ϵ_2 and at the same instant the tip denoted by ϵ_1 at the lower position captures a payload (red) brought up from Earth, noting that the Lunavator remains fully laden at this point.

By alternating the transfer times of the trans-Luna and trans-Earth transfer trajectories such they are each successively even then odd, the logistical requirements of the overall system configuration can be arranged when no waiting time at perilune is the more suitable configuration. A drawback of this which becomes evident is that it takes a whole revolution of the Moon about Earth to allow a payload picked up from the Moon's surface to be launched onto a trans-Earth trajectory, furthermore it takes the same time period to allow the payload captured at the Lunavator's upper tip to be placed onto the Moon's surface. It is therefore obvious that this is not the most suitable logistical configuration for this purpose, however the necessity for the use of this configuration will become evident when the transfer configuration is established and data accumulated on the required logistical configurations become accessible.

2.5   Conclusions

The parameters which allow the establishment of a continuous Earth-Moon payload exchange have been identified and these must be satisfied for a continuous system to exist. These are dependent upon the orbital periods of the EMMET, Lunavator and Moon and employ integer harmonic relationships to ensure the occurrence of a given configuration relative to Earth for each orbit of the Moon about Earth. Additionally, the rotation rates of the tethers themselves have also been found to be essential to this system. These are crucial in allowing the passage of pay-

loads along the tether systems and in allowing the systems to perform alternative catch and throw operations thus allowing alternate payloads to be launched at successive transfer opportunities. Furthermore, these can be adjusted to more closely to match the tether's upper tip velocities to those required for the most efficient transfers between the two MMETs in orbit. To ensure that the payloads arrive at the tether tips at the correct instant; transfer times between the MMETs must also be integer harmonic with the orbital periods of the MMETs and subsequently the Moon. Modifications to the system are also possible and various configurations are capable of accommodating the oscillatory motion of the Moon's ascending node whilst maintaining the overall logistics. This is achieved by conducting transfers earlier or later than originally intended and are accommodated by varying payload transfer times between the MMETs accordingly.

Having defined the logistics of the system and possible modifications, these logistical requirements will serve as a guideline for the entire design of the payload exchange system with all trajectory design having to fit within this framework. Attention now turns to determining how a system can be setup which will track a specific point in the Moon's orbit to allow payloads to be transferred each time the Moon reaches this point when taking into consideration orbital perturbations and the complex nature of the Moon's orbit about Earth.

3. Moon Tracking Orbit

To provide an EMMET system which allows payload transfers between the Earth and Moon over an extended time period; a suitable transfer configuration must be established which can be repeated periodically with the Moon's orbit about Earth. To accomplish this, a point in the Moon's orbit must be chosen which allows transfers to be conducted successively over any given time period. Obvious choices for such a position would be the apogee or perigee of the Moon's orbit or alternatively its ascending or descending node relative to an Earth centred equatorial or ecliptic frame of reference. As a result of the third body perturbations of the Sun and other planets within the Solar system, the orbit of the Moon is extremely complex and cannot be treated using the precessing inclined ellipse model [41]. This results in variations in the argument of perigee and the right ascension of the ascending node of the lunar orbit which affects all possible transfer positions. To conduct successive transfers to the perigee or apogee of the Moon's orbit under these conditions would be extremely difficult as its latitude would vary in addition to its position in the fundamental plane of the reference frame. Similarly to the method used by Hoyt and Uphoff [28], by conducting transfers to either the ascending or descending node of the Moon's orbit; only variations in position in the fundamental plane of the reference frame would have to be accounted for.

To account for variations in the lunar orbit's node position; the EMMET's orbit must be configured such that it returns to the required transfer configuration relative to Earth and the Moon, periodically with the Moon's own motion about Earth, whilst altering its orbital elements in such a manner that it accounts for these changes in node position. Several possible configurations which satisfy these requirements present themselves, however each requires alterations to its orbital elements by means of orbital manoeuvres and would therefore require either fuel to be brought up from Earth, via the payloads bound for the Moon, and

fed down fuel lines located through the centre of the tether sub-spans; or by solar cells located on the central facility; or by using an electro-dynamic tether and utilising the magnetic field of Earth [4] to produce thrust, however for this to occur the system would have to orbit in a low Earth orbit which means that atmospheric drag effects would have to be accounted for. By supplying additional fuel to the EMMET to conduct orbital alterations, questions relating to fuel efficiency and the timing of the orbital manoeuvers are raised. The answers however, are straightforward: the most efficient times to perform these manoeuvers will be when the velocity of the EMMET is at its lowest and, due to present specifications, when it is fully unladen and its mass is at a min-imum, occurring when payloads are on their way to, or returning from, the Moon. A caveat to be heeded, however, is that no orbital adjust-ment should be undertaken by an unladen EMMET between payload release and capture operations, which disadvantages the return payload. The implications of these answers with regards to fuel efficiency will be examined on individual merit at the key stages of this chapter.

This chapter can be dissected as follows; an outline of single manoeu-vre moon-tracking orbit designs will be given, followed by a description of the dual manoeuvre methods devised to track the Moon's ascending node: these tracking designs are also all applicable to the Moon's de-scending node. The remainder of the chapter will then be dedicated to the derivation of the formulas required to calculate the necessary adjust-ments to the EMMET's ascending node and argument of perigee which are required to maintain these moon tracking orbits.

3.1 Outline of Moon Tracking Method

To begin a description of the methods designed to track the ascending or descending node of the Moon's orbit, a short description of the Moon's motion is warranted, and this will perhaps highlight the challenges as-sociated with designing such a method for practical applications. The motion of the Moon relative to both the geocentric equatorial and ecliptic frames of reference can be summarised from Roncoli [41] as follows:

i. The principal perturbation acting on the Moon is due to the third body gravitational attraction of the Sun, the result of this is that the Moon's motion cannot be described by the precessing inclined ellipse model.

ii. The Moon's orbit has a nearly constant inclination with respect to an Earth centred ecliptic frame but a varying inclination relative to Earth's equatorial frame.

iii. Relative to the ecliptic frame, the longitude of the ascending node has a secular rate with a period of 18.6 years. However, relative to the equatorial frame it has no secular rate and oscillates about a right ascension of $0°$ with an 18.6 year period.

iv. The Moon's argument of perigee precesses with a period of 8.85 years relative to both the ecliptic and equatorial reference frames.

As a result of this complex motion, no configuration which utilises only the perturbing effects of an oblate Earth is sufficient to allow the EM-MET to be correctly located to transfer and receive payloads with the Moon on a regular (per lunar orbit) basis. The concepts of single and dual orbital manoeuvre methods to adjust the argument of perigee and ascending node of the EMMET's orbit with each having their own merits and disadvantages will now be discussed.

3.1.1 Single Manoeuvre Moon Tracking

One method of conceivably tracking the Moon's ascending node is to arrange the EMMET's orbit in a polar inclination relative to Earth's equatorial frame to ensure that no precession of its ascending node occurs. In addition to this, by making small adjustments to the orbit's ascending node angle via orbital manoeuvres, the oscillation of the Moon's own ascending node about an ascending node angle of $0°$ can be accounted for allowing a continuous alignment of their apse lines to be maintained. Furthermore, by ensuring that their ascending node angles are $180°$ out of phase, payloads are exchanged between the EMMET and Moon when the EMMET's freely precessing argument of perigee becomes re-aligned
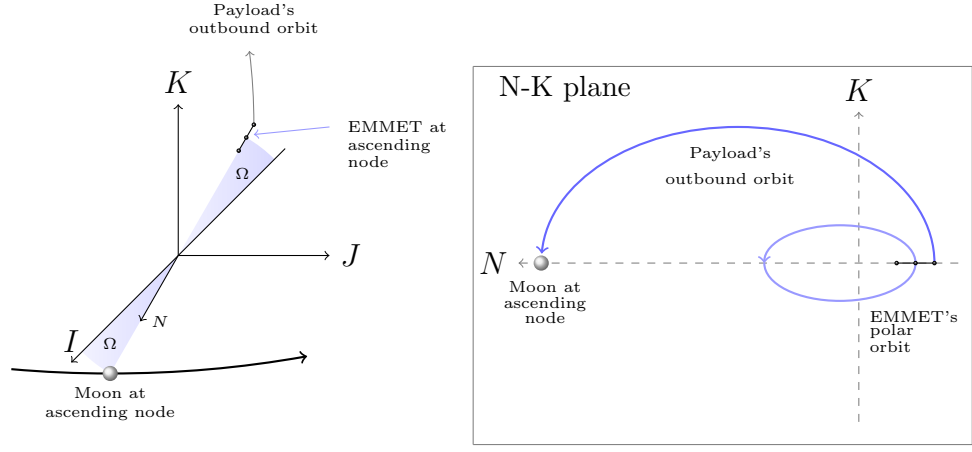
Figure 3.1: Polar Inclination Moon-Tracking Configuration

with the equatorial plane as the Moon crosses its ascending or descending node. By maximising the rate of the argument of perigee's regression, by adjustments to the eccentricity and semi-major axis, a minimum realignment time for the argument of perigee can be obtained. The configuration of this method is shown in Figure (3.1) with I, J, K denoting the axes of Earth's equatorial frame, N denoting a unit vector directed towards the ascending node of the Moon's orbit about Earth and Ω denoting the angle of the Moon's ascending node. A possible drawback to this method is its realignment period with the equatorial plane and data on this will be presented in Chapter 5.

A second method of tracking the Moon's ascending node relative to Earth's equatorial frame consists of configuring the EMMET's orbit with a critical inclination, denoted i_c, of either 63.4° or 116.6° which renders its argument of perigee stationary. This is set to 0° and ensures that the ascending node and perigee of the EMMET's orbit coincide. Under these circumstances, the angle of ascending node of the EMMET's orbit will have a secular rate, however, this can be minimised by careful selection of its semi-major axis and eccentricity and in addition to this, orbital adjustments are performed to arrange the EMMET's ascending node such that it regresses to the correct position with its apse line aligning itself with the node line of the Moon's orbit as it crosses the ascending node of its orbit, at this instant payload catch and throw operations are conducted. The configuration of this method is shown in Figure (3.2) with
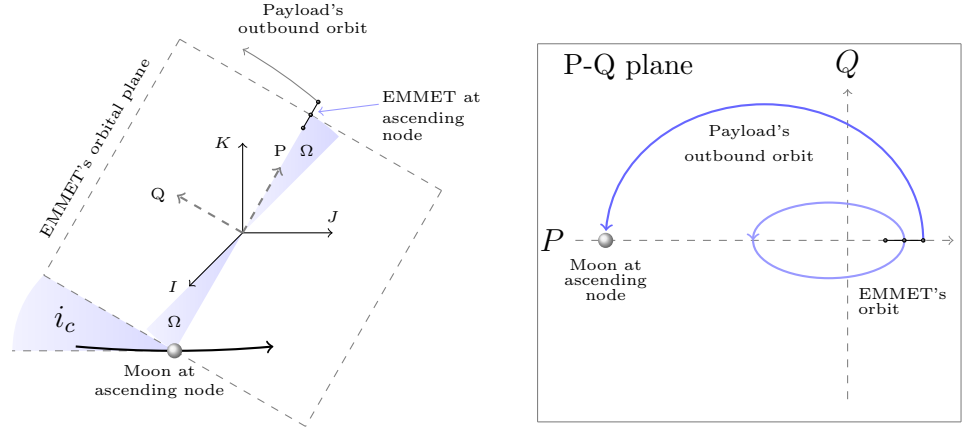
Figure 3.2: Critical Inclination Moon-Tracking Configuration

P, Q denoting axes of the EMMET's perifocal, or orbit-centred, frame of reference. Possible drawbacks of this method are the magnitude of the velocity changes required to adjust the ascending node angle, however this method is the more promising of the equatorial configurations and data on the magnitude of these adjustments will also be presented in Chapter 5.

An alternative single manoeuvre moon-tracking method utilises the secular rate of the ascending node of the Moon relative to the ecliptic frame. By arranging the EMMET orbit's inclination, semi-major axes and eccentricity such that its own ascending node relative to the ecliptic frame regresses at the same rate as the Moon's then their apse lines can remain in continual alignment. In addition to this, these arrangements could also minimise the rate of precession of the argument of perigee with orbital manoevres performed to adjust this such that it would regress/precess into alignment with the ecliptic plane at the correct instant to pass or receive payloads from the Moon which, at this point, is also aligned with the ecliptic plane and at its ascending or descending node. The main drawback of this method, however, is that any arrangement to the inclination of the EMMET's orbit to ensure that its ascending node regresses at the same rate as the Moon's ascending node, has to be configured relative to the equatorial frame, and as the ascending node regresses about the equatorial z-axis the divergence between the ecliptic frame and equatorial frames grows and recedes which introduces a varying inclination of the EMMET's orbit relative to the ecliptic frame

causing variations in the orbital inclination of incoming and outgoing payloads.

3.1.2 Dual Manoeuvre Moon Tracking

Tracking the Moon's ascending node relative to Earth's equatorial frame using the dual tracking manoeuvre can be achieved firstly by arranging the right ascension of the EMMET's orbit to remain at a constant angle, achieved using a polar orbit of 90° inclination, and secondly by allowing the EMMET's argument of perigee to regress, due to additional perturbations resulting from a non-spherical Earth, at a known rate which is dependent upon the orbit's inclination, semi-major axis and eccentricity. Payload transfers are conducted to the Moon when the apse line of the EMMET's orbit is aligned with the node line of the lunar orbit. To conduct payload catch and throw operations; the ascending node of the EMMET's orbit must be diametrically opposite to the Moon's ascending node at the instant of payload release which is satisfied by them being 180° out of phase. In addition to this, its argument of perigee must lie within the Earth's equatorial plane which is satisfied by the coincidence of the EMMET's ascending node and perigee positions and occurs when the argument of perigee is 0°. In reality, the argument of perigee will continue to regress whilst the EMMET is completely unladen and the catch and throw operations will be performed at arguments of perigee which are symmetrical about the 0° point, for greater or lesser time periods between these operations the argument of perigee adjustment manoeuvre can itself be adjusted without affecting the overall design.

Variations in the Moon's ascending node and the EMMET's argument of perigee can be accounted for by means of two orbital manoeuvers: the first manoeuvre alters the ascending node of the EMMET's orbit to align it with the predicted lunar orbit node line at the succeeding payload transfer opportunity whilst the second manoeuvre alters the argument of perigee of the EMMET's orbit to the required position such that it will regress into alignment with the equatorial plane at the correct instant for transfers to occur. By performing these adjustment manoeuvres for every orbit of the Moon about Earth; payload transfers can be conducted

on every occasion that the Moon crosses the ascending node of its orbit about Earth. The modification to the logistical requirements of the system and the timing of the systems operational procedure as result of the oscillation of the Moon's ascending node about a mean right ascension of $0°$ can be incorporated into the overall system design by performing the operational procedure time periods an even integer harmonic of the EM-MET's orbital period earlier or later in the Moon's orbit about Earth in order to accommodate the regression of the ascending node as described in Section 2.4.

Having described several methods by which the Moon's ascending node can be tracked over an extended time period, the focus of this chapter will turn to the derivation of the positions in the EMMET's trajectory at which these orbital manoeuvers should be conducted for the adjustment of their respective orbital parameters, and in addition to this the changes in velocity required to perform these manoeuvres.

3.2 Ascending Node Adjustment

According to Vallado [42], the right ascension of the ascending node of a circular orbit or an elliptical polar orbit can be modified by a single impulse manoeuvre occurring at one of two common points of intersection between the initial and final orbits. Impulses occurring at points other than these points of intersection will cause alterations to both the orbital inclination and the ascending node. For the purpose of tracking the ascending node of the Moon's orbit; the impulsive change in velocity must occur at a point of intersection between the EMMET's initial and final orbits to retain orbital inclination. For moon-tracking configurations that allow precession of the ascending node, the final orbit must have an ascending node which takes into account the predicted regression of the EMMET's ascending node during the time interval between payload launch and capture as well as the time interval between payload transfer opportunities. In addition to this, the change in the ascending node angle of the Moon's orbit must be incorporated into the adjustment to ensure correct alignment at the next transfer opportunity. For critically

inclined moon-tracking orbits, the ascending node of the final orbit will be positioned such that its apse line will precess into alignment with the Moon's node line in the time period between the adjustment manoeuvre and the succeeding payload transfer opportunity. For polar inclined moon-tracking orbits the manoeuvre required is simply the alignment of the EMMET's apse line with the predicted position of the Moon's node line at the next transfer opportunity. The change in velocity required to perform the manoeuvre can be calculated by first, determining the points of intersection of the initial and final orbits, obtained by finding the true anomaly of the trajectories at these points, and secondly, by obtaining the velocities of the orbits at the intersection. The change in velocity required is then simply the difference between the velocity vectors of the initial and final orbits at their point of intersection.

A method to calculate the true anomaly at which two orbits intersect when they are identical in every respect other than an increment in the angle of their ascending nodes will now be outlined; we begin by defining the ascending node in the final orbit, Ω_f, in terms of the ascending node in the initial orbit, Ω_i, plus some increment, $\Delta\Omega$, which we define as:

$$\Omega_f = \Omega_i + \Delta\Omega \tag{3.1}$$

The location of the EMMET's central facility in each orbit about Earth can now be determined in its perifocal frame, in this case the satellite's orbital plane [42] is the fundamental plane. The axes in this frame are denoted (P, Q, W) and its origin coincides with the centre of Earth. The P axis points towards the perigee of the satellite's orbit with the Q axis perpendicular to this in the direction of motion, the W axis points normal to the (P, Q) axes, out of the orbital plane. We begin by designating the perifocal position vectors of the initial, $\vec{r_i}$, and final, $\vec{r_f}$, trajectories as:

$$\vec{r_i} = \begin{bmatrix} x_i & y_i & 0 \end{bmatrix}^T \tag{3.2}$$

$$\vec{r_f} = \begin{bmatrix} x_f & y_f & 0 \end{bmatrix}^T \tag{3.3}$$

These perifocal positions are converted into the geocentric equatorial frame, the coordinate frame in which the adjustments to the ascending node are to be made. The equatorial frame also originates at the centre

of Earth with the equator as its fundamental plane [42]. The axes in this frame are denoted (I, J, K) with the I axis pointing towards the vernal equinox, defined as the ascending node of the Sun as viewed from Earth [42], the J axis lies perpendicular to this, in an anti-clockwise direction, and the K axis points towards the North Pole. The conversion from perifocal position, $\vec{r}_{per}$, to geocentric equatorial position, $\vec{r}_{eq}$, is achieved by the application of the perifocal to equatorial transformation matrix, R_G, to the perifocal position:

$$\vec{r}_{eq} = R_G.\vec{r}_{per} \tag{3.4}$$

Where the perifocal to equatorial transformation matrix is defined as [42]:

$$R_G =$$

$$\begin{bmatrix} \cos\Omega\cos\omega - \sin\Omega\sin\omega\cos i & -\cos\Omega\sin\omega - \sin\Omega\cos\omega\cos i & \sin\Omega\sin i \\ \sin\Omega\cos\omega + \cos\Omega\sin\omega\cos i & -\sin\Omega\sin\omega + \cos\Omega\cos\omega\cos i & -\cos\Omega\sin i \\ \sin\omega\sin i & \cos\omega\sin i & \cos i \end{bmatrix}$$

$$\tag{3.5}$$

The transformation matrix relates the equatorial frame to the perifocal frame by a series of three rotations, as shown in Figure (3.3); the first rotation is about the K axis through an angle equal to the angle of ascending node of the orbit, denoted by Ω, the second is about an axis which was initially coincident with the I axis through an angle equal to the orbital inclination, denoted by i, and finally about an axis which was initially coincident with the new K axis through an angle equal to the argument of perigee, denoted by ω.

For the initial and final orbits to intersect, their equatorial position vectors must be equal, as must be their vector components at these points. From the conversion of the position vectors at the point of intersection we have three scalar equations, one for each component in the equatorial frame. Here the (x, y) coordinates of intersection in the perifocal frames of the initial, (x_i, y_i), and final orbits, (x_f, y_f), are the four unknowns. In this case, the change in ascending node is between two orbits which differ only in their angle of ascending node whilst their inclination and argument of perigee remain identical. Equating the I axis
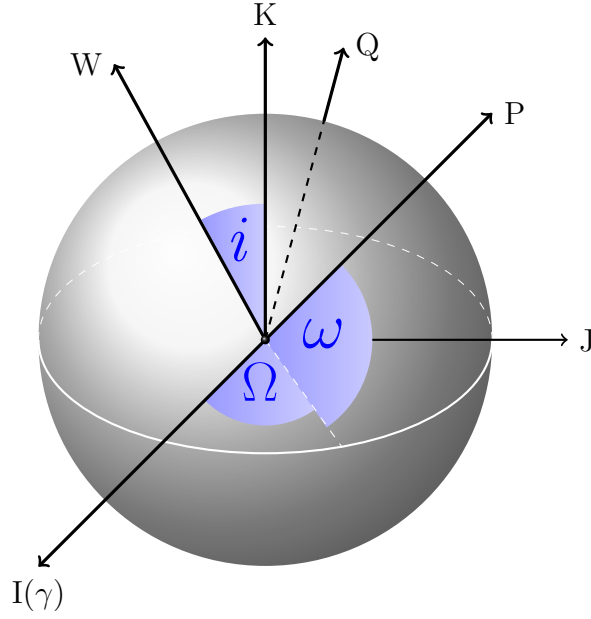
Figure 3.3: Perifocal and equatorial frame orientation

components of the initial and final orbits in the equatorial frame yields:

$$(cos\Omega_i cos\omega - sin\Omega_i sin\omega cosi)x_i - (cos\Omega_i sin\omega + sin\Omega_i cos\omega cosi)y_i =$$
$$(cos\Omega_f cos\omega - sin\Omega_f sin\omega cosi)x_f - (cos\Omega_f sin\omega + sin\Omega_f cos\omega cosi)y_f$$

$$(3.6)$$

Equating the J axis components of the initial and final orbits yields:

$$(sin\Omega_i cos\omega + cos\Omega_i sin\omega cosi)x_i - (sin\Omega_i sin\omega - cos\Omega_i cos\omega cosi)y_i =$$
$$(sin\Omega_f cos\omega + cos\Omega_f sin\omega cosi)x_f - (sin\Omega_f sin\omega - cos\Omega_f cos\omega cosi)y_f$$

$$(3.7)$$

Equating the K axis components of the initial and final orbits yields:

$$(sin\omega sini)x_i + (cos\omega sini)y_i = (sin\omega sini)x_f + (cos\omega sini)y_f \qquad (3.8)$$

The (x, y) components of the orbits in their perifocal frames can be re-written in plane polar coordinates in terms of radial distance, r, and true anomaly, θ:

$$x = rcos\theta \qquad (3.9)$$

$$y = rsin\theta \qquad (3.10)$$

Applying equations (3.9) and (3.10), in addition to the fact that the radial distance from the centre of Earth to the point of intersection is

the same for both the initial and final orbits irrespective of the coordinate frame, equation (3.8) becomes:

$$sin\omega sin i cos\theta_i + cos\omega sin i sin\theta_i = sin\omega sin i cos\theta_f + cos\omega sin i sin\theta_f \quad (3.11)$$

The only unknowns are now the true anomalies at the points of intersection in the initial, θ_i, and final, θ_f, orbits. Canceling the common inclination terms and using trigonometric sum and difference formulas [43] yields:

$$sin(\theta_i + \omega) = sin(\theta_f + \omega) \quad (3.12)$$

Canceling the sine and argument of perigee terms results in:

$$\theta_i = \theta_f \quad (3.13)$$

The initial and final trajectories unsurprisingly intersect at the same true anomaly in both orbital paths. The true anomaly at which the orbits intersect can be found in the following way; firstly, by replacing the (x, y) coordinates in the perifocal frame by their polar form in either equation (3.6) or (3.7), in this case equation (3.6) is used; secondly, by canceling out the common radial distance terms; and finally, substituting in the true anomaly of the final orbit for that of the initial orbit, yielding:

$$(cos\Omega_i cos\omega - sin\Omega_i sin\omega cos i)cos\theta_f - (cos\Omega_i sin\omega + sin\Omega_i cos\omega cos i)sin\theta_f =$$
$$(cos\Omega_f cos\omega - sin\Omega_f sin\omega cos i)cos\theta_f - (cos\Omega_f sin\omega + sin\Omega_f cos\omega cos i)sin\theta_f$$
$$(3.14)$$

Multiplying out and collecting like terms gives:

$$(cos\Omega_i - cos\Omega_f)cos\omega cos\theta_f - (sin\Omega_i - sin\Omega_f)sin\omega cos i cos\theta_f =$$
$$(cos\Omega_i - cos\Omega_f)sin\omega sin\theta_f + (sin\Omega_i - sin\Omega_f)cos\omega cos i sin\theta_f \quad (3.15)$$

This is further simplified using trigonometric sum and difference formulas [43]:

$$(cos\Omega_i - cos\Omega_f)cos(\theta_f + \omega) = (sin\Omega_i - sin\Omega_f)cos i sin(\theta_f + \omega) \quad (3.16)$$

Further rearrangement and the application of the sum to product rule for trigonometric functions [43] yields the equation for the true anomaly of intersection:

$$tan(\theta_f + \omega) = -tan\left(\frac{\Omega_i + \Omega_f}{2}\right)sec i = -tan\left(\Omega_i + \frac{\Delta\Omega}{2}\right)sec i \quad (3.17)$$

56

At this point the quadrants of the two points of intersection can be determined in the standard manner and their true anomalies are found by subtracting the argument of perigee, ω, from the angles obtained.

For moon-tracking orbits which have polar inclinations relative to the equatorial frame, equation (3.17) will tend to infinity as a result of the $sec i$ term. A method of establishing the true anomaly at which two polar orbits intersect can be obtained by again utilising equations (3.9) and (3.10), in addition to the radial distance at the point of intersection being the same for both the initial and final orbits. Having established that the true anomaly at the point of intersection will be the same in both orbits, we replace the true anomaly of both the initial and final orbits by θ and then, by collecting like trigonometric terms, equation (3.7) becomes:

$$(cos\Omega_i - cos\Omega_f)cos\omega cos\theta - (sin\Omega_i - sin\Omega_f)sin\omega cos i cos\theta =$$

$$(cos\Omega_i - cos\Omega_f)sin\omega sin\theta + (sin\Omega_i - sin\Omega_f)cos\omega cos i sin\theta \qquad (3.18)$$

Application of the trigonometric sum and difference formulas [43] and rearrangement of equation (3.18) yields:

$$cos(\theta + \omega) = sin(\theta + \omega)\left(\frac{sin\Omega_i - sin\Omega_f}{cos\Omega_i - cos\Omega_f}\right)cos i \qquad (3.19)$$

For polar inclinations; $cos\ i = 0$, therefore:

$$\theta + \omega = \qquad 90° \qquad or \qquad 270° \qquad (3.20)$$

Depending upon our choice for the argument of perigee for the EMMET's orbit, the true anomaly at the first point of intersection of the initial and final orbits will occur at:

$$\theta = 90° - \omega \qquad or \qquad 270° - \omega \qquad (3.21)$$

Having determined the true anomaly at which the orbital manoeuvre should take place, the velocity at this point in each orbit can be determined and ultimately the change in velocity required to perform the manoeuvre. This will be the focus of the following section.

3.2.1 Velocity Requirements

The next step is to determine the velocity vectors of the two orbits at their point of intersection and the change in velocity required to perform
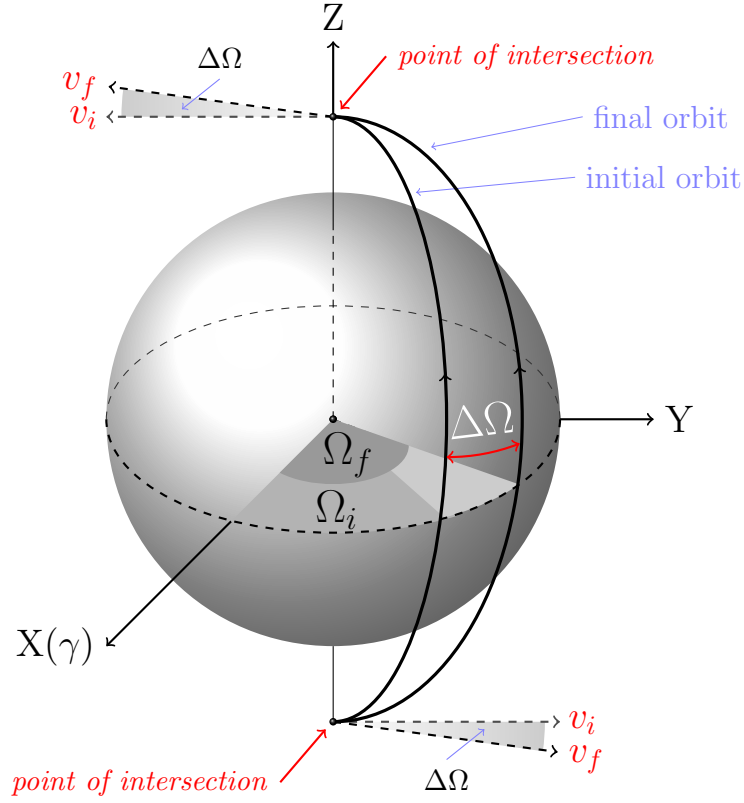
Figure 3.4: Polar orbit intersections for $\Delta\Omega$

the manoeuvre between them. To change the angle of ascending node of an orbit relative to Earth's equatorial frame without affecting the other orbital parameters, it is evident from the manoeuvre occurring at the same true anomaly on both orbits that the manoeuvre required is simply the rotation of the velocity vector of the initial orbit at its point of intersection, about the equatorial K axis, through an angle $\Delta\Omega$ equal to the required change in right ascension. This can be accomplished by means of the Rodriguez Formula [44][45] which is the kinematic form of the rotation matrix and expresses the matrix required to transform the initial velocity vector to the final velocity vector in terms of the angle of rotation and a unit vector along the axis of rotation. In this case, the rotation matrix, R_K, can be written [44][45]:

$$R_K(\Delta\Omega) = [I + S sin\Delta\Omega + S^2(1 - cos\Delta\Omega)] \qquad (3.22)$$

Where I is the 3x3 identity matrix and S, in this case, is a particularly simple skew symmetric matrix:

$$S = \begin{bmatrix} 0 & -1 & 0 \\ 1 & 0 & 0 \\ 0 & 0 & 0 \end{bmatrix} \tag{3.23}$$

The velocity of the final orbit, $\vec{v}_f$, relative to the equatorial frame can be found by applying equation (3.22) to the velocity of the initial orbit, $\vec{v}_i$, at the point of intersection:

$$\vec{v}_f = R_K(\Delta\Omega)\vec{v}_i \tag{3.24}$$

The velocity of the body in the initial orbit at the point of intersection relative to the equatorial frame can be calculated from its velocity relative to the perifocal frame. Standard practice assumes that the perifocal frame is fixed in space relative to the equatorial frame, but in the moon-tracking configurations described the orbit is being treated as a precessing inclined ellipse with a time-varying argument of perigee or ascending node, or both; it must therefore be treated as a rotating frame of reference. Dependent upon the moon-tracking method used, the rotational rate of the perifocal frame will consist of a rotation about the perifocal W axis at a rate identical to the rate of change of the argument of perigee, $\dot{\omega}$, and a rate identical to the rate of change of the ascending node, $\dot{\Omega}$, about the K axis of the equatorial frame. The velocity of the body in the perifocal frame, $\vec{v}_{per}$, is subsequently transformed into the equatorial frame, $\vec{v}_{eq}$, using the basic kinematic equation [42]:

$$\vec{v}_{eq} = \vec{v}_{per} + \vec{\Omega}_{eq} \times \vec{r}_{per} + \vec{v}_o \tag{3.25}$$

All the terms in equation (3.25) have components measured relative to the equatorial frame. The first term in equation (3.25) is simply the orbital velocity of the EMMET in the perifocal frame with its components transformed into the equatorial frame, $\vec{v}_{per}$. As a result of the moon-tracking method used; the angular velocity vector of the perifocal frame, $\vec{\Omega}_{per}$, potentially has components in same direction as the W axis of the perifocal frame measured relative to the equatorial frame, potentially components in the K direction of the equatorial frame or a precessional

rate consisting of both. The velocity of the origin of the perifocal frame, $\vec{v}_o$, the final term in equation (3.25), is zero as its origin remains coincident with that of the equatorial frame at the centre of Earth. The change in velocity required to perform the orbital manoeuvre, $\Delta \vec{v}$, can be written, using equation (3.24), solely in terms of the velocity of the initial orbit relative to the equatorial frame and the required change in the angle of ascending node as:

$$\Delta \vec{v} = \vec{v}_f - \vec{v}_i = R_K(\Delta \Omega)\vec{v}_i - \vec{v}_i = (R_K(\Delta \Omega) - I)\vec{v}_i \qquad (3.26)$$

Equation (3.26) will be used in Chapter 5 to calculate the change in velocity required to perform this orbital adjustment for different configurations of the EMMET's orbit. It has been shown that this manoeuvre must be conducted at a true anomaly where the two orbits intersect which is not necessarily at a point where the orbital velocity is at a minimum, it would therefore be most efficient for this manoeuvre to be conducted between payload launch and capture operations as long as the change in ascending node was small enough not to significantly affect overall trajectory design and disadvantage the return payload. Data accumulated on the magnitude of the required change will clarify matters.

3.3   Argument of Perigee Adjustment

According to Curtis [47], the opportunity to transfer between intersecting orbits which have a common focus but have apse lines which are not collinear, via a single impulse manoeuvre, occurs at points where the two orbits intersect. To make the required adjustment to the argument of perigee, the impulsive manoeuvre must occur where the EMMET's initial and final orbits intersect. Furthermore, for moon-tracking configurations that allow precession of the argument of perigee and perform manoeuvres to correctly align it, the final orbit must have an argument of perigee which takes into account the predicted regression of the argument of perigee during the time interval between payload launch and capture as well as the time interval between payload transfer opportunities. The argument of perigee of the final orbit will be positioned is such a manner that it will regress into its required launch position in the time

period between the adjustment manoeuvre and the succeeding payload transfer opportunity. The total adjustment required can be most simply expressed as being equal to the angle through which the EMMET's argument of perigee will regress in the time taken for the Moon to orbit the Earth, as this will account for all variations to this parameter in the intervening time period between adjustment manoeuvers. The velocity change required to perform the manoeuvre can be calculated in a similar way to that required for the ascending node adjustment. Firstly, the points of intersection of the initial and final orbits are determined by obtaining the true anomaly of the respective orbits at these points of intersection, and secondly, the velocities of the orbits at these intersections are then determined. The velocity change required is simply the difference in the velocity vectors of the initial and final orbits.

3.3.1 Position Requirements

As in the ascending node case the initial, ω_i, and final, ω_f, orbits are identical except for a positive increment in the argument of perigee, $\Delta\omega$, of the final orbit from the initial orbit which we can define as:

$$\omega_f = \omega_i + \Delta\omega \tag{3.27}$$

For orbits which have regressing arguments of perigee, a positive increment in the argument of perigee is required and satisfied by equation (3.27). For those with precessing arguments of perigee, equation (3.27) should be redefined as $\omega_i = \omega_f + \Delta\omega$. For two co-planar elliptical orbits with an increment in the argument of perigee of one relative to another but otherwise identical; the orbits will intersect at two points. The radial distance from the centre of Earth to these points of intersection are identical for both orbits and we begin by equating the radial distance of these points of intersection and re-writing the equations in terms of the components of the initial and final orbits relative to their respective perifocal frames:

$$r_i = \sqrt{x_i^2 + y_i^2} = \sqrt{x_f^2 + y_f^2} = r_f \tag{3.28}$$

Simplifying equation (3.28) and re-arranging yields:

$$(x_i^2 - x_f^2) = -(y_i^2 - y_f^2) \tag{3.29}$$

Re-writing the perifocal components in their polar form using equations (3.9) and (3.10) and canceling out common radial distance terms we obtain:

$$(cos^2\theta_i - cos^2\theta_f) = -(sin^2\theta_i - sin^2\theta_f) \qquad (3.30)$$

Again, by equating the radial distance of the points of intersection in each orbit, but in this instance substituting in the equation for an elliptical orbit, we obtain [47]:

$$r_i = \frac{h_i^2}{\mu(1 + e_i cos\theta_i)} = \frac{h_f^2}{\mu(1 + e_f cos\theta_f)} = r_f \qquad (3.31)$$

where h and e are the specific angular momentum and eccentricity of the EMMETs orbit, which will be defined in Chapters 4 and 5, respectively; and μ is Earth's gravitational parameter. The only difference between the orbits is in the argument of perigee, therefore equation (3.31) reduces to:

$$cos\theta_i = cos\theta_f \qquad (3.32)$$

Substituting equation 3.32 into equation 3.30 we obtain:

$$sin\theta_i = \pm sin\theta_f \qquad (3.33)$$

A positive (anti-clockwise) rotation of the argument of perigee, as well the initial and final orbits, are shown in Figure (3.5). For the points of intersection between the initial and final orbits; the point of intersection in the final orbit will lag a quadrant behind the point of intersection in the initial orbit relative to their respective perifocal frames. Furthermore, this intersection will occur in the region between their respective x axes and is denoted by $\Delta\omega$. For a negative rotation of the argument of perigee, the point of intersection in the initial orbit will lag a quadrant behind the point of intersection in the final orbit. Having located the EMMET's central facility relative to the perifocal frame, its position is again converted into the equatorial frame, using equation (3.5). Once again, by equating the position vectors of the initial and final orbits, we obtain three scalar equations. However, on this occasion, the difference is the argument of perigee of the initial and final orbits. Equating the I axis components of the initial and final orbits relative to the equatorial
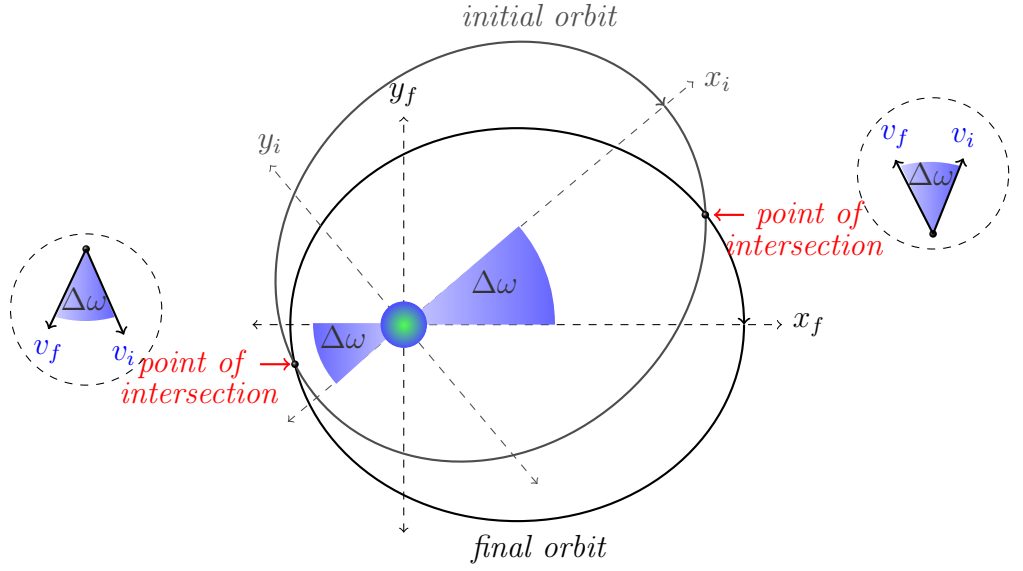
Figure 3.5: Intersection quadrants for positive $\Delta\omega$

frame yields:

$$(cos\Omega cos\omega_i - sin\Omega cos isin\omega_i)x_i - (cos\Omega sin\omega_i + sin\Omega cos icos\omega_i)y_i =$$
$$(cos\Omega cos\omega_f - sin\Omega cos isin\omega_f)x_f - (cos\Omega sin\omega_f + sin\Omega cos icos\omega_f)y_f$$
$$(3.34)$$

Substituting in equations (3.9) and (3.10); equation (3.34) becomes:

$$(cos\Omega cos\omega_i - sin\Omega cos isin\omega_i)cos\theta_i - (cos\Omega sin\omega_i + sin\Omega cos icos\omega_i)sin\theta_i =$$
$$(cos\Omega cos\omega_f - sin\Omega cos isin\omega_f)cos\theta_f - (cos\Omega sin\omega_f + sin\Omega cos icos\omega_f)sin\theta_f$$
$$(3.35)$$

Treating each side of equation (3.35) as a linear combination of sine and cosine functions [43] and assuming that Ω and i are positive yields:

$$sin(\theta_i + \omega_i + \pi + \xi) = sin(\theta_f + \omega_f + \pi + \xi) \qquad (3.36)$$

where:

$$\xi = arcsin\left(\frac{cos\Omega}{\sqrt{1 - sin^2\Omega sin^2 i}}\right)$$

Canceling out the sine and the other common terms we obtain:

$$\theta_i + \omega_i = \theta_f + \omega_f \qquad (3.37)$$

Re-arranging equation 3.37 and substituting in equation (3.27) yields:

$$\theta_i = \theta_f + \Delta\omega \qquad (3.38)$$

We can now calculate the true anomaly of both orbits at the point of intersection in the first quadrant of the initial orbit and from Figure (3.5) we see that this will occur in the fourth quadrant of the final orbit. In this case, the cosines of the true anomalies in both orbits will be positive but the sine of the true anomaly in the final orbit will be the negative of the sine of the true anomaly in the initial orbit. Replacing the (x, y) coordinates in equation (3.34) with their polar form and substituting the true anomalies in the final orbit with their equivalents in the initial orbit, we cancel out common radius terms to obtain:

$$(cos\Omega cos\omega_i - sin\Omega cos i sin\omega_i)cos\theta_i - (cos\Omega sin\omega_i + sin\Omega cos i cos\omega_i)sin\theta_i =$$
$$(cos\Omega cos\omega_f - sin\Omega cos i sin\omega_f)cos\theta_i + (cos\Omega sin\omega_f + sin\Omega cos i cos\omega_f)sin\theta_i$$
$$(3.39)$$

Collecting like terms yields:

$$(cos\omega_i - cos\omega_f)cos\Omega cos\theta_i - (sin\omega_i - sin\omega_f)sin\Omega cos i cos\theta_i =$$
$$(sin\omega_i + sin\omega_f)cos\Omega sin\theta_i + (cos\omega_i + cos\omega_f)sin\Omega cos i sin\theta_i \qquad (3.40)$$

Utilising the trigonometric sum-to-product formulas [43] and canceling like terms we obtain:

$$cos\theta_i sin\left(\frac{\Delta\omega}{2}\right) = sin\theta_i cos\left(\frac{\Delta\omega}{2}\right) \qquad (3.41)$$

Equation 3.41 simplifies to:

$$\theta_i = \frac{\Delta\omega}{2} \qquad (3.42)$$

From equation 3.38, the true anomaly at the point of intersection in the final orbit becomes:

$$\theta_f = -\frac{\Delta\omega}{2} \qquad (3.43)$$

Alterations to orbital parameters are most efficient when conducted close to the apogee of an orbit as the velocities are minimised. For the adjustment to the argument of perigee to occur close to the apogee of the initial orbit; this corresponds to the third quadrant of the initial orbit and the second quadrant of the final orbit. In this case, the cosines of the true anomalies will both be negative, but the sine of the true anomaly of the initial orbit will be negative whilst the sine of the true anomaly of the

final orbit will be positive. Following the method used previously the true anomaly at the point of intersection in the initial orbit is found to be:

$$\theta_i = \pi + \frac{\Delta\omega}{2} \tag{3.44}$$

This is as expected and yields the true anomaly in the final orbit as:

$$\theta_f = \pi - \frac{\Delta\omega}{2} \tag{3.45}$$

Having determined the true anomaly at which the adjustment to the argument of perigee should occur, the velocity at this point in both the initial and final orbits will be determined allowing the required change in velocity to be calculated, and this will be the focus of the final section of this chapter.

3.3.2 Velocity Requirements

The final step is to determine the velocity vectors of the two orbits at their intersection and the change in velocity required to perform the manoeuvre between them. We can define the velocity at the point of intersection in each orbit by its perifocal velocity vector as:

$$\vec{v}_{per} = \left(\frac{\mu}{h}\right) \begin{bmatrix} -sin\theta & e + cos\theta & 0 \end{bmatrix}^T \tag{3.46}$$

From equation (3.33) and Figure (3.5) we can see that at the points of intersection close to perigee and apogee, the cosines of the true anomaly in both orbits are identical whilst their sine functions differ only in direction. Therefore, the manoeuvre required is simply the rotation of the velocity vector of the initial orbit at its point of intersection about the W axis of its perifocal frame through an angle $\Delta\omega$, equal to the required change in the argument of perigee. The Rodriguez Formula [44][45] can again be utilised and is written as:

$$R_K(\Delta\omega) = [I + Ssin\Delta\omega + S^2(1 - cos\Delta\omega)] \tag{3.47}$$

In this case, the skew symmetric matrix, S, can be written in terms of the unit vector along the axis of rotation relative to the equatorial frame. The unit vector of the perifocal frame W axis relative to the equatorial

frame, denoted $\vec{i}_W$, is:

$$\vec{i}_W = \begin{bmatrix} sin\Omega sini \\ -cos\Omega sini \\ cosi \end{bmatrix} \qquad (3.48)$$

The skew symmetric matrix, S, can therefore be written:

$$S = \begin{bmatrix} 0 & -cosi & cos\Omega sini \\ cosi & 0 & -sin\Omega sini \\ -cos\Omega sini & sin\Omega sini & 0 \end{bmatrix} \qquad (3.49)$$

The velocity of the final orbit relative to the equatorial frame can be found by applying equation (3.47) to the velocity of the initial orbit at the point of intersection:

$$\vec{v}_f = R_K(\Delta\omega)\vec{v}_i \qquad (3.50)$$

Again the initial velocity at the point of intersection relative to the perifocal frame is converted into the equatorial frame using the basic kinematic equation, equation (3.25). As in the previous case, the argument of perigee is time varying, and the angular velocity term is the result of this variation and will be identical to that for the ascending node case. The change in velocity required to perform the orbital manoeuvre can be written:

$$\Delta\vec{v} = \vec{v}_f - \vec{v}_i = (R_K(\Delta\omega) - I)\vec{v}_i \qquad (3.51)$$

We have now obtained an expression in equation (3.51) which allows us to calculate the magnitude of the change in velocity required to adjust the argument of perigee from its value in the initial orbit to the specified configuration required for a successive orbital transfer manoeuvre to be undertaken relative to the equatorial frame which will be utilised in Chapter 5. It has been shown that this manoeuvre can be conducted close to the apogee of the EMMET's orbit where its velocity is at a minimum. However, depending upon the rate of regression of the argument of perigee it remains to be seen whether this manoeuvre can be performed between payload launch and capture operations, when the EMMET's mass is at a minimum, without significantly compromising the perigee position of the return payload. This will become clearer in Chapter 5 when numerical data can be obtained.

3.4   Conclusions

Several configurations which allow the EMMET's orbit to track the ascending or descending node of the Moon's orbit relative to both the geocentric equatorial and ecliptic frames of reference have been described. As a result of the variation in the orbital inclination of an EMMET configured relative to the ecliptic frame and resulting from the increased attraction to Earth's equator when in orbit, configurations relative to this frame have been disregarded. It was found that the most promising configurations for moon-tracking were for EMMET's in either polar or critically inclined orbits. For critically inclined orbits, a single adjustment to the angle of the ascending once per-lunar-orbit would allow the EMMET's apse line to become aligned with the Moon's ascending node when a known regression of this apse line was accounted for. For polar orbits, either single manoeuvre or dual manoeuvre configurations are available, however the single manoeuvre case is dependent upon the frequency of re-alignment of the EMMET's apse line with the fundamental plane of the equatorial frame. It is unlikely that the frequency of this re-alignment will be sufficient and it is predicted that the dual manoeuvre configuration will prove more favourable for transfer opportunities using a polar orbit conclugation.

Having described means by which the EMMET can track the Moon's nodes, equations were derived for both polar and non-polar inclination orbits which allowed the points of intersection between two almost identical orbits, with the exception being in differing angles of ascending node, to be calculated. For polar orbits this intersection was found to occur at a true anomaly of 90°, for non-polar orbits this true anomaly occurs at the same point in each orbit and is dependent upon the orbital inclination. Additionally, the Rodriguez formula was utilised to formulate expressions for the velocity change required to translate from one orbit to another solely in terms of the velocity in the initial orbit at the point of intersection. This was found to consist of a rotation of the velocity vector about the K axis of the equatorial frame. Equations were also derived which allowed the points of intersection for two non-critically in-

clined orbits to be calculated when they differed only in their arguments of perigee. This intersection was found to occur at a true anomaly equal to half the required alteration to the argument of perigee. Furthermore, the Rodriguez formula was again utilised to express the velocity change required to translate from one orbit to another solely in terms of the velocity in the initial orbit at this calculated point of intersection. In this case, the rotation of the velocity vector was about an axis parallel with the angular velocity vector of the orbit relative to the equatorial frame. Having described several possible configurations which will allow the EMMET to be configured to conduct payload exchanges when the Moon crosses the ascending or descending node of its orbit, our attention now turns to the derivation of the EMMET's dynamics which will allow us to determine the position, velocity and acceleration acting on the EMMET and payloads at any point in their orbit about Earth, in addition to allowing us to determine the velocity of the payloads at their instant of release from their tether tips. Furthermore, the accelerations acting on the system can be used to determine the maximum tension acting on the tether sub-spans as a result of the EMMET's motion about Earth in addition to the attachment of their payload masses to the tips. This is the focus of the following chapter with the aim that, in conjunction with the current focus, data can be generated in later chapters which will allow the magnitude of the adjustments required to track the Moon's orbit to be obtained and, in conjunction with later trajectory designs, the most efficient transfer configuration can be identified.

4.   EMMET Dynamics

The equations used to describe the position, velocity and acceleration of
the central facility; upper and lower payloads; as well as any point along
the tether sub-spans will now be developed for the EMMET relative to
the geocentric equatorial frame of reference. This model can be developed
most simply by considering the two-body problem, and only the most
significant gravitational perturbations resulting from Earth's oblateness.
To simplify matters further; these equations will be developed for pay-
loads treated as point masses in addition to initially inextensible tether
sub-spans, and the resulting acceleration terms will be utilised to formu-
late expressions for the tension occurring within these sub-spans. The
maximum angular velocity that the tether sub-spans can withstand as a
result of their rotation about the central facility will then be developed
with the aim of determining the maximum increment to velocity that a
given EMMET configuration can impart to a payload mass. This will
be used, in Chapter 5, to determine the maximum launch velocity of the
payload from the upper EMMET tip, which occurs at the instant that
the central facility is at the perigee of its orbit, where orbital velocity
is greatest, and when the tether sub-spans are aligned along the local
gravity gradient, giving the largest upper tip velocity relative to Earth
as a result of tether rotation. Ultimately, this allows us to determine
whether a specified EMMET configuration is suitable for imparting suf-
ficient velocities to payloads released from the upper tether tip for them
to reach the Moon.

4.1   Position, Velocity and Acceleration

The position, velocity and acceleration of the components of the EM-
MET are initially defined relative to a body fixed frame coincident with
the EMMET's central facility. These components are transformed into
the perifocal frame and finally into the geocentric equatorial frame, the
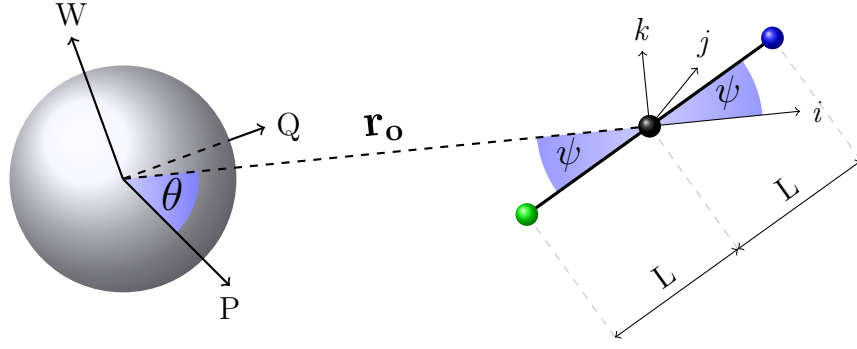
Figure 4.1: Body frame and EMMET configuration

frame in which the Earth-Moon trajectories will be designed. The derivation of these equations will focus on the upper payload at present but can be adjusted for the central facility, by setting the tether sub-span length equal to zero; for the lower payload, by adjusting the tether rotation angle relative to the body frame by 180°, or any point along the tether sub-span, by defining its distance along the length and whether it is along the instantaneous upper or lower sub-span. As the payloads are treated as point masses, the payload's position is coincident with the tether tip and their velocity and acceleration are identical. We will therefore derive the position, velocity and acceleration of the upper tip in the following subsections and references to upper payload or upper tip can be considered as being one and the same.

Body Frame Components

We begin by defining the position vector of the upper tip relative to a body fixed frame. The body frame has its origin located at the central facility and its fundamental plane is co-planar with the EMMET's orbital plane. The i axis points along the local gravity gradient with its positive direction away from Earth, its j axis is perpendicular to this in an anti-clockwise direction and its k axis is perpendicular to this fundamental plane. The upper tip's position is defined by two coordinates, L is the tether sub-span length and ψ is the angle that the tip makes with the body frame i axis, shown in Figure (4.1). The velocity and acceleration as functions of time are found by successive differentiation of the position vector. The position, velocity and acceleration vectors relative to the

body frame are defined as:

$$\vec{r}_u = \begin{bmatrix} Lcos\psi & Lsin\psi & 0 \end{bmatrix}^T \tag{4.1}$$

$$\vec{v}_u = \begin{bmatrix} -\dot{\psi}Lsin\psi & \dot{\psi}Lcos\psi & 0 \end{bmatrix}^T \tag{4.2}$$

$$\vec{a}_u = \begin{bmatrix} -L\left(\ddot{\psi}sin\psi + \dot{\psi}^2cos\psi\right) & L\left(\ddot{\psi}cos\psi - \dot{\psi}^2sin\psi\right) & 0 \end{bmatrix}^T \tag{4.3}$$

The following subsection will show how these components are transformed into the perifocal frame and will derive their components relative to this frame.

Perifocal Frame Components

The position of the upper tip relative to the body frame, $\vec{r}_u$, can be transformed into the upper tip position relative to the perifocal frame, $\vec{r}_{u-per}$, using the following equation:

$$\vec{r}_{u-per} = \vec{r}_o + R_W(\theta)\vec{r}_u \tag{4.4}$$

Where the origin of the body frame, $\vec{r}_o$, relative to the perifocal frame is simply the position of the central facility relative to the perifocal frame, shown in Figure (4.1) and is found in terms of its radial distance, r and true anomaly, θ, by equations (3.9) and (3.10). The position of the upper payload relative to the body fixed frame is transformed into the perifocal frame using the true anomaly of the central facility and the following elementary rotation matrix about the W axis of the perifocal frame:

$$R_W(\theta) = \begin{bmatrix} cos\theta & -sin\theta & 0 \\ sin\theta & cos\theta & 0 \\ 0 & 0 & 1 \end{bmatrix} \tag{4.5}$$

The velocity of the payload relative to the perifocal frame, $\vec{v}_{u-per}$, is found by differentiation of equation (4.4) with respect to time:

$$\vec{v}_{u-per} = \vec{v}_o + R_W(\theta)\vec{v}_u + \dot{R}_W(\theta)\vec{r}_u \tag{4.6}$$

The velocity of the EMMET's central facility relative to the perifocal frame, $\vec{v}_o$, is identical to that of the origin of the body frame relative to the perifocal frame and is found using [47]:

$$\vec{v}_o = \sqrt{\frac{\mu}{p}} \begin{bmatrix} -sin\theta & e + cos\theta & 0 \end{bmatrix}^T \tag{4.7}$$

In equation (4.7), the orbital parameter is denoted by p and e denotes the orbital eccentricity. The orbital parameter can be obtained from the specific angular momentum, h, of the EMMET's orbit via [47]:

$$p = \frac{h^2}{\mu} \tag{4.8}$$

The specific angular momentum is obtained from the semi-major axis, a, and eccentricity [47]:

$$h = \sqrt{\mu a \left(1 - e^2\right)} \tag{4.9}$$

The partial derivative with respect to time of equation (4.5), found in equation (4.6), is [43]:

$$\dot{R}_W(\theta) = \frac{\partial R_W(\theta)}{\partial t} = \dot{\theta} \begin{bmatrix} -sin\theta & -cos\theta & 0 \\ cos\theta & -sin\theta & 0 \\ 0 & 0 & 0 \end{bmatrix} \tag{4.10}$$

The rate of change of the true anomaly, denoted by $\dot{\theta}$ in equation (4.10), is equal to the magnitude of the orbital angular velocity of the EMMET's central facility, and is obtained from the specific angular momentum and the radial distance of the EMMET's central facility via the following [47]:

$$\dot{\theta} = \frac{h}{r_o^2} \tag{4.11}$$

The acceleration of the upper payload relative to the perifocal frame, $\vec{a}_{u-per}$, is found by direct differentiation of equation (4.6) with respect to time:

$$\vec{a}_{u-per} = \vec{a}_o + R_W(\theta)\vec{a}_u + 2\dot{R}_W(\theta)\vec{v}_u + \ddot{R}_W(\theta)\vec{r}_u \tag{4.12}$$

The acceleration of the origin of the body frame relative to the perifocal frame, $\vec{a}_o$, is simply the gravitational acceleration acting on the central facility and is given by [44]:

$$\vec{a}_o = -\frac{GM_E}{r_o^3}\vec{r}_o \tag{4.13}$$

where G is the universal gravitation constant and M_E is the mass of Earth. The partial derivative with respect to time of equation (4.10), found in equation (4.12), is [43]:

$$\ddot{R}_W(\theta) = \ddot{\theta} \begin{bmatrix} -sin\theta & -cos\theta & 0 \\ cos\theta & -sin\theta & 0 \\ 0 & 0 & 0 \end{bmatrix} + \dot{\theta}^2 \begin{bmatrix} -cos\theta & sin\theta & 0 \\ -sin\theta & -cos\theta & 0 \\ 0 & 0 & 0 \end{bmatrix} \tag{4.14}$$

Equation (4.14) is simplified by the fact that the angular acceleration acting on the body, $\ddot{\theta}$, is zero as a result of the gravitational force being entirely radial. The position, velocity and acceleration of the upper payload relative to the perifocal frame can be written:

$$\vec{r}_{u-per} = \begin{bmatrix} r_o cos\theta + Lcos(\theta + \psi) \\ r_o sin\theta + Lsin(\theta + \psi) \\ 0 \end{bmatrix} \tag{4.15}$$

$$\vec{v}_{u-per} = \begin{bmatrix} -\sqrt{\frac{\mu}{p}}sin\theta - L(\dot{\theta} + \dot{\psi})sin(\theta + \psi) \\ \sqrt{\frac{\mu}{p}}(e + cos\theta) + L(\dot{\theta} + \dot{\psi})cos(\theta + \psi) \\ 0 \end{bmatrix} \tag{4.16}$$

$$\vec{a}_{u-per} = \begin{bmatrix} -\ddot{\psi}Lsin(\theta + \psi) - (\dot{\theta} + \dot{\psi})^2 Lcos(\theta + \psi) \\ \ddot{\psi}Lcos(\theta + \psi) - (\dot{\theta} + \dot{\psi})^2 Lsin(\theta + \psi) \\ 0 \end{bmatrix} - \frac{GM_E}{r_o^3}\vec{r}_o \tag{4.17}$$

The following subsection will show how these components are transformed into the equatorial frame and will derive their components relative to this frame.

Equatorial Frame Components

The position of the upper tip relative to the equatorial frame, $\vec{r}_{u-eq}$, is equal to the transformation of the position in the perifocal frame by application of equation (3.4), this simple relation is a result of the origin of the perifocal frame coinciding with the origin of the equatorial frame:

$$\vec{r}_{u-eq} = R_G.\vec{r}_{u-per} \tag{4.18}$$

The velocity of the upper payload relative to the equatorial frame, $\vec{v}_{u-eq}$, is found by differentiating equation (4.18) with respect to time:

$$\vec{v}_{u-eq} = R_G.\vec{v}_{u-per} + \dot{R}_G.\vec{r}_{u-per} \tag{4.19}$$

The partial derivative, with respect to time, of equation (3.5), the perifocal to equatorial transformation matrix, is more easily obtained when factors are taken into account which simplify the matrix prior to differentiation. The acceleration of the upper payload relative to the equatorial frame, $\vec{a}_{u-eq}$, is found by differentiating equation (4.19) with respect to

time:

$$\vec{a}_{u-eq} = R_G.\vec{a}_{u-per} + 2\dot{R}_G.\vec{v}_{u-per} + \ddot{R}_G.\vec{r}_{u-per} \qquad (4.20)$$

The equatorial position, velocity and acceleration equations derived will now be applied to the moon-tracking orbit configurations described in Chapter 3

4.1.1 Moon Tracking Components

The equatorial position, velocity and acceleration derived in the preceding section will now be utilised to obtain the position, velocity and acceleration of the EMMET when configured to orbit Earth in each of the moon-tracking orbit configurations described in Chapter 3. In addition to this, their components at the perigee of their orbits will be also obtained for each case.

Moon-Tracking with Polar Inclinations

For moon-tracking orbits relative to the equatorial frame of reference which utilise polar inclinations to render the EMMET's angle of ascending node stationary, be it a single or dual manoeuvre configuration, the perifocal to equatorial transformation matrix, equation (3.5), becomes:

$$R_G = \begin{bmatrix} \cos\Omega\cos\omega & -cos\Omega sin\omega & sin\Omega \\ sin\Omega cos\omega & -sin\Omega sin\omega & -cos\Omega \\ sin\omega & cos\omega & 0 \end{bmatrix} \qquad (4.21)$$

The derivative of equation (4.21) is simplified by the fact that its precession is due solely to the change in argument of perigee of the EMMET's orbit and this is obtained as [43]:

$$\dot{R}_G = \dot{\omega}\begin{bmatrix} -\cos\Omega sin\omega & -cos\Omega cos\omega & 0 \\ -sin\Omega sin\omega & -sin\Omega cos\omega & 0 \\ cos\omega & -sin\omega & 0 \end{bmatrix} \qquad (4.22)$$

The angular rate in equation (4.22) is equal to the rate of change of the argument of perigee, $\dot{\omega}$, of the EMMET's orbit due to the oblateness effects of a non-spherical Earth and the rate of this change will be defined in Chapter 5. The derivative of equation (4.22) is again simplified by the

fact that its change is due solely to the change in argument of perigee of the EMMET orbit [43]:

$$
\ddot{R}_G =
$$

$$
\ddot{\omega} \begin{bmatrix} -\cos\Omega sin\omega & -cos\Omega cos\omega & 0 \\ -sin\Omega sin\omega & -sin\Omega cos\omega & 0 \\ cos\omega & -sin\omega & 0 \end{bmatrix} + \dot{\omega}^2 \begin{bmatrix} -\cos\Omega cos\omega & cos\Omega sin\omega & 0 \\ -sin\Omega cos\omega & sin\Omega sin\omega & 0 \\ -sin\omega & -cos\omega & 0 \end{bmatrix}
$$

$$(4.23)$$

Equation (4.23) is simplified further by the assumption that the angular rate of the argument of perigee is constant and un-accelerated. Using an argument of perigee aligned with the Moon's node line, i.e. $\omega = 0$, as described in Chapter 3, allows us to obtain more simply the position, velocity and acceleration of the upper tip relative to the equatorial frame. Equatorial position, equation (4.18), becomes:

$$
\vec{r}_{u-eq} = \begin{bmatrix} cos\Omega(r_o cos\theta + Lcos(\theta + \psi)) \\ sin\Omega(r_o cos\theta + Lcos(\theta + \psi)) \\ r_o sin\theta + Lsin(\theta + \psi) \end{bmatrix}
$$

$$(4.24)$$

Equatorial velocity, equation (4.19), becomes:

$$
\vec{v}_{u-eq} =
$$

$$
\begin{bmatrix} -cos\Omega\left(\left(\sqrt{\frac{\mu}{p}} + \dot{\omega}r_o\right)sin\theta + L(\dot{\theta} + \dot{\psi} + \dot{\omega})sin(\theta + \psi)\right) \\ -sin\Omega\left(\left(\sqrt{\frac{\mu}{p}} + \dot{\omega}r_o\right)sin\theta + L(\dot{\theta} + \dot{\psi} + \dot{\omega})sin(\theta + \psi)\right) \\ \left(\sqrt{\frac{\mu}{p}}\left(1 + \frac{e}{cos\theta}\right) + \dot{\omega}r_o\right)cos\theta + L(\dot{\theta} + \dot{\psi} + \dot{\omega})cos(\theta + \psi) \end{bmatrix}
$$

$$(4.25)$$

Equatorial acceleration, equation (4.20), becomes:

$$
\vec{a}_{u-eq} =
$$

$$
\begin{bmatrix} -cos\Omega(\ddot{\psi}Lsin(\theta + \psi) + L(\dot{\theta} + \dot{\psi} + \dot{\omega})^2cos(\theta + \psi) + \alpha cos\theta) \\ -sin\Omega(\ddot{\psi}Lsin(\theta + \psi) + L(\dot{\theta} + \dot{\psi} + \dot{\omega})^2cos(\theta + \psi) + \alpha cos\theta) \\ \ddot{\psi}Lcos(\theta + \psi) - L(\dot{\theta} + \dot{\psi} + \dot{\omega})^2sin(\theta + \psi) - \beta sin\theta \end{bmatrix}
$$

$$(4.26)$$

With α, β denoting:

$$
\alpha = \frac{GM_E}{r_o^2} + 2\dot{\omega}\sqrt{\frac{\mu}{p}}\left(1 + \frac{e}{cos\theta}\right) + \dot{\omega}^2 r_o
$$

$$
\beta = \frac{GM_E}{r_o^2} + 2\dot{\omega}\sqrt{\frac{\mu}{p}} + \dot{\omega}^2 r_o
$$

The largest velocity that can be imparted by the EMMET at the instant of payload launch occurs when it is at the perigee of its orbit, where its orbital velocity is highest, and the rotating tether sub-spans are aligned along the local gravity gradient, allowing rotational velocity to be added directly to orbital velocity. At this instant, angles θ and ψ are zero and the equatorial position, velocity and acceleration simplify to:

$$\vec{r}_{u-eq} = \begin{bmatrix} cos\Omega(r_o + L) \\ sin\Omega(r_o + L) \\ 0 \end{bmatrix} \tag{4.27}$$

$$\vec{v}_{u-eq} = \begin{bmatrix} 0 \\ 0 \\ \sqrt{\frac{\mu}{p}}(1 + e) + \dot{\omega}r_o + L(\dot{\theta} + \dot{\psi} + \dot{\omega}) \end{bmatrix} \tag{4.28}$$

$$\vec{a}_{u-eq} = \begin{bmatrix} -cos\Omega((\dot{\theta} + \dot{\psi} + \dot{\omega})^2 L + \alpha) \\ -sin\Omega((\dot{\theta} + \dot{\psi} + \dot{\omega})^2 L + \alpha) \\ \ddot{\psi}L \end{bmatrix} \tag{4.29}$$

Our focus now turns to deriving the EMMET's components when it has a moon-tracking configuration which includes a critically inclined orbit and again these will derived for an arbitrary true anomaly and also when the EMMET is at the perigee of its orbit when configured for payload capture and launch operations.

Moon-Tracking with Critical Inclination

For moon-tracking orbits relative to the equatorial frame of reference which utilise the critical inclination of 63.4°, denoted i_c, to render the EMMET's argument of perigee stationary, the perifocal to equatorial transformation matrix, equation (3.5), for an argument of perigee equal to zero is:

$$R_G = \begin{bmatrix} cos\Omega & -sin\Omega cosi_c & sin\Omega sini_c \\ sin\Omega & cos\Omega cosi_c & -cos\Omega sini_c \\ 0 & sini_c & cosi_c \end{bmatrix} \tag{4.30}$$

The derivative of equation (4.30), in this case is simplified by the fact that its precession is due solely to the change in angle of ascending node

of the EMMET's orbit, and this is obtained as [43]:

$$\dot{R}_G = \dot{\Omega} \begin{bmatrix} -sin\Omega & -cos\Omega cosi_c & cos\Omega sini_c \\ cos\Omega & -sin\Omega cosi_c & sin\Omega sini_c \\ 0 & 0 & 0 \end{bmatrix} \qquad (4.31)$$

The angular rate in equation (4.31) is equal to the rate of change of the ascending node, $\dot{\Omega}$, of the EMMET's orbit due to the oblateness effects of a non-spherical Earth, and the rate of this change will be defined in Chapter 5. The derivative of equation (4.31) is again simplified by the fact that its change is due solely to the change in ascending node of the EMMET's orbit [43]:

$$\ddot{R}_G = \qquad \ddot{\Omega} \begin{bmatrix} -sin\Omega & -cos\Omega cosi_c & cos\Omega sini_c \\ cos\Omega & -sin\Omega cosi_c & sin\Omega sini_c \\ 0 & 0 & 0 \end{bmatrix}$$

$$+ \qquad \dot{\Omega}^2 \begin{bmatrix} -cos\Omega & sin\Omega cosi_c & -sin\Omega sini_c \\ -sin\Omega & -cos\Omega cosi_c & cos\Omega sini_c \\ 0 & 0 & 0 \end{bmatrix} \qquad (4.32)$$

Equation (4.32) is simplified further by the assumption that the angular rate of the ascending node is constant and un-accelerated. We now obtain the position, velocity and acceleration of the upper tip relative to the equatorial frame and for simplicity we set the angle of ascending node to zero. Therefore, the equatorial position given by equation (4.18), becomes:

$$\vec{r}_{u-eq} = \begin{bmatrix} r_o cos\theta + Lcos(\theta + \psi) \\ (r_o sin\theta + Lsin(\theta + \psi))cosi_c \\ (r_o sin\theta + Lsin(\theta + \psi))sini_c \end{bmatrix} \qquad (4.33)$$

Equatorial velocity, equation (4.19), becomes:

$$\vec{v}_{u-eq} =$$

$$\begin{bmatrix} -\left(\sqrt{\frac{\mu}{p}} + \dot{\Omega} r_o cosi_c\right) sin\theta - L(\dot{\theta} + \dot{\psi} + \dot{\Omega}cosi_c)sin(\theta + \psi) \\ e\sqrt{\frac{\mu}{p}}cosi_c + \left(\sqrt{\frac{\mu}{p}}cosi_c + \dot{\Omega} r_o\right)cos\theta + L((\dot{\theta} + \dot{\psi})cosi_c + \dot{\Omega})cos(\theta + \psi) \\ \left(\sqrt{\frac{\mu}{p}}(e + cos\theta) + L(\dot{\theta} + \dot{\psi})cos(\theta + \psi)\right)sini_c \end{bmatrix}$$

$$(4.34)$$

Equatorial acceleration, equation (4.20), becomes:

$$\vec{a}_{u-eq} = \begin{bmatrix} \alpha_1 & \alpha_2 & \alpha_3 \end{bmatrix}^T \tag{4.35}$$

With α_1, α_2 and α_3 denoting:

$$\begin{aligned}
\alpha_1 = & -\ddot{\psi}Lsin(\theta + \psi) - \left(2\dot{\Omega}\sqrt{\frac{\mu}{p}}cosi_c + \dot{\Omega}^2 r_o\right)cos\theta \\
& - L[(\dot{\theta} + \dot{\psi})^2 + 2\dot{\Omega}(\dot{\theta} + \dot{\psi})cosi_c + \dot{\Omega}^2]cos(\theta + \psi) \\
& - \frac{GM_E}{r_o^2}cos\theta - 2\dot{\Omega}e\sqrt{\frac{\mu}{p}}cosi_c
\end{aligned} \tag{4.36}$$

$$\begin{aligned}
\alpha_2 = & \ddot{\psi}Lcos(\theta + \psi)cosi_c - \left(2\dot{\Omega}\sqrt{\frac{\mu}{p}} + \dot{\Omega}^2 r_o cosi_c\right)sin\theta \\
& - L[(\dot{\theta} + \dot{\psi})^2 cosi_c + 2\dot{\Omega}(\dot{\theta} + \dot{\psi}) + \dot{\Omega}^2 cosi_c]sin(\theta + \psi) \\
& - \frac{GM_E}{r_o^2}sin\theta cosi_c
\end{aligned} \tag{4.37}$$

$$\begin{aligned}
\alpha_3 = & \ddot{\psi}Lcos(\theta + \psi)sini_c - L(\dot{\theta} + \dot{\psi})^2 sin(\theta + \psi)sini_c \\
& - \frac{GM_E}{r_o^2}sin\theta sini_c
\end{aligned} \tag{4.38}$$

The equatorial position, velocity and acceleration of the EMMET at the perigee of its orbit can be stated, and in this case each simplifies to:

$$\vec{r}_{u-eq} = \begin{bmatrix} r_o + L & 0 & 0 \end{bmatrix}^T \tag{4.39}$$

$$\vec{v}_{u-eq} = \begin{bmatrix} 0 \\ \left(\sqrt{\frac{\mu}{p}}(1 + e) + L(\dot{\theta} + \dot{\psi})\right)cosi_c + \dot{\Omega}(r_o + L) \\ \left(\sqrt{\frac{\mu}{p}}(1 + e) + L(\dot{\theta} + \dot{\psi})\right)sini_c \end{bmatrix} \tag{4.40}$$

$$\vec{a}_{u-eq} =$$

$$-\begin{bmatrix} \frac{GM_E}{r_o^2} + (\dot{\theta} + \dot{\psi})^2 L + 2\dot{\Omega}\left[(\dot{\theta} + \dot{\psi})L + \sqrt{\frac{\mu}{p}}(1 + e)\right]cosi_c + \dot{\Omega}^2(r_o + L) \\ -\ddot{\psi}Lcosi_c \\ -\ddot{\psi}Lsini_c \end{bmatrix} \tag{4.41}$$

Having obtained the components of the EMMET when different moon-tracking configurations are used, the velocities obtained in equations (4.28) (4.40) will be utilised in Chapter 5 to establish whether the velocity imparted to a payload launched from the upper tip of the EMMET orbiting in a given configuration is sufficient for it to reach the Moon's gravitational influence. In addition to this, by utilising the acceleration

terms obtained for a polar inclination configuration in equations (4.29) and (4.41), the tension acting at the point of connection between the central facility and tether sub-span as a result of the payload and tether sub-spans, will be obtained in the following section.

4.2   Tether Tension

We will now begin the derivation of the tether tension resulting from the accelerations acting upon the payload and tether sub-spans. By adhering to the standard orbital mechanical assumption that a satellite and an attracting body can be treated as particles [42] with all their mass concentrated at their centre of mass and furthermore, by assuming that the centre of mass of the EMMET coincides with the central facility which orbits Earth in an ellipse with no further perturbations acting upon it than those resulting from the oblateness of Earth; the EMMET can therefore be treated as a particle orbiting the Earth at the distance of the central facility with a gravitational force acting on it which is proportional to its orbital radius. The largest tension occurring within the tether sub-spans will be at their point of connection to the central facility and result from the difference in the forces acting on the tether sub-spans and payload masses to those acting on the centre of mass of the system. This tension will consist of terms resulting from a combination of a variation in gravitational acceleration, as radial distance from Earth varies, and inertial acceleration terms arising from the motion of the non-inertial body-fixed and perifocal frames relative to the geocentric equatorial frame. The tension occurring at the connection point can be written as the sum of the tether sub-span tension, and the tension due to the payload. We will begin by developing the tension acting on the upper tether sub-span's upper tip as a result of the acceleration of the upper payload's mass. This tension is considered to be instantly transmitted along the tether and contributes to the tension at the point of connection to the central facility. We will then calculate the tension resulting from the upper tether sub-span at the connection point and obtain the total tension acting at that point. A similar procedure will be

followed for the tension resulting from the lower sub-span and payload at the lower central facility connection point, and we will again obtain the total tension acting at the connection point. The chapter will conclude with a comparison between the tensions acting at the upper and lower connection points to determine whether the tensions are equal, and if not to determine the point at which the greatest tension occurs. From this maximum tension we will derive the maximum angular velocity that the tether sub-spans can endure dependent upon the properties of the material they are composed of. The description of the derivation of the maximum tension and angular velocity for the EMMET will be given in detail for the EMMET in a polar orbit with the expression for the maximum angular velocity when the EMMET has a critically inclined orbit being stated once the corresponding equation for the polar case has been obtained. The maximum angular velocity when the EMMET is freely inclined can be obtained from the corresponding equation for the Lunavator which is also applicable, and this case is derived in detail in Chapter 7.

4.2.1 Upper Tether Tension

The tension acting at the connection point between the tether and central facility will now be derived for the upper tether sub-span and payload of an EMMET in a polar orbit with the aim of determining the point at which the greatest tension acting on the EMMET is located.

Upper Payload Tension

The net force, $\vec{F}_{net}$, acting on the upper payload can be written in terms of the gravitational force, $\vec{F}_g$, and the tension acting on it. This is equal to the product of the payload's mass and its acceleration relative to Earth's equatorial frame of reference. For the payload attached to the upper tether tip, this can be written as:

$$\vec{F}_{net} = m_p \vec{a}_{u-eq} = \vec{F}_g + \vec{T}_{u-p} \qquad (4.42)$$

Payload mass is denoted by m_p, tension is denoted by $\vec{T}_{u-p}$ and the force of gravity acting on the payload relative to the equatorial frame is defined

as:

$$\vec{F_g} = -\frac{Gm_pM_E}{r_{u-eq}^3}\vec{r}_{u-eq} \tag{4.43}$$

The tension can be written in terms of the acceleration relative to the equatorial frame and the force of gravity at that point:

$$\vec{T}_{u-p} = m_p\vec{a}_{u-eq} - \vec{F_g} \tag{4.44}$$

The equatorial acceleration term can be re-written, by extracting the gravitational term from the first term in equation (4.20), as:

$$\vec{a}_{u-eq} + \frac{GM_E}{r_o^3}\vec{r}_{o-eq} = \left(R_G.\vec{a}_{u-per} + \frac{GM_E}{r_o^3}\vec{r}_{o-eq}\right) + 2\dot{R}_G.\vec{v}_{u-per} + \ddot{R}_G.\vec{r}_{u-per} \tag{4.45}$$

where the gravitational term is simply the acceleration of the body frame origin, equation (4.13), transformed into the equatorial frame, in both coordinates frames the radial distance remains the same:

$$R_G.\vec{a}_o = -\frac{GM_E}{r_o^3}\vec{r}_{o-eq} \tag{4.46}$$

The tension can therefore be written in terms of the change in gravitational force acting on the payload's mass as a result of its displacement from the origin of the body frame and inertial acceleration terms, resulting from the payload's rotation about the EMMET's central facility in conjunction with the orbital motion of the entire tether system about Earth:

$$\vec{T}_{u-p} = m_p\left(\vec{a}_{u-eq} - R_G.\vec{a}_o\right) + Gm_pM_E\left(\frac{\vec{r}_{u-eq}}{r_{u-eq}^3} - \frac{\vec{r}_{o-eq}}{r_o^3}\right) \tag{4.47}$$

The maximum tension resulting from the acceleration of the payload will occur when the EMMET is at the perigee of its orbit, where its orbital velocity and its acceleration due to gravity are greatest, and when it is aligned along the local gravity gradient, where its centrifugal acceleration due to tether rotation is largest. Utilising equation (4.29) and assuming that no angular acceleration of the payload is taking place in the form of motor torque, the inertial acceleration of the upper payload in the equatorial frame can be written as:

$$\vec{a}_{u-eq} - R_G.\vec{a}_o = \begin{bmatrix} -cos\Omega((\dot{\theta} + \dot{\psi} + \dot{\omega})^2L + 2\dot{\omega}\sqrt{\frac{\mu}{p}}(1+e) + \dot{\omega}^2r_o) \\ -sin\Omega((\dot{\theta} + \dot{\psi} + \dot{\omega})^2L + 2\dot{\omega}\sqrt{\frac{\mu}{p}}(1+e) + \dot{\omega}^2r_o) \\ 0 \end{bmatrix} \tag{4.48}$$

81

The resulting tension acting on the payload is found from equation (4.37):

$$\vec{T}_{u-p} = -m_p \begin{bmatrix} cos\Omega \left((\dot{\theta} + \dot{\psi} + \dot{\omega})^2 L + 2\dot{\omega}\sqrt{\frac{\mu}{p}}(1+e) + \dot{\omega}^2 r_o - \gamma\,(GM_E) \right) \\ sin\Omega \left((\dot{\theta} + \dot{\psi} + \dot{\omega})^2 L + 2\dot{\omega}\sqrt{\frac{\mu}{p}}(1+e) + \dot{\omega}^2 r_o - \gamma\,(GM_E) \right) \\ 0 \end{bmatrix}$$

(4.49)

With γ defined as:

$$\gamma = \left(\frac{1}{(r_o + L)^2} - \frac{1}{r_0^2} \right)$$

A binomial series expansion can be used to approximate the gravitational terms of equation (4.49) as follows [48]:

$$\gamma = \frac{1}{r_o^2}\left(\left(1 + \frac{L}{r_o}\right)^{-2} - 1 \right) = -\frac{1}{r_o^2}\left(2\left(\frac{L}{r_o}\right) - 3\left(\frac{L}{r_o}\right)^2 + 4\left(\frac{L}{r_o}\right)^3 - ... \right)$$

(4.50)

This expansion is valid for $|\frac{L}{r_o}| < 1$. By retaining only up to squared terms of the series, as $L \ll r_o$, the tension acting on the payload can be written as:

$$\vec{T}_{u-p} = -m_p \begin{bmatrix} cos\Omega \left((\dot{\theta} + \dot{\psi} + \dot{\omega})^2 L + 2\dot{\omega}\sqrt{\frac{\mu}{p}}(1+e) + \dot{\omega}^2 r_o + \left(\frac{GM_E}{r_0^2}\right)\Gamma \right) \\ sin\Omega \left((\dot{\theta} + \dot{\psi} + \dot{\omega})^2 L + 2\dot{\omega}\sqrt{\frac{\mu}{p}}(1+e) + \dot{\omega}^2 r_o + \left(\frac{GM_E}{r_0^2}\right)\Gamma \right) \\ 0 \end{bmatrix}$$

(4.51)

With Γ defined as:

$$\Gamma = \left(2\left(\frac{L}{r_o}\right) - 3\left(\frac{L}{r_o}\right)^2 \right)$$

Having now defined the tension acting on the payload as a result of the acceleration acting on it, we can define the tension acting on the upper tether tip and subsequently the connection point to the central facility by the application of Newton's third law . The tension acting at the central facility connection point, $\vec{T}_u$, as a result of the acceleration of the payload is equal in magnitude but opposite in direction to the tension acting on the payload and can be defined as follows:

$$\vec{T}_u = m_p \begin{bmatrix} cos\Omega \left((\dot{\theta} + \dot{\psi} + \dot{\omega})^2 L + 2\dot{\omega}\sqrt{\frac{\mu}{p}}(1+e) + \dot{\omega}^2 r_o + \left(\frac{GM_E}{r_0^2}\right)\Gamma \right) \\ sin\Omega \left((\dot{\theta} + \dot{\psi} + \dot{\omega})^2 L + 2\dot{\omega}\sqrt{\frac{\mu}{p}}(1+e) + \dot{\omega}^2 r_o + \left(\frac{GM_E}{r_0^2}\right)\Gamma \right) \\ 0 \end{bmatrix}$$

(4.52)

Having obtained an expression for the tension at the central facility connection point resulting from the acceleration acting on the payload mass, we will now derive an expression for the tension resulting from the acceleration of the tether sub-span.

Upper Tether Sub-span Tension

We can calculate the tension resulting from the acceleration of the entire tether sub-span at the point of connection to the central facility by firstly obtaining an expression for the tension resulting from an infinitesimal point an arbitrary distance along the sub-span and then secondly, integrating this expression over the entire sub-span. We begin by discretising the sub-span into infinitesimal intervals of length, δs, each of mass δm. We can then define the net force acting on an arbitrary interval at some distance, s, along the tether sub-span in a similar way to that used for the payload. Beginning with equation (4.42) we follow an identical procedure as before and arrive at equation (4.52) for the tension acting on the central facility connection point as a result of the length interval δs, in this case tether sub-span length, L, is replaced by the distance along the sub-span, s:

$$\vec{T}_{u-s} = \delta m \begin{bmatrix} cos\Omega \left((\dot{\theta} + \dot{\psi} + \dot{\omega})^2 s + 2\dot{\omega}\sqrt{\frac{\mu}{p}} \left(1 + e \right) + \dot{\omega}^2 r_o + \left(\frac{GM_E}{r_0^2} \right) \Gamma_s \right) \\ sin\Omega \left((\dot{\theta} + \dot{\psi} + \dot{\omega})^2 s + 2\dot{\omega}\sqrt{\frac{\mu}{p}} \left(1 + e \right) + \dot{\omega}^2 r_o + \left(\frac{GM_E}{r_0^2} \right) \Gamma_s \right) \\ 0 \end{bmatrix}$$

$$(4.53)$$

with Γ_s defined as:

$$\Gamma_s = \left(2 \left(\frac{s}{r_o} \right) - 3 \left(\frac{s}{r_o} \right)^2 \right)$$

The tension can be re-defined in terms of the differential mass, the magnitude of the acceleration acting on it at point s along the sub-span, and a unit vector directed along the sub-span, as:

$$\vec{T}_{u-s} = \delta m \left((\dot{\theta} + \dot{\psi} + \dot{\omega})^2 s + 2\dot{\omega}\sqrt{\frac{\mu}{p}} \left(1 + e \right) + \dot{\omega}^2 r_o + \left(\frac{GM_E}{r_0^2} \right) \Gamma_s \right) \vec{i}_s$$

$$(4.54)$$

where the unit vector directed along the sub-span, $\vec{i}_s$, is defined as:

$$\vec{i}_s = \begin{bmatrix} cos\Omega & sin\Omega & 0 \end{bmatrix}^T$$

From equation (4.54), the magnitude of the acceleration acting at point s can be defined as:

$$a(s) = (\dot{\theta} + \dot{\psi} + \dot{\omega})^2 s + 2\dot{\omega}\sqrt{\frac{\mu}{p}}(1 + e) + \dot{\omega}^2 r_o + \left(\frac{GM_E}{r_0^2}\right)\Gamma_s \quad (4.55)$$

Writing the differential mass in terms of the tether's material density, ρ, cross sectional area, A, and differential length δs as:

$$\delta m = \rho A \delta s \quad (4.56)$$

The tension resulting from this infinitesimal tether element can therefore be expressed as:

$$\vec{T}_{u-s} = (\rho A a(s) \delta s)\,\vec{i}_s \quad (4.57)$$

The net tension resulting from all of the differential elements which compose the tether sub-span can now be found by integrating equation (4.57) over the entire length:

$$\vec{T}_U = \left[\int_0^L \rho A a(s) \delta s\right]\vec{i}_s \quad (4.58)$$

As a result of $\vec{i}_s$ being independent of the length variable s, the integral along the entire sub-span simplifies to an integral of the magnitude of the acceleration over the entire sub-span as:

$$T_U = \int_0^L \rho A a(s) \delta s \quad (4.59)$$

Performing the integration yields a tension resulting from the entire sub-span of:

$$\vec{T}_U = m_T \left(\frac{1}{2}(\dot{\theta} + \dot{\psi} + \dot{\omega})^2 L + 2\dot{\omega}\sqrt{\frac{\mu}{p}}(1 + e) + \dot{\omega}^2 r_o + \left(\frac{GM_E}{r_0^2}\right)\Gamma_U\right)\vec{i}_s$$
$$(4.60)$$

where the total mass of the tether $m_T = \rho A L$ and Γ_U is defined as:

$$\Gamma_U = \left(\left(\frac{L}{r_o}\right) - \left(\frac{L}{r_o}\right)^2\right)$$

An expression for the total tension resulting from the tether sub-spans and payload tension will now be obtained.

Upper Connection Point Tension

The tension acting at the connection point between the tether sub-span and the central facility is the resultant of the payload and tether sub-span

tensions acting at that point. By similarly defining the payload tension to that of the sub-span tension in terms of mass, magnitude of acceleration, and a unit vector defined along the tethers sub-span, equation (4.60), the total tension acting at the connection point can be defined as:

$$\vec{T}_{net} = (T_{net})\,\vec{i}_s \tag{4.61}$$

with the magnitude of the tension acting at the connection point defined as:

$$
\begin{aligned}
T_{net-upper} \;=\; & (\dot{\theta} + \dot{\psi} + \dot{\omega})^2 L\left(m_p + \frac{1}{2}m_T\right) \\
& + \left(2\dot{\omega}\sqrt{\frac{\mu}{p}}\,(1+e) + \dot{\omega}^2 r_o\right)(m_p + m_T) \\
& + \left(\frac{GM_E}{r_0^2}\right)\left((2m_p + m_T)\left(\frac{L}{r_o}\right) - (3m_p + m_T)\left(\frac{L}{r_0}\right)^2\right)
\end{aligned}
\tag{4.62}
$$

Having obtained the magnitude of the tension acting at this point, we will now derive the tension acting at the lower connection point.

4.2.2 Lower Tether Tension

The tension acting at the connection point between the tether and central facility will now be derived for the lower tether sub-span and payload and the net tension acting at this point will be compared to that acting on the upper tether with the aim of determining the location of greatest tension.

Lower Payload Tension

The tension acting on the lower payload can be found by again using equation (4.42) but in this case the acceleration term denotes that of the lower payload. This is obtained by adding 180° to the tether rotation angle ψ in equation (4.26). As is the case for the upper tension, the greatest tension occurring in the lower connection point will occur when the EMMET is at perigee and aligned along the local gravity gradient. The acceleration acting on the lower payload is found to be:

$$
\vec{a}_{l-eq} =
\begin{bmatrix}
cos\Omega\left((\dot{\theta} + \dot{\psi} + \dot{\omega})^2 L - \frac{GM_E}{r_o^2} - 2\dot{\omega}\sqrt{\frac{\mu}{p}}(1+e) - \dot{\omega}^2 r_o\right) \\
sin\Omega\left((\dot{\theta} + \dot{\psi} + \dot{\omega})^2 L - \frac{GM_E}{r_o^2} - 2\dot{\omega}\sqrt{\frac{\mu}{p}}(1+e) - \dot{\omega}^2 r_o\right) \\
-\ddot{\psi}L
\end{bmatrix}
\tag{4.63}
$$

Following a similar procedure to that used for the upper payload we arrive at an equation similar to equation (4.49) for the lower payload:

$$\vec{T}_{l-p} = m_p \begin{bmatrix} cos\Omega \left((\dot{\theta} + \dot{\psi} + \dot{\omega})^2 L - 2\dot{\omega}\sqrt{\frac{\mu}{p}} \left(1 + e \right) - \dot{\omega}^2 r_o + \lambda \left(GM_E \right) \right) \\ sin\Omega \left((\dot{\theta} + \dot{\psi} + \dot{\omega})^2 L - 2\dot{\omega}\sqrt{\frac{\mu}{p}} \left(1 + e \right) - \dot{\omega}^2 r_o + \lambda \left(GM_E \right) \right) \\ 0 \end{bmatrix}$$

(4.64)

with λ defined as:

$$\lambda = \left(\frac{1}{(r_o - L)^2} - \frac{1}{r_0^2} \right)$$

Utilising the binomial series expansion [48], valid for $|\frac{L}{r_o}| < 1$, to approximate λ yields:

$$\lambda = \frac{1}{r_o^2} \left(\left(1 + \left(-\frac{L}{r_o} \right) \right)^{-2} - 1 \right)$$

$$= \frac{1}{r_o^2} \left(2\left(\frac{L}{r_o} \right) + 3\left(\frac{L}{r_o} \right)^2 + 4\left(\frac{L}{r_o} \right)^3 + ... \right)$$

(4.65)

Retaining only up to squared terms, equation (4.64) becomes:

$$\vec{T}_{l-p} = m_p \begin{bmatrix} cos\Omega \left((\dot{\theta} + \dot{\psi} + \dot{\omega})^2 L - 2\dot{\omega}\sqrt{\frac{\mu}{p}} \left(1 + e \right) - \dot{\omega}^2 r_o + \Lambda \left(GM_E \right) \right) \\ sin\Omega \left((\dot{\theta} + \dot{\psi} + \dot{\omega})^2 L - 2\dot{\omega}\sqrt{\frac{\mu}{p}} \left(1 + e \right) - \dot{\omega}^2 r_o + \Lambda \left(GM_E \right) \right) \\ 0 \end{bmatrix}$$

(4.66)

with Λ defined as:

$$\Lambda = \frac{1}{r_o^2} \left(2\left(\frac{L}{r_o} \right) + 3\left(\frac{L}{r_o} \right)^2 \right)$$

Having defined the tension acting on the payload as a result of the additional acceleration terms occurring as a result of the payload's displacement from the centre of mass, the tension acting on the connection point to the central facility can be found from Newton's third law as:

$$\vec{T}_l = -m_p \begin{bmatrix} cos\Omega \left((\dot{\theta} + \dot{\psi} + \dot{\omega})^2 L - 2\dot{\omega}\sqrt{\frac{\mu}{p}} \left(1 + e \right) - \dot{\omega}^2 r_o + \Lambda \left(GM_E \right) \right) \\ sin\Omega \left((\dot{\theta} + \dot{\psi} + \dot{\omega})^2 L - 2\dot{\omega}\sqrt{\frac{\mu}{p}} \left(1 + e \right) - \dot{\omega}^2 r_o + \Lambda \left(GM_E \right) \right) \\ 0 \end{bmatrix}$$

(4.67)

Having obtained an expression for the tension at the central facility connection point resulting from the acceleration acting on the lower payload mass, we will now derive an expression for the tension resulting from the acceleration of the lower tether sub-span.

Lower Tether Sub-span Tension

By similarly discretising the lower tether sub-span with the method used for the upper tether sub-span, the tension acting along the lower tether sub-span can be found by means of an integral identical to equation (4.58), in this case the acceleration term, a_s, can be defined as:

$$a_s = \left((\dot{\theta} + \dot{\psi} + \dot{\omega})^2 s - 2\dot{\omega}\sqrt{\frac{\mu}{p}} (1 + e) - \dot{\omega}^2 r_o + \left(\frac{GM_E}{r_0^2} \right) \Lambda_s \right) \quad (4.68)$$

Where Λ_s is defined as:

$$\Lambda_s = \left(2 \left(\frac{s}{r_o} \right) + 3 \left(\frac{s}{r_o} \right)^2 \right)$$

The resulting tension acting at the point of connection can be found by integrating over the entire sub-span and applying Newton's third law as:

$$\vec{T}_L = -m_T \left(\frac{1}{2} (\dot{\theta} + \dot{\psi} + \dot{\omega})^2 L - 2\dot{\omega}\sqrt{\frac{\mu}{p}} (1 + e) - \dot{\omega}^2 r_o + \left(\frac{GM_E}{r_0^2} \right) \Lambda_L \right) \vec{i}_s$$
$$(4.69)$$

where Λ_L is defined as:

$$\Lambda_L = \left(\left(\frac{L}{r_o} \right) + \left(\frac{L}{r_o} \right)^2 \right)$$

An expression for the total tension resulting from the tether sub-spans and payload tension will now be obtained.

Lower Connection Point Tension

The net tension acting on the lower connection point can again be defined by equation (4.61). In this case, the unit vector $\vec{i}_s$ has a direction opposite to that for the upper tension case, the magnitude of the tension can therefore be defined as:

$$
\begin{aligned}
T_{net-lower} = \ & (\dot{\theta} + \dot{\psi} + \dot{\omega})^2 L \left(m_p + \frac{1}{2} m_T \right) \quad (4.70) \\
& - \left(2\dot{\omega}\sqrt{\frac{\mu}{p}} (1 + e) + \dot{\omega}^2 r_o \right) (m_p + m_T) \\
& + \left(\frac{GM_E}{r_0^2} \right) \left((2m_p + m_T) \left(\frac{L}{r_0} \right) + (3m_p + m_T) \left(\frac{L}{r_0} \right)^2 \right)
\end{aligned}
$$

Having obtained the magnitude of the tension acting at the upper and lower connection points they will now be compared to establish the point of maximum tension, and an expression for the maximum rotational velocity that the tether can withstand due to this tension will be obtained.

4.2.3   Maximum Tension and Rotational Velocity

Having obtained expressions for the tensions acting at the upper and lower connection points we can now determine if these two tensions are equal and if not the magnitude of the maximum tension can be identified. As a result of the assumption that the central facility orbits Earth with no other perturbations acting on it other than those arising from Earth's oblateness, the tensions acting on the central facility due to the the upper payload and sub-span and lower payload and sub-span should be opposite and equal according to Newton's third law. This can be established by:

$$\vec{T}_{net-lower} + \vec{T}_{net-upper} = \vec{0} \tag{4.71}$$

However, implementing the magnitudes of net tensions results in:

$$\left(2\dot{\omega}\sqrt{\frac{\mu}{p}}\left(1+e\right) + \dot{\omega}^2 r_o\right)(m_p + m_T)-$$
$$\left(\frac{GM_E}{r_0^2}\right)\left((3m_p + m_T)\left(\frac{L}{r_0}\right)^2\right) \neq 0 \tag{4.72}$$

The two tensions are therefore unequal, and as the ascending node's rate of regression is negative, due to the polar inclination, the central facility experiences a net negative force as a result of equation (4.72). This means that the tension on the lower connection point is greater. This however raises a interesting situation with regards to our assumption that there are no other perturbations acting on the EMMET's centre of mass other than those resulting from an oblate Earth. A hypothesis will be postulated in Chapter 9 which attempts to explain this mismatch between upper and lower tether tension which, additionally, is observed in the case of the Lunavator in Chapter 7. However, for the moment we will remain within the confines of standard orbital dynamic assumptions and concern ourselves with establishing the maximum rotational velocity that the sub-spans can endure, in addition to the development of the minimum requirements that must be satisfied for a continuous Earth-Moon payload exchange to be established.

Maximum Rotational Velocity

Having determined that the maximum tension occurring in the EMMET system will occur at the connection point between the lower tether sub-

span and central facility, we will now derive an expression for the maximum angular velocity which the sub-spans can rotate at which is dependent upon tether length, payload mass and the characteristics of the material that the tether sub-spans are composed of. To begin with, the tension in the tether can be re-written in terms of the tensile stress of the material, denoted by σ, and cross sectional area of the tether sub-span [4] as:

$$T = \sigma A \tag{4.73}$$

The maximum tension that the tether sub-span can endure can be written in terms of cross sectional area of the tether and the maximum tensile stress, σ_{max}, that the tether material can endure, and a factor of safety, SF, has been included:

$$T_{max} = \left(\frac{\sigma_{max}}{SF}\right) A \tag{4.74}$$

Re-arranging equation (4.70) and replacing tension with equation (4.74), the maximum rotational velocity, $\dot{\psi}_{max}$, that the tether can endure for a moon tracking orbit which has a polar inclination relative to the equatorial frame can be expressed as:

$$\dot{\psi}_{max} = \sqrt{\frac{1}{L\left(m_p + \frac{1}{2}m_T\right)}\left(\left(\frac{\sigma_{max}}{SF}\right)A + \nu\right)} - (\dot{\theta} + \dot{\omega}) \tag{4.75}$$

where ν can be defined as:

$$
\begin{aligned}
\nu =\ & \left(2\dot{\omega}\sqrt{\frac{\mu}{p}}\left(1 + e\right) + \dot{\omega}^2 r_o\right)(m_p + m_T) \\
& - \left(\frac{GM_E}{r_0^2}\right)\left((2m_p + m_T)\left(\frac{L}{r_0}\right) + (3m_p + m_T)\left(\frac{L}{r_0}\right)^2\right)
\end{aligned}
$$

Comparing this with the expression derived by Zeigler [49] for the maximum angular velocity that a tether can endure:

$$\dot{\psi}_{max} = \sqrt{\frac{\sigma A}{L\left(m_p + \frac{1}{2}\rho A\right)}} \tag{4.76}$$

It can be seen that equation (4.75) contains all of the terms in equation (4.76), where $m_T = \rho A L$, but also includes terms which account for tensions arising in the tether as a result of gravity gradient, in addition to tensions arising from precession of the EMMET's argument of perigee. The maximum angular velocity that the EMMET can withstand when

89

configured to orbit Earth in a critically inclined moon-tracking configuration is derived in a manner identical to that of the polar case and is obtained as:

$$\dot{\psi}_{max} = \sqrt{\left(\frac{1}{L\left(m_p + \frac{1}{2}m_T\right)}\left[\left(\frac{\sigma_{max}}{SF}\right)A + \nu\right] - \dot{\Omega}^2\right)} - (\dot{\theta} + \dot{\Omega}cosi_c)$$

(4.77)

Where ν can be defined, in this case, as:

$$\begin{aligned}
\nu = & \left(2\dot{\Omega}\sqrt{\frac{\mu}{p}}\left(1 + e\right)cosi_c + \dot{\Omega}^2 r_o\right)(m_p + m_T) \\
& - \left(\frac{GM_E}{r_0^2}\right)\left((2m_p + m_T)\left(\frac{L}{r_0}\right) + (3m_p + m_T)\left(\frac{L}{r_0}\right)^2\right)
\end{aligned}$$

It can be seen that equation (4.77) differs from equation (4.75) due to the terms resulting from the rate of the ascending node of the EMMET's orbit and no terms due to the precession of the argument of perigee as this is stationary in this case.

4.3 Conclusions

A means by which to transform dynamic components from the body fixed frame of reference to Earth's equatorial frame have been obtained. These have been applied to the configurations for the polar and critically inclined moon-tracking orbits and furthermore these have been utilised to obtain the position, velocity and acceleration of the EMMET and its tips at the perigee of its orbit in each of these configurations. Utilising the expressions for the upper and lower tip's acceleration relative to the equatorial frame and obtaining these when the accelerations are greatest, occurring at the perigee of the EMMET's orbit; expressions for the maximum tension along the tether sub-spans have been derived. A surprising result was obtained which showed that the tension occurring along the lower sub-span and payload was greater than that of the upper. This contradicts the assumption that the forces are balanced at the centre of mass of the system which is coincident with the central facility. A hypothesis to explain this phenomenon has been proposed in Chapter 9. Having obtained the maximum tension acting, this tension was expressed in terms of the material properties of the tether sub-spans and

expressions were obtained for the maximum rotational rates which these sub-spans are capable of withstanding when taking into account payload and tether sub-span masses.

The expressions obtained in this chapter will now be used to determine whether a given EMMET configuration is capable of providing the velocity required to inject a payload onto a trans-Luna trajectory from a given upper tip position whilst remaining within the constraints imposed by the maximum angular velocity that the tether sub-spans can safely operate at. In addition to this, by utilising the velocities derived for each configuration in conjunction with expressions derived in the previous chapter for the magnitude of the velocity required to adjust the EMMET's parameters, the most efficient moon-tracking configuration can be established.

5. EMMET Parameters

Several configurations have now been described which will allow us to track the ascending or descending node of the Moon's orbit relative to the equatorial frame. In addition to this, expressions have been derived for the maximum velocity increment that the EMMET's sub-spans are capable of imparting to the payloads as a result of the properties of the material which they are composed of, and the maximum tension that the sub-spans can be subjected to. The velocity at which payloads are released onto trans-Luna trajectories from the EMMET's upper tip can now be calculated for EMMET configurations which satisfy the requirements of each of the moon-tracking orbits. Suitable input parameters for each moon-tracking configuration can then be determined and any limitations of the configurations assessed, the culmination of this will be a set of design parameters which satisfy the requirements of the Earth orbiting tether for a continuous payload exchange. Having defined suitable input parameters, the moon-tracking configuration which is most suitable for this purpose in terms of transfer opportunities and manoeuvre efficiency will be preliminarily determined; with the most suitable configuration being capable of exchanging payloads each time the Moon crosses its ascending or descending node in addition to the adjustment manoeuvres having the lowest required velocity changes. The simulations and data presented in this chapter were produced using the mathematical software programme $MATHEMATICA^{\text{TM}}$ but the formulation is not restricted exclusively to this package. This chapter will begin with the determination of the orbital parameters most suitable for providing both the single and dual configuration moon-tracking orbits when using the EMMET in a polar inclination, and by determining the launch velocity of the payloads from the EMMET's upper tip under these conditions the range of input parameters suitable for these configurations can be obtained. Having obtained the input parameters for these configurations, the magnitude of the velocity changes required to configure the EMMET correctly to track

the Moon's ascending or descending node, when using the polar moon-tracking configuration can be determined. The next step will repeat this process, but in this case the focus will turn to the EMMET orbiting with a critical inclination about Earth. Having obtained the changes in velocity required to maintain the moon-tracking configurations, and in some cases, the time period between transfer opportunities, the most suitable moon-tracking configuration can be preliminarily determined.

5.1   Polar Inclinations Parameters

For both the single and dual manoeuvre moon-tracking orbits which utilise the EMMET in a polar orbit about Earth to render its angle of ascending node stationary, it is necessary that the rate at which the EMMET's argument of perigee precesses relative to Earth is pre-determined. In the single manoeuvre case, this allows the time period to be determined for the precession of the argument of perigee through one complete revolution resulting in the re-alignment of the EMMET's apse line with the equatorial plane, and this indicates the frequency at which payload exchanges can be conducted for a given orbital configuration. In the dual manoeuvre case, this precessional rate allows the change in argument of perigee between successive payload exchanges to be determined and allows the required adjustment manoeuvre to be calculated such that the argument of perigee precesses into the required position for exchanges to occur at the required instant. The rate at which the EMMET's argument of perigee varies, $\dot{\omega}$, is dependent upon the semi-major axis and eccentricity of the orbit in addition to its orbital inclination and can be found by means of the following equation [47]:

$$\dot{\omega} = -\left[\frac{3}{2}\frac{\sqrt{\mu}J_2 R_E{}^2}{\left(1-e^2\right)^2 a^{7/2}}\right]\left(\frac{5}{2}sin^2 i - 2\right) \tag{5.1}$$

where Earth's gravitational parameter is denoted by μ; J_2 is Earth's second zonal harmonic; R_E is Earth's equatorial radius; e is orbital eccentricity; a is the semi-major axis; and orbital inclination is denoted i. For polar orbits this simplifies to:

$$\dot{\omega} = -\left[\frac{3}{4}\frac{\sqrt{\mu}J_2 R_E{}^2}{\left(1-e^2\right)^2 a^{7/2}}\right] \tag{5.2}$$

93

The two remaining variables in this equation are the semi-major axis and eccentricity. The semi-major axis [47] of the orbit can be calculated as a function of the orbital period, T, as follows:

$$a = - \left(\frac{T \sqrt{\mu}}{2\pi} \right)^{2/3} \tag{5.3}$$

To satisfy the logistical requirements stated in Chapter 2, the EMMET must arrive at the perigee of its orbit periodically with the arrival of the Moon at the ascending node of its orbit and this is achieved by arranging the orbital period of the Moon to be an even integer multiple of the EMMET's orbital period which is satisfied by equation (2.1), where m is the orbital variable. The semi-major axis can therefore be defined as:

$$a = - \left(\frac{T_{moon} \sqrt{\mu}}{2\pi m} \right)^{2/3} \tag{5.4}$$

The eccentricity [47] can be found as a function of the semi-major axis and the EMMET orbit's perigee distance as follows:

$$e = 1 - \frac{r_{perigee}}{a} \tag{5.5}$$

The rate of change of the argument of perigee can therefore be represented most simply as a function of the orbital variable m and the perigee position of the orbit.

To negate any effects of atmospheric drag on the EMMET's orbit, it must orbit in the Exosphere region of Earth's atmosphere, where these drag effects are considered to be negligible. This region is commonly considered to begin at an altitude of 600 km but varies due to solar activity and has been estimated up to an altitude of 1000 km [50]. Considering this as the most suitable region for the EMMET to orbit and using this in conjunction with a maximum tether sub-span length of 100 km we obtain an initial estimate for the EMMET's central facility perigee altitude of 1100 km or a distance of 7478 km from Earth's centre. Using this perigee altitude, the rate of regression of the argument of perigee of the EMMET's orbit was plotted as a function of the orbital variable m and this is shown in Figure (5.1). From this it can be seen that this rate of regression increases with an increasing integer variable and results from a reduction in the EMMET's apogee distance which correlates to
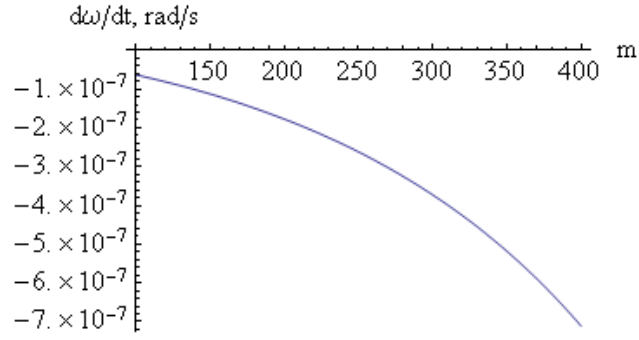
Figure 5.1: Argument of perigee variation with m

an increasing effect of the J_2 zonal harmonic on the EMMET's orbit. To minimise the time period for the revolution of the argument of perigee and maximise the frequency of alignment of the EMMET's apse line with the equatorial plane to allow more opportunities for payload exchanges for the single manoeuvre moon-tracking orbit with a polar inclination, the orbital variable m should be maximised. For the dual manoeuvre polar inclination case, we require the change in the argument of perigee to be minimised, and therefore the velocity change for this manoeuvre is also minimised and this is achieved by minimising the orbital variable m.

Maintaining our focus on the single manoeuvre configuration in the region where the orbital variable m is large, the time period taken to re-align the EMMET's apse line with Earth's equatorial plane was plotted as a function of the Moon's orbital period about Earth and this is shown in Figure (5.2). Optimally there would be a one-to-one correspondence for the period of revolution of the argument of perigee to the orbital period of the Moon, and this would allow transfers to the Moon's ascending node to occur once for every orbital period of the Moon about Earth. This one-to-one correspondence occurs for a value of the integer variable of approximately 610 and this corresponds to the EMMET undertaking 610 revolutions of Earth in the time period for the Moon to orbit Earth. A circular orbit (minimum energy and minimum period path) at the perigee radius of the EMMET's central facility has an orbital period corresponding to an integer variable value of 366 and this corresponds to the maximum practical value that the orbital variable can take and

represents the lowest orbital period that the EMMET orbit can have without traversing a path which enters into the lower atmospheric layers. It is obvious from these results that this configuration is incapable of providing a transfer opportunity for every orbit of the Moon about Earth and at best can provide a transfer opportunity every 5 lunar months when the EMMET undertakes a circular orbit about Earth. The single manoeuvre polar moon-tracking orbit will therefore be considered an inappropriate configuration hereafter.

Having determined the rate at which the EMMET's argument of perigee will regress as a function of the Moon's orbital period when the EMMET has the dual manoeuvre moon-tracking configuration, the next issue to consider is the velocity of the EMMET's upper tip relative to Earth at the instant of release as this parameter determines the perigee velocity of the payload as it begins its trans-Luna trajectory. Payload release is designed to occur when the EMMET's central facility is at perigee and the tether is aligned along the local gravity gradient; the condition under which the orbital and rotational velocities add to impart the greatest launch velocity to the payload. The maximum achievable velocity upon release at this instant can be determined as the magnitude of equation (4.28) when the tether rotation rate is at a maximum:

$$v_{u-eq} = \sqrt{\frac{\mu}{p}}(1+e) + \dot{\omega}r_o + L(\dot{\theta} + \dot{\psi} + \dot{\omega}) \qquad (5.6)$$

Any configuration of the EMMET orbit, as the orbital variable is adjusted, which does not impart a sufficient velocity for the payload to reach the boundary of the Lunar Sphere of Influence (LSI), the concep-
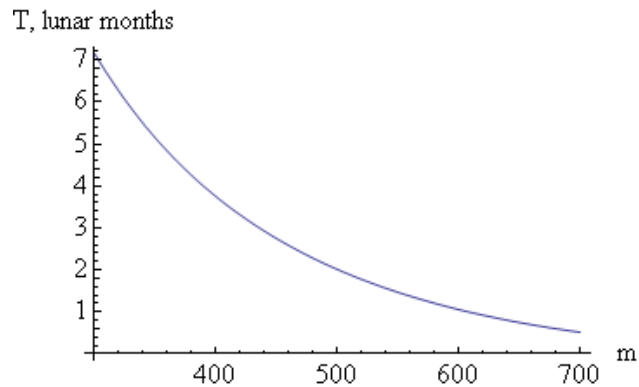
Figure 5.2: Argument of perigee re-alignment period
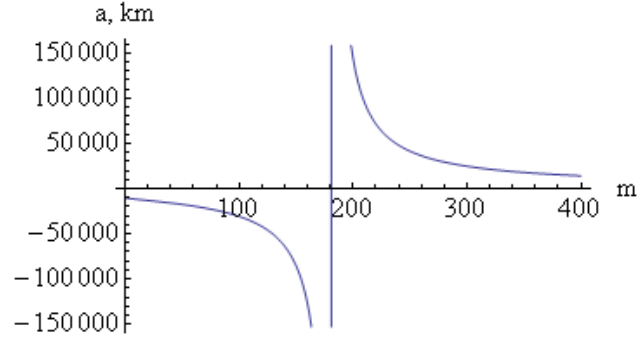
Figure 5.3: Payload semi-major axis upon release

tual boundary between Earth and the Moon's dominating gravitational influences, upon release from the upper tether tip is an inadequate configuration and is disregarded. The semi-major axis of the payload's trajectory upon release from the EMMET's upper tip can be used to determine whether or not a sufficient velocity has been imparted and this can be formulated in terms of the minimum energy, E_{min}, that the payload must possess and is found by the following relation:

$$E_{min} = \frac{\mu}{a_{min}} \tag{5.7}$$

This minimum semi-major axis, a_{min}, can also be found in terms of the required initial and final distances, r_1 and r_2, respectively, of the payload and the magnitude of the chord length, c, connecting these two positions [44]:

$$a_{min} = \frac{1}{4}(r_1 + r_2 + c) \tag{5.8}$$

For this purpose; the minimum suitable configuration equates to a trajectory from perigee at the upper tip distance, to the closest boundary
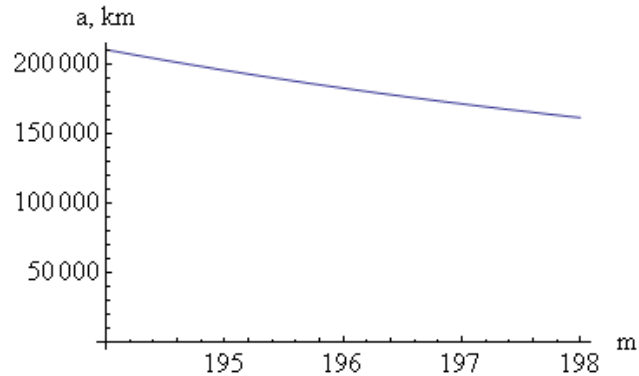
Figure 5.4: Minimum semi-major axis upon release

point of the LSI using a maximum true anomaly of 180°. Any trajectory which does not have a semi-major axis greater than this is unsuitable. At this maximum true anomaly of 180°; the chord length is equal to the addition of the initial (perigee) and final (apogee) distances of the trajectory [44]. Taking the worst case scenario to ensure that the payload can reach the Moon at any point throughout its orbital profile, we subtract the distance of the LSI in the direction of Earth, approximately 52142.75 km [44], from the apogee distance of the Moon, approximately 406731 km [51], to obtain a minimum final distance from Earth of 354588.25 km. Using this in conjunction with an initial distance of 7578 km (EMMET perigee distance plus tether sub-span length), the minimum semi-major axis required is found to be 181083.125 km from equation (5.8). Having determined the minimum semi-major axis of the payload that is required, we obtain the semi-major axis of the payload's trans-Luna transfer trajectory, $a_{payload}$, from the 'vis-viva' equation [47] using the distance and speed of the EMMET's upper tip at the payload's point of release:

$$a_{payload} = \frac{\mu}{v^2 - \frac{2\mu}{r}} \tag{5.9}$$

The range of obtainable semi-major axes for payloads released from the upper tip of a tether sub-span composed of Spectra 2000 material and rotating at maximum angular velocity relative to the central facility, found in equation (4.75), was plotted for EMMET orbits varying as functions of the orbital variable and this is shown in Figure (5.3). The data was generated using a payload mass of 500 kg, a uniform tether cross sectional area of 65 mm^2, tether sub-span density of 970 kg/m^3, maximum tensile stress of 3.25x10^9 Pa and a factor of safety of 2. The vertical line occurring at an orbital variable of 190 in Figure (5.3) and negative semi-major axis values below this are the result of the payload undertaking parabolic and hyperbolic trajectories, respectively, at these values and by reducing tether sub-span rotational rates adequate transfer velocities can be obtained. The orbital variable at which the minimum semi-major axis occurs is more easily identified by examining Figure (5.4) and this can be seen to occur at an orbital variable value of approximately 196. Any EMMET configuration which has an integer variable greater than 196, when utilising this moon-tracking configuration, is disregarded.

5.1.1 Ascending Node Velocity Change

Now that we have determined the orbital variable value above which the payload released from the upper EMMET tip is no longer able to reach the boundary of the LSI, we can now determine the change in velocity required to align the EMMET's apse line with the predicted node line of the Moon's orbit for orbital variables which are sufficient for lunar transfers. This will give an indication of the magnitude of the velocity change required to perform the manoeuvre and the orbital variables which minimise this velocity change. Assuming that the orbital manoeuvre takes place at the first opportunity within the orbit, occurring at a true anomaly of 90°, we obtain the velocity of the EMMET at the point of manoeuvre within its initial orbit, $\vec{v}_{i_1}$, by setting the sub-span length equal to zero in equation (4.25), this equation can be further simplified by assuming that the ascending node angle is 0° from which we obtain:

$$\vec{v}_{i_1} = \left[-\sqrt{\tfrac{\mu}{p}} + \dot{\omega} r_{i_1} \quad 0 \quad \sqrt{\tfrac{\mu}{p}} e \right]^T \tag{5.10}$$

At this true anomaly, orbital distance, r_{i_1}, is found to be equal to the orbital parameter and is obtained from equations (3.31) and (4.8) as:

$$\vec{r}_{i_1} = \left[0 \quad 0 \quad \tfrac{h^2}{\mu} \right]^T \tag{5.11}$$

The rotation matrix from equation (3.22) which transforms the EMMET's velocity vector from the initial to the final orbit is determined as:

$$R_K(\Delta\Omega) = \begin{bmatrix} cos(\Delta\Omega) & -sin(\Delta\Omega) & 0 \\ sin(\Delta\Omega) & cos(\Delta\Omega) & 0 \\ 0 & 0 & 1 \end{bmatrix} \tag{5.12}$$

According to Roncoli [41], the ascending node of the Moon's orbit oscillates about an ascending node angle of 0° with an amplitude of approximately 13.5° with an 18.6 year period, this results in a maximum angular variation in the ascending node of 0.22°(0.00384 radians) for an orbit of the Moon about Earth with equation (5.12) becoming:

$$R_K(0.00384) = \begin{bmatrix} 1 & -0.00384 & 0 \\ 0.00384 & 1 & 0 \\ 0 & 0 & 1 \end{bmatrix} \tag{5.13}$$
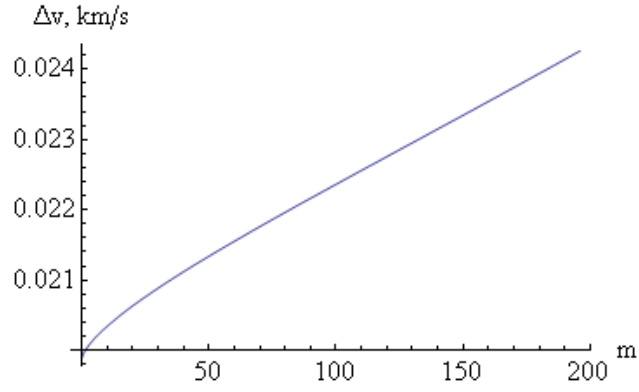
Figure 5.5: EMMET ascending node adjustment

The equation giving the change in the velocity required for the manoeuvre, equation (3.26), can now be written as:

$$\Delta \vec{v}_1 = \begin{bmatrix} 0 & -0.00384 \left(\sqrt{\frac{\mu}{p}} - \frac{\dot{\omega} h^2}{\mu} \right) & 0 \end{bmatrix}^T \tag{5.14}$$

As the orbital parameter and specific angular momentum are dependent upon the semi-major axis and orbital eccentricity which are themselves dependent upon the orbital variable, the required velocity change of the EMMET to perform the manoeuvre can be found in terms of the orbital variable and this is plotted in Figure (5.5). From this the magnitude of the change in velocity required to realign the ascending node of the EMMET's orbit with the the Moon's predicted ascending node can be found for a specific value of the orbital variable. It can be noted at this point that it requires a greater change in velocity to accomplish the manoeuvre at higher values of the orbital variable, this is a result of the manoeuvre being performed closer to Earth when the orbital variable is larger, in addition to orbits with smaller semi-major axes having larger (x, y) velocity components at a true anomaly of 90° than those with larger semi-major axes which still have a greater proportion of their velocity vector directed along the equatorial K axis.

5.1.2 Argument of Perigee Velocity Change

The next step is to determine the velocity change required to adjust the argument of perigee of the EMMET's orbit, and to begin with the true anomaly at which the orbital manoeuvre should take place will be obtained. As noted previously, a more efficient transfer can be had by
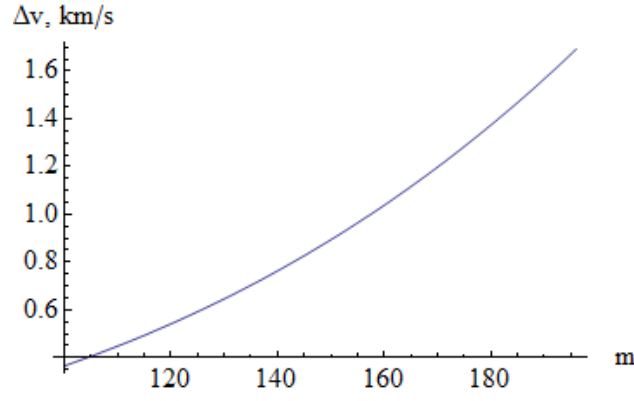
Figure 5.6: EMMET argument of perigee adjustment

performing the manoeuvre close to the apogee of the orbit. At this point of intersection, the true anomaly of the initial orbit is found from equation (3.44). The velocity of the EMMET's central facility at this point can be found from equation (4.25) and continuing with the assumption that the initial ascending node angle was zero, and also that the ascending node manoeuvre precedes the argument of perigee adjustment, the ascending node angle is now $0.22°\,(0.00384$ radians). The small angle approximation is applicable here and in addition to this, there is no loss in the simplifying assumption that the argument of perigee of the initial orbit is zero degrees at the instant of manoeuvre because the magnitude of the adjustment will be the same irrespective of the argument of perigee of the initial orbit. The velocity of the EMMET's central facility at the true anomaly of the manoeuvre, $\vec{v}_{i_2}$ is obtained as:

$$\vec{v}_{i_2} = \begin{bmatrix} \left(\sqrt{\frac{\mu}{p}} + \dot{\omega}r_{i_2}\right)sin\left(\frac{\Delta\omega}{2}\right) \\ 0 \\ \left(\sqrt{\frac{\mu}{p}}e - \left(\sqrt{\frac{\mu}{p}} + \dot{\omega}r_{i_2}\right)cos\left(\frac{\Delta\omega}{2}\right)\right) \end{bmatrix} \tag{5.15}$$

The distance of the EMMET's central facility at the point of manoeuvre is denoted by r_{i_2} and is obtained from equations (3.31) and (4.24) as:

$$\vec{r}_{i_2} = \frac{h^2/\mu}{1 - ecos\left(\frac{\Delta\omega}{2}\right)}\begin{bmatrix} -cos\left(\frac{\Delta\omega}{2}\right) & 0 & -sin\left(\frac{\Delta\omega}{2}\right) \end{bmatrix}^T \tag{5.16}$$

The adjustment to the argument of perigee of the EMMET's orbit is defined as the angle through which the argument of perigee of the EMMET's orbit regresses in the time period for an orbit of the Moon about Earth. By accounting for this regression we can align the argument of

101

perigee such that it allows the EMMET to perform catch and throw manoeuvres for every orbit of the Moon about Earth. The required angle of adjustment can be obtained by multiplying the regression rate of the EMMET's central facility, equation (5.2), by the orbital period of the Moon. We will now obtain the rotation matrix required for the manoeuvre. For a polar orbit with small angle assumptions applied, the skew symmetric matrix of equation (3.49) becomes:

$$S = \begin{bmatrix} 0 & 0 & 1 \\ 0 & 0 & 0 \\ -1 & 0 & 0 \end{bmatrix} \tag{5.17}$$

This yields the following rotation matrix from equation 3.47:

$$R_K(\Delta\omega) = \begin{bmatrix} cos(\Delta\omega) & 0 & sin(\Delta\omega) \\ 0 & 1 & 0 \\ -sin(\Delta\omega) & 0 & cos(\Delta\omega) \end{bmatrix}$$

$$\tag{5.18}$$

The change in velocity can be found from equation (3.51) as:

$$\Delta\vec{v}_2 = \begin{bmatrix} -2\left(\sqrt{\frac{\mu}{p}} + \dot{\omega}r_{i2}\right)sin(\frac{\Delta\omega}{2}) + \sqrt{\frac{\mu}{p}}esin(\Delta\omega) \\ 0 \\ -\sqrt{\frac{\mu}{p}}e\left(1 - cos(\Delta\omega)\right) \end{bmatrix} \tag{5.19}$$

The velocity change required to perform the manoeuvre, equation (5.19), varies as a function of the orbital variable and this is plotted in Figure (5.6). It is clear that a smaller velocity change is required for manoeuvres which occur close to the apogee of orbits with lower orbital variable values and thus larger semi-major axes. This is a result of their having smaller velocities closer to apogee than orbits with smaller semi-major axes, and this is in addition to the lessened effect of Earth's oblateness on larger orbits and a smaller rate of regression of the argument of perigee which results in a smaller change in the argument of perigee between transfer opportunities.

Having obtained the magnitude of the velocity changes required to adjust both the ascending node and argument of perigee of the EMMET's orbit when configured in a polar moon-tracking orbit, the total velocity
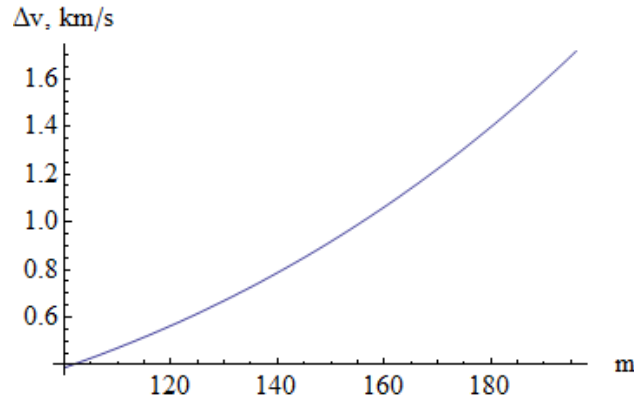
Figure 5.7: Total velocity change for polar configuration

change required to align the EMMET correctly can be obtained as the sum of these two velocity adjustments. The total velocity change required can therefore be presented as a function of the orbital variable of the EMMET's orbit and this is shown in Figure (5.7). It is evident from this that the majority of the velocity change required is to align correctly the freely precessing argument of perigee in this configuration.

5.2   Critical Inclination Parameters

Having obtained the magnitude of the velocity changes required to perform the manoeuvres required to configure the EMMET in the dual manoeuvre polar inclination case, our attention now turns to the moon-tracking configuration which utilises the EMMET with a critical inclination to render the argument of perigee stationary. At the critical inclination, the angle of ascending node of the EMMET's orbit will precess as a result of the oblateness effects of Earth's orbit, and a manoeuvre will have to be undertaken between payload exchange opportunities which takes into account this precession in addition to accounting for the oscillation of the Moon's ascending node about a mean angle of $0°$ to ensure that the EMMET's apse line precesses into alignment with the Moon's node line at the correct instant to perform payload exchanges. To obtain the magnitude of the velocity changes required to adjust correctly the EMMET's angle of ascending node first we must obtain the rate at which the ascending node precesses. As was the case with the precessional rate
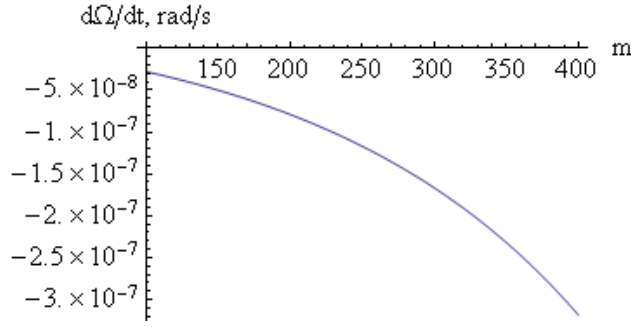
Figure 5.8: Ascending node variation with m

of the EMMET's argument of perigee, the angle of ascending node's precessional rate is dependent upon the semi-major axis and eccentricity of the orbit, in addition to its orbital inclination, and is therefore ultimately a function of the orbital variable m, assuming that the EMMET's perigee altitude remains the same. The rate at which the ascending node precesses, $\dot{\Omega}$, can be found by the following equation [47]:

$$\dot{\Omega} = -\left[\frac{3}{2} \frac{\sqrt{\mu} J_2 R_E{}^2}{(1 - e^2)^2 \, a^{7/2}} \right] cos i \qquad (5.20)$$

The orbital inclination in this case is set to a critical inclination of 63.4° as we require a prograde orbit for the EMMET. The variation of the rate of precession of the ascending node was plotted against the variation in the orbital variable and this is shown in Figure (5.8) and from this it is evident that this rate is of a comparable magnitude to that of the freely precessing argument of perigee, shown in Figure (5.8), for the polar configuration. In addition to this, it is also obvious that the rate of precession increases with increasing orbital variable and results from an increasing proximity to Earth as the orbit's geometry decreases. Having obtained the precessional rate as the orbital variable is adjusted, the range of orbital variables which provide sufficient semi-major axis for the payloads launched from the upper tips can be determined. By maintaining a minimum semi-major axis of 181083.125 km and a payload perigee distance of 7578 km, the semi-major axis of the payloads at launch can be determined from equation (5.9) where the magnitude of

104
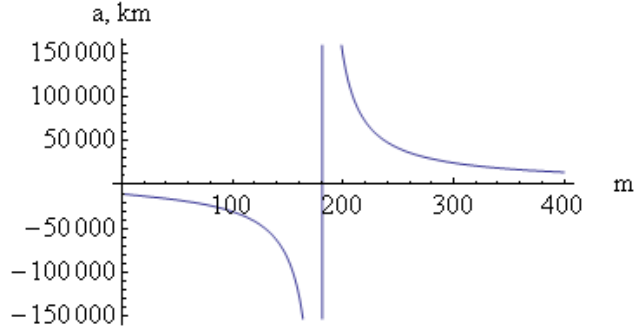
Figure 5.9: Semi-major axis upon release

the upper tip velocity in this case is determined from equation (4.40) as:

$$
\begin{aligned}
v_{u-eq}^2 &= \left(\sqrt{\frac{\mu}{p}}(1+e) + L(\dot{\theta} + \dot{\psi}) + \dot{\Omega}(r_o + L) \right)^2 \qquad (5.21)\\
&- 2\dot{\Omega}(r_o + L)\left(\sqrt{\frac{\mu}{p}}(1+e) + L(\dot{\theta} + \dot{\psi}) \right)(1 - cosi_c)
\end{aligned}
$$

Where i_c is defined as the critical inclination of the EMMET's orbit. The range of obtainable semi-major axes for payloads released from the upper tip of a tether sub-span composed of Spectra 2000 material with the material characteristics stated in section 5.1 and rotating at maximum angular velocity relative to the central facility, found in equation (4.77), was plotted for EMMET orbits varying as functions of the orbital variable, and this is shown in Figure (5.9). As expected, a plot identical to Figure (5.3) was produced and the orbital variable at which the minimum semi-major axis for payload transfers to the Moon was again found to occur at m equal to 196.

Using this moon-tracking configuration, the only orbital adjustment necessary to configure the EMMET is the adjustment of the EMMET's ascending node such that it regresses into alignment with the Moon's node line at the instant of launch. As the Moon's ascending node position varies by $0.22°(0.00384$ radians) relative to the equatorial frame for every revolution about Earth, as calculated in sub-section 5.1.2, the maximum change in ascending node angle of the EMMET's orbit can be expected when this variation in the Moon's ascending node is opposite in direction to the precession of the EMMET's ascending node. The worst case ascending node angle change will be the sum of the Moon's own ascending node variation and the variation in the EMMET's angle

of ascending node in the time period of a single orbit of the Moon about Earth. To calculate the change in velocity required to configure the EM-MET's orbit we must first determine the true anomaly in its current orbit at which the manoeuvre must be undertaken. Assuming an initial EMMET ascending node angle of $0°$, for simplicity, and an argument of perigee set to $0°$, the true anomaly of intersection is obtained from equation (3.17) as:

$$\theta_i = tan^{-1}\left(-tan\left(\frac{\Delta\Omega}{2}\right)seci_c\right) \qquad (5.22)$$

The velocity of the EMMET's central facility at this true anomaly can be obtained by setting the tether sub-span length equal to zero in equation (4.34) and is obtained as:

$$\vec{v}_i = \begin{bmatrix} -\left(\sqrt{\frac{\mu}{p}} + \dot{\Omega}r_icosi_c\right)sin\theta_i \\ \sqrt{\frac{\mu}{p}}(e + cos\theta_i)cosi_c + \dot{\Omega}r_icos\theta_i \\ \sqrt{\frac{\mu}{p}}(e + cos\theta_i)sini_c \end{bmatrix} \qquad (5.23)$$

Where the central facility distance, r_i, is obtained from the equation of an elliptical orbit:

$$r_i = \frac{h^2}{\mu(1 + ecos\theta_i)} \qquad (5.24)$$

The change in velocity required to adjust the ascending node of the EM-MET's orbit can be expressed solely in terms of the velocity of the initial orbit and the rotation matrix as shown in equation (3.26). As the rotation axis for the adjustments to the ascending node angle of the EMMET's orbit coincides with Earth's polar axis, the required rotation matrix for the application of the Rodriguez formula can be expressed identically to that obtained in equation (5.12). The change in velocity required to perform the ascending node adjustment when the EMMET is in a critically inclined orbit is therefore:

$$\Delta\vec{v} = \begin{bmatrix} \alpha \\ \beta \\ 0 \end{bmatrix} \qquad (5.25)$$
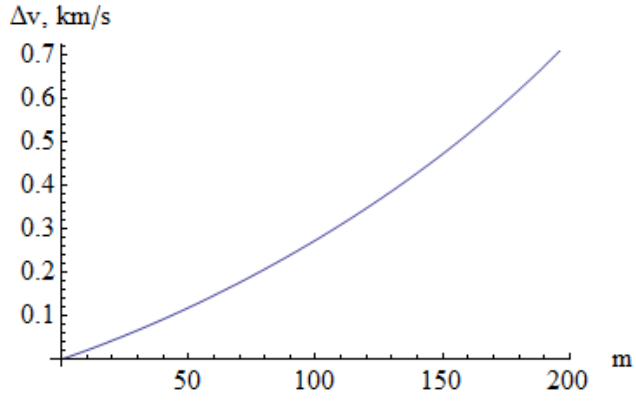
Figure 5.10: Velocity change for critical configuration

with

$$
\begin{aligned}
\alpha &= -\left(\sqrt{\frac{\mu}{p}} + \dot{\Omega}r_i cosi_c\right)sin\theta_i(cos(\Delta\Omega) - 1) \\
&\quad - \left(\sqrt{\frac{\mu}{p}}(e + cos\theta_i)cosi_c + \dot{\Omega}r_i cos\theta_i\right)sin(\Delta\Omega) \\
\beta &= -\left(\sqrt{\frac{\mu}{p}} + \dot{\Omega}r_i cosi_c\right)sin\theta_i sin(\Delta\Omega) \\
&\quad + \left(\sqrt{\frac{\mu}{p}}(e + cos\theta_i)cosi_c + \dot{\Omega}r_i cos\theta_i\right)(cos(\Delta\Omega) - 1)
\end{aligned}
$$

Having obtained an expression for the change in velocity required to adjust the ascending node of the EMMET's orbit when it has a critical inclination, this change in velocity was plotted as a function of the orbital variable and this is shown in Figure (5.10). Again the velocity increases as the orbital variable increases and results from the EMMET's increasing proximity to Earth as its orbital geometry decreases. In this case, the change in velocity required is smaller than the freely precessing argument of perigee in the polar inclination case and results from the ascending node rate being smaller in this case than the rate of the argument of perigee in the polar inclination case.

5.3 Tether Efficiency and Performance

Having defined the EMMET's parameters relative to Earth it is useful to determine the most efficient configuration to conduct payload transfers and this is dependent upon the semi-major axis of the EMMET's orbit, tether sub-span length and the rotational rate of the sub-spans

themselves. By determining the dependency of the payload's launch configuration on each of these variables, the most efficient configuration that provides the payload with the minimum semi-major axis required to reach the Moon's LSI at all times in its orbital profile can be determined. Previous studies have been conducted on the performance and effiency of symmetrically laden hanging, librating and motorised tethers by Zeigler and Cartmell [22], [49] which were based upon the altitude gained and lost by payloads released from the upper and lower tip positions of a motorised tether system with varying tether sub-span lengths orbiting Earth in circular orbits only. As the designs presented here require the EMMET to orbit Earth in elliptical orbits so that the payload released from the upper tip has sufficient velocity to reach the Moon, the performance and efficiency indexes presented by Zeigler and Cartmell [22], [49] have been modified to account for the launch velocity's dependency upon the perigee velocity of the central facility's orbit in addition to the tether sub-span length and rotational rates. To accomplish this the focus has switched from payload altitude gain and loss half an orbit after release from the upper and lower tips, respectively, of an Earth orbiting MMET to a more general gain or loss of specific orbital energy, which is a constant of the payload's subsequent trajectory, and this gives a more satisfactory measure of the performance and efficiency when variations in the EMMET's semi-major axis, tether sub-span length and rotational rates are taken into account. Similarly to Zeigler and Cartmell's own formulation [22], [49]; the oblateness effects of Earth are ignored for the moment; the tether's sub-spans are assumed to lie within the orbital plane; the tether sub-spans are assumed to be of uniform cross sectional area and density; and the tethers are rigid and of a fixed length. However, in this case, the analysis will only be conducted for a tether at the perigee of its orbit about Earth with the sub-spans aligned along the local gravity gradient, and this is consistent with the optimum configuration for a trans-luna payload's launch position. We will begin with an assessment of the payload's gain or loss of specific energy when the semi-major axis or the tether sub-span lengths are adjusted for the hanging tether case, with the aim of finding the nature of the relationship between the

change in energy and the adjustment of the variables, and from this the EMMET's performance and efficiency in terms of this energy change will be obtained. The performance and efficiency of a motorised tether will then be obtained and we will conclude the current chapter with a comparison of the performance and efficiency of the hanging and motorised cases to those obtained in previous literature.

5.3.1   Hanging Tether Parameters

To generalise the performance and efficiency of an MMET in an elliptical orbit about Earth with payloads of equal mass attached symmetrically to the upper and lower tips such that variations in tether sub-span length and semi-major axis can be accounted for, the resultant configuration of the payloads at their instant of release must be expressed in terms of their resultant gain or loss of their energy per unit mass (or specific energy) relative to Earth. In the preceding literature with the central facility in a circular orbit [49], the resultant gain or loss in altitude was sufficient to determine performance and efficiency. However, when the central facility orbits Earth with an elliptical geometry, variation in its semi-major axis must also be accounted for. Firstly, to establish the nature of the relationship between the gain and loss of specific energy as the tether sub-span length is varied, the semi-major axis of the EMMET is defined as identical to that of equation (5.9) and is set to a constant value by setting the orbital variable m to a constant. The specific energy of the EMMET's orbit, E_{EM} is found by the following equation:

$$E_{EM} = -\frac{\mu_E}{a_{EM}} \qquad (5.26)$$

where μ_E is Earth's gravitational parameter and a_{EM} is the EMMET's semi-major axis. The specific energy of the payloads released from the EMMET's upper and lower tips, denoted by E_u and E_l, respectively, are found from an equation of identical form to equation (5.26), with the semi-major axis in each case obtained from equation (5.9). At perigee, the radial distance in equation (5.9) is simply the addition of the tether sub-span length to the EMMET's perigee distance for the upper payload case and for the lower payload case it is simply the subtraction of the

sub-span length from the perigee distance. Ignoring Earth's oblateness effects for the moment, the velocity of the upper payload at the instant of release, v_u, in equation (5.9) is the magnitude of equation (4.16) with the true anomaly set to zero which results in:

$$v_u = \sqrt{\frac{\mu}{p}}(1 + e) + L(\dot{\theta} + \dot{\psi}) \qquad (5.27)$$

The lower payload's velocity at the point of release, v_l, is obtained as:

$$v_l = \sqrt{\frac{\mu}{p}}(1 + e) - L(\dot{\theta} + \dot{\psi}) \qquad (5.28)$$

For a hanging tether the sub-span's angular rate $\dot{\psi}$ is zero. The energy gain of the payload, ΔE_u, as a result of its release from the EMMET's upper tip can be simply expressed as:

$$\Delta E_u = E_u - E_{EM} \qquad (5.29)$$

The loss of specific energy, ΔE_l, for a payload released from the EMMET's lower tip can be expressed as:

$$\Delta E_l = E_l - E_{EM} \qquad (5.30)$$

A plot was produced of the gain and loss of the specific energy of the payloads as a result of release from the tips of the EMMET using an EMMET perigee distance of 7478 km, an orbital variable of 150, corresponding to a semi-major axis of 13573.1 km, and varying the sub-span length between 0 and 200 km, which are shown in Figures (5.11) and (5.12), respectively. It is clear that the specific energy of the payloads varies linearly with the tether sub-span length, and the gain in energy of a payload at some arbitrary sub-span length above the central facility corresponds to a payload with an identical loss in specific energy at the same sub-span length below the central facility. It can be concluded from this that whatever the energy that is gained by the upper payload is also lost by the lower one, resulting in the energy of the entire EMMET system remaining constant. The performance of a MMET was previously defined as the gain or loss of distance experienced by the payload half an orbit after release from the MMET [22], [49], as specific energy is constant at all points in the payload's orbit; we can define performance as
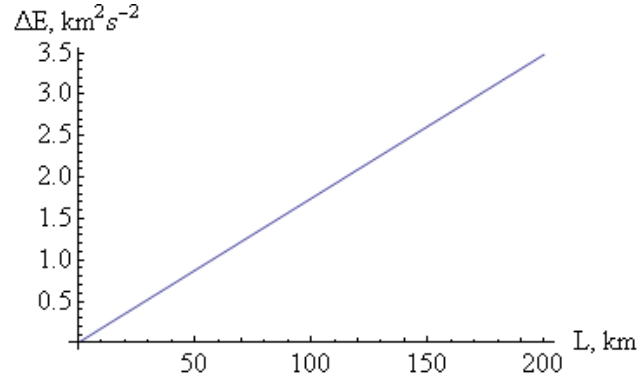
Figure 5.11: Upper payload energy gain with length
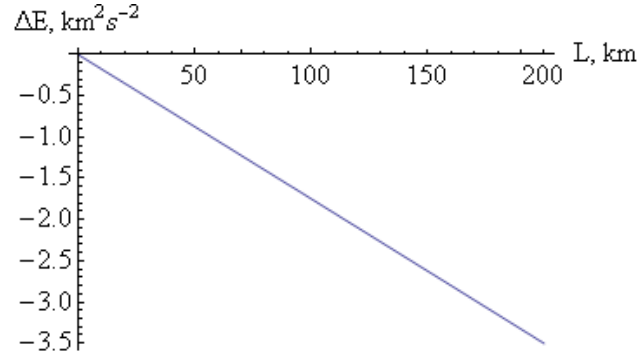
Figure 5.12: Lower payload energy loss with length

the gain or loss in energy of the payload at the instant of release. Using this definition, it can be seen that there is a larger gain in energy of the upper payload when larger tether sub-spans are used, additionally, there is a larger loss in energy in this case too. It can be concluded from this that longer tether sub-spans have better performance characteristics for the respective gain and loss of energy. Putting this into terms of payload raising and lowering; the greater the energy the payload has upon release from the upper tip results in it having a larger semi-major, axis and consequently a larger apogee distance. It is therefore performing better at payload raising; the greater the energy loss of the payload at release from the lower tip, the lower its semi-major axis will be resulting in increasingly closer perigee distances to Earth and therefore performs better at payload lowering.

Tether efficiency was defined by Zeigler and Cartmell [22], [49] as the ratio of the altitude gain or loss to the tether's sub-span length. Here we will define the efficiency in terms of the ratio of the specific energy of

111
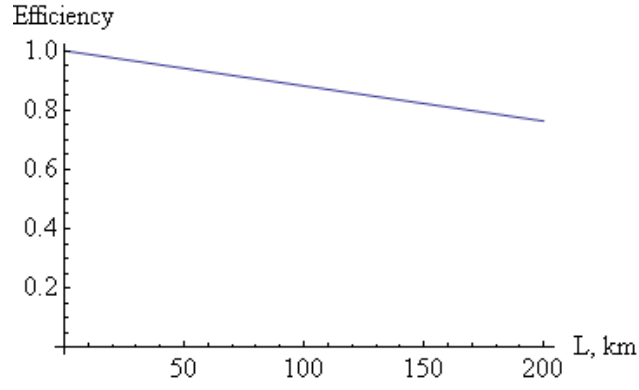
Figure 5.13: Upper payload efficiency with length
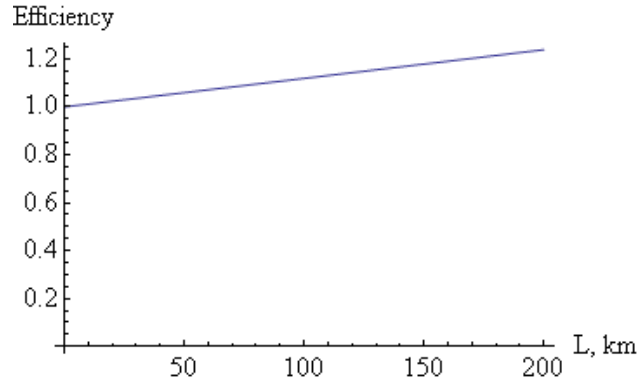
Figure 5.14: Lower payload efficiency with length

the payload after release to the energy of the EMMET's orbit, and this can be interpreted as the ratio of the output energy to the input energy. The efficiency is derived from equation (5.29) or (5.30) and is defined as:

$$\text{efficiency} = 1 + \frac{\Delta E}{E_{EM}} \qquad (5.31)$$

Plotting the efficiency for the energy imparted and detracted from the upper and lower payloads as the tether sub-span is varied allows us to establish the dependency of this energy change on sub-span length, and these are shown for the upper and lower payloads in Figures (5.13) and (5.14), respectively. In the field of orbital mechanics, the energy of a body in orbit about a central mass is negative which corresponds to the negative potential well model applied in these cases. The potential energy of the mass is taken to increase in energy from -∞ to its current location with the total required energy to reach the boundary of the body's gravitational influence equal to zero, and actually to escape the gravity field the energy must exceed this and become positive. Applying

112

this model to the specific energy of the payloads upon release, the EM-MET's efficiency actually increases as the ratio of the output energy to the input energy decreases because this corresponds to the payload upon release increasing in the positive direction towards zero from the initial negative energy of the EMMET in its orbit about Earth. We will therefore define a more efficient system for increasing payload energy as one which gives increasingly smaller efficiency ratios, as defined in equation (5.31). Furthermore, we will define a more efficient system for decreasing payload energy as one which gives increasingly larger efficiency ratios. Using this definition, it can be seen that the efficiency of the upper payload's energy gain increases with increasing tether sub-span length for the upper payload, correspondingly, efficiency increases with increasing sub-span length for the lower payload. It is obvious from this that the most efficient configuration for payload altitude gain or loss is when the tether sub-span length is maximised. Physically, this can be interpreted as the upper payload gaining an increasingly larger velocity relative to the velocity required to remain on the same trajectory after release and similarly for the lower payload; this loses an increasingly larger proportion of the velocity required to remain on the same trajectory after release. In both cases, the energy input is simply the energy required to place the EMMET's central facility in the correct orbit with the resultant energy gain and loss of the upper and lower payloads a result of their position relative to Earth and the central facility, in addition to the kinetic energy of the central facility.

To establish the relationship between the variation in the semi-major axis of the EMMET's orbit and the corresponding change in specific energy, an identical method used for the variation in the sub-span length was utilised but in this case the sub-span length was set to 100 km and the orbital variable was varied between 100 and 366, the orbital harmonic corresponding to a circular orbit, in order to adjust the semi-major axis of the orbit. Plots of the upper and lower payloads energy gain and loss are shown in Figures (5.15) and (5.16), respectively. In this case, there is an almost linear relationship between the change in the orbital variable m, corresponding to a change in the semi-major axis of the EMMET,
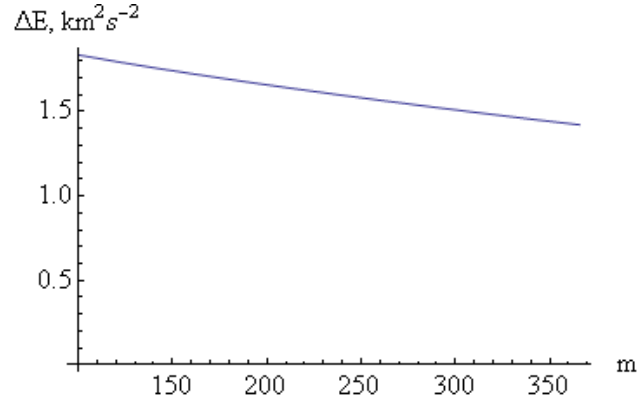
Figure 5.15: Upper payload energy gain with semi-major axis
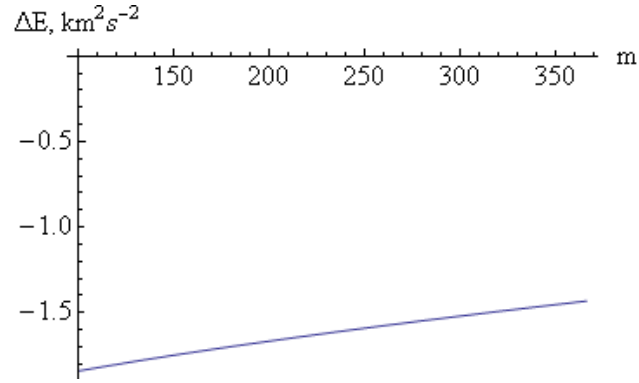
Figure 5.16: Lower payload energy loss with semi-major axis
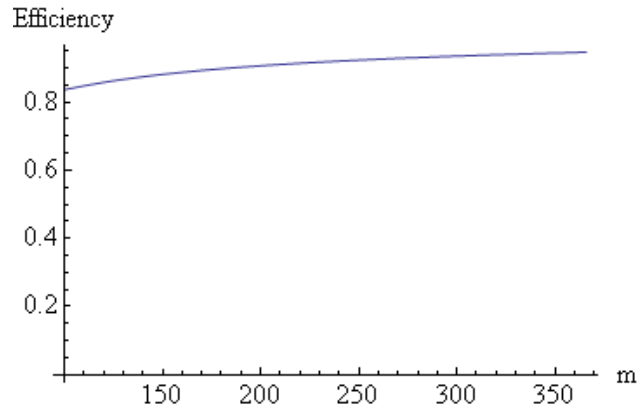
Figure 5.17: Upper payload efficiency with semi-major axis

and the change in specific energy of the payloads upon release. The specific energy of the upper payload is found to decrease as the semi-major axis of the EMMET's orbit decreases with increasing orbital variable m. This can be interpreted very simply as the energy of the upper payload decreasing as the input energy of the EMMET's orbit decreases as a direct result of a decrease in the semi-major axis of the EMMET's orbit.
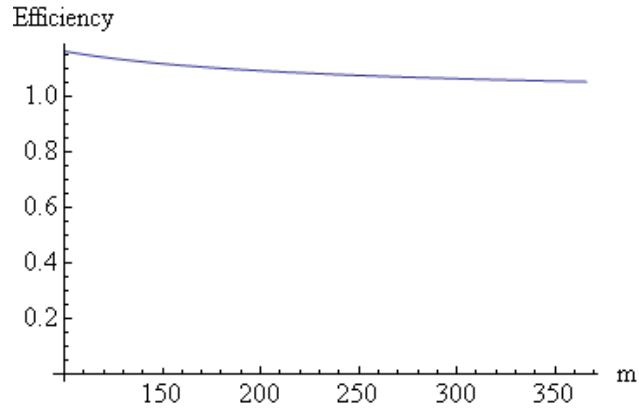
Figure 5.18: Lower payload efficiency with semi-major axis

Similarly, the energy of the lower payload increases with a decreasing semi-major axis and increasing orbital variable m and corresponds to less energy being detracted from the lower payload as the semi-major axis and thus the orbital energy supplied by the EMMET are decreased. As was the case with variation in tether sub-span length, the specific energy gained by the upper payload at a certain sub-span length corresponds to the energy lost by the lower payload at this length. Defining the performance in a similar manner to that of the tether sub-span variation case, the performance of the EMMET in imparting or detracting energy from the upper and lower payloads decreases with decreasing semi major axis and corresponds to an increasing orbital variable m and a decrease in the energy input from the EMMET's orbit. It can therefore be concluded that decreasing the semi-major axis results in poorer performance of the EMMET when considering payload energy gain or loss, or correspondingly payload raising or lowering. Tether efficiency was obtained for the energy imparted and detracted from the upper and lower payloads as the EMMET's semi-major axis was varied with the tether sub-span lengths remaining constant, and these are shown for the upper and lower payloads in Figures (5.17) and (5.18), respectively. By again defining a more efficient EMMET for imparting energy as one which produces the smallest ratio between input and output energy, corresponding to a positive increase in energy towards zero, it can be seen that the system becomes less efficient at imparting energy to the upper payload with increasing orbital variable which corresponds to a decreasing semi-major axis, cor-

115
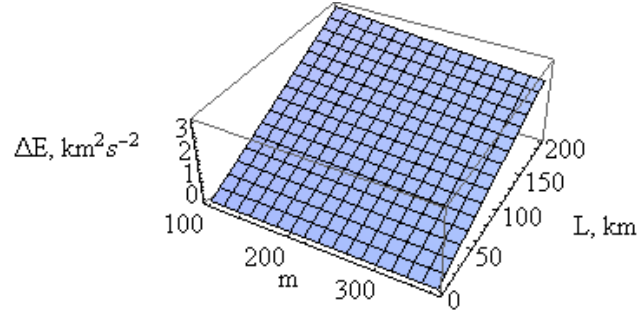
Figure 5.19: Upper energy gain with semi-major axis and length
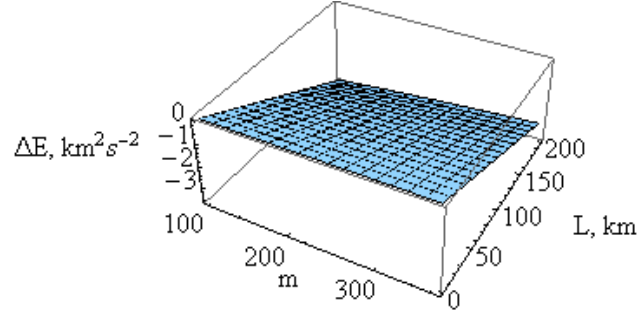
Figure 5.20: Lower energy loss with semi-major axis and length
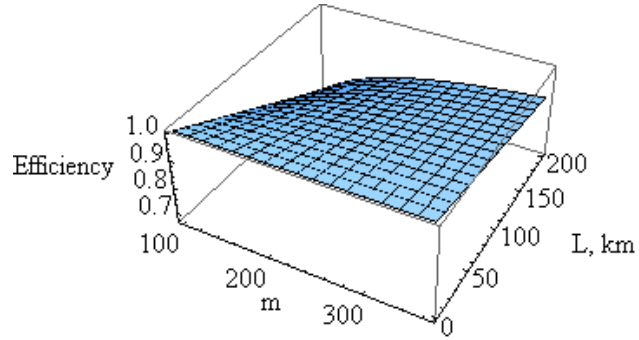
Figure 5.21: Upper efficiency with semi-major axis and length

respondingly the system becomes less efficient at extracting energy from the lower payload with decreasing semi-major axis for the lower payload.

Having obtained data for the variation in the performance and efficiency when only the tether sub-spans or semi-major axis of the central facility was varied, plots were obtained for the performance and efficiency when both of these were changed. Performance is shown for the upper and lower payloads in Figures (5.19) and (5.20), respectively, and efficiency is shown in Figures (5.21) and (5.22). From the plots on performance for the upper and lower payloads, Figures (5.19) and (5.20), respectively,

116
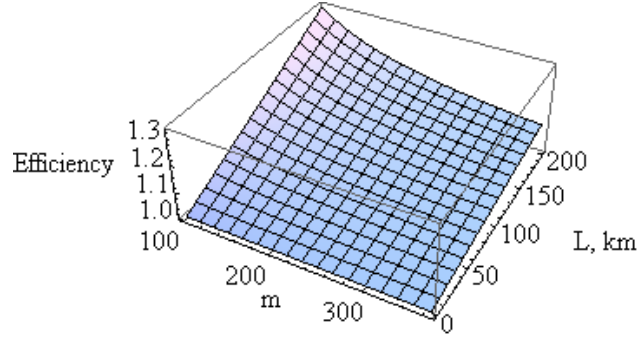
Figure 5.22: Lower efficiency with semi-major axis and length

the best performing configuration for imparting energy to the payload is one which has the largest semi-major axis and tether sub-span length additionally, this also corresponds to the best performing configuration for detracting energy from the lower payload. It can therefore be concluded that energy gain and loss is a direct result of the orbital energy imparted to the EMMET, and the separation between the payloads and central facility at the instant of release. Furthermore, by examining the plots for the energy efficiency when both the semi-major axis and tether sub-span lengths are varied, Figures (5.21) and (5.22), it is obvious that the EMMET is most efficient for both payload raising and lowering at the configuration at which the best performance is obtained for energy gain and loss, therefore no distinction can be made between the measurement of performance and efficiency and either one or the other can be utilised.

Comparing the change in energy for both the upper and lower payloads when both the tether sub-span length and semi-major axis are varied seems to suggest that the adjustment to tether sub-span length has a much greater influence on the addition or subtraction of payload energy than any variations to the semi-major axis which are made. To compare this correctly, we calculate the change in payload specific energy between a sub-span length of 50 km and 100 km as 0.9 km^2s^{-2} from Figure (5.11) and we also calculate the change between an initial semi-major axis of 136233.1 km and 13573.1 km and orbital variable values of 149.063 and 150 for which we obtain 0.062 km^2s^{-2}. The change in energy as a function of tether sub-span length is a factor of 10 greater than the energy change resulting from the corresponding change in semi-major axis.

5.3.2 Motorised Tether Parameters

Having defined the performance and efficiency of a hanging tether when variations in tether sub-span length and semi-major axis are made, we will now obtain data on the performance and efficiency of the EMMET for imparting and subtracting energy when the EMMET is motorised and the sub-spans are rotating relative to the central facility. Once again the energy of the payloads at their instant of release are determined using an equation identical to equation (5.26), with the upper tip position at perigee again denoted as the EMMET's perigee distance plus sub-span length L and the lower position as the EMMET's perigee position minus sub-span length L. The velocity of the upper and lower tips are again obtained using equations (5.27) and (5.28) and in this case the angular rate $\dot{\psi}$ is non-zero and its maximum value is dependent upon sub-span length and is obtained from equation (4.75), by setting the secular rates equal to zero, as:

$$\dot{\psi}_{max} =$$
$$\sqrt{\frac{\left(\left(\frac{\sigma_{max}}{SF}\right)A - \frac{GM_E}{r_0^2}\left((2m_p + m_T)\left(\frac{L}{r_0}\right) + \left(\frac{L}{r_0}\right)^2(3m_p + m_T)\right)\right)}{L\left(m_p + \frac{1}{2}m_T\right)}} - \dot{\theta}$$
$$(5.32)$$

Defining the specific kinetic energy, $KE_{specific}$, of rotation of the sub-spans as:

$$KE_{specific} = \frac{1}{2}L^2\dot{\psi}^2 \qquad (5.33)$$

The change in kinetic energy of either payload as a result of the rotation of the sub-spans was plotted as a function of tether sub-span length for the maximum rotational rate and using a semi-major axis of 13573.1 km, the results are shown in Figure (5.23). It can be seen that the maximum gain in kinetic energy as a function of tether sub-span length and resulting from the tether rotating at the maximum rate which it can comfortably withstand at this length occurs for a tether sub-span length of 100km and for values close to this. Having determined that the payload gains most kinetic energy when rotating at maximum angular velocity with a sub-span of 100 km and that the effect of altering the semi-major axis
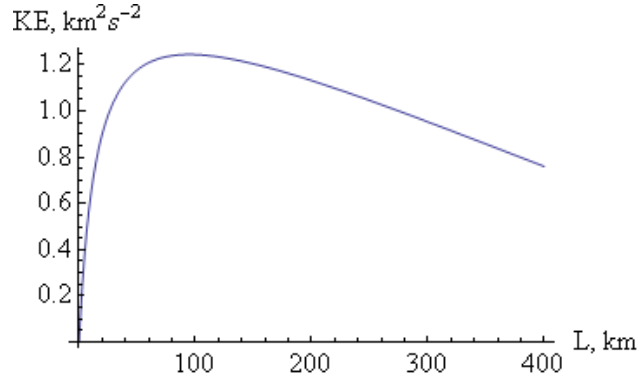
Figure 5.23: Change in payload kinetic energy

of the EMMET's orbit is at least a factor of 10 smaller than altering the sub-span length, our focus will turn the performance and efficiency of the tether when taking into account the variation in sub-span rotational rate. To achieve this, modifications to our definitions of performance and efficiency must be made to account for the energy put into the system to rotate the sub-spans. We therefore re-define performance of the upper and lower sub-spans to account for this additional kinetic energy, as:

$$\Delta E = E - \left(E_{EM} + \frac{1}{2}\dot{\psi}^2 L^2 \right) \tag{5.34}$$

The performance of the EMMET can be similarly re-defined as:

$$\text{efficiency} = 1 + \frac{\Delta E}{\left(E_{EM} + \frac{1}{2}\dot{\psi}^2 L^2 \right)} \tag{5.35}$$

The energy gain and loss of the upper and lower payloads was plotted for variations in the rotational rate of the tether sub-spans from zero to their maximum rates using a sub-span length of 100 km and a semi-major axis of 13573.1 km, and the performance of the EMMET is shown for the upper and lower payloads in Figures (5.24) and (5.25), respectively. Comparing the performance with that of the hanging tether at the same tether length and semi-major axis, it can be seen that the motorised tether gives the upper payload an energy increase of 10 times that of the hanging tether with the same sub-span length and semi-major axis when rotating at maximum rate, and the lower payload receives a corresponding energy loss in comparison with the hanging tether case. The efficiency of the motorised EMMET was also obtained. By retaining our definition of efficiency for upper payload energy gain, the system's efficiency is in-
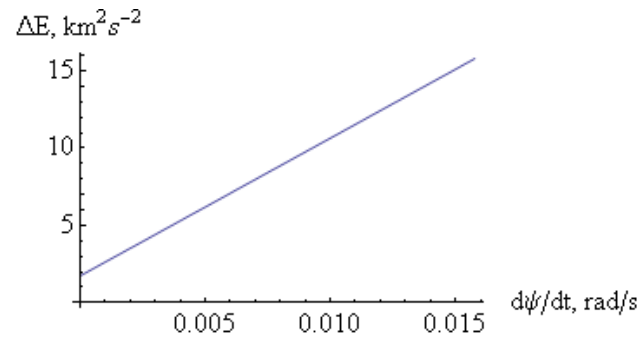
Figure 5.24: Upper payload energy gain with rotation rate
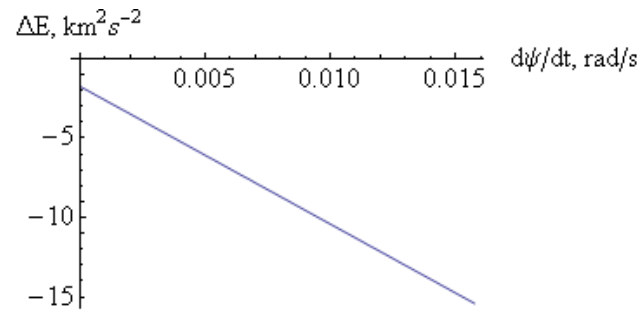
Figure 5.25: Lower payload energy loss with rotation rate
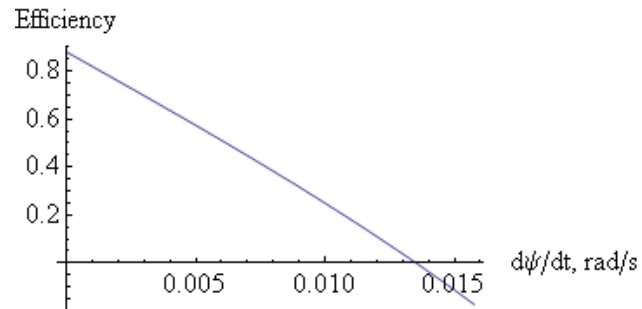
Figure 5.26: Upper payload energy efficiency with rotation rate
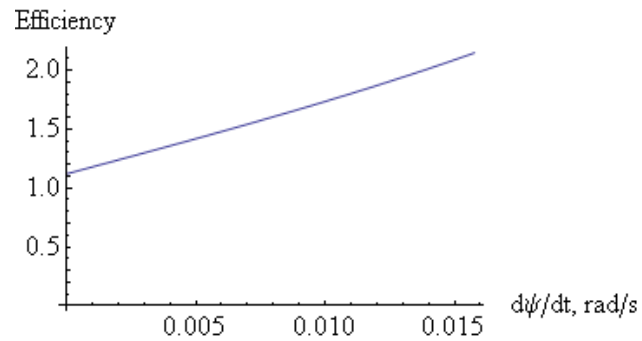
Figure 5.27: Lower payload energy efficiency with rotation rate

creasing with increasing angular rate, furthermore, the point at which the data plot crosses the x-axis corresponds to the payload having zero energy and being able to reach the boundary of Earth's gravitational influence. The data also shows that this configuration is also capable of providing enough energy to escape Earth's gravity, and corresponds to negative efficiency in the plot. Continuing with the definition of efficiency for detracting energy from the lower payload, the efficiency of the system also increases with increasing angular rate. Therefore, the performance and efficiency also correspond for the motorised tether case.

5.4   Conclusions

Using the equations for the rate of change of the argument of perigee it was found that a single manoeuvre polar moon-tracking configuration would give insufficient re-alignment frequency with the fundamental plane of the equatorial frame. This configuration was subsequently disregarded as a viable solution. Additionally, by utilising the maximum angular speeds which the tether sub-spans can withstand in this configuration, derived in Chapter 4, in conjunction with the minimum payload semi-major axis upon release which is required to reach the Moon: it was found that the maximum orbital harmonic between the EMMET and Moon sufficient for lunar transfers occurred at m equal to 196. The maximum angle through which the EMMET orbit's velocity vector must be rotated to adjust the apse line of the EMMET's polar orbit was determined by calculating the rate at which the Moon's ascending node oscillates about the equatorial frame's x axis. The velocity change required to perform this manoeuvre as a function of harmonic m was then determined. These adjustments were found to increase with increasing orbital harmonic and resulted from an increased proximity of the EMMET to the Earth resulting in increased precessional rate. Furthermore, the magnitude of the velocity change required to adjust the freely precessing argument of perigee of the EMMET into alignment with the fundamental plane of the equatorial frame was obtained as a function of harmonic m thus allowing the optimum configuration to perform these

velocity changes to be determined. It was noted that the adjustments to the freely precessing argument of perigee was much more significant than those required to re-align the EMMET's apse line with the Moon's node line.

Again, the semi-major axes of the payloads upon release for EMMET's in critically inclined orbits was determined thus allowing the maximum value of harmonic m to be determined. This was again found to occur at m equal to 196. By determining the rate at which the freely precessing angle of ascending node varies for critically inclined orbits the change in velocity required to transfer from one orbit to another was determined and from this the optimum configuration could be obtained. It was found that the change in velocity required to adjust the freely precessing angle of ascending node in this case also increased with increasing orbital harmonic again as a result of increasing proximity to Earth, resulting in increased precessional rate in this case. However, this velocity change was found to be smaller in comparison to that required to adjust the freely precessing argument of perigee.

Performance and efficiency indexes have been derived for both the hanging and motorised tether cases which are based upon the gain or loss of the specific energy of a payload at the instant of release. It was found that an increase in tether sub-span length improved both the performance and efficiency of the system for upper payload energy gain and lower payload energy loss in comparison with alterations to the semi-major axis of the system. An increase in the semi-major axis of the system was also found to improve the performance of the tether for both energy loss or gain as a result of this coinciding with an increase in orbital energy for the system. A significant result was found when numerical analysis of the motorised tether system was undertaken which showed that the maximum increase in the kinetic energy of a payload at the tip of sub-span rotating at maximum angular velocity occurred on a small plateau centred at a sub-span length of 100 km. The motorised tether system performed ten times better than the hanging tether case in imparting energy to the upper payload and detracting energy from the lower payload.

6.   Circumlunar Design

The following chapter will begin with an outline of the procedure used
to configure a circumlunar trajectory with the outbound payload from
Earth launched from the upper tip of the EMMET and captured by the
upper tip of the Lunavator; the return payload, after a logistical delay,
is launched on a trajectory to Earth from the upper tip of the Lunavator
and is captured at Earth by the upper tip of the EMMET. This proce-
dure was very much influenced by the procedure outlined by Battin [44]
and though dissimilar in many ways it could not exist without it. The
main differences between this method, Battin's or any other method is
that this procedure is designed to allow a circumlunar trajectory to be
arranged which is consistent with the logistical framework required for
a continuous payload exchange defined in Chapter 2. Unlike previous
methods, the point of in and outbound payload perigee positions can-
not be freely chosen nor can the perilune positions of the payloads at
the Moon be freely chosen. Furthermore, times of flight between these
positions are restricted by the system's logistics. Having given our out-
line, a description of the mechanisation of the procedure is given as well
as a detailed account of how the trajectories between the MMETs were
constructed with the aim of satisfying the logistical requirements of the
system's design.

6.1   Design Outline

To establish a circumlunar trajectory in order to conduct payload ex-
changes between the EMMET and Lunavator when the Moon is at the
ascending or descending node of its orbit about Earth; the initial step
in the procedure is to establish a patched conic approximation for the
motions of the payloads relative to Earth and the Moon. In this chapter
focus will remain with the ascending node case. The patched conic ap-
proximation does not give a precise reference orbit [44] but allows us to

explore the initial and final conditions of the payload's motion about the Earth and Moon when variations to the trajectories between the MMETs are made. According to Battin [44], when a precise orbit is obtained based on the patched conic approximation, certain quantities such as the time of flight, as well as the launch and return perigees, are invariant. The method utilised here consists of configuring three conics, the first is the hyperbolic trajectory about the Moon of the payload, or in this case payloads, beginning at the payload's entry point to the Moon's gravitational influence, termed Lunar Sphere of Influence (LSI), and terminating at the exit point of the hyperbola from the LSI. The second and third conics to be configured are the elliptical orbits about the Earth which connect the LSI entry and exit points to the launch and return perigee positions, respectively; it is useful in reducing any velocity mismatches if these elliptical transfer arcs are symmetrical portions of the same elliptical trajectory resulting in coincident perigee positions. Although the ellipses about Earth and the hyperbola coincide at the entry and exit points to the LSI their velocities at these points relative to the Moon or Earth do not necessarily coincide, however by making small adjustments to these trajectories the velocities at the junction points can be matched and subsequently a circumlunar trajectory can be established. To achieve our overall aims, we treat the payload travelling to the Moon, which we term trans-Luna, and the payload traveling to Earth, termed trans-Earth, as a single payload and establish a patched conic approximation for the circumlunar trajectory which incorporates a short delay when the payload reaches perilune corresponding to the waiting time logistical requirement outlined in Chapter 2, and the transfer times for these motions must also satisfy the logistical requirements also described in that chapter. Furthermore, by configuring the EMMET's and Lunavator's upper tips to coincide with the payload's perigee position and velocity and perilune position and velocity, respectively; the required configurations for the MMETs to perform payload launch and capture operations can be established whilst minimising any velocity mismatches at these points. Once a circumlunar trajectory has been established, the magnitude of the change in velocity required to correct for any irreconcilable

mismatches over the course of the trajectory design can be established. Having described the general method for a patched conic approximation, we will now outline the method used to establish the circumlunar trajectory which will be utilised for a continuous payload exchange between the EMMET and Lunavator.

6.1.1   Payload Exchange Trajectory Design

Firstly, a time period for transfer operations to begin is chosen and we obtain the configuration of the Moon at this instant, from this the Moon's orbital elements are obtained and the time to its next occurrence at its ascending node is established. In addition to this, we configure the EMMET's ascending node to be 180° out of phase with the Moon's ascending node at this time. Now we begin the construction of the circumlunar trajectory for the payload exchange method and establish an initial approximation for the single hyperbola about the Moon corresponding to the motion of both the trans-Earth and trans-Luna payloads within the LSI. A single hyperbola is constructed between the LSI entry and exit positions and this allows the same upper tip position and velocity of the Lunavator to be matched to the perilune position and velocity of both payloads thereby reducing any velocity mismatches at this point. The time of flight for the hyperbola is simply the time taken for a single payload to travel between the LSI entry and exit points with the logistical waiting time ignored for the moment. By adjusting the LSI entry and exit points, relative to the Moon, a sufficient perilune position can be obtained which is generally within 200-300km of the Moon's surface. At this point, the upper and lower tip velocities of the Lunavator can be calculated and this determines whether a satisfactory perilune position and velocity has been obtained. By maintaining the time of flight of this hyperbola but now including the waiting time; the orbital elements of the trajectory at LSI entry and exit relative to Earth are obtained, and the payload's inclinations are matched to one another and the inclination of the EMMET's orbit by making small adjustments to the entry time to LSI and adjustments to the exit time through variation of the waiting time at perilune. Particular attention is also paid to the argument

of perigee of the payloads relative to Earth and these should match as closely as possible the argument of perigee of the EMMET to reduce any mismatches between the velocities of the elliptical trajectories between the EMMET and LSI, at the instant of LSI contact, and the payload velocities at LSI entry and exit required for the configured hyperbola. Attention is also paid to the eccentricity of these payloads relative to Earth to ensure that they are actually undertaking elliptical trajectories before and after undertaking the hyperbola about the Moon, and do not have sufficient velocities to undertake hyperbolic trajectories about Earth.

Having obtained a sufficient hyperbola about the Moon, the elliptical trajectories between the EMMET's perigee position and the LSI entry point, in addition to the LSI exit point and EMMET perigee position, are then established. By setting an initial time of flight between these points, the orbital inclination, ascending node angle and argument of perigee of the trajectories can be determined. By adjusting the times of entry and exit to the LSI, the inclination and angle of ascending node of these trajectories can be varied. Although this affects the inclination of the required hyperbola relative to Earth this is more dependent upon the actual entry and exit positions than the elliptical arcs are. By matching the inclinations of the trans-Luna and trans-Earth elliptic arcs to one another, in addition to matching these to the EMMET's inclination, velocity changes at payload capture and launch resulting from differences in orbital inclination are negated. At this point the LSI entry and exit position and time are adjusted by small amounts until the inclinations of the inbound and outbound trajectories from LSI relative to Earth match those of the elliptic arcs. Furthermore, by matching the angle of ascending node of the elliptical transfer arcs to that of the EMMET, the apse lines of the transfer arcs and the EMMET's orbit coincide and negate any velocity differences occurring as a result of a divergence in ascending node angle. Once again, LSI entry and exit positions and times are adjusted until the inclination of the LSI motion relative to Earth matches that of the elliptic arcs, and in addition to the alignment of their ascending nodes with that of the EMMET's orbit this results in

any velocity differences, arising between the LSI entry and exit velocity and the elliptical arcs at LSI contact due to inclination or ascending node discrepancies, being minimised. Finally, by adjusting the time of flight between LSI and perigee, and vice-versa, the argument of perigee of the elliptical transfer arcs can be reduced to as close to zero as possible whilst obeying the logistical requirements imposed on the time of flight, and this minimises any velocity change required as a result of a discrepancy between the argument of perigee of the transfer arcs and that of the EMMET. Small variations in the time of flight for both the elliptic arcs and payload's hyperbola about the Moon allows the argument of perigee of the trajectories to be matched at LSI contact, however when obeying such strict logistical requirements this is not always possible and some velocity change is expected at these points. The final step is to arrange the rotational rate of the EMMET's tether sub-spans such that its upper tip closely matches the perigee velocity of the trans-Luna and trans-Earth transfer arcs.

An identical procedure is carried out for the configuration of the Moon at its next arrival at the ascending node of its orbit with the adjustments to the Lunavator's argument of perilune, orbital inclination and ascending node being made to accommodate the transfer procedure. In the Lunavator's case the only invariants are the perilune altitude of the central facility and the tether sub-span lengths.

6.2 Mechanisation of the Design Procedure

Having outlined the general procedure utilised to configure the circumlunar trajectories of the transferred payloads such that the logistical requirements of the system are adhered to and the velocity changes required to perform the payload exchanges are minimised, our attention now turns to the means by which we calculate and configure these trajectories.

6.2.1 Input Variables and Time

The first step in the mechanisation procedure is the input of the gravitational parameters of Earth and the Moon, μ_e and μ_m; the magnitude of

their oblateness parameters, J_2 and J_{2m}; their physical radii, R_E and R_M; and their mass, M_E and M_M; in addition to this the orbital period of the Moon, T_{moon}, is also obtained. To allow the configuration of the Moon to be determined, an arbitrary date and time is selected for the operational procedures to be undertaken, and these are implemented into the on-line solar system data and ephemeris calculator *Horizon* [52] which is provided by NASA's Jet Propulsion Laboratory (*JPL*). As we assume that both the EMMET and Lunavator are both composed of *SPECTRA 2000* material of uniform density and cross sectional area, we implement in the material properties (A, σ, ρ) for the tether sub-spans in addition to a factor of safety (SF). Having obtained these constants we now describe the means by which we determine the configuration of the Moon at the time period of operations.

6.2.2 Moon Configuration at Input Time

The configuration of the Moon at its next arrival at its ascending node after some arbitrary time selected to conduct operations can be determined using a combination of methods, firstly, the JPL Horizon [52] system is used to obtain the Moon's velocity and position vector at the system input time. This system is the most accurate available and numerically integrates the equations of motion of the Moon forward in time to our selected time. Taking these position and velocity vectors, the orbital elements of the Moon at this instant are determined using the state vector of the system [47]. This state vector is a vector of the six classical orbital elements $(h, i, \Omega, e, \omega, \theta)$ which describe the configuration of an orbiting body from its position and velocity relative to the attracting body at that instant. The state vector is derived from the position and velocity vectors using the following method as described by Curtis [47]. Firstly, the magnitude of the velocity vector directed radially is determined as:

$$v_r = \frac{\vec{r}.\vec{v}}{r} \tag{6.1}$$

The vector of specific angular momentum (the angular momentum per unit mass of the body) of the orbit is directed perpendicularly to the orbital plane and is determined as the vector cross product between the

position and velocity vectors of the Moon at the system's input time:

$$\vec{h} = \vec{r} \times \vec{v} \tag{6.2}$$

The magnitude of the specific angular momentum vector which forms part of the state vector is determined from the dot product of the specific angular momentum vector. The orbital inclination of the Moon about Earth is defined as the angle between the Moon's specific angular momentum vector and the unit vector K directed along Earth's equatorial z-axis and is obtained from the dot product of these two vectors as:

$$i = cos^{-1}\left(\frac{h_z}{h}\right) \tag{6.3}$$

where h_z is the magnitude of the specific angular momentum vector projected along the equatorial z-axis. The vector from the centre of Earth to the point at which the Moon's orbit crosses Earth's equatorial plane is termed the node line and this is determined as the vector cross product between the unit vector K directed along Earth's equatorial z-axis and the Moon's specific angular momentum vector as:

$$\vec{N} = \vec{K} \times \vec{h} \tag{6.4}$$

The angle of ascending node of the Moon's orbit is then defined as the angle between the unit vector I directed along the x-axis of the Earth's equatorial frame and the Moon's node line vector and is obtained by application of the vector dot product as:

$$\Omega = cos^{-1}\left(\frac{N_x}{N}\right) \tag{6.5}$$

where N_x is the magnitude of the node line projected on to the equatorial x-axis. A quadrant ambiguity arising from this equation can be remedied by taking equation (6.5) exactly when the component N_y is positive and $360°$ minus equation (6.5) when N_y is negative. The eccentricity of the Moon's orbit about Earth is a measure of the deviation of its orbital geometry from that of a true circle and so the Moon's eccentricity vector can be determined from:

$$\vec{e} = \left(\frac{1}{\mu_e}\right)\left(\left(v^2 - \frac{\mu_e}{r}\right)\vec{r} - rv_r\vec{v}\right) \tag{6.6}$$

The magnitude of the eccentricity vector which forms part of the state vector is determined from the dot product of the eccentricity vector. The argument of perigee of the Moon's orbit is defined as the angle between the Moon's node line vector and its eccentricity vector which is directed towards the perigee of the Moon's orbit and is determined by calculating this angle in terms of the vector dot product between these two vectors as:

$$\omega = cos^{-1}\left(\frac{\vec{N}.\vec{e}}{Ne}\right) \tag{6.7}$$

Any quadrant ambiguity is resolved by examining the sign of the equatorial z-component of the eccentricity vector; if the z-component is positive, the perigee of the orbit occurs in the upper hemisphere of the Earth and indicates that the argument of perigee is identically equation (6.7), a negative component indicates that the perigee occurs in the lower hemisphere of Earth and indicates that its argument of perigee is 360° minus equation (6.7). The last orbital element to form part of the state vector is the true anomaly of the Moon in its orbit about Earth at this point and this is defined as the angle between the Moon's eccentricity vector, directed towards the perilune of its orbit, and its current position vector as:

$$\theta = cos^{-1}\left(\frac{\vec{e}.\vec{r}}{er}\right) \tag{6.8}$$

Any quadrant ambiguity is resolved by examining the sign of the radial velocity defined in equation (6.1); if the radial velocity is positive the Moon is moving away from the Earth and its true anomaly is identical to equation (6.8), if its radial velocity is negative the Moon is moving towards Earth and its true anomaly is 360° minus equation (6.8). Having determined the state vector of the Moon at the arbitrary input time, the true anomaly within the Moon's orbit about Earth at which its ascending node occurs is determined from:

$$\theta_{AN} = 360° - \omega \tag{6.9}$$

Furthermore, the time elapsed since the last perigee passage is obtained in terms of the eccentric anomaly of the Moon's orbit, which will be defined in subsection 6.2.3, and the Moon's orbital period in the following

equation [47] which will be utilised later:

$$t_p = \left(\frac{T_m}{\pi}\right) \cdot \left((1 - esin)tan^{-1}\left[\sqrt{\frac{1-e}{1+e}}tan\left(\frac{\theta}{2}\right)\right]\right) \qquad (6.10)$$

The configuration of the Moon at the selected time period for operations has been determined, it is assumed that any variation between the Moon's configuration and its next arrival at its ascending node about Earth is negligible and can be ignored. It should be noted however, that some error has been introduced into the Moon's motion by the use of the state vector to obtain its position and velocity as this assumes that the Moon orbits Earth in a perfectly closed orbit which does not occur as a result of the additional gravitational attractions acting on the Moon from the other bodies which occupy the Solar System. We now have the ability to calculate the position and velocity vectors of the Moon at later times in its orbit which allows us to determine its configuration at the instant of arrival and departure of payloads at the boundary to its gravitational influence.

6.2.3   LSI Configuration at Payload Contact

Having determined the orbital configuration of the Moon at the system's input time, the position of the Moon at a later instant in its orbit about Earth can be determined, and this is utilised to determine the position and velocity of the Moon relative to Earth when it is close to the ascending node of its orbit, and the chosen time for payload arrival and departure. From this we can determine the position at which the payload transferred from the EMMET's upper tip crosses into the region of the Moon's dominating gravitational influence relative to both the Earth and Moon, and furthermore the position at which the payload transferred from the upper tip of the Lunavator crosses from the Moon to Earth's dominating gravitational relative to both the Earth and Moon. These changes from one gravitational influence to another allow us to piece together the hyperbolic trajectory about the Moon with the elliptic transfer phases about Earth, in addition to determining any changes in velocity required at these points.

LSI Configuration at Payload Arrival

The time and true anomaly of the Moon at the instant of arrival of the payload at the LSI is dependent upon the transfer time variable η_{LSI} defined as the trans-Luna payload's time of arrival at LSI after the system input time. Due to the Moon's orbit about Earth having an elliptical geometry, the true anomaly of the Moon at the instant of arrival of the payload at the LSI must first be obtained in terms of the mean anomaly of the Moon in its orbit about Earth. This mean anomaly is defined as the azimuth position of a fictitious body moving around the ellipse at a constant angular speed and is defined as [47]:

$$M_e = \left(\frac{2\pi}{T_m}\right)(t_p + \eta_L) \tag{6.11}$$

The addition of the time since perigee passage at the system's input time and the LSI arrival time after system input time, η_L, in equation (6.11) gives the mean anomaly that the Moon has passed through since its last instance at perigee. At this point an auxiliary angle called the eccentric anomaly, E, is introduced which is a geometric means of obtaining the area swept out between perigee and the current position, and allows the current time to be calculated from Kepler's second law [42]. We obtain an initial estimate for the eccentric anomaly in terms of the mean anomaly and orbital eccentricity as [47]:

$$E_0 = M_e - \frac{e}{2} \tag{6.12}$$

Once the initial estimate of the eccentric anomaly has been obtained, we form the function [47]:

$$f(E) = E - esinE - M_e \tag{6.13}$$

We calculate the derivative of equation (6.13) with respect to this eccentric anomaly as:

$$f'(E) = 1 - ecosE \tag{6.14}$$

We apply Newton's method to equations (6.12), (6.13) and (6.14) to obtain a value for the eccentric anomaly to within five significant figures. We can then simply obtain the true anomaly at the instant in question

in terms of the eccentric anomaly as [47]:

$$tan\left(\frac{\theta}{2}\right) = \sqrt{\frac{1+e}{1-e}}tan\left(\frac{E}{2}\right) \qquad (6.15)$$

Having obtained the true anomaly of the Moon at the instant of payload arrival at the LSI we calculate its position and velocity in its perifocal frame by first obtaining its distance from Earth at this true anomaly as:

$$r = \frac{a(1-e^2)}{1+ecos\theta} \qquad (6.16)$$

With its semi-major axis, a, and eccentricity, e, defined by equations (5.3) and (5.5), respectively. The position of the Moon in its perifocal frame of its orbit about Earth can then be determined as:

$$\vec{r}_{perifocal} = r \begin{bmatrix} cos\theta & sin\theta & 0 \end{bmatrix}^T \qquad (6.17)$$

The Moon's perifocal velocity at this true anomaly can be determined using equation (3.46) and its position and velocity relative to Earth's equatorial frame can be obtained by the application of the basic dynamic equations and a perifocal to equatorial conversion matrix for the Moon. The perifocal position of the Moon can be transformed into Earth's equatorial frame using the following equation [42]:

$$\vec{r}_{moon} = R_G.\vec{r}_{perifocal} \qquad (6.18)$$

Where the transformation matrix, R_G, is simply equation (3.5) with the inclination, ascending node and argument of perigee replaced with those elements calculated for the Moon in section (6.2.2). The velocity of the Moon relative to the equatorial frame at this point is obtained as:

$$\vec{v}_{moon} = R_G.\vec{v}_{perifocal} + \dot{R}_G.\vec{r}_{perifocal} \qquad (6.19)$$

As a result of the oscillation of the Moon's ascending node relative to the equatorial frame and to reduce the risk of introducing mistakes into our calculations through extensive derivations of transformation matrices, we will only treat the secular rate of the Moon's argument of perigee as a variable when deriving the first derivative of the Moon's perifocal to equatorial transformation matrix and this becomes:

$$\dot{R}_G = \dot{\omega} \begin{bmatrix} -\cos\Omega sin\omega - sin\Omega cos\omega cosi & -cos\Omega cos\omega + sin\Omega sin\omega cosi & 0 \\ -sin\Omega sin\omega + cos\Omega cos\omega cosi & -sin\Omega cos\omega - cos\Omega sin\omega cosi & 0 \\ cos\omega sini & -sin\omega sini & 0 \end{bmatrix}$$

Having determined the position and velocity of the Moon at the instant of payload arrival, we now turn our attention to locating the payload's entry point into the LSI in terms of its position relative to the Moon. Within the LSI (Lunar Sphere of Influence), the Moon's gravity is the dominating force and the Moon's centre becomes the origin of the majority of coordinate systems used to determine a satellite's motion within this region. Outwith this sphere of influence, Earth's gravity is the dominating force. The choice of the correct coordinate system to use, and which is the dominating force, is determined as the ratio of the disturbing force and the central force when a body, m_3, is in the presence of two bodies, m_1 and m_2. The smallest disturbing force to central force ratio is the correct coordinate system to use [44]. Furthermore, due to the proximity of the Moon to Earth, this region of Lunar gravitational influence cannot be treated simply as a sphere but the magnitude of its boundary at an arbitrary angle to the Earth-Moon line can be approximated as [44]:

$$r_L = \left(\left(\frac{M_M(M_M + m_p)}{M_E(M_E + m_p)} \right)^{-\frac{1}{5}} (1 + 3cos^2\alpha)^{\frac{1}{10}} + \left(\frac{2}{5} \right) cos\alpha \left(\frac{1 + 6cos^2\alpha}{1 + 3cos^2\alpha} \right) \right)^{-1}$$

(6.21)

The mass of Earth is denoted by M_E, the mass of the Moon is denoted by M_M and the mass of the payload is denoted by m_p. Angle α between the Earth-Moon line and the point on the boundary of the LSI can be defined as the angle between the negative I_m axis of the selenocentric frame of reference and the vector from the centre of the Moon to the point on the boundary of the LSI, and is obtained as the angle from the vector dot product between the two unit vectors. At this point it is necessary to define the selenocentric frame of reference; it is a Moon centred, body fixed frame of reference [41] with the unit vector K_m directed along the instantaneous orbit normal of the Moon about Earth, the unit vector I_m is in the same direction as the Moon from Earth and rotates at a rate equal to the Moon about Earth, the unit vector J_m lies within the

orbital plane in the direction of motion and completes the coordinate frame axes. The selenocentric frame is the coordinate frame in which all motion within the LSI will be referenced. The unit vector in the direction of the point on the LSI can be defined relative to the selenocentric frame as:

$$\vec{i}_L = \begin{bmatrix} cos(\pi + \phi_L)cos\delta_L \\ sin(\pi + \phi_L)cos\delta_L \\ sin\delta_L \end{bmatrix} = \begin{bmatrix} -cos\phi_L cos\delta_L \\ -sin\phi_L cos\delta_L \\ sin\delta_L \end{bmatrix} \qquad (6.22)$$

where ϕ_L is the angle between the negative I_m axis of the selenocentric frame and the projection of the unit vector onto the selenocentric (I_m, J_m) plane and δ_L is the angle between the selenocentric (I_m, J_m) plane, and the unit vector in the direction of the LSI point. In addition to this, angles ϕ_L and δ_L are variables of the overall transfer design and allow the entry point of the payload into the LSI to be determined and varied, and these are utilised when constructing the hyperbolic trajectory taken by the payloads about the Moon. Angle α is then obtained by the application of the vector dot product as:

$$\alpha = cos^{-1}(cos\phi_L cos\delta_L) \qquad (6.23)$$

The position of the payload's point of entry into the LSI can then be determined relative to the selenocentric frame as:

$$\vec{r}_L = r_L \vec{i}_L \qquad (6.24)$$

Having obtained the payload's entry point into the LSI relative to the Moon, it is useful to determine this entry point relative to Earth and this will be utilised later. To convert the selenocentric coordinates into the geocentric equatorial frame we first convert its selenocentric position into the perifocal frame of the Moon's orbit and add to this the perifocal position vector of the Moon at this instant, and so to achieve this we first apply the selenocentric to perifocal conversion matrix to the LSI entry point position vector as:

$$R_{sp} = \begin{bmatrix} cos\theta_a & -sin\theta_a & 0 \\ sin\theta_a & cos\theta_a & 0 \\ 0 & 0 & 1 \end{bmatrix} \qquad (6.25)$$

135

where θ_a is the true anomaly of the Moon at the instant of payload arrival and r_a is its distance from Earth. The perifocal position of the payload's entry point relative to Earth is then:

$$\vec{r}_{ap} = \begin{bmatrix} r_a cos\theta_a - r_{L-a} cos(\theta_a + \phi_a) cos\delta_a \\ r_a sin\theta_a - r_{L-a} sin(\theta_a + \phi_a) cos\delta_a \\ r_{L-a} sin\delta_a \end{bmatrix} \qquad (6.26)$$

The position vector of the payload's entry point into the LSI is obtained relative to the equatorial frame by direct application of the perifocal to equatorial rotation matrix defined in equation (3.5) with its inclination, argument of perigee and ascending node angles replaced with those of the Moon's configuration at the time period of payload arrival

LSI Configuration at Payload Departure

The configuration of the Moon at the instant of payload departure is determined using a method identical to that used previously, however, in this case, the time at which the payload departs the LSI is an integer multiple of the Lunavator's orbital period after the arrival of the payload from Earth. The mean anomaly of the Moon at the payload's departure from the LSI is therefore defined as:

$$M_e = \left(\frac{2\pi}{T_m}\right)(t_p + \eta_L + \Theta T_{LV}) \qquad (6.27)$$

with ΘT_{LV} defined as the time between payload entry and exit from the LSI and includes payload transfer times to and from perilune and a waiting time between Lunavator capture and Launch operations. Here, Θ is the integer multiple of the Lunavator's orbital period T_{LV} but some flexibility can be accommodated with variations in the time spent within LSI so long as the overall system logistics are satisfied. By obtaining the eccentric anomaly at the point of departure from the LSI, the Moon's true anomaly at this point, θ_d, can be obtained by the application of Newton's method which subsequently enables the Moon's position vector, $\vec{r}_d$, to be calculated at this point. The LSI departure point relative to the Moon is again determined by utilising equations (6.21) and (6.23) with variables ϕ_d and δ_d at our chosen departure point from the LSI in the direction of

unit vector $\vec{i}_d$. The position of this departure point is then determined relative to the Moon's perifocal frame as:

$$\vec{r}_{dp} = \begin{bmatrix} r_d cos\theta_d - r_{L-d}cos(\theta_d + \phi_d)cos\delta_d \\ r_d sin\theta_d - r_{L-d}sin(\theta_d + \phi_d)cos\delta_d \\ r_{L-d}sin\delta_d \end{bmatrix} \quad (6.28)$$

This is the transformed into Earth's equatorial frame using equation (3.5) with its inclination, argument of perigee and ascending node angles replaced with those of the Moon's configuration at the time period of payload departure.

Having specified the entry and exit points of the payload from the LSI, a hyperbolic trajectory about the Moon can be constructed by specifying a transfer time between these points which excludes any waiting time at perilune, and this will be the subject of the following subsection.

6.2.4   EMMET's Orbit about Earth

Having obtained the configuration of the Moon at system input time, the EMMET's orbit relative to Earth is configured using the orbital harmonic of the Moon's orbital period to that of the EMMET's orbital period, defined as m, in addition to the rotational harmonic of its rotational period to its orbital period, defined as p, and this allows the position and velocity of the central facility and tips to be determined. The orbital inclination of the EMMET is dependent upon the moon-tracking configuration being used and as the optimum argument of perigee is $0°$, the only remaining component of its orbit required to determine its position is its angle of ascending node relative to the equatorial frame. The ascending node of the EMMET's orbit is required to be arranged such that it is diametrically opposite to the ascending node of the Moon's orbit about Earth to allow symmetrical transfers to and from the EMMET when the Moon is close to its ascending node. The ascending node of the EMMET's orbit can therefore be expressed in terms of the ascending node of the Moon's orbit as:

$$\Omega_{EM} = \pi + \Omega_m \quad (6.29)$$

where Ω_m is the ascending node of the Moon's orbit at system input time and determined using equation (6.5). Now that the ascending node

of the EMMET's orbit has been obtained, the position and velocity of its central facility can be obtained using equations (4.27) and (4.28), respectively, and by setting the tether sub-span length equal to zero. The upper tip's position and velocity are obtained by using equations (4.27) and (4.28) in their exact form, and these determine the perigee position and velocity at which the payloads are released onto their trans-Luna orbits and their perigee position and velocity at which they end their trans-Earth trajectories from the Moon. Finally, the lower tip's position and velocity are obtained by adjusting the tether rotation angle by π radians in equations (4.27) and (4.28) respectively. Having determined the configuration of the EMMET at payload release relative to the equatorial frame, our attention now turns to the configuration of the payload's hyperbolic trajectory about the Moon.

6.2.5   Hyperbolic Trajectory about the Moon

Having defined the entry and exit points of the payload into and from the LSI, our attention now turns to constructing a hyperbola about the Moon, relative to the selenocentric frame of reference, which satisfies our timing requirements from LSI entry to perilune and from perilune to LSI exit, in addition to providing a suitable perilune position and velocity. By ensuring that the inbound and outbound payloads undertake different portions of the same hyperbolic trajectory about the Moon we ensure that they have the same perilune velocity and therefore only a single upper tip velocity for the Lunavator is required to match this. Furthermore, by configuring the same hyperbola to be undertaken by both payloads we also ensure that the orbital elements for both trajectories will be identical, thus allowing a single Lunavator configuration to be suitable for both phases. To ensure that the inbound and outbound payloads undertake the same hyperbola, we construct a single hyperbola between the LSI entry and exit points occurring in a time period suitable for our LSI to perilune and perilune to LSI transfer phases and for the moment ignore any waiting time at the Lunavator which, in itself, has no effect on the transfer hyperbola and is solely a logistical necessity. This subsection will firstly, describe the means by which we construct the hyperbola be-

tween the LSI entry and exit points initially by obtaining the change in true anomaly between these two points by means of Lambert's Theorem, and then by utilising the Lagrange Coefficients to obtain the velocity of the payloads at these entry and exit points. The second step will be to transform the trans-Earth and trans-Luna payloads' velocities relative to Earth's equatorial frame which will be utilised later to patch the payload's hyperbolic velocity to their corresponding elliptical velocities about Earth and allow us to determine whether any velocity adjustments are required at our entry and exit points to the LSI. In the final part of this subsection, the perilune position and velocity of the payloads will be determined for the single hyperbola about the Moon which allows the Lunavator's orbit to be configured.

Trajectory between LSI Boundary Points

To construct this single hyperbola about the Moon we employ the method given by Curtis [47] which will be outlined here, firstly we employ Lambert's Theorem which states that *the orbital transfer time depends only upon the semi-major axis, the sum of the distances of the initial and final points of the arc from the centre of force, and the length of the chord joining these points* [44]. Having already defined the two points on the arc as the LSI entry and exit points, we set the transfer time between these points to obtain the true anomaly through which the payload passes as it traverses this path. The first step is determine the quadrant of the Moon's selenocentric frame through which the payload passes and this is determined by whether the trajectory is prograde or retrograde in addition to the Z-axis component of the cross-product of the LSI entry point position vector, which we will denote here as $\vec{r}_1$, and exit point position vector, which we will denote here as $\vec{r}_2$, as:

$$(\vec{r}_1 \times \vec{r}_2)_Z = r_1 r_2 sin\Delta\theta cosi \qquad (6.30)$$

The payload's trajectory about the Moon is required to be retrograde therefore, when equation (6.30)is negative the change in true anomaly for the trajectory is determined as:

$$cos\Delta\theta = \frac{\vec{r}_1.\vec{r}_2}{r_1 r_2} \qquad (6.31)$$

139

For a positive value of equation (6.30), the change in true anomaly is 360° minus equation (6.31). Having obtained the change in true anomaly between the entry and exit points, the next step is to determine the trajectory between these points and this can be found in terms of the Lagrange Coefficients. These coefficients are derived from the premise that if the position and velocity of a body are known at one instant they can be found at a later instant in terms of these initial components [47]. The Lagrange coefficients are obtained by first expressing them in terms of the universal anomaly, χ, which is a generalised anomaly [44], similar to the eccentric anomaly for elliptical orbits or the hyperbolic anomaly for hyperbolic orbits, but is valid for all orbit types as:

$$f = 1 - \frac{\chi^2}{r_1}C(z) \tag{6.32}$$

$$g = \Delta t - \frac{1}{\sqrt{\mu}}\chi^3 S(z) \tag{6.33}$$

$$\dot{f} = \frac{\sqrt{\mu}}{r_1 r_2}\chi(zS(z) - 1) \tag{6.34}$$

$$\dot{g} = 1 - \frac{\chi^2}{r_2}C(z) \tag{6.35}$$

where μ is the gravitational parameter of the central body, variable $z = \alpha\chi^2$ with α defined as the reciprocal of the semi-major axis of the hyperbola, Δt is flight time between the entry and exit points, excluding waiting time, and defined as $\gamma \times T_{LV}$ with γ being an orbital harmonic, and finally, C(z) and S(z) are infinite series known as Stumpff functions and are related to the circular and hyperbolic trigonometric functions. For hyperbolic trajectories, S(z) and C(z) can be defined as [47]:

$$S(z) = \frac{sinh\sqrt{-z} - \sqrt{-z}}{(\sqrt{-z})^3} \tag{6.36}$$

$$C(z) = \frac{cosh\sqrt{-z} - 1}{-z} \tag{6.37}$$

This allows χ to be defined as:

$$\chi = \sqrt{\frac{y(z)}{C(z)}} \tag{6.38}$$

where

$$y(z) = r_1 + r_2 + A\frac{zS(z) - 1}{\sqrt{C(z)}} \tag{6.39}$$

and

$$A = sin\Delta\theta\sqrt{\frac{r_1 r_2}{1 - cos\Delta\theta}} \tag{6.40}$$

The only unknown is now function z and we utilise Newton's approximation by forming the following equation:

$$z_{i+1} = z_i - \frac{F(z_i)}{F'(z_i)} \tag{6.41}$$

where the function F(z) and its derivative are defined as:

$$F(z) = \left(\frac{y(z)}{C(z)}\right)^{\frac{3}{2}} S(z) + A\sqrt{y(z)} - \sqrt{\mu}\Delta t \tag{6.42}$$

$$F'(z) = \begin{cases} \left(\frac{y(z)}{C(z)}\right)^{\frac{3}{2}} \left(\frac{1}{2z}\left(C(z) - \frac{3}{2}\frac{S(z)}{C(z)}\right) + \frac{3}{4}\frac{S(z)^2}{C(z)}\right) \\ + \frac{A}{8}\left(3\frac{S(z)}{C(z)}\sqrt{y(z)} + A\sqrt{\frac{C(z)}{y(z)}}\right) & (z \neq 0) \\[2em] \frac{\sqrt{2}}{40}y(0)^{\frac{3}{2}} + \frac{A}{8}\left[\sqrt{y(0)} + A\sqrt{\frac{1}{2y(o)}}\right] & (z = 0) \end{cases} \tag{6.43}$$

Taking our initial estimate as $z=0$, with $C(0)=\frac{1}{2}$ and $S(0)=\frac{1}{6}$ we apply Newton's method to obtain a solution for z to five significant figures, we then obtain a final value for y(z) and calculate the Lagrange coefficients as:

$$f = 1 - \frac{y(z)}{r_1} \tag{6.44}$$

$$g = A\sqrt{\frac{y(z)}{\mu}} \tag{6.45}$$

$$\dot{f} = \frac{\sqrt{\mu}}{r_1 r_2}\sqrt{\frac{y(z)}{C(z)}}(zS(z) - 1) \tag{6.46}$$

$$\dot{g} = 1 - \frac{y(z)}{r_2} \tag{6.47}$$

The velocities of the payload at LSI entry, $\vec{v}_1$, and exit, $\vec{v}_2$, are then obtained as:

$$\vec{v}_1 = \frac{1}{g}(\vec{r}_2 - f\vec{r}_1) \tag{6.48}$$

$$\vec{v}_2 = \frac{1}{g}(\dot{g}\vec{r}_2 - \vec{r}_1) \tag{6.49}$$

Having obtained the velocities of the payload at the entry and exit points to LSI, the orbital elements of the hyperbolic motion of the payloads about the Moon are obtained by a means identical to that utilised to obtain the state vector of the Moon in subsection (6.2.2).

Entry and Exit Velocities at LSI Boundary

Having obtained the velocities of the payloads at their entry and exit from the LSI relative to the selenocentric frame, it is useful at this point to transform these velocities into Earth's equatorial frame of reference. By obtaining these velocities relative to the equatorial frame we can determine the elliptical velocity at LSI contact required to undertake the correct hyperbolic trajectory to perilune in the case of LSI entry, or the elliptical trajectory which will be undertaken about Earth at LSI exit of the payload. Furthermore, these velocities can be used to match the elliptical to hyperbolic velocities and if an incompatible velocity mismatch occurs which compromises the overall trajectory design, the magnitude of the velocity change required to correct for any mismatch can be obtained.

Having described a means to obtain the position vectors of the LSI entry and exit points relative to the equatorial frame in subsection (6.2.3), the velocities of these payloads relative to Earth's equatorial frame can be obtained firstly by transforming the selenocentric velocities at contact in equations (6.48) and (6.49) into the perifocal frame of the Moon's orbit. The payload's velocity at LSI entry is transformed into the perifocal frame of the Moon's orbit by utilising equation (6.25) and its first derivative with respect to time and implementing these into the following equation:

$$\vec{v}_{1p} = \vec{v}_{mpa} + R_{sp}\vec{v}_1 + \dot{R}_{sp}\vec{r}_1 \qquad (6.50)$$

where $\vec{v}_{mpa}$ is defined as the perifocal velocity of the Moon at LSI entry. The payload's velocity at LSI exit is transformed into the perifocal frame of the Moon's orbit by replacing the true anomaly terms in equation (6.25) with those of the Moon at payload departure, and so we obtain the perifocal velocity of the payload at LSI exit as:

$$\vec{v}_{2p} = \vec{v}_{mpd} + R_{sp}\vec{v}_2 + \dot{R}_{sp}\vec{r}_2 \qquad (6.51)$$

where $\vec{v}_{mpd}$ is defined as the perifocal velocity of the Moon and R_{sp} is equation (6.25)at LSI exit. The perifocal velocities of the payloads at LSI entry and exit are transformed into the equatorial frame by means of the following equation:

$$\vec{v}_{eq} = R_G\vec{v}_p + \dot{R}_G\vec{r}_p \qquad (6.52)$$

where $\vec{v}_{eq}$ is the equatorial velocity of the payload at either LSI entry or exit, R_G and $\dot{R}_G$ are the perifocal to Earth equatorial transformation matrix for the Moon at the system input time, and its first derivative, and these are defined in equations (3.5) and (6.20), respectively. Furthermore, $\vec{v}_p$ and $\vec{r}_p$ are the perifocal velocity and position of the payload at either LSI entry or exit.

Having obtained a means by which we transform the velocities of the payloads at LSI entry and exit into Earth's equatorial frame, we obtain the state vectors of the payload's motion at LSI entry and exit relative to Earth using the method described in subsection 6.2.2, allowing us to determine the inclination, argument of perigee and ascending node of this motion which is used to match the LSI entry and exit parameters to those of the elliptic arcs about Earth. Attention now turns to the perilune parameters of the payload's hyperbolic trajectory about the Moon which determine the configuration of the Lunavator's orbit and this will form the remainder of this subsection.

Payload Perilune Parameters

Having obtained the state vector of the hyperbolic trajectory about the Moon, the exact time of flight of the payload to the perilune of its orbit can be determined firstly by obtaining the true anomaly of the trans-Luna payload within its hyperbolic trajectory at entry into the LSI, determined by means of the eccentricity of its hyperbola and the position vector of this payload at LSI entry. From this true anomaly the hyperbolic anomaly, defined as an auxiliary equilateral hyperbola with eccentricity equal to $\sqrt{2}$, and the hyperbolic equivalent of the eccentric anomaly, can be determined as [42]:

$$H = 2tan^{-1}\left(\sqrt{\frac{e_h - 1}{e_h + 1}}tan\left(\frac{\theta_{in}}{2}\right)\right) \qquad (6.53)$$

where e_h is the eccentricity of the payload's hyperbola and θ_{in} is the payload's true anomaly at LSI entry. We obtain the mean anomaly at this point in terms of the hyperbolic anomaly as [42]:

$$M_h = e_h sinH - H \qquad (6.54)$$

143

Finally, the time to perilune from LSI entry can be obtained in terms of this mean anomaly as [42]:

$$t_{perilune} = \sqrt{\frac{-a_h{}^3}{\mu_m}} M_h \tag{6.55}$$

where the negative sign in front of the semi-major axis, a_h, is necessary to prevent a number with a complex component as the semi-major axis for hyperbolic orbits is negative. From the transfer time to perilune from LSI entry, the exact time at which the trans-Earth payload exits the LSI can be obtained by subtracting the time to perilune from the transfer time of the hyperbola, Δt, between LSI entry and exit points.

Having obtained the exact transfer times for the payloads to and from perilune, the position and velocity of the payloads at perilune will now be obtained. Firstly, we can obtain the perilune distance and speed of the hyperbola as [42]:

$$r_{perilune} = a_h(1 - e_h) \tag{6.56}$$

and

$$v_{perilune} = \sqrt{\frac{2\mu}{r_{perilune}} - \frac{\mu}{a_h}} \tag{6.57}$$

The perifocal position and velocity at perilune are simply:

$$\vec{r}_{perilune} = \begin{bmatrix} a_h(1 - e_h) & 0 & 0 \end{bmatrix}^T \tag{6.58}$$

and

$$\vec{v}_{perilune} = \begin{bmatrix} 0 & \frac{\mu(1+e_h)}{h_h} & 0 \end{bmatrix}^T \tag{6.59}$$

with the magnitude of the velocity obtained by expressing equation (6.57) solely in terms of the semi-major axis of the orbit and then substituting the specific angular momentum, h_h, of payload's hyperbola into the resulting expression. The position and velocity of the payload's hyperbola at perilune is transformed into the selenocentric frame of reference by means of the following transformation matrix:

$$R_S = \begin{bmatrix} \alpha_1 & \alpha_2 & \alpha_3 \\ \beta_1 & \beta_2 & \beta_3 \\ \gamma_1 & \gamma_2 & \gamma_3 \end{bmatrix} \tag{6.60}$$

where

$$\alpha_1 = \cos\Omega_h cos\omega_h - sin\Omega_h sin\omega_h cosi_h$$

$$\alpha_2 = -cos\Omega_h sin\omega_h - sin\Omega_h cos\omega_h cosi_h$$

$$\alpha_3 = sin\Omega_h sini_h$$

$$\beta_1 = sin\Omega_h cos\omega_h + cos\Omega_h sin\omega_h cosi_h$$

$$\beta_2 = -sin\Omega_h sin\omega_h + cos\Omega_h cos\omega_h cosi_h$$

$$\beta_3 = -cos\Omega_h sini_h$$

$$\gamma_1 = sin\omega_h sini_h$$

$$\gamma_2 = cos\omega_h sini_h$$

$$\gamma_3 = cosi_h$$

where the angle of ascending node, argument of perilune (the Moon centred equivalent to the argument of perigee) and the orbital inclination are those of the payload's hyperbola about the Moon. These are denoted by the subscript h and were calculated using the state vector for the hyperbola using the method described to calculate the state vector of the Moon in subsection (6.2.2). Here we consider, for simplicity, a hyperbolic trajectory to be a singular trajectory and by this it is meant that since the body, in this case the payload, that is undertaking the hyperbola about the Moon is only under the influence of the Moon's gravity for a short period of time, and this is the case for all hyperbolic trajectories as by their very nature they allow escape from the region of gravitational influence, in conjunction with the magnitude of the Moon's oblateness being limited; we consider the hyperbola to be a fixed orbit relative to the Moon during the body's period of motion and free from any precessional effects. Using this assumption gives a very simple transformation equation between the position and velocity of the hyperbola at perilune in the perifocal frame and the selenocentric frame. The position of the payload at perilune can be obtained in the selenocentric frame as:

$$\vec{r}_{ps} = R_S.\vec{r}_{perilune} = a_h(1-e_h)\begin{bmatrix} \cos\Omega_h cos\omega_h - sin\Omega_h sin\omega_h cosi_h \\ sin\Omega_h cos\omega_h + cos\Omega_h sin\omega_h cosi_h \\ sin\omega_h sini_h \end{bmatrix} \quad (6.61)$$

As there is no secular rate of the argument of perilune or angle of as-

cending node and the inclination is assumed to be constant, the first derivative of R_S with respect to time is zero and the velocity of the payload at perilune relative to the selenocentric frame is obtained as:

$$\vec{v}_{ps} = \frac{\mu(1+e_h)}{h_h} \begin{bmatrix} -cos\Omega_h sin\omega_h - sin\Omega_h cos\omega_h cosi_h \\ -sin\Omega_h sin\omega_h + cos\Omega_h cos\omega_h cosi_h \\ cos\omega_h sini_h \end{bmatrix} \qquad (6.62)$$

Having obtained the perilune position and velocity of the payload's hyperbola about the Moon, we can now configure the Lunavator's orbit about the Moon. As the configuration required for this is considerable, it will be described in detail in the following chapter, Chapter 7, dedicated to the Lunavator's dynamics, design and configuration. However, by defining the upper tip velocity of the Lunavator relative to the selenocentric frame of reference as $\vec{v}_{Lsu}$ we can obtain an expression for the velocity adjustment to be performed by the payload at its instant of arrival or departure at the Lunavator's upper tip to ensure that no velocity mismatch between the upper tip and payload occurs, in addition to ensuring that the payload undertakes the correct hyperbolic trajectory about the Moon as:

$$\Delta\vec{v}_{ps} = \vec{v}_{Lsu} - \vec{v}_{ps} \qquad (6.63)$$

For the moment, we will turn our attention to describing the method used to configure the trajectory of the trans-Earth and trans-Luna payloads' elliptical trajectories between the LSI and the EMMET's upper tip.

6.2.6   Elliptical Trajectories about Earth

Having configured the hyperbolic trajectories of the payloads about the Moon, the complete circumlunar trajectory can be completed, firstly by the configuration of an elliptical arc between the position of the trans-Earth payload at its point of exit from the LSI and its perigee position at Earth which is coincident with the EMMET's upper tip position at perilune with its sub-spans aligned along the local gravity gradient, and finally by the configuration of an elliptical arc between an identical perigee position and the position of the trans-Luna payload at its entry point to the LSI. Once again, the trajectories between these points will

be obtained by the application of Lambert's Theorem and the Lagrange Coefficients, collectively termed Lambert's Problem, with the time periods between the beginning and end of these elliptic arcs being consistent with the logistical requirements described in Chapter 2.

LSI to Earth Trajectory

To calculate the elliptic arc that the payload will traverse between its exit point from the LSI and its perigee position at Earth we again employ Lambert's Theorem to calculate the change in true anomaly between the LSI exit point and perigee. To calculate this, we first evaluate the cross-product between the initial and final position vectors, which in this case are the LSI exit point of the payload, obtained by the application of the perifocal to equatorial transformation matrix to equation (6.28), and from this point on we will define this as $\vec{r}_{exit}$, and the EMMET's upper tip position at perigee with sub-spans aligned along the local gravity gradient, defined in equation (4.27) as $\vec{r}_{u-eq}$. As we require a prograde trajectory for the return elliptical arc to Earth, for positive Z-axis components of the cross product between the initial and final position vectors the change in true anomaly will identically be equation (6.31) and for negative values of this component the change in true anomaly will be 360° minus equation (6.31), which is opposite to the case for retrograde trajectories. Having obtained the change in true anomaly, the next step in the configuration of the elliptical trajectory to Earth is to specify the transfer time for this trajectory. To identify easily the shortest time period that this transfer can be undertaken in, we calculate the parabolic flight time for a trajectory between these two positions and this sets the lower limit for our transfer time. This parabolic flight time is calculated as [47]:

$$t_{parabolic-r} = \left(\frac{r_{exit} + 2r_{u-eq}}{3} \right) \sqrt{\frac{2(r_{exit} - r_{u-eq})}{\mu_e}} \qquad (6.64)$$

Where r_{exit} and r_{u-eq} are the respective LSI exit and perigee distances from Earth. Having calculated this parabolic flight time, the shortest time period that the transfer can occur in is a time period equal to an even integer multiple of the EMMET's orbital period closest to this parabolic flight time without exceeding it. Accounting for the boundary

set by the parabolic flight time, the transfer transfer time between LSI exit and perigee is defined as:

$$\Delta t_r = n_r T_{EM} \qquad \text{for} \qquad \Delta t_r < t_{parabolic-r} \qquad (6.65)$$

Where T_{EM} is the orbital period of the EMMET's orbit and n_r is an even orbital harmonic for the flight time between LSI and perigee. Having obtained the change in true anomaly and specified a time of flight between the initial and final position vectors, the Lagrange Coefficients are again obtained using a method similar to that utilised for the hyperbolic trajectory about the Moon. We begin by expressing the universal variable, χ, in terms of variable z and Stumpff functions $C(z)$ and $S(z)$ but in this case these are related to the circular trigonometric functions by:

$$S(z) = \frac{\sqrt{z} - sin\sqrt{z}}{(\sqrt{z})^3} \qquad (6.66)$$

$$C(z) = \frac{1 - cos\sqrt{z}}{z} \qquad (6.67)$$

Utilising equation (6.41) and setting our initial estimate for variable z as zero, we apply Newton's method to obtain a value for variable z to five significant figures, and from this we again calculate our Lagrange Coefficients as defined in equations (6.44) to (6.47) and obtain the payload's velocity at LSI exit and perigee from equations (6.48) and (6.49), respectively. Having obtained the velocities at these points, the state vector of the payload's trajectory to perigee can be obtained beginning from the position and velocity at either LSI exit or perigee, and this is useful for matching the orbital parameters of the payload's outbound trajectory from LSI to the parameters for the current elliptic trajectory back to Earth. Furthermore, by comparing the payload's velocity at the beginning of this elliptic arc when the payload is at the boundary of the LSI, denoted by $\vec{v}_{exit}$, to the the hyperbolic velocity at LSI exit relative to the equatorial frame, obtained from equation (6.52) and defined as $\vec{v}_{2eq}$, the velocity adjustment required at the payload's exit from the LSI can be expressed as:

$$\Delta \vec{v}_{exit} = \vec{v}_{exit} - \vec{v}_{2eq} \qquad (6.68)$$

In addition to this, by comparing the velocity at the end of the elliptic arc when it is at perigee, denoted by $\vec{v}_{perigee-r}$, to the upper tip velocity

of the EMMET when it is at perigee and its sub-spans are aligned along the local gravity gradient, denoted by $\vec{v}_{u-eq}$, the magnitude of the velocity required at the payload's arrival at the EMMET's upper tip can be expressed as:

$$\Delta\vec{v}_{perigee-r} = \vec{v}_{u-eq} - \vec{v}_{perigee-r} \tag{6.69}$$

Having configured the elliptical arc back to perigee our attention now turns to configuring the outbound elliptic arc from perigee to the LSI entry point for the trans-Luna payload.

Earth to LSI Trajectory

The elliptic arc between the EMMET's upper tip, coincident with the perigee position of the trans-Luna payload's trajectory, and the LSI entry point is again calculated as a solution to Lambert's Problem using a method identical to the LSI to Earth case. The orbital motion is again prograde and between the payload's perigee position, $\vec{r}_{u-eq}$, and the LSI entry point, obtained by the application of the Moon's perifocal to equatorial transformation matrix to equation (6.26) and from this point on we will define this as $\vec{r}_{entry}$. The change in true anomaly between these points is obtained by equation (6.31) and the limiting parabolic flight time in this case is defined as [47]:

$$t_{parabolic-l} = \left(\frac{r_{u-eq} + 2r_{entry}}{3}\right)\sqrt{\frac{2(r_{u-eq} - r_{entry})}{\mu_e}} \tag{6.70}$$

Adhering to the logistical requirements of the system, the time of flight between these two positions can be expressed as:

$$\Delta t_l = n_l T_{EM} \qquad \text{for} \qquad \Delta t_l < t_{parabolic-l} \tag{6.71}$$

Where T_{EM} is again the orbital period of the EMMET's orbit and n_l is an even orbital harmonic for the flight time between perigee and LSI. We again obtain the Lagrange Coefficients for the motion by applying Newton's method to evaluate variable z and finally obtain the velocities at perigee, denoted as $\vec{v}_{perigee-l}$, and LSI entry, denoted as $\vec{v}_{entry}$, from equations (6.48) and (6.49), respectively. Having obtained these velocities, the state vector for the motion is again obtained and the change in velocity required to ensure that the payload undertakes the correct

elliptical trajectory to LSI which is performed at the instant of payload release from the EMMET's upper tip can be expressed as:

$$\Delta\vec{v}_{perigee-l} = \vec{v}_{perigee-l} - \vec{v}_{u-eq} \tag{6.72}$$

In addition to this, the state vector allows a comparison of the inbound LSI motion to that of the trans-Luna elliptic arc and the change in velocity performed at the instant of arrival of the payload at the LSI entry point can be expressed as the difference between the payload's velocity at this point in its elliptic arc and the velocity required to undertake the correct hyperbolic trajectory to perilune, obtained using equation (6.52) and defined as $\vec{v}_{1eq}$. This velocity change can be expressed as:

$$\Delta\vec{v}_{entry} = \vec{v}_{1eq} - \vec{v}_{entry} \tag{6.73}$$

Having described the means by which the elliptic trajectories to and from LSI can be configured, our attention now turns to satisfying the overall logistical requirements of the system.

6.2.7 Logistical Parameters and Velocity Changes

The final step in the procedure is simply a check of the overall system to ensure that the logistics are being satisfied in each transfer phase and collectively. In addition to this a comparison is made between the state vectors of the hyperbolic trajectories undertaken by the trans-Luna and trans-Earth payloads to ensure that these match and in addition to this, a comparison is made between the trans-Luna and trans-Earth elliptic arcs to ensure that their state vectors are almost identical to one another however, a little deviation between them can be accommodated. Finally, the sum of the changes in velocity required for the entire transfer are calculated.

Our attention now turns to the description of the dynamics and design of the Lunavator's orbit about the Moon, in addition to the derivation of the central facility and tip's position and velocity relative to the selenocentric frame of reference which will be the subject of the following chapter.

6.3 Conclusions

A patched conic method for configuring the trajectories between the EM-MET and Lunavator tethers' upper tips has been established whilst remaining consistent with the logistical design of the system. The method utilises payloads undertaking elliptical trajectories between the EMMET's upper tip and the LSI boundary and undertaking hyperbolic trajectories between LSI and perilune. It was found that by means of an iterative procedure that the elliptical and hyperbolic trajectories could be patched together at the intersection points coinciding with their points of contact with the LSI and velocity differences minimised by means of this iterative procedure. Trajectories were configured to satisfy the timing requirements of the transfers by calculating the transfers about Earth and the Moon as solutions to Lambert's problem with the required velocity at the beginning and end points of the trajectory calculated by utilising Lagrange coefficients. By alterations to the times of entry and exit to LSI, the orbital elements of these transfers about Earth could be closely matched to those of the EMMET in either of the moon-tracking configurations. Furthermore, by adjustment to the transfer time of the hyperbolic trajectory about the Moon and to the positions of entry and exit themselves; a sufficient perilune distance could be had whilst matching the orbital elements of the trajectories at the boundary relative to Earth closely to those of the EMMET and payload's elliptical trajectory about Earth.

Having determined a method of calculating the required transfer trajectories which satisfy the system's logistical requirements, these will be used in conjunction with the EMMET configured in a chosen moon-tracking configuration and the configuration of the Lunavator about the Moon to allow the motion of each component of the system to be identified at any point during operations. These will be implemented into simulations and the magnitude of the velocity changes required to implement this system will be determined.

7. Lunavator Design

Having defined a means of configuring the transferred payload's hyperbolic trajectory about the Moon, the Lunavator's orbit must be arranged such that its upper tip coincides with the payload's perilune position when it is itself at the perilune of its orbit with its tether sub-spans aligned along the local gravity gradient, at the same instant its lower tip must almost touch the Moon's surface. To reduce any velocity mismatch between the upper tip and payload, and reduce the risk of mechanical shock along the tether sub-spans at the instant of payload capture, the Lunavator's orbital and rotational angular velocities must combine at the upper tip to match to the payload's perilune velocity as closely as possible, and additionally, this allows both the inbound and outbound payloads to undertake sequential portions of the same hyperbolic trajectory about the Moon, with chemical propulsion being utilised to correct for any irreconcilable velocity mismatches. An additional criterion that must be accommodated into the payload's hyperbolic trajectory design is the payload having a large enough perilune velocity. Therefore, by matching the velocity of the Lunavator's upper tip to this the relative velocity of the Lunavator's lower tip is as close to zero as possible and this allows the payload attached to the lower tip to be placed onto the Moon's surface.

To allow the inbound payload and Lunavator's upper tip to meet at their respective perilunes, as well as facilitating the outbound payload's launch from the same position, the Lunavator's orbital inclination must match that of the inbound hyperbola, and in addition to this the apse lines of the payload's hyperbolic trajectory and the Lunavator's orbit about the Moon must be coincident. This is achieved by matching the Lunavator's ascending node and argument of perilune to that of the payload's hyperbolic trajectory about the Moon. As was the case with the effects of Earth's oblateness on the EMMET's orbit about Earth, effects of similar magnitude will be evident and result from the Lunavator's close

proximity to the Moon, with secular rates for the argument of perilune and angle of ascending node. As a result of the magnitude of these variations, adjustments to the ascending node or argument of perilune on every occasion that the Lunavator becomes unladen are again necessary. In addition to this, as variations in the inclination of the payload's hyperbola about the Moon occur due to the fact that no single circumlunar configuration for the payload's motion can be configured as a result of the complex motion of the Moon, alterations to the orbital inclination of the Lunavator's orbit are also necessary.

This chapter begins similarly to Chapter 4 with the derivation of the Lunavator's upper tip position, velocity and acceleration, relative firstly, to a body fixed frame attached to the Lunavator's central facility, secondly to the Lunavator's perifocal frame, and finally to the Moon centred, body fixed Selenocentric frame of reference [46]. Again, as with the EMMET, the equations derived for the upper tip can be easily adjusted to obtain the dynamic equations for the central facility, by setting the tether sub-span length equal to zero, and for the lower tip, by adding π radians to the tether rotation angle at this point. The maximum tension acting on the fully laden Lunavator will then be derived, and an expression for the maximum angular velocity that the Lunavator can withstand will be obtained. The orbital adjustments required to configure correctly the Lunavator's orbit will then be defined and the chapter will conclude with a set of simulations which will allow us firstly to determine the rate at which the orbital elements of the Lunavator's orbit are varying; and then determine the upper and lower tip velocities for a range of Lunavator configurations, allowing it to be determined whether a zero velocity touchdown velocity at the lower tip is a realistic goal; and finally, allow the magnitude of the velocity changes required to perform these adjustments to be obtained.

7.1   Lunavator Dynamics

To satisfy the requirements of the overall logistical design, defined in Chapter 2, and the dynamic requirements of the payload's hyperbolic

trajectory about the Moon, defined in Chapter 6, the Lunavator must obtain sufficient upper tip velocity through orbital and rotational rates to match the hyperbolic velocity of the payload at perilune whilst ensuring that its orbital period remains at an odd integer harmonic with the EMMET's orbital period and its rotational rate remains at an odd integer harmonic plus an additional rotational fraction with the Lunavator's orbital period. To allow the incoming payload from Earth to be captured at the Lunavator's upper tip position, whilst simultaneously picking up a payload from the Moon's surface, the Lunavator's central facility must be located mid-way between the hyperbolic trajectory's perilune distance and the minimum Lunavator touchdown position defined previously, at this point the Lunavator's sub-span lengths can be defined as:

$$L_L = \frac{r_{perilune} - r_m}{2} \qquad (7.1)$$

where r_m is the minimum lower tip position defined previously and equal to 1741.476km. This results in the perilune distance of the central facility being defined as:

$$r_L = r_m + L_L \qquad (7.2)$$

Having defined these two parameters, the central facility's orbital period can be defined using equation (2.2) and an arbitrary value of orbital variable n. From this, the Lunavator's semi-major axis, a_L, and orbital eccentricity, e_L, can be defined using equations (5.3) and (5.5), respectively. The perilune velocity of the central facility can then be obtained by the re-arrangement of equation (5.9) as:

$$v_L = \sqrt{\frac{2\mu_m}{r_L} - \frac{\mu_m}{a_L}} \qquad (7.3)$$

where μ_m is the gravitational parameter of the Moon. A body frame is attached to the Lunavator's central facility which allows us to define the upper tip's position, velocity and acceleration relative to this frame and in addition to the central facility's perilune distance and speed this provides a means of converting these components into the perifocal frame and ultimately the selenocentric frame. Again, as was the case in section 4.1 the focus will remain on the upper tip's components, but the equations obtained can be easily adjusted for the central facility or the lower tip.

Body frame Components

We begin by denoting the position vector of the upper tip relative to a body fixed frame and define this frame similarly to that in section 4.1; the i_m axis is directed along the local gravity gradient with its positive direction directed away from the Moon, the j_m axis is orientated perpendicular to this and its k_m axis is perpendicular to the plane of the i_m and j_m components. We again define the upper tip's components relative to the body frame using the tether sub-span length, L_L, and tether rotation angle, ψ_L, and its derivatives as the sub-span length is assumed to be a fixed length. The upper tip position, velocity and acceleration are defined relative to the body frame as:

$$\vec{r}_{Lu} = \begin{bmatrix} L_L cos\psi_L \\ L_L sin\psi_L \\ 0 \end{bmatrix} \tag{7.4}$$

$$\vec{v}_{Lu} = \begin{bmatrix} -\dot{\psi}_L L_L sin\psi_L \\ \dot{\psi}_L L_L cos\psi_L \\ 0 \end{bmatrix} \tag{7.5}$$

$$\vec{a}_{Lu} = \begin{bmatrix} -L_L \left(\ddot{\psi}_L sin\psi_L + \dot{\psi}_L^2 cos\psi_L \right) \\ L_L \left(\ddot{\psi}_L cos\psi_L - \dot{\psi}_L^2 sin\psi_L \right) \\ 0 \end{bmatrix} \tag{7.6}$$

Having obtained these components relative to the body fixed frame, they will now be transformed into the perifocal frame of the Lunavator's orbit by the application of an elementary rotation matrix and the addition of the perifocal components of the origin of the body frame coincident with the Lunavator's central facility.

Perifocal Components

The components of the upper tip can now be determined in the perifocal frame of the Lunavator's orbit about the Moon. The perifocal frame, as described in section 3.2, is a satellite based coordinate frame centred at the Moon, with its P_m axis directed towards the perilune of the Lunavator's orbit, its Q_m axis is perpendicular to this in the direction of orbital motion and its W_m axis is perpendicular to the orbital plane.

The dynamic components of the Lunavator's upper tip relative to the perifocal frame, can be determined by transforming the upper tip's body frame components into the perifocal frame and adding to this the perifocal components of the Lunavator's central facility. The position of the upper tip relative to the perifocal frame is determined as follows:

$$\vec{r}_{Lpu} = \vec{r}_{Lp} + R_{W_L}(\theta_L).\vec{r}_{Lu} \tag{7.7}$$

where the perifocal position of the central facility at true anomaly θ_L in its orbit is defined as:

$$\vec{r}_{Lp} = r_L \begin{bmatrix} cos\theta_L \\ sin\theta_L \\ 0 \end{bmatrix} \tag{7.8}$$

The transformation matrix between the body fixed and perifocal frames is defined as:

$$R_{W_L}(\theta_L) = \begin{bmatrix} cos\theta_L & -sin\theta_L & 0 \\ sin\theta_L & cos\theta_L & 0 \\ 0 & 0 & 1 \end{bmatrix} \tag{7.9}$$

Implementing equations 7.8 and 7.9 into equation 7.7 yields an upper tip position of:

$$\vec{r}_{Lp} = \begin{bmatrix} r_L cos\theta_L + L_L cos(\theta_L + \psi_L) \\ r_L sin\theta_L + L_L sin(\theta_L + \psi_L) \\ 0 \end{bmatrix} \tag{7.10}$$

The velocity of the upper tip relative to the perifocal frame can be determined by the derivation of equation 7.7 with respect to time, and this is obtained as:

$$\vec{v}_{Lpu} = \vec{v}_{Lp} + R_{W_L}(\theta_L).\vec{v}_{Lu} + \dot{R}_{W_L}(\theta_L).\vec{r}_{Lu} \tag{7.11}$$

In this case, the velocity of the central facility relative to the perifocal frame can be defined as:

$$\vec{v}_{Lp} = \sqrt{\frac{\mu_m}{p_L}} \begin{bmatrix} -sin\theta_L & e_L + cos\theta_L & 0 \end{bmatrix}^T \tag{7.12}$$

where p_L is determined from the specific angular momentum of the Lunavator's orbit as defined in equation (4.8). In equation (7.11), the first derivative of equation (7.9) with respect to time is defined as $\dot{R}_{W_L}$, and

together with equation (7.12) yields a perifocal velocity of:

$$\vec{v}_{Lpu} = \begin{bmatrix} -\sqrt{\frac{\mu_m}{p_L}}sin\theta_L - L_L(\dot{\theta}_L + \dot{\psi}_L)sin(\theta_L + \psi_L) \\ \sqrt{\frac{\mu_m}{p_L}}(e + cos\theta_L) + L_L(\dot{\theta}_L + \dot{\psi}_L)cos(\theta_L + \psi_L) \\ 0 \end{bmatrix} \quad (7.13)$$

The perifocal acceleration of the upper tip is simply the second derivative of equation 7.9 from which we obtain:

$$\vec{a}_{Lpu} = \vec{a}_{Lp} + R_{W_L}(\theta_L).\vec{a}_{Lu} + 2\dot{R}_{W_L}(\theta_L).\vec{v}_{Lu} + \ddot{R}_{W_L}(\theta_L).\vec{r}_{Lu} \quad (7.14)$$

In this case, $\ddot{R}_{W_L}(\theta_L)$ is the second derivative of equation 7.9 with respect to time and is simplified by the fact that the angular acceleration acting on the body is zero as a result of the gravitational force being entirely radial in nature. The acceleration of the origin of the body frame is simply the gravitational acceleration acting on the central facility and is defined as:

$$\vec{a}_{Lp} = -\frac{GM_M}{r_L^3}\vec{r}_{Lp} \quad (7.15)$$

Where G is the universal gravitational constant and M_M is the mass of the Moon. The acceleration of the upper tip relative to the perifocal frame is obtained as:

$$\vec{a}_{Lpu} = \begin{bmatrix} -\frac{GM_M}{r_L^2}cos\theta_L - L_L(\ddot{\psi}_L sin(\theta_L + \psi_L) - (\dot{\theta}_L + \dot{\psi}_L)^2 cos(\theta_L + \psi_L)) \\ -\frac{GM_M}{r_L^2}sin\theta_L + L_L(\ddot{\psi}_L cos(\theta_L + \psi_L) - (\dot{\theta}_L + \dot{\psi}_L)^2 sin(\theta_L + \psi_L)) \\ 0 \end{bmatrix}$$
$$(7.16)$$

Having obtained the perifocal components of the upper tip we can obtain its components relative to the selenocentric frame by the application of the perifocal to selenocentric rotation matrix and the basic kinematic equations.

Selenocentric Components

The selenocentric frame of reference is defined as a Moon centred, body fixed frame of reference [41] with the unit vector K_m with a direction along the instantaneous orbit normal of the Moon about Earth, the unit vector I_m is in the same direction as the Moon from Earth and rotates at a rate equal to the Moon about Earth, the unit vector J_m lies within

the orbital plane in the direction of motion and completes the coordinate frame axes. As a result of the necessity for the Lunavator's orbital parameters to be dependent upon those of the payload's hyperbola about the Moon, no precautions can be taken to stop any variations in the argument of perilune and angle of ascending node of the Lunavator's orbit relative to the selenocentric frame as a result of the Moon's oblateness: the perifocal frame of the Lunavator's orbit therefore has components varying relative to the selenocentric frame which must be accounted for where transforming from one coordinate frame to another. The position of the Lunavator's upper tip relative to the selenocentric frame is obtained by the application of the perifocal to selenocentric transformation matrix to the upper tip's perifocal position vector:

$$\vec{r}_{Lsu} = R_{LV}.\vec{r}_{Lpu} \tag{7.17}$$

The transformation matrix between the Lunavator's perifocal frame and its selenocentric frame is denoted by R_{LV} in equation (7.17) and is composed entirely of components obtained from the payload's hyperbola about the Moon. This transformation matrix is identical to that for the payload's hyperbola about the Moon when the Lunavator is at the optimum position for payload capture and launch operations but deviates from this when oblateness effects have caused a precession of the Lunavator's orbital elements, and prior to any manoeuvre required to correct for variations in the hyperbola's inclination relative to the Moon. The Lunavator's perifocal to selenocentric transformation matrix is defined as follows:

$$R_{LV} = \begin{bmatrix} a_{11} & a_{12} & a_{13} \\ a_{21} & a_{22} & a_{23} \\ a_{31} & a_{32} & {}_{33} \end{bmatrix} \tag{7.18}$$

where

$$a_{11} = \cos\Omega_h\cos\omega_h - \sin\Omega_h\sin\omega_h\cos i_h$$

$$a_{12} = -\cos\Omega_h\sin\omega_h - \sin\Omega_h\cos\omega_h\cos i_h$$

$$a_{13} = \sin\Omega_h\sin i_h$$

$$a_{21} = \sin\Omega_h\cos\omega_h + \cos\Omega_h\sin\omega_h\cos i_h$$

$$a_{22} = -\sin\Omega_h\sin\omega_h + \cos\Omega_h\cos\omega_h\cos i_h$$

$$a_{23} = -\cos\Omega_h\sin i_h$$

$$a_{31} = \sin\omega_h\sin i_h$$

$$a_{32} = \cos\omega_h\sin i_h$$

$$a_{33} = \cos i_h$$

with the subscript h notation denoting orbital parameters obtained from the payload's hyperbolic trajectory about the Moon. Implementing equations (7.10) and (7.18) into (7.17) yields a selenocentric upper tip position of:

$$\vec{r}_{Lsu} = \begin{bmatrix} b_1 & b_2 & b_3 \end{bmatrix}^T \tag{7.19}$$

where

$$b_1 = L_L\sin(\theta_L + \omega_h + \psi_L) - \sin\Omega_h\cos i_h(r_L\sin(\theta_L + \omega_h))$$
$$+ \cos\Omega_h(r_L\cos(\theta_L + \omega_h) + L_L\cos(\theta_L + \omega_h + \psi_L))$$
$$b_2 = L_L\sin(\theta_L + \omega_h + \psi_L) + \cos\Omega_h\cos i_h(r_L\sin(\theta_L + \omega_h))$$
$$+ \sin\Omega_h(r_L\cos(\theta_L + \omega_h) + L_L\cos(\theta_L + \omega_h + \psi_L))$$
$$b_3 = \sin i_h(r_L\sin(\theta_L + \omega_h) + L_L\sin(\theta_L + \omega_h + \psi_L))$$

The velocity of the upper tip relative to the selenocentric frame can be obtained by deriving the selenocentric position vector, from equation (7.17), with respect to time and is obtained as:

$$\vec{v}_{Lsu} = R_{LV}.\vec{v}_{Lpu} + \dot{R}_{LV}.\vec{r}_{Lpu} \tag{7.20}$$

where $\dot{R}_{LV}$ is defined as the first derivative of equation (7.18) and is obtained as:

$$\dot{R}_{LV} = \dot{\Omega}_h \begin{bmatrix} a_{11} & a_{12} & a_{13} \\ a_{21} & a_{22} & a_{23} \\ a_{31} & a_{32} & a_{33} \end{bmatrix} + \dot{\omega}_h \begin{bmatrix} b_{11} & b_{12} & b_{13} \\ b_{21} & b_{22} & b_{23} \\ b_{31} & b_{32} & b_{33} \end{bmatrix} \tag{7.21}$$

where

$$a_{11} = -sin\Omega_h cos\omega_h - cos\Omega_h sin\omega_h cosi_h$$

$$a_{12} = sin\Omega_h sin\omega_h - cos\Omega_h cos\omega_h cosi_h$$

$$a_{13} = cos\Omega_h sini_h$$

$$a_{21} = cos\Omega_h cos\omega_h - sin\Omega_h sin\omega_h cosi_h$$

$$a_{22} = -cos\Omega_h sin\omega_h - sin\Omega_h cos\omega_h cosi_h$$

$$a_{23} = -sin\Omega_h sini_h$$

$$a_{31} = 0$$

$$a_{32} = 0$$

$$a_{33} = 0$$

$$b_{11} = -cos\Omega_h sin\omega_h - sin\Omega_h cos\omega_h cosi_h$$

$$b_{12} = -cos\Omega_h cos\omega_h + sin\Omega_h sin\omega_h cosi_h$$

$$b_{13} = 0$$

$$b_{21} = -sin\Omega_h sin\omega_h + cos\Omega_h cos\omega_h cosi_h$$

$$b_{22} = -sin\Omega_h cos\omega_h - cos\Omega_h sin\omega_h cosi_h$$

$$b_{23} = 0$$

$$b_{31} = cos\omega_h sini_h$$

$$b_{32} = -sin\omega_h sini_h$$

$$b_{33} = 0$$

By implementing equations (7.10), (7.11), (7.18) and (7.21) into equation (7.20) we obtain the selenocentric velocity of the upper tip as:

$$\vec{v}_{Lsu} = \begin{bmatrix} -\alpha_L cos\Omega_h - \beta_L sin\Omega_h cosi_h \\ -\alpha_L sin\Omega_h + \beta_L cos\Omega_h cosi_h \\ \gamma_L sini_h \end{bmatrix} \quad (7.22)$$

with α_L, β_L and γ_L are defined as:

$$\alpha_L = \sqrt{\frac{\mu_m}{p_L}}(e_L sin\omega_h + sin(\theta_L + \omega_h)) + (\dot{\Omega}_h cosi_h + \dot{\omega}_h)(r_L sin(\theta_L + \omega_h)$$
$$+ L_L sin(\theta_L + \omega_h + \psi_L)) + L_L(\dot{\theta}_L + \dot{\psi}_L)sin(\theta_L + \omega_h + \psi_L) \quad (7.23)$$

160

$$\beta_L = \sqrt{\frac{\mu_m}{p_L}}(e_L cos\omega_h + cos(\theta_L + \omega_h)) + \left(\frac{\dot{\Omega}_h}{cosi_h} + \dot{\omega}_h\right)(r_L cos(\theta_L + \omega_h)$$

$$+ L_L cos(\theta_L + \omega_h + \psi_L)) + L_L(\dot{\theta}_L + \dot{\psi}_L)cos(\theta_L + \omega_h + \psi_L) \quad (7.24)$$

$$\gamma_L = \sqrt{\frac{\mu_m}{p_L}}(e_L cos\omega_h + cos(\theta_L + \omega_h)) + \dot{\omega}_h(r_L cos(\theta_L + \omega_h)$$

$$+ L_L cos(\theta_L + \omega_h + \psi_L)) + L(\dot{\theta}_L + \dot{\psi}_L)cos(\theta_L + \omega_h + \psi_L) \quad (7.25)$$

At this point some clarification may be required: in the above equations the rates of change of the argument of perilune and angle of ascending node are the rates occurring within the Lunavator's orbit as a result of matching the Lunavator's orbital elements to those of the payload's hyperbola about the Moon rather than any rate occurring within the hyperbola itself which is considered fixed relative to the Moon at that instant in time. The acceleration of the upper tip relative to the selenocentric frame can be obtained by deriving the selenocentric velocity vector, equation (7.20) with respect to time and is obtained as:

$$\vec{a}_{Lsu} = R_{LV}.\vec{a}_{Lpu} + 2\dot{R}_{LV}.\vec{v}_{Lpu} + \ddot{R}_{LV}.\vec{r}_{Lpu} \quad (7.26)$$

Assuming that the rates of the argument of perilune and angle of ascending node are constant and unaccelerated, the second derivative with respect to time of the perifocal to selenocentric transformation matrix is obtained as:

$$\ddot{R}_{LV} = \begin{bmatrix} -\xi a_{11} & \xi a_{12} & -\dot{\Omega}_h^2 a_{13} \\ -\xi a_{21} & \xi a_{22} & -\dot{\Omega}_h^2 a_{23} \\ -\dot{\omega}_h^2 a_{31} & -\dot{\omega}_h^2 a_{32} & a_{33} \end{bmatrix} + 2\dot{\Omega}_h\dot{\omega}_h \begin{bmatrix} b_{11} & b_{12} & b_{13} \\ b_{21} & b_{22} & b_{23} \\ b_{31} & b_{32} & b_{33} \end{bmatrix} \quad (7.27)$$

where

$$a_{11} = cos\Omega_h cos\omega_h - sin\Omega_h sin\omega_h cosi_h$$

$$a_{12} = cos\Omega_h sin\omega_h + sin\Omega_h cos\omega_h cosi_h$$

$$a_{13} = sin\Omega_h sini_h$$

$$a_{21} = sin\Omega_h cos\omega_h + cos\Omega_h sin\omega_h cosi_h$$

$$a_{22} = (sin\Omega_h sin\omega_h - cos\Omega_h cos\omega_h cosi_h)$$

$$a_{23} = cos\Omega_h sini_h$$

$$a_{31} = sin\omega_h sini_h$$

$$a_{32} = cos\omega_h sini_h$$

$$a_{33} = 0$$

$$b_{11} = sin\Omega_h sin\omega_h - cos\Omega_h cos\omega_h cosi_h$$

$$b_{12} = sin\Omega_h cos\omega_h + cos\Omega_h sin\omega_h cosi_h$$

$$b_{13} = 0$$

$$b_{21} = -cos\Omega_h sin\omega_h - sin\Omega_h cos\omega_h cosi_h$$

$$b_{22} = -cos\Omega_h cos\omega_h + sin\Omega_h sin\omega_h cosi_h$$

$$b_{23} = 0$$

$$b_{31} = 0$$

$$b_{32} = 0$$

$$b_{33} = 0$$

with ξ defined as $(\dot{\Omega}_h^2 + \dot{\omega}_h^2)$. Implementing this into equation (7.26) we obtain:

$$\vec{a}_{Lsu} = \begin{bmatrix} -\chi_1 cos\Omega_h + (\chi_2 + \dot{\Omega}_h^2\eta_L)sin\Omega_h cosi_h + \chi_3 sin\Omega_h - \chi_4 cos\Omega_h cosi_h \\ -\chi_1 sin\Omega_h - (\chi_2 + \dot{\Omega}_h^2\eta_L)cos\Omega_h cosi_h - \chi_3 cos\Omega_h - \chi_4 sin\Omega_h cosi_h \\ \chi_2 sini_h \end{bmatrix}$$

(7.28)

with the χ_n terms in equation (7.28) defined as:

$$\chi_1 = \delta_L + 2\dot{\omega}_h\beta_L + (\dot{\Omega}_h^2 + \dot{\omega}_h^2)\zeta_L \tag{7.29}$$

$$\chi_2 = \epsilon_L + 2\dot{\omega}_h(\alpha_L + \dot{\omega}_h\eta_L) \tag{7.30}$$

$$\chi_3 = 2\dot{\Omega}_h(\alpha_L + \dot{\omega}_h\eta_L) \tag{7.31}$$

$$\chi_4 = 2\dot{\Omega}_h(\beta_L + \dot{\omega}_h\zeta_L) \tag{7.32}$$

where δ_L, ϵ_L, ζ_L and η_L are defined as follows:

$$\delta_L = \ddot{\psi}_L L_L sin(\theta_L + \omega_h + \psi_L) + \frac{GM_M}{r_L^2}cos(\theta_L + \omega_h) \qquad (7.33)$$

$$+ \ (\dot{\theta}_L + \dot{\psi}_L)^2 L_L cos(\theta_L + \omega_h + \psi_L)$$

$$\epsilon_L = -\ddot{\psi}_L L_L cos(\theta_L + \omega_h + \psi_L) + \frac{GM_M}{r_L^2}sin(\theta_L + \omega_h) \qquad (7.34)$$

$$+ \ (\dot{\theta}_L + \dot{\psi}_L)^2 L_L sin(\theta_L + \omega_h + \psi_L)$$

$$\zeta_L = r_L cos(\theta_L + \omega_h) + L_L cos(\theta_L + \omega_h + \psi_L) \qquad (7.35)$$

$$\eta_L = r_L sin(\theta_L + \omega_h) + L_L sin(\theta_L + \omega_h + \psi_L) \qquad (7.36)$$

As stated previously, by replacing the orbital elements in equations (7.19), (7.22) and (7.28) with those of an arbitrarily inclined EMMET orbiting Earth; its the position, velocity and acceleration of the components at any point in its orbit can be obtained. Now that the selenocentric components of the Lunavator have been derived, an expression for the maximum tension occurring within the tether as a result of its orbital and rotational motion will be obtained with the aim of deriving an expression for the maximum angular velocity that the Lunavator is capable of being subjected to on an operational basis.

7.1.1 Maximum Tension and Rotational Velocity

Similarly to the derivation in section 4.2, the point of maximum tension along the Lunavator's sub-span occurs at the connection point between the central facility and the lower tether sub-span, as a result of increased gravitational attraction of the Moon on the lower payload and sub-span, and occurs when the Lunavator is at the perilune of its orbit with its sub-spans aligned along the local gravity gradient. At this point accelerations resulting from the centrifugal force are largest. To derive this tension we first obtain the tension acting on the payload and tether sub-span which results from the increment in gravitational attraction as the payload and sub-span are displaced from the Lunavator's centre of mass, in addition to the inertial acceleration terms arising from the Lunavator's orbital and rotational motion. Once we have obtained these expressions, we obtain the tension acting at the lower sub-span's point of connection to the central facility by the application of Newton's third law. To simplify the

derivation some assumptions will be made *a priori*: firstly, it is assumed that the tether sub-spans are at the required rotational velocity and that there is no motor torque acting on the system; secondly, we assume that the the tether sub-spans are aligned along the local gravity gradient with the Lunavator at the perilune of its orbit about the Moon; thirdly, to simplify the derivation and without loss of generality, we assume that the argument of perilune of the Lunavator is zero. We begin by deriving an expression for the tension acting on the lower payload of the Lunavator at its instant of arrival at perilune.

Lower Payload Tension

The tension acting on the lower payload can be found in terms of the net and gravitational forces acting on the payload. The net force results from the Lunavator's motion and is obtained as the product of the payload's mass and its net acceleration. The payload is assumed to be coincident with the Lunavator's lower tip, therefore the net acceleration acting on the payload is identical to that defined for the lower tip by modifying equation 7.28. The tension acting on the payload is defined as:

$$\vec{T}_{Lp} = m_p \vec{a}_{Lsl} - \vec{F}_g \tag{7.37}$$

where $\vec{F}_g$ is the gravitational force of the Moon acting on the payload and defined as:

$$\vec{F}_g = -\frac{GM_M}{r_{Lsl}^3} \vec{r}_{Lsl} = -\frac{GM_M}{(r_L - L_L)^2} \begin{bmatrix} cos\Omega_h & sin\Omega_h & 0 \end{bmatrix}^T \tag{7.38}$$

The acceleration of the lower payload, $\vec{a}_{Lsl}$, is obtained from equation (7.28) by the addition of π radians to the tether rotation angle, ψ_L, and is obtained as:

$$\vec{a}_{Lsl} = -a_{Lsl} \cdot \begin{bmatrix} cos\Omega_h & sin\Omega_h & 0 \end{bmatrix}^T \tag{7.39}$$

where the magnitude of the payload's acceleration, a_{Lsl}, is defined as

$$
\begin{aligned}
a_{Lsl} &= \left(3(\dot{\Omega}_h^2 + \dot{\omega}_h^2) + 4\dot{\Omega}_h\dot{\omega}_h cosi_h + \frac{2\dot{\Omega}_h\dot{\omega}_h}{cosi_h} \right)(r_L - L_L) \\
&\quad - ((\dot{\theta}_L + \dot{\psi}_L)^2 + 2(\dot{\Omega}_h cosi_h + \dot{\omega}_h)(\dot{\theta}_L + \dot{\psi}_L))L_L \\
&\quad + 2\sqrt{\frac{\mu_m}{p_L}}(1 + e_L)(\dot{\Omega}_h cosi_h + \dot{\omega}_h) + \frac{GM_M}{r_L^2}
\end{aligned}
\tag{7.40}
$$

164

Extracting the gravitational term from the lower tip acceleration, equation (7.39) can be re-written as:

$$\vec{a}_{Lsl} + \frac{GM_M}{r_L^3}\vec{r}_L = -\left(a_{Lsl} - \frac{GM_M}{r_L^2}\right) \cdot \begin{bmatrix} cos\Omega_h & sin\Omega_h & 0 \end{bmatrix}^T \quad (7.41)$$

The tension acting on the payload can now be written in terms of the force arising from the inertial and angular acceleration in addition to the increment in gravitational force between the central facility and lower payload:

$$\vec{T}_{Lp} = m_p \left(\vec{a}_{Lsl} + \frac{GM_M}{r_L^3}\vec{r}_L\right) - \left(\vec{F}_g + \frac{GM_M m_p}{r_L^3}\vec{r}_L\right) \quad (7.42)$$

with the increment in gravitational force simplifying to:

$$\left(\vec{F}_g + \frac{GM_M m_p}{r_L^3}\vec{r}_L\right) = -GM_M m_p \left(\frac{1}{(r_L - L_L)^2} - \frac{1}{r_L^2}\right) \begin{bmatrix} cos\Omega_h \\ sin\Omega_h \\ 0 \end{bmatrix} \quad (7.43)$$

Extracting the radial terms in equation (7.43) and applying a binomial series expansion for $\left(\frac{L_L}{r_L}\right) < 1$ yields:

$$\frac{1}{(r_L - L_L)^2} - \frac{1}{r_L^2} = \frac{1}{r_L^2}\left(2\left(\frac{L_L}{r_L}\right) + 3\left(\frac{L_L^2}{r_L^2}\right) + 4\left(\frac{L_L^3}{r_L^3}\right) + ...\right) \quad (7.44)$$

Retaining up to squared terms only we obtain:

$$\upsilon_P = \frac{1}{r_L^2}\left(2\left(\frac{L_L}{r_L}\right) + 3\left(\frac{L_L^2}{r_L^2}\right)\right) \quad (7.45)$$

We now define the magnitude of the inertial and rotational accelerations which comprise the second part of the first term in equation (7.42) as:

$$\begin{aligned} \lambda_P = {} & \left(3(\dot{\Omega}_h^2 + \dot{\omega}_h^2) + 4\dot{\Omega}_h\dot{\omega}_h cosi_h + \frac{2\dot{\Omega}_h\dot{\omega}_h}{cosi_h}\right)(r_L - L_L) \\ & - ((\dot{\theta}_L + \dot{\psi}_L)^2 + 2(\dot{\Omega}_h cosi_h + \dot{\omega}_h)(\dot{\theta}_L + \dot{\psi}_L))L_L \\ & + 2\sqrt{\frac{\mu_m}{p_L}}(1 + e_L)(\dot{\Omega}_h cosi_h + \dot{\omega}_h) \end{aligned} \quad (7.46)$$

The tension acting on the lower payload can now be defined as:

$$\vec{T}_{Lp} = m_p \left(\lambda_P + GM_M \upsilon_P\right) \begin{bmatrix} cos\Omega_h & sin\Omega_h & 0 \end{bmatrix}^T \quad (7.47)$$

Applying Newton's third law, we obtain the tension acting as a result of the central facility, at the connection point to the central facility as:

$$\vec{T}_{LP} = -m_p \left(\lambda_P + GM_M \upsilon_P\right) \begin{bmatrix} cos\Omega_h & sin\Omega_h & 0 \end{bmatrix}^T \quad (7.48)$$

We now now derive an expression for the tension acting at the connection point which results from the lower tether sub-span.

Lower Lunavator Sub-span Tension

To calculate the total tension acting along the tether sub-span we use a method identical to that outlined in section 4.2, by obtaining an expression for the tension acting on an infinitesimal mass element of the sub-span an arbitrary distance along the sub-span's length and we can integrate this expression over the entire length to obtain the total tension along the sub-span. We begin by defining the tension acting on the infinitesimal mass element an arbitrary distance s along the sub-span as:

$$\vec{T}_{Ls} = \delta m \left(\lambda_s + GM_M \upsilon_s \right) \begin{bmatrix} cos\Omega_h & sin\Omega_h & 0 \end{bmatrix}^T \quad (7.49)$$

with λ_s and υ_s defined as:

$$
\begin{aligned}
\lambda_s &= \left(3(\dot{\Omega}_h^2 + \dot{\omega}_h^2) + 4\dot{\Omega}_h\dot{\omega}_h cosi_h + \frac{2\dot{\Omega}_h\dot{\omega}_h}{cosi_h} \right)(r_L - s_L) \\
&- \left((\dot{\theta}_L + \dot{\psi}_L)^2 + 2(\dot{\Omega}_h cosi_h + \dot{\omega}_h)(\dot{\theta}_L + \dot{\psi}_L) \right)s_L \\
&+ 2\sqrt{\frac{\mu_m}{p_L}}(1 + e_L)(\dot{\Omega}_h cosi_h + \dot{\omega}_h) \quad (7.50)
\end{aligned}
$$

$$\upsilon_s = \frac{1}{r_L^2} \left(2\left(\frac{s_L}{r_L}\right) + 3\left(\frac{s_L^2}{r_L^2}\right) \right) \quad (7.51)$$

The tension acting on the infinitesimal element can be re-defined in terms of a magnitude of force directed along the sub-span's length as:

$$\vec{T}_{Ls} = \delta m \left(\lambda_s + GM_M m_p \upsilon_s \right)\vec{i}_s \quad (7.52)$$

Where the unit vector along the sub-spans length, $\vec{i}_s$, is defined as:

$$\vec{i}_s = \begin{bmatrix} cos\Omega_h & sin\Omega_h & 0 \end{bmatrix}^T \quad (7.53)$$

Writing the element's mass in terms of the sub-span's material density, cross sectional area and infinitesimal length δs, the tension acting on the element can be expressed as:

$$\vec{T}_{Ls} = \left(\rho A \left(\lambda_s + GM_M m_p \upsilon_s \right) \delta s \right)\vec{i}_s \quad (7.54)$$

The total tension acting over the entire tether sub-span is obtained by integrating equation (7.54) over the entire sub-span length and from this we obtain:

$$\vec{T}_{Lt} = m_{TL} \left(\lambda_L + GM_M m_p \upsilon_L \right)\vec{i}_s \quad (7.55)$$

where the total mass of the tether is $m_T = \rho A L_L$, with λ_L and v_L defined as:

$$\lambda_L = \left(3(\dot{\Omega}_h^2 + \dot{\omega}_h^2) + 4\dot{\Omega}_h\dot{\omega}_h cosi_h + \frac{2\dot{\Omega}_h\dot{\omega}_h}{cosi_h}\right)\left(r_L\frac{L_L}{2}\right)$$

$$- ((\dot{\theta}_L + \dot{\psi}_L)^2 + 2(\dot{\Omega}_h cosi_h + \dot{\omega}_h)(\dot{\theta}_L + \dot{\psi}_L))\left(\frac{L_L}{2}\right)$$

$$+ 2\sqrt{\frac{\mu_m}{p_L}}(1 + e_L)(\dot{\Omega}_h cosi_h + \dot{\omega}_h) \tag{7.56}$$

$$v_L = \frac{1}{r_L^2}\left(\left(\frac{L_L}{r_L}\right) + \left(\frac{L_L}{r_L}\right)^2\right) \tag{7.57}$$

Applying Newton's third law, we obtain the tension acting at the connection to the central facility resulting from the entire sub-span as:

$$\vec{T}_{LT} = -m_{TL}\left(\lambda_L + GM_M m_p v_L\right)\vec{i}_s \tag{7.58}$$

Now that we have obtained expressions for the tensions acting at the connection point due to the payload and sub-span separately, an expression for the total tension acting at this point will now be obtained.

Maximum Tension and Angular Velocity

The maximum tension acting at the connection point between the central facility and lower tether sub-span can now be found as the vector sum of the tension acting at the connection point as a result of the payload and the tether sub-span and is defined as:

$$\vec{T}_{net} = \vec{T}_{LP} + \vec{T}_{LT} = T_{net}\vec{i}_s$$

$$= -\left(m_{TL}\left(\lambda_L + GM_M v_L\right) + m_p\left(\lambda_P + GM_M v_P\right)\right)\vec{i}_s \tag{7.59}$$

The magnitude of the tension acting on the connection point is defined as:

$$T_{net} = -\left(3(\dot{\Omega}_h^2 + \dot{\omega}_h^2) + 4\dot{\Omega}_h\dot{\omega}_h cosi_h + \frac{2\dot{\Omega}_h\dot{\omega}_h}{cosi_h}\right)(m_p + m_{TL})r_L$$

$$- \left(3(\dot{\Omega}_h^2 + \dot{\omega}_h^2) + 4\dot{\Omega}_h\dot{\omega}_h cosi_h + \frac{2\dot{\Omega}_h\dot{\omega}_h}{cosi_h}\right)\left(m_p + \frac{m_{TL}}{2}\right)L_L$$

$$+ \left(((\dot{\theta}_L + \dot{\psi}_L)^2 + 2(\dot{\Omega}_h cosi_h + \dot{\omega}_h)(\dot{\theta}_L + \dot{\psi}_L))L_L\right)\left(m_p + \frac{m_{TL}}{2}\right)$$

$$- \frac{GM_M}{r_L^2}\left((2m_p + m_{TL})\left(\frac{L_L}{r_L}\right) + (3m_p + m_{TL})\left(\frac{L_L}{r_L}\right)^2\right)$$

$$- \left(2\sqrt{\frac{\mu_m}{p_L}}(1 + e_L)(\dot{\Omega}_h cosi_h + \dot{\omega}_h)\right)(m_p + m_{TL}) \tag{7.60}$$

Having defined the maximum tension acting at the lower sub-span's point of connection to the central facility, we substitute in an expression for the tension in terms of the maximum tensile stress that the material can endure, tether cross sectional area and factor of safety, defined in equation (4.62), into equation (7.60) and re-arrange the resulting equation to make the maximum angular rotational velocity, $\dot{\psi}_L$, of the tether sub-spans the subject of the equation. The maximum angular velocity of the Lunavator sub-spans is therefore obtained as:

$$
\dot{\psi}_L = \\
\sqrt{\frac{1}{\left(m_p + \frac{m_{TL}}{2}\right)L_L}\left(\left(\frac{\sigma_{max}}{SF}\right)A + \nu_L\right) + (\dot{\Omega}_h cosi_h + \dot{\omega}_h)^2} \\
- (\dot{\theta}_L + \dot{\Omega}_h cosi_h + \dot{\omega}_h) \tag{7.61}
$$

with ν_L defined as:

$$
\nu_L = \left(3(\dot{\Omega}_h^2 + \dot{\omega}_h^2) + 4\dot{\Omega}_h\dot{\omega}_h cosi_h + \frac{2\dot{\Omega}_h\dot{\omega}_h}{cosi_h}\right)(m_p + m_{TL})r_L
$$
$$
+ \left(3(\dot{\Omega}_h^2 + \dot{\omega}_h^2) + 4\dot{\Omega}_h\dot{\omega}_h cosi_h + \frac{2\dot{\Omega}_h\dot{\omega}_h}{cosi_h}\right)\left(m_p + \frac{m_{TL}}{2}\right)L_L
$$
$$
+ \frac{GM_M}{r_L^2}\left((2m_p + m_{TL})\left(\frac{L_L}{r_L}\right) + (3m_p + m_{TL})\left(\frac{L_L}{r_L}\right)^2\right)
$$
$$
+ \left(2\sqrt{\frac{\mu_m}{p_L}}(1 + e_L)(\dot{\Omega}_h cosi_h + \dot{\omega}_h)\right)(m_p + m_{TL}) \tag{7.62}
$$

This takes a similar form to those for the EMMET's maximum angular velocity in both cases and contains terms for both precessional rates. By replacing the elements in equation (7.61) by those of an arbitrarily inclined EMMET in orbit about Earth, the maximum angular velocity that the EMMET's sub-spans can withstand can be obtained. Having obtained an expression for the maximum angular velocity that the Lunavator sub-spans can safely rotate at, we will turn our attention to obtaining expressions for the velocity changes required for the orbital adjustments which will keep the Lunavator correctly positioned relative to the Moon to ensure that it has the correct position to perform payload capture and launch operations.

7.2   Orbital Adjustments

Due to the necessity for the Lunavator's orbit to be arranged such that its upper tip velocity matches that of the payload's hyperbola at perilune, no arrangements can be made to negate the effects of oblateness on the Lunavator's orbital elements, and subsequently both the angle of the ascending node and the argument of perilune will have secular rates which result in a deviation of the Lunavator from the optimum position to perform payload catch and throw operations. Adjustments to these orbital elements are therefore necessary to ensure that the Lunavator is correctly aligned for operations, and allocations must be made to include the change in these elements between the time of the manoeuvre and the instants of payload capture and launch. In addition to this adjustments to the orbital inclination of the Lunavator will also be undertaken to match its inclination with that of the payload's current hyperbola about the Moon which varies as a result of the circumlunar trajectory design and the complex motion of the Moon; the change in the secular rates of the argument of perilune, and the ascending node angle due to this change in inclination must also be accounted for. Three separate manoeuvres will be undertaken which will firstly adjust the angle of ascending node, secondly, adjust its argument of perigee and finally, adjust the orbital inclination of the Lunavator's orbit which, when these are complete, will result in the correct alignment of that orbit. Furthermore, by separating these orbital adjustments into individual procedures we ensure that the initial and final orbits in each case actually intersect as this is not necessarily the case when taking into account the deviations in the ascending node, argument of perilune and orbital inclination between the initial and final orbits. To find the change in velocity necessary to perform these orbital adjustments, we must first obtain the true anomaly in each orbit at which the manoeuvre must be performed and secondly, obtain the velocity vector of the Lunavator in each orbit at these true anomalies. The required velocity change is then, simply, the vector required to rotate the Lunavator's velocity vector at the true anomaly of manoeuvre.

7.2.1 Ascending Node Adjustment

According to Vallado [42], the ascending node of an elliptical orbit can be modified by a single impulse manoeuvre occurring at one of two common points of intersection between the current and required orbit. To alter the Lunavator's orbit about the Moon from the initial orbit to the final orbit necessary for operations, three manoeuvres are necessary. The first manoeuvre alters the Lunavator's angle of ascending node to the required angle without modification to its argument of perilune or orbital inclination. This ensures that the alteration to the argument of perilune and inclination consist simply of rotations of the Lunavator's velocity vector at the true anomaly of intersection and node point, respectively. To obtain the velocity required to perform the adjustment we first obtain the true anomalies of the two points in each orbit at which intersection occurs. To obtain the true anomaly of intersection a method similar to section 3.2 is utilised; firstly, the selenocentric components at the point of intersection of the two orbits are equated and we substitute in the polar form for the perifocal (x,y) components, in this case only the angle of ascending node differs in both orbits. Again, we find an expression relating the true anomaly in the first orbit to that of the second orbit using the equated K_m components of the selenocentric frame and from this find that the intersection occurs at the same true anomaly in both orbits. We then substitute in the same true anomaly into the equated I_m components and obtain the expressions for the true anomaly of intersection in the first and second orbits in terms of the angle of ascending node, argument of perigee and orbital inclination. The true anomaly of the first point of intersection in the first orbit can be obtained as:

$$\theta_1 = tan^{-1}\left(-tan\left(\Omega_1 + \frac{\Delta\Omega_L}{2}\right)sec(i_1)\right) - \omega_1 \qquad (7.63)$$

with the subscript (1) denoting components of the Lunavator's first orbital configuration and $\Delta\Omega_L$ denoting the change in the Lunavator's angle of ascending node. The second point of intersection in the first orbit is displaced by π radians from this first point of intersection. Likewise, the true anomaly at the first point of intersection in the second orbit can be

obtained as:

$$\theta_2 = tan^{-1}\left(-tan\left(\Omega_2 - \frac{\Delta\Omega_L}{2}\right)sec(i_1)\right) - \omega_1 \qquad (7.64)$$

With the subscript (2) denoting components of the Lunavator's second orbit. Again, the second point of intersection is displaced π radians from this point in the second orbit. The change in velocity required to alter the Lunavator's angle of ascending node from the first to the second orbit is most simply obtained as the rotation of the Lunavator's velocity vector at the point of intersection in the first orbit through an angle equal to the change in argument of perigee about the Moon's polar axis. This rotation matrix is again obtained using the Rodriguez formula [44], [45] and is obtained as a modified version of equation (3.22), with skew-symmetric matrix S_{an} identical to the skew-symmetric matrix defined in equation (3.23), and obtained as:

$$R_{K_m}(\Delta\Omega_L) = [I + S_{an}sin\Delta\Omega_L + S_{an}^2(1 - cos\Delta\Omega_L)] \qquad (7.65)$$

The velocity of the Lunavator in the second orbit is obtained by the application of the rotation matrix defined in equation (7.65) to the velocity vector in the first orbit, defined in equation (7.22). From this we obtain an equation analogous to equation (3.26) thus obtaining the change in velocity required to perform the manoeuvre in terms of the velocity of the first orbit and the rotation matrix. The change in velocity is obtained and simplified using a linear combination of trigonometric terms [43] as:

$$\Delta\vec{v}_{LV-AN} = \begin{bmatrix} \gamma & \delta & 0 \end{bmatrix}^T \qquad (7.66)$$

with

$$\gamma = -\left(\alpha_1cos\Omega_1 + \beta_1sin\Omega cosi_1\right)(cos(\Delta\Omega_L) - 1)$$
$$+ (\alpha_1sin\Omega_1 - \beta_1cos\Omega cosi_1)sin(\Delta\Omega_L)$$
$$\delta = -\left(\alpha_1cos\Omega_1 + \beta_1sin\Omega cosi_1\right)sin(\Delta\Omega)$$
$$- (\alpha_1sin\Omega_1 - \beta_1cos\Omega cosi_1)(cos(\Delta\Omega) - 1)$$

with α_1 and β_1 defined as:

$$\alpha_1 = \sqrt{\frac{\mu_m}{p_L}}(e_Lsin\omega_1 + sin(\theta_1 + \omega)) + (\dot{\Omega}_1cosi_1 + \dot{\omega}_1)r_1sin(\theta_1 + \omega_1) \qquad (7.67)$$

$$\beta_1 = \sqrt{\frac{\mu_m}{p_L}}(e_L \cos\omega_1 + \cos(\theta_1 + \omega)) + \left(\frac{\dot{\Omega}_1}{\cos i_1} + \dot{\omega}_1\right) r_1 \cos(\theta_1 + \omega_1) \tag{7.68}$$

with $\dot{\Omega}_1$ and $\dot{\omega}_1$ denoting the secular rates of the ascending node and argument of perilune, respectively, at the current inclination of the first orbit and subscript L denoting invariant elements which are constants of the Lunavator's orbit. Now that we have obtained an expression for the change in velocity required to adjust the angle of ascending node of the Lunavator's orbit we will now obtain a similar expression for the change in velocity required to perform the adjustment to the Lunavator's argument of perilune.

7.2.2 Argument of Perilune Adjustment

Having performed the adjustment to align the ascending node of the Lunavator's orbit correctly, the adjustment to the argument of perilune is achieved by rotating the argument of perilune of the Lunavator's second orbital configuration within the orbital plane to the correct alignment with the third orbital configuration in preparation for the Lunavator to perform catch and throw operations. We obtain the true anomaly of intersection by utilising the method of subsection 3.3.1 and by equating the selenocentric components of the second and third orbital configurations we obtain:

$$\theta_2 = \theta_3 + \Delta\omega_L \tag{7.69}$$

This makes physical sense as a positive rotation of the argument of perilune from the second to third orbits will reduce the true anomaly of intersection in the third orbit. By rewriting the equated I_m components in terms of a single true anomaly, an equation for the true anomaly at the first point of intersection can be obtained for each orbit. The true anomaly of intersection in the second orbit is obtained as:

$$\theta_2 = \frac{\Delta\omega_L}{2} \tag{7.70}$$

With the true anomaly at the point of intersection in the third orbit obtained as:

$$\theta_3 = -\frac{\Delta\omega_L}{2} \tag{7.71}$$

where $\Delta\omega_L$ is defined as the change in argument of perilune of the Luna-vator's orbit. As was the case with the ascending node adjustment, the second of point of intersection in both orbits is displaced π radians from the first point. By examining the velocity vectors of the orbits at their points of intersection, as was done in subsection 3.3.1, we find that the only difference in their respective velocity vectors is in the direction of the I_m velocity components. Therefore, the manoeuvre to be performed at the point of intersection between the second and third orbits consists, simply, of a rotation of the second velocity vector at the point of inter-section about the W_m direction of the Lunavator's perifocal frame. To obtain the required rotation matrix, we once again employ the Rodriguez formula which requires that we obtain the direction of the rotation axis relative to the selenocentric frame of reference; this can be obtained easily by transforming the unit vector directed along the W_m direction of the Lunavator's perifocal frame into the selenocentric frame, and is obtained as:

$$i_{W_m} = \begin{bmatrix} sin\Omega_h sini_1 \\ -cos\Omega_h sini_1 \\ cosi_1 \end{bmatrix} \tag{7.72}$$

where the subscript h denotes the Lunavator's orbital elements that are matched to the elements of the payload's hyperbola about the Moon, which at this configuration is only the ascending node angle. The skew-symmetric matrix, S_{ap}, required for the application of the Rodriguez formula can be obtained as:

$$S_{ap} = \begin{bmatrix} 0 & -cosi_1 & -cos\Omega_h sini_1 \\ cosi_1 & 0 & -sin\Omega_h sini_1 \\ cos\Omega_h sini_1 & sin\Omega_h sini_1 & 0 \end{bmatrix} \tag{7.73}$$

The rotation matrix can therefore be defined as:

$$R_{W_m}(\Delta\omega_L) = [I + S_{ap}sin\Delta\omega_L + S_{ap}^2(1 - cos\Delta\omega_L)] \tag{7.74}$$

Utilising equation (7.74), the velocity of the Lunavator at the point of intersection in the third orbit can be written in terms of the rotation matrix and the velocity of the Lunavator in the second orbit. The change in velocity required to perform the adjustment can therefore be written

solely in terms of the rotation matrix and the velocity of the Lunavator in the second orbit as:

$$\Delta \vec{v}_{LV-AP} = (R_{W_m} - I)\vec{v}_2 \qquad (7.75)$$

where $\vec{v}_2$ is defined as:

$$\vec{v}_2 = \begin{bmatrix} -\alpha_2 cos\Omega_h - \beta_2 sin\Omega_h cosi_1 \\ -\alpha_2 sin\Omega_h + \beta_2 cos\Omega_h cosi_1 \\ \gamma_2 sini_1 \end{bmatrix} \qquad (7.76)$$

with α_2, β_2 and γ_2 are defined as:

$$
\begin{aligned}
\alpha_2 &= \sqrt{\frac{\mu_m}{p_L}} \left(e_L sin\omega_1 + sin\left(\omega_1 + \frac{\Delta\omega_L}{2}\right)\right) \qquad (7.77)\\
&+ (\dot{\Omega}_1 cosi_1 + \dot{\omega}_1)r_2 sin\left(\omega_1 + \frac{\Delta\omega_L}{2}\right)\\
\beta_2 &= \sqrt{\frac{\mu_m}{p_L}} \left(e_L cos\omega_1 + cos\left(\omega_1 + \frac{\Delta\omega_L}{2}\right)\right) \qquad (7.78)\\
&+ \left(\frac{\dot{\Omega}_1}{cosi_1} + \dot{\omega}_1\right) r_2 cos\left(\omega_1 + \frac{\Delta\omega_L}{2}\right)\\
\gamma_2 &= \sqrt{\frac{\mu_m}{p_L}} \left(e_L cos\omega_1 + cos\left(\omega_1 + \frac{\Delta\omega_L}{2}\right)\right) \qquad (7.79)\\
&+ r_2\dot{\omega}_1 cos\left(\omega_1 + \frac{\Delta\omega_L}{2}\right)
\end{aligned}
$$

Having obtained expressions for the changes in velocity required to alter the Lunavator's argument of perilune to that required to obtain the optimum position for catch and throw operations we will now derive the velocity required to alter the inclination of the Lunavator's orbit to the correct value.

7.2.3 Inclination Adjustment

The third and final adjustment to be performed which completes the alignment of the Lunavator with the optimum position for catch and throw operations is the alteration to the Lunavator's orbital inclination. According to Vallado [42], alterations to the inclination of an orbit, without affecting the angle of ascending node, must be conducted at either the ascending and descending node of the orbit at the instant that it crosses the orbital plane. By definition, the true anomaly at which an

orbit crosses its ascending node is:

$$\theta_{AN} = 2\pi - \omega \tag{7.80}$$

As the inbound hyperbola is configured such that it enters the LSI above and in front of the Moon and exits behind and below it, the perilunes of the Lunavator and inbound hyperbola occur close to the descending node of their orbits. Therefore, to reduce the magnitude of the velocity changes required to alter the Lunavator's inclination the manoeuvre should be undertaken close to the apolune (furthest point in the orbit from the Moon) of the Lunavator's orbit at its ascending node. The change in velocity required to alter the Lunavator's inclination from the third orbital configuration to the final configuration is most simply obtained using the Rodriguez formula [44], [45] and consists of the rotation of the Lunavator's velocity vector at the ascending node of its orbit through an angle equal to the change in inclination and about an axis directed along the Lunavator's line of node which has a unit vector relative to the selenocentric frame. Initially defining the unit vector of the ascending node at its true anomaly in the perifocal frame, with its true anomaly is obtained by equation (7.80), as:

$$\vec{i}_{AN-P} = \begin{bmatrix} cos\omega_h & -sin\omega_h & 0 \end{bmatrix}^T \tag{7.81}$$

Applying the Lunavator's perifocal to selenocentric transformation matrix but in this case with the inclination terms replaced by those of the Lunavator's inclination prior to the adjustment manoeuvre, we obtain the unit vector relative to the selenocentric frame about which the Lunavator's vector must be rotated to obtain our required inclination as:

$$\vec{i}_{AN} = \begin{bmatrix} cos\Omega_h & sin\Omega_h & 0 \end{bmatrix}^T \tag{7.82}$$

This results in the skew-symmetric matrix required for the Rodriguez formula as:

$$S_i = \begin{bmatrix} 0 & 0 & sin\Omega_h \\ 0 & 0 & -cos\Omega_h \\ -sin\Omega_h & cos\Omega_h & 0 \end{bmatrix} \tag{7.83}$$

The rotation matrix for the adjustment to the Lunavator's inclination can be expressed as:

$$R(\Delta i) = [I + S_i sin\Delta i + S_i^2(1 - cos\Delta i)] \tag{7.84}$$

175

Once again, the change in velocity required to perform the adjustment can be written solely in terms of the rotation matrix and the velocity of the Lunavator in the final orbital configuration as:

$$\Delta \vec{v}_{LV-i} = (R(\Delta i) - I)\vec{v}_3 \tag{7.85}$$

where $\vec{v}_3$ is the Lunavator's velocity vector at its ascending node and is defined as:

$$\vec{v}_3 = \begin{bmatrix} -\alpha_3 cos\Omega_h - \beta_3 sin\Omega_h cosi_1 \\ -\alpha_3 sin\Omega_h + \beta_3 cos\Omega_h cosi_1 \\ \gamma_3 sini_1 \end{bmatrix} \tag{7.86}$$

with α_3, β_3 and γ_3 are defined as:

$$\alpha_3 = \sqrt{\frac{\mu_m}{p_L}}\left(e_L sin\omega_h\right) \tag{7.87}$$

$$\beta_3 = \sqrt{\frac{\mu_m}{p_L}}\left(1 + e_L cos\omega_h\right) + \left(\frac{\dot{\Omega}_1}{cosi_1} + \dot{\omega}_1\right)r_2 \tag{7.88}$$

$$\gamma_3 = \sqrt{\frac{\mu_m}{p_L}}\left(1 + e_L cos\omega_h\right) + r_2\dot{\omega}_h \tag{7.89}$$

Having obtained expressions for the velocity changes required to alter the Lunavator's orbital elements, our attention will now turn to obtaining data by means of simulations of the magnitude of these velocity changes in addition to determining whether a zero relative velocity of the Lunavator's lower tip relative to the Moon's surface is a realistic objective.

7.3   Lunavator Simulations and Data

Now that expressions for the Lunavator's maximum angular velocity have been obtained, its upper and lower tip velocities, in addition to the changes in velocity required to adjust the central facilities' orbit; simulations will now be carried out to establish, firstly, the magnitude of the rate of precession of the Lunavator's orbital elements, secondly, the magnitude of the adjustments required to correctly align the Lunavator, and finally, whether the maximum angular velocity that the Lunavator's sub-spans can be subjected to is sufficient to allow us to obtain a zero relative velocity between the Lunavator's lower tip and the Moon's surface and if obtainable what are the constraints upon this velocity match.

7.3.1 Secular Rates for Orbital Elements

Although the effects of the Moon's oblateness are small compared to those of the Earth's, the Moon's second zonal harmonic is approximately a fifth of that of Earths, the proximity of the Lunavator's orbit to the Moon results in a magnification of this phenomenon and results in its effects being of a comparable magnitude to those experienced by the EMMET in orbit about Earth. The secular rate of the Lunavator's argument of perilune which results from these oblateness effects can be obtained using equation 5.1 and is the same equation as that for the effects of Earth's oblateness on the argument of perigee of the EMMET's orbit. In this case, the inclination of the Lunavator's orbit is matched to that of the payload's hyperbola about the Moon, the gravitational parameter of the Moon, μ_m, is 4902 $km^3 s^{-2}$ [47] and the Moon radius, R_M, is 1738 km [41]. The semi-major axis and eccentricity of the Lunavator's orbit are obtained by the application of equations (5.3) and (5.5) respectively with the orbital period of the Lunavator's orbit satisfying the logistical requirement defined in equation (2.2). In addition to the secular rate for the Lunavator's argument of perilune, the angle of ascending node also has a secular rate which can be obtained via the following equation:

$$\dot{\Omega} = -\left[\frac{3}{2}\frac{\sqrt{\mu_m}J_2 R_M{}^2}{(1-e_L^2)^2 \, a_L^{7/2}}\right] cos i \qquad (7.90)$$

The rate at which the Lunavator's argument of perilune precesses as a result of a variation in its orbital inclination was simulated using a tether sub-span length of 29.262 km, a central facility perilune distance of 1770.738 km, an orbital harmonic, m, between the Moon and EMMET of 130 and an orbital harmonic, n, between the EMMET and Lunavator of 3. The Lunavator's sub-spans were again assumed to be composed of Spectra 2000 material with the same material properties that were specified in Chapter 5. In this instance the data was generated using code written in $MATHEMATICA$™ and a plot of precessional rate against orbital inclination was obtained and is shown in Figure 7.1. As expected, the rate of change of the Lunavator's argument of perilune decreases with increasing inclination and changes from a positive precession to a negative regression as it crosses the critical inclination of 1.157 radians
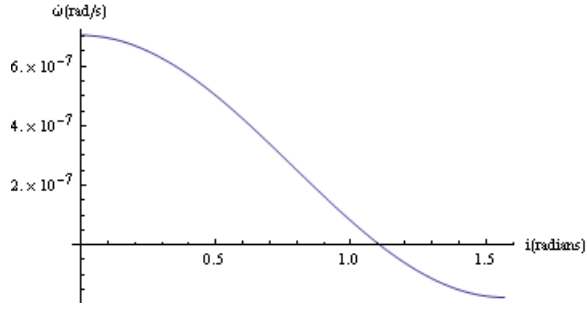
Figure 7.1: Rate of argument of perilune against inclination
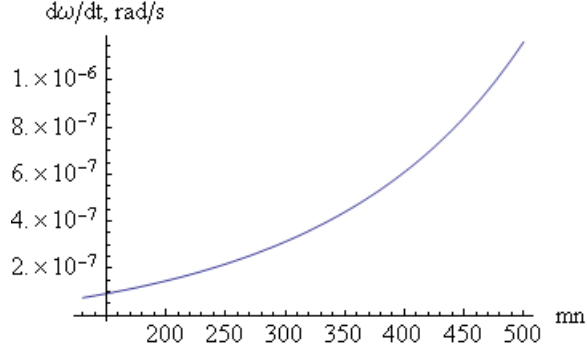
Figure 7.2: Rate of argument of perilune against orbital harmonic mn

(66.3°). The rate of variation of the argument of perilune is smaller than that about Earth but of a similar magnitude. Similarly, the argument of perilune's rate varies as the eccentricity and semi-major axis vary as a result of adjustments to the Lunavator's orbital harmonic, mn, with the Moon. Maintaining the Lunavator's perilune distance and sub-span length whilst setting the orbital inclination to 0.5 radians (28.65°) we again obtain a plot of the Lunavator's rate of argument of perilune and this is shown in Figure 7.2. From this it can be easily seen that the Lunavator's rate of argument of perilune increases with increasing orbital harmonic with the Moon and this correlates to the Lunavator's orbit being brought increasingly closer to the Moon as its semi major axis decreases and these effects are evident in the increased rate of variation of the argument of perilune of the Lunavator's orbit.

The rates at which the angle of ascending node of the Lunavator's orbit varies as a result of this oblateness can also be determined when variations in the orbital inclination, semi-major axis and orbital eccentricity are considered. Maintaining a Lunavator sub-span length of 29.262 km,

178
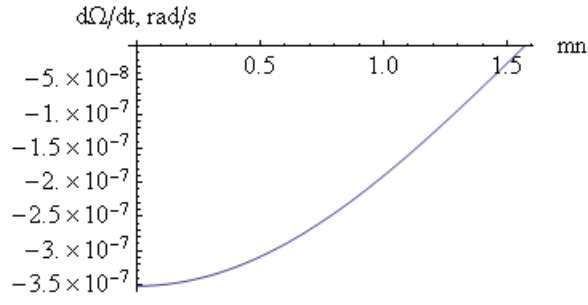
Figure 7.3: Rate of ascending node against inclination
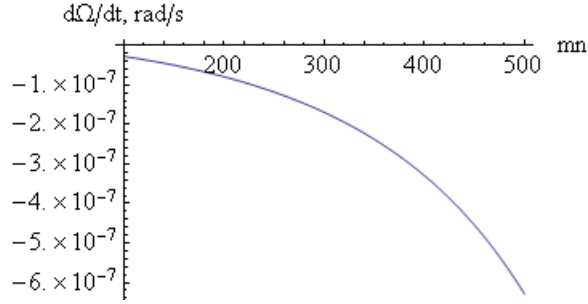
Figure 7.4: Rate of ascending node against orbital harmonic mn

a central facility perilune distance of 1770.738km, an orbital harmonic, m, of 130 and an orbital harmonic, n, of 3; the rate at which the precession of the angle of the ascending node occurred was determined when the inclination was varied between 0 and 90° and the results of this are shown in Figure 7.3. As expected, the maximum rate of regression of the ascending node occurs when the Lunavator is in an almost equatorial Moon orbit when the attractive influence of the Moon's equator is most strongly felt. This attractive influence decreases as the inclination increases and becomes zero when the Lunavator's inclination equals that of a polar orbit. The angle of ascending node also varies as the eccentricity and semi-major axis vary as a result of adjustments to the Lunavator's orbital harmonic, mn with the Moon. Maintaining perilune distance and sub-span length and setting the orbital inclination to 0.5 radians (28.65°) we obtain a plot of the Lunavator's rate of angle of ascending node and the plot obtained is shown in figure 7.4. These results show an increase in the rate of the angle of ascending node as the semi-major axis and orbital eccentricity of the Lunavator's orbit decrease and corresponds to an increase in the attractive influence of the Moon's equator as the Lu-

179

navator becomes increasingly closer to the Moon throughout its orbit as the geometry of its orbit decreases.

It has been shown that the oblateness effects of the Moon, although small in comparison to those of the Earth, have effects of comparable magnitude due to the Lunavator's proximity to the Moon. Therefore, as stated earlier, adjustments to the Lunavator's orbital parameters must be carried out with a similar frequency to those performed for the EMMET to minimise the velocity required to perform these adjustments.

7.3.2 Upper and Lower Tip Velocities

Having obtained data for the rate at which the angle of ascending node and argument of perilune vary as a result of variations in orbital inclination and the Lunavator's orbital harmonic with the Moon, the upper and lower tip velocities that the Lunavator is capable of producing when its inclination, orbital harmonic with the Moon, perilune distance and tether sub-span length are varied will now be obtained. Plots of the gathered data will be produced with the aim of determining whether a zero relative velocity between the Lunavator's lower tip and the Moon's surface is a realistic objective and if so, what is the required upper tip velocity and whether a practical hyperbolic trajectory of the payload about the Moon be configured in this event.

Noting that the rates of the angle of ascending node and argument of perilune are small in magnitude in comparison to the orbital velocity, the main proportion of the tip velocities of the Lunavator are a result of the orbital and sub-span rotational velocities and are not due to these oblateness effects, we therefore will focus our attention on variations in the Lunavator's orbital parameters through variation in perilune distance. This is achieved by means of adjustment to the Lunavator's orbital harmonic with the Moon, and through rotational parameters by means of variation in the perilune distance of the payload's hyperbolic trajectory about the Moon, so this subsequently determines Lunavator's sub-span length and central facility distance, we will therefore set the inclination of the Lunavator's orbit to 0.5 radians for the remainder of this chapter. Plotting the lower tip velocity of the Lunavator, using a modified form
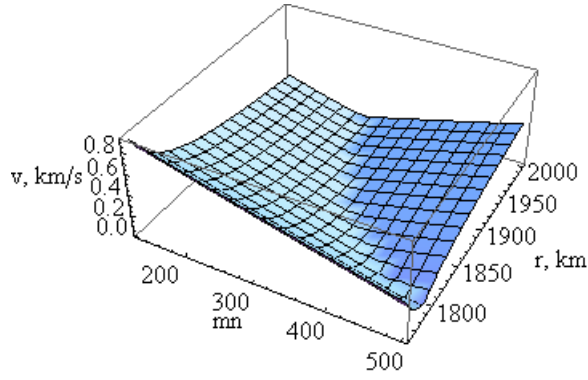
Figure 7.5: Lunavator's lower tip velocity at perilune

of equation (7.22), against variations in both orbital harmonic with the Moon, *mn*, between a range of 130 and 500 and varying the payload's hyperbolic perilune position between 1761.476 and 2000km, corresponding to a Lunavator sub-span range between 10 and 129.262km, we obtain a 3-dimensional plot of the variation in the Lunavator's lower tip, and this is shown in Figure 7.5. From this it is indeed evident that the Lunavator is in fact capable of producing a zero relative velocity at its lower tip for a range of sub-span lengths, and this zero relative velocity can be identified as the border between the light and darker blue regions of the plot. Furthermore, the light blue region indicates the regions where the lower tip has a positive velocity in the same direction as the Lunavator's orbital motion and the darker region indicates that the sub-span's rotational rate in combination with its length, is of sufficient magnitude to negate orbital velocity in addition to producing a net lower tip velocity in the direction opposite to orbital motion. A plot of the Lunavator's upper tip velocity was obtained over this same data range by utilising equation (7.22) and this is shown in Figure 7.6. This produces a range of upper tip velocities between 2.6 and 3.7 kms^{-1} with a decrease in velocity, correlating with an increase in the Lunavator's orbital harmonic with the Moon. This is unsurprising given that the Lunavator's orbital geometry and perilune velocity decrease with increasing orbital harmonic. An increase in the upper tip velocity is found to correspond to an increase in tether sub-span length, with the maximum velocity occurring when the orbital harmonic is at a minimum and sub-span length is at a maximum. Our attention now turns to determining the magnitude of the

181
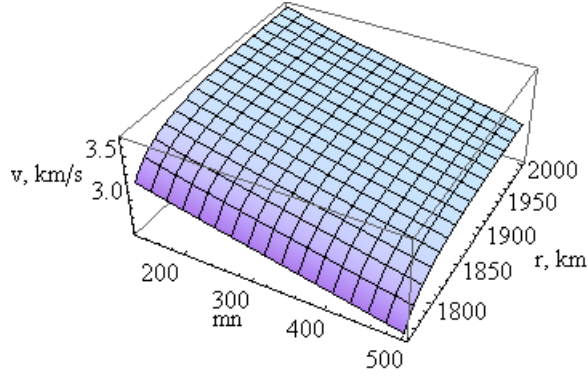
Figure 7.6: Lunavator's upper tip velocity at perilune

orbital adjustments required to position the Lunavator correctly for payload capture and throw operations, with the aim of obtaining an estimate of the required changes in velocity for this to occur. However, it remains to be determined whether a practical hyperbolic perilune velocity for the payload is obtainable at the Lunavator's upper tip which will produce a zero relative velocity at the lower tip and this will be examined in Chapter 8.

7.3.3 Orbital Adjustment Velocity Requirements

The magnitude of the velocity changes necessary to perform the orbital adjustments required to align correctly the Lunavator will now be determined when the orbital harmonic between the Lunavator and Moon is varied. For simplicity and without loss, we set the angle of the ascending node and argument of perilune of the Lunavator's orbit equal to zero in equation (7.66) which yields a required change in velocity for some arbitrary increment in the Lunavator's angle of ascending node as:

$$\Delta \vec{v}_{LV-AN} = - \begin{bmatrix} \alpha_1(cos(\Delta\Omega_L) - 1) + \beta_1 cosi_1 sin(\Delta\Omega_L) \\ \alpha_1 sin(\Delta\Omega_L) - \beta_1 cosi_1(cos(\Delta\Omega_L) - 1) \\ 0 \end{bmatrix} \quad (7.91)$$

with α_1 and β_1 defined as:

$$\alpha_1 = \left(\sqrt{\frac{\mu_m}{p_L}} + (\dot{\Omega}_1 cosi_1 + \dot{\omega}_1)r_1 \right) sin(\theta_1) \quad (7.92)$$

$$\beta_i = \sqrt{\frac{\mu_m}{p_L}}e_L + \left(\sqrt{\frac{\mu_m}{p_L}} + \left(\frac{\dot{\Omega}_1}{cosi_1} + \dot{\omega}_1 \right) r_1 \right) cos(\theta_1) \quad (7.93)$$
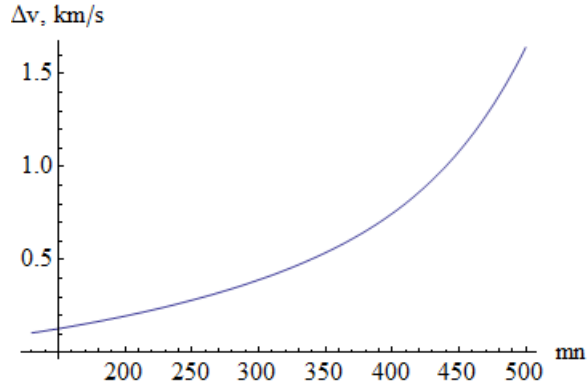
Figure 7.7: Velocity change for ascending node adjustment

The true anomaly at the point of intersection in the first orbital configuration for some arbitrary increment in the Lunavator's angle of ascending node is defined as:

$$\theta_1 = tan^{-1}\left(-tan\left(\frac{\Delta\Omega_L}{2}\right)sec(i_1)\right) \qquad (7.94)$$

The rate at which the angle of the ascending node of the Lunavator's orbit precesses is greatest at low inclinations, however for equatorial orbits, zero orbital inclination, the angle of ascending node and argument of perilune become undefined because there is no equatorial crossing point and any precessional effects are combined and termed precession of the longitude of perilune. We therefore take the worst case scenarios for the rate of ascending node when the Lunavator is at low inclinations and in our simulation of the change in velocity required to perform the adjustment to the angle of ascending node we take our orbital inclination as 0.1 radians (5.73°). In addition to this, we take a Lunavator central facility perilune altitude of 1770.738 km resulting in a sub-span length of 29.262km, and finally assuming the manoeuvre to occur at the first point of intersection between the first and second orbital configurations, data of the change in velocity required to perform the manoeuvre each time the Lunavator becomes unladen, which correlates to the adjustment in ascending node required to correct for the deviation in optimum position occurring in the time period for the orbit of the Moon about Earth, was obtained when the Lunavator's orbital harmonic was varied, this plot is shown in Figure 7.7. It is evident from this data that a one-to-one correlation between the orbital period of the EMMET and Lunavator may be

the preferred choice to minimise the change in velocity required for the adjustment to the Lunavator's ascending node. The maximum velocity change correlates to a change in ascending node angle of π radians.

Our attention now turns to the required change in velocity required to adjust the Lunavator's argument of perilune which will also be designed to occur when the Lunavator is fully unladen and at the point of intersection between the second and third orbital configurations occurring closest to apolune. We again assume, for the purposes of simplification, that the argument of perilune and angle of ascending node are both zero in the second orbit, and from equations (7.75) and (7.76) we obtain the required change in velocity as:

$$\Delta \vec{v}_{LV-AP} = (R_{W_m} - I) \begin{bmatrix} -\alpha_2 \\ \beta_2 cosi_1 \\ \gamma_2 sini_1 \end{bmatrix} \tag{7.95}$$

Defining the true anomaly in the second orbit at the point of intersection closest to apogee as:

$$\theta_2 = \pi + \frac{\Delta \omega_L}{2} \tag{7.96}$$

The components α_2, β_2 and γ_2 of equation 7.85 are defined as:

$$\alpha_2 = -\sqrt{\frac{\mu_m}{p_L}} sin\left(\frac{\Delta \omega}{2}\right) - (\dot{\Omega}_1 cosi_1 + \dot{\omega}_1) r_2 sin\left(\frac{\Delta \omega}{2}\right) \tag{7.97}$$

$$\beta_2 = \sqrt{\frac{\mu_m}{p_L}} \left(e_L - cos\left(\frac{\Delta \omega}{2}\right)\right) - \left(\frac{\dot{\Omega}_1}{cosi_1} + \dot{\omega}_1\right) r_2 cos\left(\frac{\Delta \omega}{2}\right) \tag{7.98}$$

$$\gamma_2 = \sqrt{\frac{\mu_m}{p_L}} \left(e_L - cos\left(\frac{\Delta \omega}{2}\right)\right) - r_2 \dot{\omega}_1 cos\left(\frac{\Delta \omega}{2}\right) \tag{7.99}$$

The matrix, $(R_{W_m} - I)$, to be directly applied to the second orbit's velocity becomes:

$$\begin{bmatrix} a_{11} & a_{12} & a_{13} \\ a_{21} & a_{22} & a_{23} \\ a_{31} & a_{32} & a_{33} \end{bmatrix}$$

$$\tag{7.100}$$
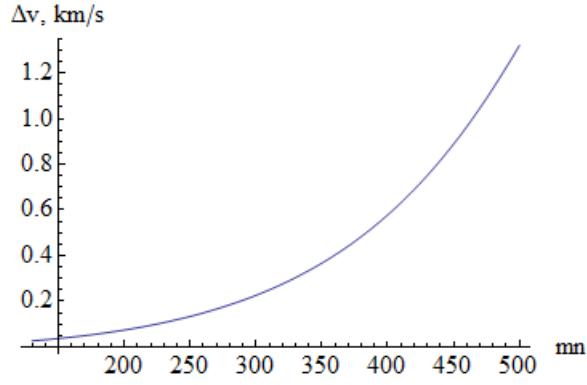
Figure 7.8: Velocity change for argument of perilune adjustment

where

$$a_{11} = -\cos^2 i_1 + \cos^2 i_1 \cos\Delta\omega$$

$$a_{12} = -\cos i_1 \sin\Delta\omega$$

$$a_{13} = 0$$

$$a_{21} = \cos i_1 \sin\Delta\omega$$

$$a_{22} = -\cos^2 i_1 + \cos^2 i_1 \cos\Delta\omega$$

$$a_{23} = 0$$

$$a_{31} = 0$$

$$a_{32} = 0$$

$$a_{33} = 0$$

Utilising the parameters used for the ascending node case, the change in velocity required to adjust the argument of perilune between the second and third orbital configurations was plotted against the variation in the Lunavator's orbital harmonic with the Moon, this plot is shown in Figure (7.8). This again supports the case for a one-to-one correlation between the Lunavator and EMMET's orbital periods.

Our attention now turns to the change in velocity required to adjust the Lunavator's inclination which is designed to occur when the Lunavator is at the ascending node of its orbit and close to, or at, apolune. Without loss of generality we can assume that the ascending node of the Lunavator's orbit is π radians and this results in the change in velocity between the third and final orbital configurations obtained from equation

185
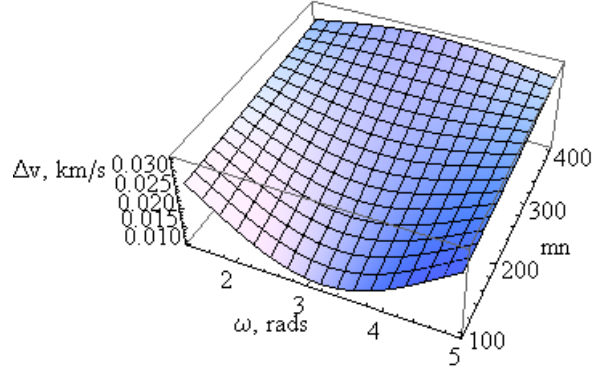
Figure 7.9: Velocity change required for Lunavator's inclination adjustment against mn

(7.86) as:

$$\Delta \vec{v}_{LV-i} = \begin{bmatrix} 0 \\ -\beta_3 \cos i (1 - \cos \Delta i) + \gamma_3 \sin i \sin \Delta i \\ -\beta_3 \cos i \sin \Delta i - \gamma_3 \sin i (1 - \cos \Delta i) \end{bmatrix} \qquad (7.101)$$

Initially, the change in velocity required to perform some arbitrary change in inclination is obtained from equation (7.101) as a function of the change in argument of perilune of the Lunavator's orbit in addition to the change in orbital harmonic. To arrange the perilune the Lunavator's orbit to occur close to its descending node, the argument of perilune must be close to π radians in addition to the ascending node also being π radians. Setting the initial inclination of the Lunavator's orbit to 45.84° with a central facility perilune altitude of 1770.503km, the velocity change required to alter the inclination of the Lunavator's orbit by 1° when variations in the orbital harmonic and argument of perilune are made is shown in Figure (7.9). From Figure (7.9) it can be seen that the velocity change required increases with increasing orbital harmonic and this is a result of the Lunavator's ascending node velocity increasing as the orbital geometry decreases. In addition to this, the velocity adjustment is minimised when the argument of perilune of the Lunavator's orbit is exactly π radians and this is a result of the Lunavator's ascending node coinciding exactly with the Lunavator's apolune and results in the manoeuvre being undertaken when the Lunavator's velocity is low-

est. Data was also accumulated on the required velocity change when variation and direction of the inclination change was performed, taking the initial inclination of the orbit to be 45°, the magnitude of the velocity adjustment required to change the inclination to 0° and 90° was plotted as the argument of perilune of the Lunavator's orbit was varied and using a orbital harmonic mn of 130 and this is shown in Figure (7.10). It can be seen from Figure (7.10) that the magnitude of the velocity change increases with increasing inclination change angle and again it can be seen that the velocity required to perform the manoeuvre is minimised when the argument of perilune is zero.

To verify the previous discussion concerning the logistical requirements of the system, moon-tracking orbits, and EMMET and Lunavator designs; simulations will now be undertaken to obtain data on the operations of the system when the ascending node of the Moon's orbit occurs at points closes to perigee and apogee within the Moon's orbit which will yield maximum and minimum configurations for the system. The data gathered from these simulations will be discussed in the following chapter.
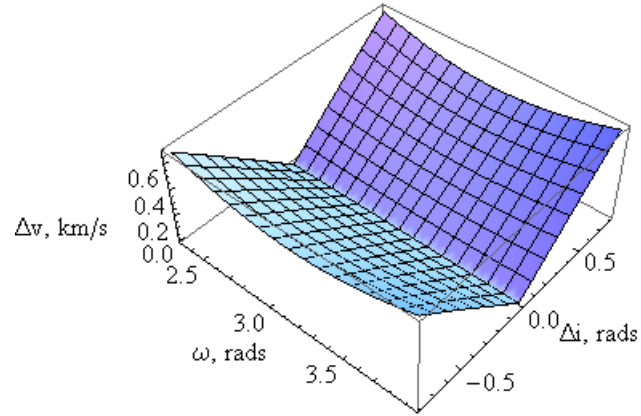
Figure 7.10: Velocity change required for Lunavator's inclination adjustment against inclination

7.4   Conclusions

Having determined the manoevres required to arrange the Lunavator such that its upper tip is in the required position on each occasion that a payload arrives from Earth or when a payload is required to be launched back to Earth, it was found that these were every bit as complex as configuring the EMMET for moon-tracking but for altogether different reasons. The Lunavator's argument of perilune, ascending node and orbital inclination all require alterations to ensure a correct configuration for payload capture or release. This is a result of the Moon reaching its ascending node earlier or later in each orbit. This requires an adjustment to the payload flight time which in turn affects the hyperbola about the Moon which is accommodated by altering the Lunavator's orbital elements. In comparison to the EMMET, which requires alteration to its orbital elements for moon-tracking, it was expected that any adjustments to the Lunavator's elements would be more easily achieved in terms of fuel consumption as a result of the lower gravitational attraction of the Moon and reduced oblateness. Similarly to the velocity adjustments required for the EMMET's orbit, the Rodriguez formula was utilised to formulate these adjustments in terms of a rotation matrix and the velocity at the point of orbital intersection in the initial orbit. In the Lunavator's case, a further rotation occurring at the ascending node of its orbit was required to also adjust the orbital inclination.

Conducting analysis of the velocity changes required to perform these adjustments revealed that these rates were of a comparable magnitude to those occurring within the EMMET's orbit and were a result of the Lunavator's close proximity to the Moon even though its actual oblateness is very much less significant. Again the magnitude of the adjustments required to configure the Lunavator's freely precessing argument of perilune and angle of ascending node were found to increase with increasing orbital harmonic with the Moon's orbit and were of a comparable magnitude in both cases. Furthermore, analysis revealed that the Lunavator was in fact capable of completely removing orbital velocity from a payload at its upper tip and producing zero relative velocity with the Moon's

surface at its lower tip. However, numerical simulations in Chapter 8 will reveal whether this is a realistic goal whilst satisfying the logistical requirements during the trajectory design phase.

The EMMET and Lunavator configurations in addition to the circumlunar transfer configuration described will now be used to simulate the operational phases for the payload exchange mechanism using different moon-tracking configurations and occurring at different times. The results of this are presented in Chapter 8

8.   Simulations and Data

Having established the theoretical basis for the continuous payload exchange system, the EMMET and Lunavator configurations were implemented with code written in $MATHEMATICA^{\text{TM}}$ in addition to the means for calculating the payload's trajectories between them, with the aim of determining whether such a system could be realistically established when these logistical requirements were adhered to, and if possible, the economy of the system in comparison with a conventional chemical propulsion system. Data for four different transfer configurations are shown each to illustrate a different aspect of the system's design, the cases are as follows:

i. Polar inclined EMMET exchanging with a Lunavator using the no-wait time logistical configuration. The system input-time is 08:40:00 on June 11th 2022 with the Moon's ascending node occurring at a true anomaly of approximately 90°.

ii. Polar inclined EMMET exchanging with a Lunavator using standard logistical configuration. The system input-time is 12:40:00 on June 16th 2020 with the Moon's ascending node occurring close to apogee at a true anomaly of approximately 180°.

iii. Critically inclined EMMET exchanging with a Lunavator using standard logistical configuration. The system input-time is 08:40:00 on June 11th 2022 with the Moon's ascending node occurring at a true anomaly of approximately 90°.

iv. Critically inclined EMMET exchanging with a Lunavator using standard logistical configuration. The system input-time is 20:40:00 on May 10th 2024 with the Moon's ascending node occurring close to perigee at a true anomaly of approximately 0°.

The first two cases are used to show the operation of the system using a polar moon-tracking orbit, the first case is used to show the system's con-

figuration when a no-wait time logistical configuration is used in comparison with the standard logistical configurations of the other cases. Case 2 is used to show the system configuration when transfers are conducted to an ascending node coinciding with the apogee of the Moon's orbit. The last two cases show the transfer configuration when critically inclined EMMET inclinations are used with Case 3 allowing a comparison with Case 1 to be made as they transfer to the same ascending node position. Case 4 is used to show the configuration of the system when transfers are conducted to an ascending node coinciding to the perigee of the Moon's orbit. The simulations all use the same basic input parameters and these are shown in Table (8.1) and in each of the following tables of data, any value followed in the next column by (-) indicates a repeated value.

Table 8.1: Simulation Input Parameters

Parameter	Input Value
Earth's Gravitational Parameter, km^3s^{-2}	398600
Moon's Gravitational Parameter, km^3s^{-2}	4902.8
Mass of Earth,kg	5.9742×10^{24}
Mass of Moon,kg	7.3483×10^{22}
Payload Mass, kg	500
Earth's J_2 Effect	0.0011
Radius of Earth, km	6378.14
Orbital Period of Moon, days	27.3207
Radius of Moon, km	1738
Moon's J_2 Effect	0.0002

8.1 Moon Configuration Data

The position and velocity vectors of the Moon at the input time of the system were obtained using the Horizon system from *JPL* [52] in addition to its state vector at that instant. The orbital configuration at the input time in each case is shown in Table (8.2). In this table t_p denotes time since perigee passage for the Moon's orbit; p denotes the Moon's orbital

parameter; and θ_ω denotes the true anomaly of the Moon's ascending node. It can be noted that the Moon's position and velocity over the course of its orbit is quite consistent and this benefits our trajectory designs. Furthermore, variations in the Moon's energy occur as a result of third body perturbations acting on the Moon and coincides with variations in eccentricity and semi-major, axis in addition to the other orbital elements.

Table 8.2: Moon configuration at input time

Case	1.	2.	3.	4.
r, km	368855	403294	368855	379255
v, kms^{-1}	1.066	0.972	1.066	1.038
$\dot\omega$, 10^{-6}rads^{-1}	1.289	-	-	-
h, km$^2 s^{-1}$	392333	392118	392333	393050
v radial, kms^{-1}	-0.065	-0.02	-0.065	0.064
i, deg	26.956	24.094	26.956	28.4827
Ω, deg	9.12	13.022	9.12	2.776
e	0.0718	0.058	0.0718	0.063
ω, deg	269.974	180.126	269.974	2.2
θ, deg	298.431	199.078	298.431	81.3344
E, km$^2 s^2$	-0.513	-0.516	-0.513	-0.512
a, km	388609	386617	388609	389325
p, km	386603	385300	386603	387768
t_p, days	-4.137	-12.04	-4.137	5.633
θ_ω, deg	90.026	179.874	90.026	357.799

8.2 System Transfer Variable Data

The transfer variables for each of the exchange configurations are shown in Table (8.3) and it can be noted that the points of payload entry and exit into the LSI are very similar in each case. The wait time d_w of zero in Case 1 denotes that the Lunavator system remains fully laden throughout the course of the exchange, and by utilising an even Earth-Moon transfer

time, c_1, and an odd Moon-Earth transfer time, c_2, and reversing this order during the next transfer phase; the logistical requirements for this arrangement are satisfied. It may be noted that the flight time within LSI, γ, is not integer harmonic with the EMMET and Lunavator's orbital periods however, this is accommodated into the logistical design such that the addition of the flight time between Earth and LSI, plus the flight time between LSI and perilune, are integer harmonic with the EMMET and Lunavator's orbital periods, the same is the case for the Lunavator to EMMET flight time.

Table 8.3: Transfer Variables

Case	1.	2.	3.	4.
ϕ_{LSIL}, deg	123.85	129.58	127.288	133.017
δ_{LSIL}, deg	18.621	16.919	11.173	11.1727
c_1	28	30	30	28
ν, days	9.845	-2.19	9.72	-6.2965
d_w	0	-1	1	-1
γ	6.81	8.5	7.347	7.831
ϕ_{LSIR}, deg	236.15	230.42	232.712	226.983
δ_{LSIR}, deg	-16.043	-15.069	-9.311	-9.31056
c_2	27	30	30	28

8.3 EMMET Perigee Data

The EMMET is composed of *SPECTRA 2000* material and its characteristics are shown, along with a factor of safety, in Table (8.4). Each case uses almost identical EMMET configurations with the only differences being in their angles of ascending node; the inclinations used in the first two cases in comparison with those used in the last two cases; and in the angular and linear velocities resulting from the increased rotational harmonic of the last two cases to that of the first two.

Table 8.4: EMMET Perigee Parameters

Case	1.	2.	3.	4.
S.F.	2	-	-	-
A, 10^{-12}km^2	65	-	-	-
ρ, 10^{11}kgkm^3	9.7	-	-	-
σ_{max}, $10^{12}Pa$	325	-	-	-
r_{ET-P}, km	7478	-	-	-
L_{ET}, km	100	-	-	-
ω_{ET}, deg	0	-	-	-
m	180	-	-	-
p_r	29	-	31	-
θ_{ET}, deg	0	-	-	-
i_{ET}, deg	90	-	63.4	-
Ω_{ET}, deg	189.12	193.022	189.12	182.776
T, hours	3.643	-	-	-
a, km	12019.4	-	-	-
e	0.378	-	-	-
v_{cf}, kms^{-1}	8.57	-	-	-
h, km$^2s^{-1}$	64085.6	-	-	-
p, km	10303.5	-	-	-
T_{rot}, min	7.409	-	6.939	-
$\dot{\psi}_{max}$, rads^{-1}	0.016	-	-	-
$\dot{\psi}$, rads^{-1}	0.014	-	0.015	-
$\dot{\theta}$, rads^{-1}	0.001	-	-	-
v_l, kms^{-1}	7.042	-	6.946	-
v_u, kms^{-1}	10.098	-	10.194	-

8.4   LSI Contact Data

The configuration of the Moon and the distance of the LSI entry and exit points relative to both Earth and the Moon are shown at the instant of payload arrival and departure from the the LSI in Table (8.5). The true anomaly of LSI entry and exit, in each case, can be seen to be almost

symmetrical about the true anomaly of the Moon's ascending node and this allows the inbound and outbound transfer trajectories to have similar inclinations and perigee positions relative to Earth.

Table 8.5: LSI Arrival and Departure Data

Case	1.	2.	3.	4.
θ_{m-arr}, deg	83.33	173.314	81.644	-9.94
r_{m-arr}, km	383403	409005	382608	365029
$\dot{\theta}_{m-arr}$, $\times 10^{-4} \mathrm{deg} s^{-1}$	1.529	1.343	1.536	1.69
$r_{LSI-arr-s}$, km	65375.1	69470.4	65032.9	61834.2
$r_{LSI-arr-eq}$, km	353285	370771	347910	326888
θ_{m-dep}, deg	97.048	186.686	98.464	5.59409
r_{m-dep}, km	390041	409005	390735	364806
$\dot{\theta}_{m-dep}$, $\times 10^{-4} \mathrm{deg} s^{-1}$	1.478	1.343	1.472	1.692
$r_{LSI-dep-s}$, km	66483	69452.2	66403.3	61785.9
$r_{LSI-dep-eq}$, km	358872	370345	355049	326423

8.5   Payload Hyperbola Data

The hyperbolic trajectories undertaken by the payloads within the LSI in each of the cases are shown in table (8.6). Differences in the orbital elements of the payload's hyperbola between the polar inclined Cases 1 and 2, and also evident in the critically inclined cases 3 and 4, can be accommodated into the system by the adjustment manoeuvres discussed in Chapter (7). Each case has a perilune altitude within 300km of the Moon's surface and it can be noted that the critically inclined Cases, 3 and 4, have hyperbolas with greater inclinations than those of the polar inclination cases: it is not clear whether this is a result of the moon-tracking orbit used or simply a coincidence of the transfer configuration. It should also be noted that Case 1 has the highest LSI boundary velocities, corresponding to larger eccentricity, which results in a higher velocity perilune: although Case 3 has the highest velocity if its perilune distance was increased to match that of Case 1 it would have a lower

velocity as a result of its inbound velocity and a decreased acceleration due to the Moon's gravitational attraction. Another point which should be noted with regards to the differences in perilune distance for each case: under the conditions that the perilune distances of succeeding payload exchanges could not be matched a solution to this would be for the Lunavator to undertake a Hoffman manoeuvre [47] to alter the perilune altitude of the Lunavator's orbit in addition to adjustment to the tether sub-span lengths this however, would require the further use of fuel.

Table 8.6: LSI Payload Hyperbola Data

Case	1.	2.	3.	4.
v_{in}, kms^{-1}	1.381	1.143	1.261	1.086
v_{out}, kms^{-1}	1.38	1.143	1.26	1.086
h, km^2s^{-1}	5188.53	5118.72	4859.56	4638.32
v radial, kms^{-1}	-1.38	-1.141	-1.259	-1.084
i, deg	159.264	159.544	167.11	166.05
Ω, deg	186.725	184.218	186.953	185.683
e	1.723	1.507	1.554	1.384
p, km	5490.92	5344.14	4816.7	4388.1
ω, deg	186.519	184.159	186.869	185.671
θ_{entry}, deg	237.883	232.221	233.429	227.819
E, km$^2s^2$	0.879	0.583	0.72	0.511
a, km	-2789.33	-4206.88	-3403.77	-4799.6
r_p, km	2016.53	2131.89	1885.9	1840.98
v_p, kms^{-1}	2.573	2.401	2.577	2.52

8.6   LSI Motion Earth Data

To ensure that the elliptical transfers about Earth are as closely matched to the hyperbolic trajectories about the Moon at the LSI boundary points, and vice versa; it is useful to compare the orbital elements of their hyperbolic trajectories relative to Earth. The orbital elements of the payload's trajectory from LSI entry to perilune are obtained relative

to Earth in Table (8.7) whilst those of the perilune to LSI hyperbolic trajectory relative to Earth are shown in Table (8.8). The inclination of the payloads of Case 1 have been intentionally matched to that of the elliptical trajectories to and from Earth whilst this has not been done in the other cases and is being used to determine the dependency of the change in velocity required at the transition point between the elliptical and hyperbolic trajectories as a result of the inclinations of the orbits relative to Earth. In both the entry and exit data sets, for each of the cases there are small discrepancies in the angle of ascending node of the payloads trajectories relative to Earth but more significantly there are large discrepancies in the argument of perigee of the payloads relative to Earth in comparison to that of the EMMET's orbit, optimally 0°. The sign of the radial velocity terms in each case are consistent with pre-apogee payload contact with LSI upon entry and post apogee payload contact upon exit and this is important in ensuring that the payload has not already entered or left LSI prior to the stated contact which is unrecognisable to the simulation.

Table 8.7: LSI Entry Data Relative to Earth

Case	1.	2.	3.	4.
v_{in}, kms^{-1}	0.824	0.699	0.77	0.702
h, km^2s^{-1}	162625	113176	88058.2	79333.5
v radial, kms^{-1}	0.684	0.628	0.728	0.659
i, deg	89.04	68.038	88.521	22.406
Ω, deg	189.155	194.398	188.238	186.395
e	0.86	0.931	0.958	0.961
p, km	66349.1	32134.3	19453.7	15789.8
ω, deg	15.176	7.362	7.8065	2.91
θ_{entry}, deg	161.037	168.948	170.337	172.157
E, km$^2s^2$	-0.788	-0.831	-0.849	-0.973

Table 8.8: LSI Exit Data Relative to Earth

Case	1.	2.	3.	4.
v_{out}, kms^{-1}	0.733	0.724	0.643	0.714
h, $km^2 s^{-1}$	175840	130939	93681	84122.1
v radial, kms^{-1}	-0.546	-0.631	-0.586	-0.666
i, deg	89.256	69.511	88.736	26.878
Ω, deg	189.079	191.91	189.863	180.461
e	0.82	0.908	0.948	0.956
p, km	77570.8	43013.2	22017.4	17753.4
ω, deg	346.225	350.051	353.195	355.016
θ_{exit}, deg	197.067	193.204	188.355	188.459
E, $km^2 s^2$	-0.842	-0.815	-0.916	-0.966

8.7 Lunavator Data

The Lunavator parameters for each of the configurations are shown in Table (8.9), the tether sub-spans in this case are again composed of *SPECTRA 2000* material. It is evident from this that the lower tip of the Lunavator is not sufficiently removing the orbital velocity from the payloads such that the lower payload can be placed with zero relative velocity on to the Moon's surface with the lowest tip velocity occurring for Case 1 at $1.22 kms^{-1}$.

8.8 Payload Elliptical Data

The orbital parameters of the LSI to Earth elliptical trajectory are shown in Table (8.10) with that of the Earth to LSI trajectory shown in Table (8.11). It can be seen that in both cases their orbital elements are closely matched to those of the EMMET's orbit with the aim of reducing any velocity change upon capture and launch; the two trajectories are in fact symmetrical about the Moon's ascending node and the perigee position of the EMMET. Some discrepancy exists between the arguments of perigee of the trajectories and that of the EMMET's orbit however, these are

Table 8.9: Lunavator Perilune Parameters

Case	1.	2.	3.	4.
S.F.	2	-	-	-
A, 10^{-12}km^2	65	-	-	-
ρ, 10^{11}kgkm^3	9.7	-	-	-
σ_{max}, $10^{12}Pa$	325	-	-	-
n	1	-	-	-
q_r	7	3	15	19
θ_{LT}, deg	0	-	-	-
L_{LT}, km	139.267	196.945	73.95	51.4897
r_{cf}, km	1877.27	1934.95	1811.95	1789.49
T, hours	3.643	-	-	-
a, km	2774.49	-	-	-
e	0.323	0.303	0.347	0.355
v_{cf}, kms^{-1}	1.859	1.817	1.909	1.927
h, km^2s^{-1}	3490.02	3515.29	3459.13	3447.94
p, km	2484.34	2520.45	2440.56	2424.8
i, deg	159.264	159.544	167.11	166.05
Ω, deg	186.725	184.218	186.953	185.683
ω, deg	186.519	184.159	186.869	185.671
T_{rot}, min	29.142	62.447	13.877	11.209
$\dot{\omega}$, $\times 10^{-7}$rads^{-1}	1.21	1.178	1.39	1.393
$\dot{\Omega}$, $\times 10^{-8}$rads^{-1}	6.689	6.511	7.225	7.287
$\dot{\psi}_{max}$, rads^{-1}	0.012	0.008	0.021	0.03
$\dot{\psi}$, rads^{-1}	0.004	0.002	0.008	0.009
$\dot{\theta}$, $\times 10^{-4}$rads^{-1}	9.903	9.389	10.54	10.767
r_l, km	1738	-	-	-
v_l, kms^{-1}	1.221	1.302	1.273	1.39
r_u, km	2016.53	2131.89	1885.9	1840.98
v_u, kms^{-1}	2.497	2.332	2.545	2.463

small in comparison to those of the hyperbolic trajectories relative to the Earth in Tables (8.7) and (8.8). Some velocity discrepancy exists

between that of the payloads at perigee and that of the EMMET's upper tip but exist as a result of adhering to the logistical requirements of the system.

Table 8.10: LSI to Earth Transfer Data

Case	1.	2.	3.	4.
$v_{LSI-exit}$, kms^{-1}	0.367	0.315	0.253	0.252
v_p, kms^{-1}	10.1544	10.156	10.15	10.14
h, $km^2 s^{-1}$	76950.2	76962.4	76914.8	76840
v_{exit} radial, kms^{-1}	-0.297	-0.237	-0.13	-0.091
i, deg	89.972	89.472	63.371	63.417
Ω, deg	189.12	193.022	189.12	182.776
e	0.964	0.96	0.959	0.955
ω, deg	359.866	0.323	0.23	0.707
θ_{exit}, deg	183.426	182.723	181.5	181.049
E, $km^2 s^2$	-1.044	-1.027	-1.091	-1.189

Table 8.11: Earth to LSI Transfer Data

Case	1.	2.	3.	4.
v_p, kms^{-1}	10.151	10.156	10.147	10.14
$v_{LSI-entry}$, kms^{-1}	0.303	0.316	0.24	0.253
h, $km^2 s^{-1}$	76915.9	76962.7	76892.7	76839.9
v_{entry} radial, kms^{-1}	0.118	0.059	0.086	0.088
i, deg	89.563	89.909	63.391	63.354
Ω, deg	189.12	193.022	189.12	182.776
e	0.959	0.961	0.958	0.955
ω, deg	358.637	359.325	359.004	358.977
θ_{entry}, deg	177.577	177.253	178.92	178.921
E, $km^2 s^2$	-1.0825	-1.025	-1.117	-1.187

8.9 Velocity Change Data

The total velocity changes required to exchange payloads for each of the configuration cases are shown in Table (8.11) which consist of the velocity adjustments required to configure the Lunavator and EMMET tethers for each of the moon-tracking methods in addition to the velocity changes required for the transfer trajectories themselves. This allows the efficiency of the system to be established when a comparison is made with the velocity requirements for a minimum energy trajectory from the Earth to the Moon's surface and back [53] which are shown in Table (8.13).

Table 8.12: Configuration Delta-V Requirements

Case	1.	2.	3.	4.
$\Delta v_{LT-Capture}$, kms^{-1}	0.0755	0.069	0.032	0.056
$\Delta v_{LT-Launch}$, kms^{-1}	0.0755	0.069	0.032	0.056
$\Delta v_{LSI-Exit}$, kms^{-1}	0.454	0.562	0.61	0.768
$\Delta v_{ET-Capture}$, kms^{-1}	0.59	0.114	0.048	0.081
$\Delta v_{ET-Launch}$, kms^{-1}	0.151	0.085	0.098	0.103
$\Delta v_{LSI-Entry}$, kms^{-1}	0.683	0.566	0.785	0.755
$\Delta v_{E-Mtotal}$, kms^{-1}	0.909	0.72	0.914	0.915
$\Delta v_{M-Etotal}$, kms^{-1}	0.589	0.745	0.685	0.905
Δv_{E-M-E}, kms^{-1}	1.498	1.465	1.599	1.819
$\Delta v_{Adjustments}$, kms^{-1}	1.63	1.63	0.85	0.85
Δv_{Total}, kms^{-1}	3.128	3.095	2.449	2.669

8.10 Conclusions

It has been shown by means of numerical simulations of the entire procedure that a continuous payload exchange system can be established by obeying the logistical and trajectory requirements of the system. These exchanges can be undertaken with significant velocity change savings in comparison to conventional chemical propulsion. However, there are sev-

Table 8.13: Conventional Propulsion Delta-V Requirements

Phase	Velocity change, kms^{-1}
Trans-Luna Injection	3.2
Mid-course correction	0.03
Lunar orbit insertion	0.89
De-orbit	0.02
Landing	1.85
Lift-off	1.83
Lunar orbit injection	0.02
Trans-Earth Injection	0.85
Mid-course correction	0.03
Earth-Moon-Earth Total	8.72

eral important issues which must be taken into account in future research of this area:

i. At every tip in every instance velocity mismatches were present between the tether tip and the incoming and outgoing payloads. This can be dealt with in two ways firstly, by ensuring that the system is robust enough to withstand this shock no further action need be taken or alternatively, the payload should undertake propulsive burns to adjust the velocity at launch and capture to the required velocity as was the case incorporated into the simulations.

ii. Significant velocity mismatches occurred at the entry and exit points to LSI between the elliptical and hyperbolic trajectories at these points. Case 1 showed that these were as significant in the case where the elliptical and hyperbolic inclinations were matched and result from the differences in their arguments of perigee at these points of conjunction and less significantly on small differences in the angle of ascending nodes. Attempts were made to remedy this but resulted in unwanted variations in the other orbital elements of the trajectories.

iii. In all cases the lower tip velocity of the Lunavator remained unac-

ceptably large and could not be reconciled. The solution to this is for the Lunavator to be placed into a circular orbit about the Moon but this also introduces further constraints into the overall system design.

It is clear that these are not optimised trajectory calculations and the velocity mismatches between the tips and payloads in addition to those existing between the hyperbolic and elliptical trajectories at conjunction could be further reduced. The extent to which this may occur remains unclear at this point. The data presented here should be considered a first step in the design of a concise circumlunar trajectory with a more detailed trajectory calculation being implemented. This would incorporate third body perturbations and would implement techniques such as linearisation of the state transition matrix to give the payload's precise circumlunar trajectories whilst retaining perigee and perilune position in addition to the times of flight between them.

9. Centre of Energy

The research conducted in this chapter was motivated by the occurrence of an anomaly in the predicted altitude of a symmetrically laden momentum exchange tether's central facility when beginning work on the use of reeling of the tether sub-span's lengths to effect orbital changes. This phenomenon was again evident in the mis-balance between the upper and lower tether tensions acting on the EMMET and Lunavator central facilities in Chapters 4 and 7. It was discovered that the system appeared not to orbit Earth at the altitude of its central facility coincident with the system's centre of mass as a result of a net force, due to variations in gravitational and centrifugal forces, acting on the system at this point. Neither did it appear to orbit at the system's centre of gravity which is not coincident with its centre of mass in a non-uniform gravitational field and additionally the point at which these forces balance. It was discovered that the system orbits about Earth at a distance coincident with the point of mean specific potential energy of the entire system and this was termed the *centre of energy*. This centre of energy is located exactly midway between its centre of mass and centre of gravity and satisfies the 'vis-viva' equation and the law of conservation of energy for the system.

9.1   Lagrangian formulation

To begin the research on tether reeling manoeuvres, a symmetrically laden tether system was conceived which connected two uniform payloads of equal mass to the central facility using rigid, massless tether sub-spans of equal length, with the aim of allowing changes caused by these reeling manoeuvres to be clearly observed. The central facility was given an initial angular velocity equal to that of a circular orbit about a perfectly spherical Earth at the central facility's orbital altitude which coincided with the centre of mass of the system. The position vectors of the central facility and upper and lower tips were obtained relative to an Earth

centered perifocal frame as implicit functions of time using a method similar to that employed in Chapter 4 as:

$$R_{cf} = R[t] \begin{bmatrix} cos\theta[t] & sin\theta[t] & 0 \end{bmatrix}^T \tag{9.1}$$

$$R_{upper} = R_{cf} + L \begin{bmatrix} cos(\theta[t] + \psi[t]) & sin(\theta[t] + \psi[t]) & 0 \end{bmatrix}^T \tag{9.2}$$

$$R_{lower} = R_{cf} - L \begin{bmatrix} cos(\theta[t] + \psi[t]) & sin(\theta[t] + \psi[t]) & 0 \end{bmatrix}^T \tag{9.3}$$

The generalised coordinates used here are the radius of the central facility, R; the true anomaly of the central facility within its orbit, θ; and the tether rotation angle, ψ: the tether sub-span length was initially set at a constant length to ensure that the equations for the tether system were being correctly set up. The velocity of the central facility, in addition to the velocities of the upper and lower tips were defined as the derivatives of the respective position vectors and by assuming that the central facility in addition to the upper and lower payloads could be adequately modeled as point masses, each of mass M, for the initial set up of the system. Therefore, the total potential energy of the system was defined as:

$$U = -\mu M \left(\frac{1}{r_{cf}} + \frac{1}{r_{upper}} + \frac{1}{r_{lower}} \right) \tag{9.4}$$

Additionally, the total kinetic energy of the system was defined as:

$$KE = \frac{1}{2} M \left(v_{cf}^2 + v_{upper}^2 + v_{lower}^2 \right) \tag{9.5}$$

These were used to form the Lagrangian of the system, KE-U, and following the standard procedure, the variational equations for each of the generalised coordinates were obtained by implementing the Lagrangian of the system into the variational equation of the form [54]:

$$\frac{\partial L}{\partial q} - \frac{d}{dt} \left(\frac{\partial L}{\partial \dot{q}} \right) = 0 \tag{9.6}$$

with q defining each of the generalised coordinates of the system and $\dot{q}$ defining its first derivative with respect to time. To obtain the equations of motion of the system and to accumulate data of how the system's parameters varied with time, these variational equations were numerically integrated using code written in $Mathematica^{\text{TM}}$.

Using an initial radial distance for the central facility of 7378 km and a radial velocity of zero, corresponding to the central facility being at either the apogee or perigee of its orbit; an initial true anomaly of 0° with
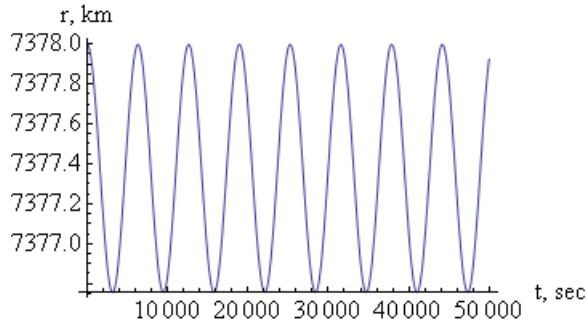
Figure 9.1: Oscillation of tether's centre of mass in a circular orbit
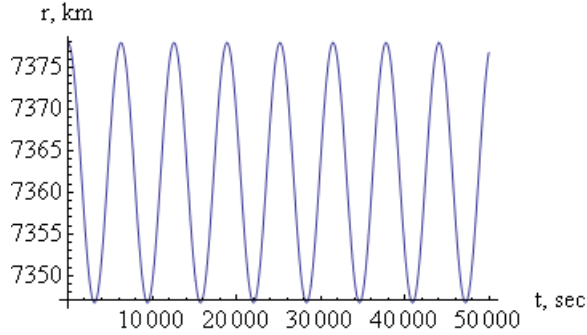

Figure 9.2: Increased oscillation of system's centre of mass

an orbital angular velocity of 0.0009955 rad/s which is equal to that of a circular orbit at this altitude; and an initial tether rotation angle of 0° with a spin angular velocity of 0.025 rad/s, data on the evolution of the system over a time interval of 100,000 seconds was accumulated using a tether sub-span length of 100 km and mass, M, equal to 1000kg. This showed a surprising result: that the oscillation of the system's centre of mass beginning at the initial altitude of the central facility, corresponding to the oscillation's peak, and with a peak to peak amplitude of approximately 1.22 km and a period marginally larger than 6000 seconds and this is shown in Figure (9.1). This anomaly was also present in similar data presented by Zeigler [49] in 2003 but was not analysed in any detail. This oscillation becomes even more pronounced when the mass of each of the system's components is increased to 5000 kg and the tether sub-span lengths are increased to 500km with the oscillation again beginning at its peak corresponding to the radius of the central facility with a peak to peak amplitude of 31 km in this case and this is shown in Figure (9.2). This oscillation was present for all values of
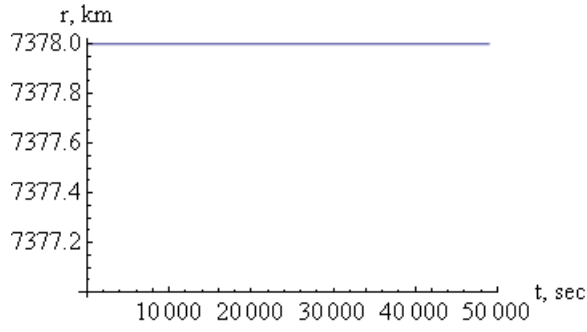
206

Figure 9.3: No oscillation of system's centre of mass for circular orbit
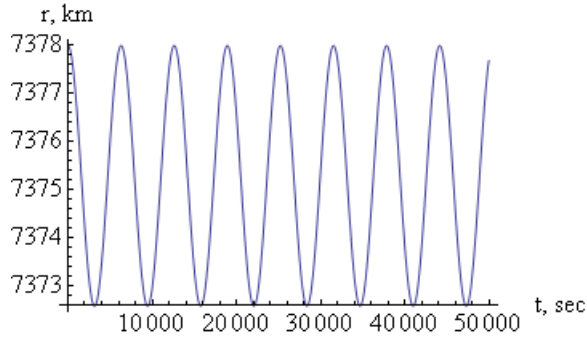

Figure 9.4: Oscillation of hanging centre of mass in a circular orbit

tether length but disappeared when the tether sub-span lengths were set to zero which corresponds to a single particle orbiting in a circular orbit at the radial distance of the central facility and this is shown in Figure (9.3). The oscillation was also found to be evident and in fact even more pronounced in the hanging tether case, and this is shown for masses, M, equal to 1000 kg and tether sub-span lengths of 100 km in Figure (9.4). A peak to peak amplitude of 5.4 km for the hanging case was observed, comparing this to a 1.22 km peak to peak for the spinning case , and a time period again marginally larger than 6000 seconds which indicates that this phenomena is not a result of the rotation of the tether sub-span and may be somewhat alleviated by spinning. Having described the observed phenomenon, a hypothesis for its cause was proposed and this is the focus of the following section.

9.2 Centre of Gravity Hypothesis

A fundamental laws in physics states [55]: *When a body or collection of particles is acted on by external forces, the centre of mass moves as though all the mass were concentrated at that point and it were acted on by a force equal to the sum of the external forces on the system.* Furthermore, according to Cosmo and Lorezini [7], for a gravity gradient stabilised tether system consisting of two satellites tethered in orbit: *The gravitational and centrifugal forces are equal and balanced at only one place: the system's center of gravity. The center of gravity (or mass), located at the midpoint of the tether when the end masses are equal, is in free fall as it orbits the Earth, but the two end masses are not. They are constrained by the tether to orbit with the same angular velocity as the center of gravity.* Additionally, these forces can be equated as follows:

$$\frac{\mu m}{r^2} = m\theta^2 r \qquad (9.7)$$

where the total mass of the system is denoted by m; the radius of the centre of mass is denoted by r; and the angular velocity of this centre of mass is denoted by θ. Our observations of the motion of the centre of mass of the symmetrically laden system contradict both of these statements. As the only forces acting on the system as a result of this simplified model are the gravitational force of Earth and the inertial centrifugal force arising as a result of the orbital motion of the tether system about Earth, the cause of the deviations cannot be explained by the effects of precession or nutation, as no out-of-plane forces are acting on the system and these oscillations must therefore be gravitational and inertial in origin. Cosmo and Lorenzini take the centre of mass and centre of gravity of the tethered system to be coincident, this however is not the case for a body which experiences a varying force of gravitational attraction, which is the case for an extended tether system in a non-uniform gravitational field [55].

At this point it could be hypothesised that these oscillations in the radius of the system's centre of mass are possibly a result of an additional torque acting due to the centre of mass and centre of gravity not being coincident for an extended body in a non-uniform gravitational field however, if this was the case these deviations would vanish for a gravity

gradient stabilised hanging tether system, but as Figure (9.4) shows, the oscillation is even more pronounced and this hypothesis must therefore be discounted. The only remaining possibility is that the central facility of the tether system, and consequently its centre of mass, is subject to a net force which arises due to a tension in the tether system as a result of the extension of the body, and consequently equation (9.7) is not valid in this case therefore the centre of mass of the system cannot be thought of as the point at which the mass can be considered to translate in a non-uniform gravitational field. If the gravitational and centrifugal forces are not balanced at this point it seems reasonable that the actual point at which translation can be considered to occur is at a point where these forces do balance and a reasonable guess would be that this occurs at the centre of gravity of the system. To establish the location of this balance of forces, a simple model of a symmetrical tether system was established which consisted of two identical masses connected by a tether aligned along the local gravity gradient and its configuration is shown in Figure (9.5). By defining the net forces acting on the system as a result of variation in gravitational and centrifugal forces, the point at which these forces are in equilibrium can be determined. The net force acting on the mass located at the lower end of the gravity gradient stabilised tether is determined as the sum of the gravitational and centrifugal forces acting at that point as:

$$\Delta F_1 = -\frac{\mu m}{R^2} + m\theta^2 R \qquad (9.8)$$

Where R is the radial distance of the lower payload from Earth; the mass of the payloads are denoted by m; the angular velocity of the system is denoted by θ; and in the following equation the entire tether length will be denoted by L. The net force acting on the payload at the upper tip
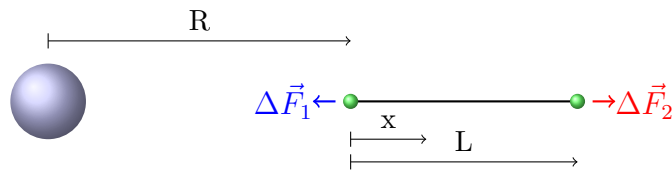

Figure 9.5: Forces acting on symmetrical tether system in orbit

can be determined as:

$$\Delta F_2 = -\frac{\mu m}{(R+L)^2} + m\theta^2(R+L) \tag{9.9}$$

By obtaining an expression for the net force acting at some arbitrary point x along the tether sub-span as:

$$\Delta F_x = -\frac{\mu m}{(R+x)^2} + m\theta^2(R+x) \tag{9.10}$$

then the point of equilibrium of the centrifugal and gravitational forces can be determined for the system by examining the equilibrium conditions for arbitrary point x along the sub-span. This equilibrium condition is defined as:

$$\Delta F_1 - \Delta F_x = \Delta F_x - \Delta F_2 \tag{9.11}$$

Implementing equations (9.8), (9.9) and (9.10) into equation (9.11) results in:

$$-\frac{\mu m}{R^2} - \frac{\mu m}{(R+L)^2} + m\theta^2 L = -2\frac{\mu m}{(R+x)^2} + 2m\theta^2 x \tag{9.12}$$

Canceling out the common mass terms; applying the binomial theorem to the first term on the right hand side; assuming that x is very small in comparison with R; and omitting squared terms we obtain:

$$\left(\frac{2\mu}{R^3} + \theta^2\right) x = \frac{1}{2}\left(\frac{\mu}{R^2} - \frac{\mu}{(R+L)^2} + \theta^2 L\right) \tag{9.13}$$

As a short numerical example: using a lower sub-span radius of 7278km; a tether length of 200km; and an angular velocity of a circular orbit at the centre of mass of the system at 7378 km equal to 0.000955 rad/s; we obtain a value of x equal to 97.2411 km. This corresponds to the forces balancing at a radius of 7375.2411 km and 2.7589 km below the centre of mass of the system. This hypothesis seems to fit the data and the oscillations observed are not, as first interpreted, fluctuations about the initial position of the system's centre of mass but are in fact the radial profile of a tether system undertaking an elliptical trajectory about Earth. This is at a point other than its centre of mass, with the observed oscillations occurring as a result of the system having too great or too little angular velocity at the system's point of orbit about Earth to undertake a circular orbit. This is due to this angular velocity being that

of a circular orbit at the radial distance of the central facility coinciding with the centre of mass.

If the system in orbit in a non-uniform gravitational field does not orbit as if all of its mass is concentrated at its centre of mass then is there a physical significance to the point of equilibrium at a distance x along the sub-span? The obvious point of translation would be at the centre of gravity itself which would obviously occur closer to Earth than the centre of mass in a non-uniform gravitational field and which is defined similarly to the centre of mass as the average location of the force of gravity acting on a body, we will define this here as:

$$\vec{R}_{cg} = \frac{-\sum_{i=1}^{n}(M_i r_i^{-2})\vec{R}_i}{\sum_{i=1}^{n}(M_i r_i^{-2})} \tag{9.14}$$

Calculating the position of the centre of gravity for the system utilised to establish the point of equilibrium of force we find that this centre of gravity occurs at a distance of 7375.29 km from Earth. Comparing this with the point of equilibrium of forces of 7375.2411 km it can be reasonably stated that by taking into the approximations made in the calculation of the equilibrium point that the point of force equilibrium and the centre of gravity are coincident.

Plotting the motion of the centre of gravity of the hanging system described in section 9.1 using a sub-span length of 100 km and mass of the payloads and central facility of 1000 kg; an initial central facility radius of 7378km and the angular velocity of a circular orbit at the distance of the centre of gravity, now calculated at 7376.2 km due to the addition of the central facility to the system, it can be determined that if the entire system undertakes a circular orbit about Earth then this is evidence that the system is orbiting Earth in an identical manner to that of a particle at the distance of the system's centre of gravity from Earth at the angular velocity of a circular orbit at this point. Data on the radius of the system's centre of gravity and centre of mass was plotted and this is shown in Figure (9.6). The motion of the centre of mass is shown in blue and that of the centre of gravity is purple, it is very clear that the system is undertaking an elliptical orbit about Earth with its perigee position coinciding with its initial conditions. Both centres subsequently traverse a trajectory to their respective apogees, furthest

from Earth and this indicates that the system has an initial angular velocity too large to remain on a circular orbit about Earth and that the system is not translating with a motion identical to that of a particle at a point coincident with the systems centre of gravity. Furthermore, by examining Figure (9.4) it can be seen that the system in this case has an initial angular velocity which is too low to remain on a circular orbit and the central facility subsequently traverses a path from apogee to the perigee of its orbit. Taking into account these two data plots allows us to conclude that for this system to undertake a circular orbit about Earth, it must have an angular velocity greater than that required for a circular orbit at its centre of mass distance but smaller than that at the distance, of its centre of gravity. Therefore, if the system can be simplified such that its motion is identical to that of a particle at a particular point along the body this must lie somewhere between its centre of mass and centre of gravity.

9.3   Centre of Energy Hypothesis

Having established that the system does not orbit Earth as a particle with all mass concentrated at its centre of mass, or as a particle with all force concentrated at the centre of gravity, we will move away from force considerations and focus upon the total energy of the system. The specific energy of a particle in orbit is composed of potential and kinetic components and is given by the *vis viva* equation which is further related to the semi-major axis of the particles motion. Defining the total orbital
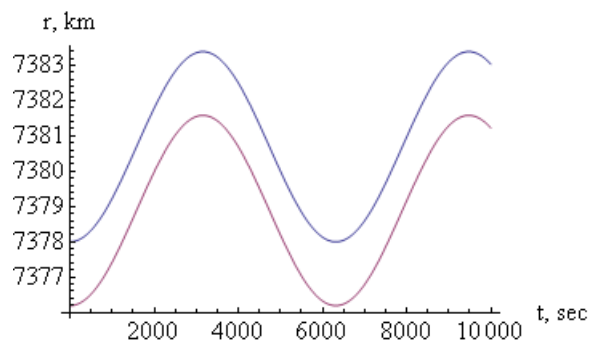

Figure 9.6: Orbit of hanging system's centre of mass and gravity about Earth

potential energy of the system as the total energy stored as a result of the position of each of the system's components within the non-uniform gravitational field: it would seem that the system's motion, if it could at all be treated as a particle, would follow the motion of a particle located at the point of specific potential energy of the entire system with a subsequent motion defined by the specific kinetic energy of that location. This hypothesis can be checked in the following way: firstly, by examining the motion of the centre of mass and centre of gravity in Figure (9.6), the centre of mass is shown in blue and the centre of gravity is shown in purple, we can write their respective semi-major axes in terms of their perigee and apogee positions and an offset distance from the point of actual motion and from this we can calculate the magnitude of this offset. Additionally, by calculating the point of mean specific potential energy of the system at perigee and then comparing this to the perigee distance of the offset point we can determine whether or not these coincide and if so, then we have a working hypothesis. To further cement this, if the entire system undergoes a circular orbit when the angular velocity of the entire system is that of a circular orbit at the point of specific potential energy then this is proposed as further proof.

Firstly, we define the semi major axis of the system's centre of mass, a_{com}, in terms of its the observed apogee, r_{a-com}, and perigee, r_{p-com}, positions and relate this to the semi-major axis of the offset, a_s; its apogee and perigee distances, r_a and r_p, respectively; and the offset from the centre of mass, s_1, as follows:

$$a_{com} = \frac{1}{2}(r_{p-com} + r_{a-com}) = \frac{1}{2}((r_p + s_1) + (r_a + s_1)) = a_s + s_1 \quad (9.15)$$

Similarly, this is done for the centre of gravity of the system using an offset distance s_2 in this case:

$$a_{cg} = a_s - s_2 \quad (9.16)$$

By utilising simultaneous equations we find that $s_1 = s_2$ and re-define this as s. The offset of the system is then obtained as:

$$s = \frac{1}{2}(a_{com} - a_{cg}) \quad (9.17)$$

By obtaining the perigee and apogee data of the centre of mass and gravity shown in Figure (9.6), the semi major axis of the centre of mass

is found to be 7380.7km and that of the centre of gravity is found to be 7378.9km resulting in an offset of 0.9km. Using either equation (9.15) or (9.16), the semi major axis of the offset point is found to be 7379.8km. Utilising this, we calculate the perigee distance of the offset point by subtracting the offset from the perigee distance of the centre of mass and find this to be 7377.1km. We now calculate the radius of the point of mean specific potential energy for the system by firstly calculating the mean specific potential energy of the system using the following equation:

$$U_{mean} = \frac{\mu}{3} \left(\frac{1}{R-L} + \frac{1}{R} + \frac{1}{R+L} \right) \tag{9.18}$$

For a central facility radius of 7378km and sub-span length of 100km this is obtained as $53.9507 km^2 s^{-2}$. Implementing this into the equation for orbital potential energy we obtain this as occur

We have established that the trajectory undertaken by a extended system in orbit cannot be simplified to a particle of equal mass located at the centre of mass or at the centre of gravity however, it can be simplified to that of a particle at the mean point of specific potential energy for the system which raises the question: *is this point located at a yet undefined physical centre for the system?* The answer to this is, that the system orbits Earth as a particle located at the mean point of specific potential energy of the system coincident with the physical centre which we will denote its *centre of energy* and define it as the mean position of the sum particles of the system weighted by the specific potential energy of each
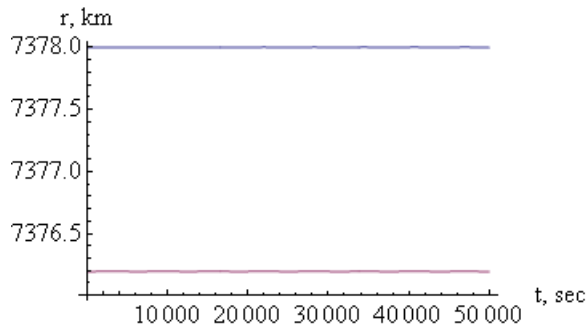

Figure 9.7: Hanging system's centre of mass and gravity at point of mean potential
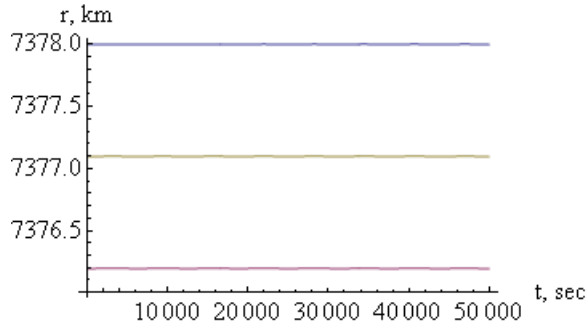
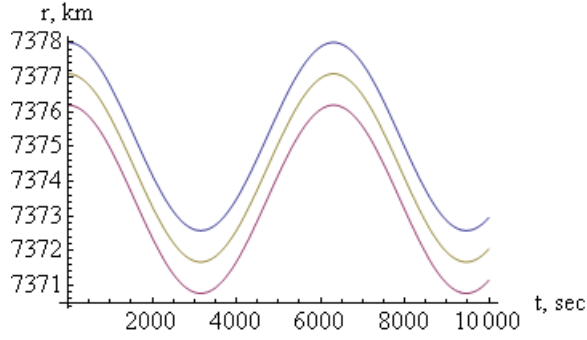**Figure 9.8:** Circular orbit of hanging system's centre of energy

Figure 9.9: Elliptical orbit of hanging system's centre of energy

particle, this can be written as:

$$\vec{R}_{cp} = \frac{-\sum_{i=1}^{n}(M_i r_i^{-1})\vec{R}_i}{\sum_{i=1}^{n}(M_i r_i^{-1})} \tag{9.19}$$

By incorporating equation (9.19) into the data plots shown in Figure (9.7), where the centre of mass is represented by the blue line and the centre of gravity is shown in purple, it becomes evident that the centre of potential lies exactly midway between the system's centre of mass and gravity. In Figures (9.8) and (9.9), the radius of the system's centre of mass is depicted by a blue line; its centre of gravity is depicted by a purple line; and its centre of potential is depicted by a golden line. For the case that the system has an orbital angular velocity equal to a circular orbit at the radius of this centre of potential, Figure (9.8), the entire system undertakes a circular orbit about Earth. For the case that an elliptical trajectory is undertaken when the entire system is given the orbital angular velocity of the system's centre of mass, Figure (9.9), the system undertakes the motion of a particle situated at the centre of potential with the orbital angular velocity of the centre of mass.

215

9.4 Conclusions

The observation of an anomaly occurring in a circular orbit of a tether system about Earth led to research into the point of balance of forces of this system. By calculating the tension acting at the centre of mass of the system, it was found that there was a mis-balance with the lower tension being greater than the upper tension at this point. It was noted that this was a result of the centrifugal and gravitational forces being unbalanced at this point for an extended body in a non-uniform gravitational field and it was found that these forces actually balance at the system's centre of gravity which is displaced from its centre of mass in this non-gravitational field. However, further work showed that the body cannot be treated as a particle acting at this point. It was discovered that the body actually orbits Earth identically to that of a particle located at the distance of mean specific potential energy of the system with an orbital geometry identical to that of a particle at this point and an angular velocity identical to that of the tether system. This point was termed the *centre of energy* of the system and the entire tether system undertook a circular orbit when given an angular velocity corresponding to that of a circular orbit at the distance of this physical centre. This certainly has many implications if verification of its existence can be obtained. This concept would redefine how the motion of extended bodies in orbit are calculated and may partly account for the presence of gravitational anomalies in many space missions.

10.   Conclusions

10.1   Discussion

An examination of the logistical requirements necessary to establish a continuous Earth-Moon payload revealed that an extremely flexible system could be configured by ensuring that the orbital periods of the EM-MET and Lunavator were integer harmonic with the orbital period of the Moon about Earth and this ensured that the system would return to its initial configuration each time the Moon arrived at the same point in its orbit relative to Earth. Furthermore, by establishing the rotational periods of the tether sub-spans such that they themselves were integer harmonic with the orbital period of their respective tethers plus some additional half rotation; quarter rotation; three-quarter rotation; or any combination of these; alternative tether tips could perform alternate catch and throw operations. It was found that to ensure that the payloads arrived at the tips of these tether systems at the correct instant, the payload exchanges conducted between the tethers occurred in time periods which were themselves integer harmonic with the orbital periods of these systems. The logistical design of the system was found to have an inherent flexibility, and by simple alterations to the rotational rates of the tips most circumstances could be accounted for. Furthermore, it was found that the system could accommodate variations in the Moon's orbital elements by altering the time at which operations were initiated without altering the operational procedure itself, however this resulted in small time mismatches between the optimum trajectories at one instant and those at another instant. It was found that these could not be accounted for, or remedied, and it was therefore found to be necessary for the logistical requirements to be rigorously adhered to and any adjustments in this case being made to the payloads' trajectories to and from Earth, and subsequently by the Lunavator in orbit about the Moon.

Several methods were conceived for tracking a significant location in the Moon's orbit with the aim of conducting payload exchanges upon the arrival of the Moon at these points. It was determined that this could be most easily achieved when the Moon crossed the ascending or descending node of its orbit relative to Earth's equatorial frame. Several methods for this were proposed with the most promising of these being:

i. Critically inclined EMMET orbit with adjustments to the freely precessing angle of ascending node being made via orbital manoeuvres

ii. Polar inclined EMMET orbit with adjustment manoeuvres utilised to align its apse line with that of the Moon's predicted node line at its next occurrence at its ascending node in addition to adjustment manoeuvres to the EMMET's freely precessing argument of perigee.

For each of these methods, the point at which the manoeuvres should take place within the EMMET's orbit were obtained in terms of the required change in orbital elements and for changes in angle of the ascending node between polar orbits this was found to occur at a true anomaly of 90°, for orbits with non-polar inclinations it was found that the point of manoeuvre occurred at the same true anomaly in both orbits and could be expressed in terms of the initial ascending node angle plus half the magnitude of the required change to this angle, in addition to the orbital inclination of the EMMET's orbit. The magnitude of the velocity change required to perform these adjustments was obtained using the Rodriguez formula and consisted of a rotation of the velocity vector of the EMMET's orbit about the equatorial frames' north pole. Similarly, the same was found to be the case for adjustments to the Lunavator's angle of ascending node with the change in velocity consisting of a rotation of the Lunavator's velocity vector at its point of manoeuvre in its initial orbit about the Moon's pole. For changes to the argument of perigee of the EMMET's orbit, in addition to the argument of perilune of the Lunavator's orbit it was found that the true anomaly of manoeuvre in each orbit occurred at a true anomaly equal to half the required alteration to this argument of perigee or perilune, furthermore it was found that the

change in velocity required to conduct this manoeuvre could be obtained in terms of the rotation of the velocity vector in the initial orbit about an axis coincident with the orbits' angular momentum vector relative to the equatorial or selenocentric frames.

The position, velocity and acceleration of the EMMET's and Lunavator's central facility and tips were derived relative to Earth's equatorial and the Moon's selenocentric frames, respectively. By taking into account the orbital elements required for both the polar and critically inclined EMMET inclination moon-tracking configurations the position, velocity and acceleration of the EMMET's orbit could be obtained for any point within the orbit also by incorporating the oblateness effects of the planetary bodies into these equations, for any instant of time afterwards. These equations were applied to the EMMET orbit at perigee in both configurations which would allow the velocity of payload release in each configuration to be assessed. These components were also derived for a Lunavator with freely precessing argument of perilune and angle of ascending node and this allowed one to obtain its position, velocity and acceleration at any point in its orbit when taking into account oblateness effects. Again an expression for these components at the perilune of its orbit were obtained with the aim of determining the velocities for payloads released at the upper and lower tips at this point. In both cases the accelerations of the system were utilised at their respective periapse to obtain expressions for the net forces acting on the payloads at these points in terms of the gravitational and inertial forces present which resulted in expressions for the tension acting on each of the payloads. Furthermore, the same methodology was applied to the tether sub-spans, and expressions for the tension occurring in each of these was obtained. By application of Newton's third law, the maximum tension within each of the tether systems, which occurred at the tether's point of connection to the central facility, was found to be equal and opposite to the sum of the tensions acting on the respective payloads and tether sub-spans. Utilising this point of maximum tension, expressions were obtained for the maximum angular velocity and which the tether sub-spans could rotate at which were based upon the material properties of tether sub-spans.

These improved upon previous maximum rotational rate expressions by their incorporation of velocity terms arising as a result of the motion of the tether system's frame of reference relative to either Earth or the Moon.

Numerical analysis of the EMMET's parameters relative to Earth was undertaken with data of the precessional rates of the argument of perigee and angle of ascending node being obtained for each configuration and this resulted in the single manoeuvre polar moon-tracking method being discounted due to the large amount of time taken to re-align the EM-MET's argument of perigee with Earth's equatorial plane as required to conduct payload exchanges. By defining the minimum semi-major axis sufficient to allow payloads launched from the EMMET's upper tip to reach the Moon at all points in its orbit when the EMMET sub-spans rotated at their maximum angular velocity it was found that a maximum orbital harmonic between the EMMET and Moon of 196 could be used which corresponds to an EMMET semi-major axis of 52224.5 km. Data of the velocity changes required to configure the EMMET's orbit in a polar inclination were obtained as a function of the EMMET's orbital harmonic with the Moon and it was found that the velocity required for these changes increased with increasing orbital harmonic resulting from an increased proximity of the EMMET to the Earth resulting in increased precessional rate in addition to this, it was noted that the adjustment to freely precessing argument of perigee was much more significant than those required to re-align the EMMET's apse line with the Moon's node line. Data was also obtained for the velocity changes required to configure the EMMET's orbit with a critical inclination, and it was found that the change in velocity required to adjust the freely precessing angle of ascending node in this case also increased with increasing orbital harmonic again as a result of increasing proximity to Earth, resulting in increased precessional rate in this case. However this velocity change was found to be smaller in comparison to that required to adjust the freely precessing argument of perigee.

Numerical analysis of the precessional rates of the argument of perilune and angle of ascending node of the Lunavator's orbit was undertaken

220

and it was observed that these rates were of a comparable magnitude to those occurring within the EMMET's orbit and were a result of the Lunavator's close proximity to the Moon even though its actual oblateness is very much less significant. The velocity adjustments required to configure the Lunavator's freely precessing argument of perilune and angle of ascending node were similarly found to increase with increasing orbital harmonic with the Moon's orbit and were of a comparable magnitude on both cases. Furthermore, it was investigated whether the Lunavator was indeed capable of completely removing orbital velocity from a payload at its upper tip and producing zero relative velocity with the Moon's surface at its lower tip, and this was indeed found to be the case and dependent upon the orbital harmonic of the Lunavator and the perilune radius of its central facility.

Numerical analysis of the performance of the tether systems was conducted in terms of the gain and loss of specific energy of the system for both the hanging and motorised cases. It was found that an increase in tether sub-span length improved both the performance and efficiency of the system for upper payload energy gain and lower payload energy loss in comparison with alterations to the semi-major axis of the system and was a direct result of the payloads experiencing increasing velocity discrepancies between current velocity and the velocity required to stay on the same orbit after release. An increase in the semi-major axis of the system was also found to improve the performance of the tether for both energy loss or gain as a result of this coinciding with an increase in orbital energy for the system. A significant result was found when numerical analysis of the motorised tether system was undertaken which showed that the maximum increase in the kinetic energy of a payload at the tip of sub-span rotating at maximum angular velocity occurred on a small plateau centred at a sub-span length of 100km. The motorised tether system performed ten times better than the hanging tether case in imparting energy to the upper payload and detracting energy from the lower payload.

A methodology for the configuration of the circumlunar trajectories between the EMMET and Lunavator's upper tips, when adhering

to the logistical requirements previously established, has been devised which utilises payloads undertaking elliptical trajectories between the EMMET's upper tip and the LSI boundary in addition to undertaking hyperbolic trajectories between LSI and perilune. It was found that by means of an iterative procedure that the elliptical and hyperbolic trajectories could be patched together at their points of intersection coinciding with their points of contact with the LSI and velocity differences minimised by means of this iteration. These trajectories were configured to satisfy the timing requirements of the transfers by calculating the transfers about Earth and the Moon as solutions to Lambert's problem with the required velocity at the beginning and end points of the trajectory calculated by utilising Lagrange coefficients. By alterations to the times of entry and exit to LSI, the orbital elements of these transfers about Earth could be closely matched to those of the EMMET in either of the moon-tracking configurations, additionally by adjustment to the transfer time of the hyperbolic trajectory about the Moon and to the positions of entry and exit themselves; a sufficient perilune distance could be had whilst matching the orbital elements of the trajectories at the boundary relative to Earth closely to those of the EMMET and payload's elliptical trajectory about Earth.

Numerical simulations of the entire circumlunar procedure were undertaken and several cases were presented which allowed the system under different logistical and moon-tracking configurations to be examined at ascending nodes occurring at different points in the Moon's orbit. By iteration of the procedure it was shown that the system could be set up according to the logistical requirements and the methodology previously endorsed with savings on the velocity requirements for the circumlunar transfer when comparing this to conventional chemical propulsion. However, several points of note arose as a result of this analysis and were present within every configuration case presented, These are as follows:

i. At every tip in every instance velocity mismatches were present between the tether tip and the incoming and outgoing payloads. This can be dealt with in two ways firstly, by ensuring that the system is robust enough to withstand this shock no further action need

be taken or alternatively, the payload should undertake propulsive burns to adjust the velocity at launch and capture to the required velocity as was the case incorporated into the simulations.

ii. Significant velocity mismatches occurred at the entry and exit points to LSI between the elliptical and hyperbolic trajectories at these points. Case 1 showed that these were as significant in the case where the elliptical and hyperbolic inclinations were matched and result from the differences in their arguments of perigee at these points of conjunction and less significantly on small differences in the angle of ascending nodes. Attempts were made to remedy this but resulted in unwanted variations in the other orbital elements of the trajectories.

iii. In all cases the lower tip velocity of the Lunavator remained unacceptably large and could not be reconciled. The solution to this is for the Lunavator to be placed into a circular orbit about the Moon but this also introduces further constraints into the overall system design and this will be discussed further in the next section.

Although an iterative procedure was undertaken for each of the transfer configuration cases, it is abundantly clear that these are not optimised trajectory calculations and the velocity mismatches between the tips and payloads in addition to those existing between the hyperbolic and elliptical trajectories at conjunction could be further reduced. The extent to which this may occur remains unclear at this point.

Having observed an anomaly occurring within the orbit of a symmetrical tether system about Earth it was noted that this was a result of the body undertaking an elliptical orbit about Earth even though it had the required orbital angular velocity for a circular orbit at its centre of mass. It was noted that this was a result of the centrifugal and gravitational forces being unbalanced at this point for an extended body in a non-uniform gravitational field and further examination found that these forces actually balance at the system's centre of gravity which is displaced from its centre of mass in this non-gravitational field. However, further work showed that neither was this the location at which the

system orbited Earth with a motion identical to a particle with the same angular velocity as the body. It was discovered that the body actually orbits Earth identically to that of a particle located at the distance of mean specific potential energy of the system with an orbital geometry identical to that of a particle at this point and an angular velocity identical to that of the tether system. This point was termed the *centre of potential* of the system and the entire tether system undertook a circular orbit when given an angular velocity corresponding to that of a circular orbit at the distance of this physical centre.

10.2 Further Work

Several issues have been raised regarding to the establishment of a continuous payload exchange system utilising momentum exchange tethers however, all of the problems can be overcome by careful design and optimisation and there are several areas which our focus should turn to. Although the system has been shown to be a realistic possibility the mission architecture at its current state does not yet present a viable alternative to chemical propulsion, when taking into account the development and system setup in the near term however, it is the author's firm belief that all of the velocity changes required, with the exception of those required to configure the EMMET and Lunavator, can be eradicated by optimisation of the trajectories between the EMMET and Lunavator tips. Furthermore, by taking into account trajectories which would minimise the required changes to the Lunavator's configuration; the optimum configuration for conducting these exchanges over the next several decades can be found and only then can a valid comparison of the efficiency of the system in comparison to current means of propulsion can be made. The next step for this research will therefore be the establishment of an optimisation process to determine the most efficient configurations for these exchanges which would utilise an EMMET in an elliptical orbit and a Lunavator in a circular orbit about the Moon with slight adjustments in the logistical arrangements to accommodate this.

Regarding the high velocity at the Lunavator's lower tip; although

this can be remedied to some extent by utilising a circular orbit about the Moon the fact remains that the Lunavator's orbit must adhere to the logistical requirements of the system which result in the circular orbit taking only those radial distances about the Moon which have orbital periods which are harmonic with the orbital period of the Moon about Earth. Furthermore, to ensure that the tip of the lower sub-span remains close to the Moon's surface without touching it when orbiting in this circular orbit; the lower tip must be at such an altitude to be within reach of the surface but far enough from it that no contact is made due to changes in surface geography. If this circular orbit cannot completely remove this velocity then a mobile mechanism located on the Moon's surface should be designed to do so and in addition to this, it would provide the boost to the payload to ensure that its velocity matched that of the lower payload in preparation for lower tip capture.

For the orbital mechanics described in this thesis it has been assumed that the tether sub-spans themselves are rigid and inextensible and although this is adequate for preliminary investigations of the orbital motion of these systems it is important that these motions can be realistically predicted. It is therefore recommended that a finite element model of a flexible and extensible tether system is constructed with an accurate model of the perturbing effects of the Earth's oblateness being implemented as a series expansion of the gravitational potential using Legendre polynomials as explained by Boas [48] . This is in addition to the perturbing effects of the Moon and the other bodies in the Solar system being treated as disturbing accelerations as explained by Battin [44]. The time evolution of the system would be obtained by numerical integration of the systems equations of motion and time was spent during the period of this Ph.D. research considering this problem but it was concluded that this would be a major period of research in itself and therefore it was unable to be undertaken.

An extremely important aspect of the system which has not been investigated in great detail is the mechanism for performing the capture and launch of the payloads at the tether tips and this is an area which requires immediate attention however, concepts have been proposed and

it possible that the grapple assembly designed by *Tethers Unlimited*™ for the *MXER* system [57] could be ideal for this application. Finally, work should be undertaken to thoroughly investigate the centre of potential of the system to understand more fully the extent of this phenomena and the implications this has for the motion of extended bodies in orbit.

Bibliography

[1] Puig-Suari, J., Longuski, J.M., and Tragesser, S.G., *A Tether Sling for Lunar and Interplanetary Exploration*, Acta Astronautica, Vol. 36, No. 6, 291-295, (1995).

[2] Cartmell, M.P., and Zeigler, S.W., *Symmetrically Laden Motorised Momentum Exchange Tethers For Continuous Two-Way Interplanetary Exchange*, 35th AIAA/ASME/SAE/ASEE Joint Propulsion Conference and Exhibit, AIAA Paper 99-2840, Los Angeles, CA, USA, (1999).

[3] Tsiolkovskii, K.E., *A Way to Stars*, Izdatelstvo AN SSSR, Moscow, (1961).

[4] Beletsky, V.V.,and Levin, E.M., *Dynamics of Space Tether Systems*, Advances in Astronautical Sciences: Volume 83, American Astronautical Society, San Diego, CA, U.S.A., 1993.

[5] Chobotov, V.A., *Gravity Gradient Excitation of a Rotating Cable Counterweight Space Station in Orbit*, Journal of Applied Mechanics, **30** (1963), 547-554.

[6] Lang, D.D., and Nolting, R.R., *Operations with Tethered Space Vehicles*, Gemini Summary Conference, February 1-2, 1967, Houston, Texas, NASA SP-138, 55-66.

[7] Cosmo, M.L., and Lorenzini, E.C., *Tethers in Space Handbook*, Third edition, Smithsonian Astrophysical Observatory, Cambridge, MA, U.S.A, 1997.

[8] Napolitano, L.G., and Bevilacqua, F., *Tethered Constellations, Their Utilisation as Microgravity Platforms and Relevant Features*, 35th International Astronautical Congress, Lausanne, Switzerland, October 7-13, 1984, Paper No 84-439.

[9] Kroll, K.R., *Tethered Propellant Resupply Technique for Space Stations*, Acta Astronautica, **12** (1985), 987-994.

[10] Bainum, P.M., Harkness, R.E., and Stuiver, W., *Attitude Stability and Damping of a Tethered Orbiting Interferometer Satellite System*, Journal of the Astronautical Sciences, **19** (1972), 364-389.

[11] Bekey, I., *Tethers Open New Space Options*, Astronautics and Aeronautics, Vol. 21, No. 4, 32-40, (1983).

[12] Forward, R.L., Hoyt, R.P., and Uphoff, C., *The Terminator Tether: A Low-Mass System for End-of-Life Deorbit of LEO Spacecraft*, Tether Technical Interchange Meeting, Huntsville, AL, September 10, 1997.

[13] Drell, S.D., Foley, H.M., and Rudderman, M.A., *Drag and Propulsion of Large Satellites in the Ionosphere: An Alfven Propulsion Engine in Space*, Journal of Geophysical Research, Vol.70, No. 13, 3131-3145, July, (1965).

[14] Vas, I.E., Kelly, T.J., and Scarl. E.A., *Space Station Reboost with Electrodynamic tethers*, Journal of Spacecraft and Rockets, Vol. 37, No. 2, 154-164.

[15] Grossi, M.D., *Spaceborne Long Vertical Wire as a Self-Powered ULF/ELF Radiator*, Journal of Oceanic Engineering , Vol. 9, No. 3, p. 211-213, July 1984.

[16] Bekey, I., and Penzo, P.A., *Tether Propulsion*, Aerospace America, Vol. 24, No. 7, 40-43, (1986).

[17] Lorenzini, E.C., Cosmo, M.L., Kaiser, M., Bangham, M.E., Vonderwell,D.J., and Johnson, L., *Mission Analysis of Spinning Systems for Transfers from Low Orbits to Geostationary*, Journal of Spacecraft and Rockets, Vol. 37, No. 2, 165-172, (2000).

[18] Carroll, J.A., *Tether Applications in Space Transportation*, Acta Astronautica, Vol. 13,No. 4 , 165-174, (1986).

[19] Crellin, E.B., and Janssens, F.L., *Some Properties of the In-plane Motion of a Dumbbell in an Elliptical Orbit*, ESTEC Working Paper, No, 1888, European Space Agency, Noordwijk, Netherlands, (1996).

[20] Moravec, H., *A Non-Synchronous Orbital Skyhook*, Journal of Astronautical Sciences, Vol. 15, No. 4, 307-322, (1977).

[21] Hoyt, R., and Forward, R.L., *Tether Transport from Sub-Earth-Orbit to the Lunar Surface and Back!*, International Space Development Conference, Orlando, Florida, May, (1997).

[22] Zeigler, S.W., and Cartmell, M.P., *Using Motorised Tethers for Payload Orbital Transfer*, Journal of Spacecraft and Rockets, Vol. 38, No. 6, (2001).

[23] Cartmell, M.P., and Zeigler, S.W., *Experimental Scale Model Testing of a Motorised Momentum Exchange Propulsion Tether*, 37th AIAA/ASME/SAE/ASEE Joint Propulsion Conference and Exhibit, AIAA Paper 2001-3914, Salt Lake City, UT, USA, (2001).

[24] McKenzie, D.J., and Cartmell, M.P., *On the Performance of a Motorised Tether using a Ballistic Launch Method*, 55th International Astronautical Congress, Vancouver, Canada, IAC-04-IAA-3.8.2.10, (2004).

[25] Chen, Y., and Cartmell, M.P., *Multi-Objective Optimisation on Motorised Momentum Exchange Tether for Payload Orbital Transfer*, 2007 IEEE Congress on Evolutionary Computation, Singapore, 2007

[26] Murray, C., and Cartmell, M.P., *Continuous Earth-Moon Payload Exchange Using Symmetrically Laden Motorised Momentum Exchange Tethers*, 59th International Astronautical Congress, Glasgow, UK, IAC-06-D4.3.03, (2008).

[27] Forward, R.L., *Tether Transport from LEO to the Lunar Surface*, 27th AIAA/ASME/SAE/ASEE Joint Propulsion Conference and Exhibit, AIAA Paper 91-2322, Sacramento, CA, USA, (1991).

[28] Hoyt, R., and Uphoff, C., *Cislunar Tether Transport System*, 35th AIAA/ASME/SAE/ASEE Joint Propulsion Conference and Exhibit, AIAA Paper 9-2690, Los Angeles, CA, USA, (1999).

[29] Cartmell, M.P., McInnes, C.R., McKenzie, D.J., *Proposals for an Earth-Moon Mission Design based on Motorised Momentum Exchange Tethers*, Plenary session paper, Proc. XXXII Summer School on Advanced Problems in Mechanics, Russian Academy of Sciences, St. Petersburg, Russia, June 2004.

[30] Forward, R., and Nordley, G., *Mars-Earth Rapid Interplanetary Tether Transport (MERITT) System*, 35th AIAA/ASME/SAE/ASEE Joint Propulsion Conference and Exhibit, AIAA Paper 9-2151, Los Angeles, CA, USA, (1999).

[31] Hoyt, R., Slostad, J., and Twiggs, R., *the Multi-Application Survivable Tether (MAST) Experiment*, 39th AIAA/ASME/SAE/ASEE Joint Propulsion Conference and Exhibit, AIAA Paper 2003-5219, Huntsville, AL, USA, (2003).

[32] [online] *SpaceRef.com*, Accessed 20-2-2011, Available at: http://www.spaceref.com/news/viewsr.rss.spacewire.html?pid=34856.

[33] Bogar, T.J., Bangham, M.E., Forward, R.L., and Lewis, M.J., *Hypersonic Airplane Space Tether Orbital Launch (HASTOL) System: Interim Study Results*, 9th International Space Planes and Hypersonic Systems and Technologies Conference, AIAA Paper 99-4802, Norfolk, VA, USA, (1999).

[34] Hoyt, R., *Design and Simulation of a Tether Boost Facility For LEO-¿GEO Transport*, 36th AIAA/ASME/SAE/ASEE Joint Propulsion Conference and Exhibit, AIAA Paper 2000-3866, Huntsville, AL, USA, (2000).

[35] Santangelo, A., Johnson, L., *Future Applications of Electrodynamic Tethers for Propulsion*, 36th AIAA/ASME/SAE/ASEE Joint Propulsion Conference and Exhibit, AIAA Paper 2000-3870, Huntsville, AL, USA, (2000).

[36] [online] *Tethers Unlimited Inc*, Accessed 22-2-2011, Available at: http://www.tethers.com/GRASP.html.

[37] [online] *Tethers Unlimited Inc*, Accessed 22-2-2011, Available at: http://www.tethers.com/microPET.html.

[38] [online] *Tethers Unlimited Inc*, Accessed 22-2-2011, Available at: http://www.tethers.com/HiVOLT.html.

[39] [online] *BETS passive electric propulsion*, Accessed 22-2-2011, Available at: http://www.thebetsproject.com/.

[40] Cartmell, M.P., *Private communication*, University of Glasgow, UK, (2008).

[41] Roncoli, R.B., *Lunar Constants and Models Document*, JPL D-32296, Jet Propulsion Laboratory, Pasadena, CA, U.S.A., (2005).

[42] Vallado, D.A.,*Fundamentals of Astrodynamics and Applications*,Microcosm Press, Hawthorne, CA, U.S.A. and Springer, New York, NY, U.S.A., (2007).

[43] Woan, G., *The Cambridge Handbook of Physics Formulas*, Cambridge University Press, Cambridge, UK, (2003).

[44] Battin, R.H, *An introduction to the Mathematics and Methods of Astrodynamics*, Revised Edition. AIAA Education Series, Reston, VA, U.S.A, (1999).

[45] Shabana, A.A., *Dynamics of Multibody Systems*, Second Edition, Cambridge University Press, Cambridge, UK, (1998).

[46] Chobotov, V.A., *Orbital Mechanics*, Third Edition, AIAA Education Series, Reston, VA, U.S.A., (2002).

[47] Curtis, H.D., *Orbital Mechanics for Engineering Students*, Elsevier Aerospace Engineering Series, Butterworth-Heinemann, Oxford, UK, (2004).

[48] Boas, M.L, *Mathematical Methods In The Physical Sciences*, Second Edition. John Wiley and Sons, U.S.A, (1983).

[49] Zeigler,S.W., *The Rigid Body Dynamics Of Tethers In Space*, Ph.D. Dissertation, Department of Mechanical Engineering, University of Glasgow, Glasgow, UK, 2003.

[50] [online] *Wikipedia*, Accessed 5-9-2010, Available at: http://en.wikipedia.org/wiki/Exosphere.

[51] [online] *Moon Fact Sheet*, Downloaded 17-12-2007, Available at: http://nssdc.gsfc.nasa.gov/planetary/factsheet/moonfact.html.

[52] [online] *Jet Propulsion Laboratory HORIZONS System*, Accessed extensively, Available at: http://ssd.jpl.nasa.gov/horizons.cgi.

[53] Langan, M.P., *First Lunar Outpost (FLO)Conceptual Flight Profile*, Engineering Directorate, Systems Engineering Division; NASA JSC, (1992).

[54] Fowles, G.R., and Cassiday, G.L., *Analytical Mechanics*, Fifth Edition, Saunders College Pub, Fort Worth, Tx, (1993).

[55] Young, H.D., and Freedman, R.A., *University Physics with Modern Physics*, Tenth Edition, Pearson Education, Addison-Wesley, (2000).

[56] [online] *NASA*, Accessed 14-6-2010, Available at: http://www.grc.nasa.gov/WWW/K-12/airplane/cg.html.

[57] [online] *Tethers Unlimited Inc.*, Acessed 1-3-2011, Available at: http://www.tethers.com/Movies/CaptureToss.mov.